KINEMATIC STUDY OF OVERCONSTRAINED LINKAGES AND DESIGN OF RECONFIGURABLE MECHANISMS

NANYANG TECHNOLOGICAL UNIVERSITY

KINEMATIC STUDY OF OVERCONSTRAINED LINKAGES AND DESIGN OF RECONFIGURABLE MECHANISMS

SONG CHAO-YANG

SCHOOL OF
MECHANICAL AND AEROSPACE ENGINEERING

2013

SONG CHAO-YANG

2013

This page is intentionally left blank.

KINEMATIC STUDY OF OVERCONSTRAINED LINKAGES AND DESIGN OF RECONFIGURABLE MECHANISMS

SONG Chao-Yang

School of Mechanical and Aerospace Engineering

A Dissertation Submitted to the Nanyang Technological University

in fulfilment of the requirement for the Degree of Doctor of Philosophy

2013

Acknowledgement

I would like to express my deepest gratitude to my advisors, Professor CHEN Yan and Professor CHEN I-Ming, for their constant support and guidance throughout these years. I am grateful to Professor CHEN Yan for giving me the opportunity to pursue a Ph.D. degree. I am greatly thankful to Professor CHEN I-Ming for his broad knowledge, patient and open-minds towards life and work, which have always been and will always be an inspiration to me. All the things I've learned from both advisors are the valuable lifetime experience which could never be found in any textbooks.

I would like to thank Prof. Karl WOHLHART for his patience, generosity and openness during communications and discussions. I would like to thank my colleagues, ZHANG Yin, LIU Sicong, SONG Jie, ZHU Shengqing and YUAN Qilong, for their friendship during these years. Many thanks to the technicians at Robotics Research Centre, Mr. LIM Eng Cheng, Ms. TAN Siok Kuan, Mr. YOU Kim San; and other technicians, Ms. TAN How Jee, Ms. LEE Koon Fong, Mr. NG Jui Hock, Mr. WONG Cher Kong, for their support in the workshop.

Last but not least, I would like to thank my parents for their encouragements. I would like to express special thanks to my best companion and my wife, WAN Fang, as I couldn't have been able to finish my study without the support from her.

Dedication

To my family

Table of Contents

List of Notations

Chapter 1

M	The mobility of a linkage
n	The number of links
j	The number of joints
f_i	The degree of freedom of joint i

Chapter 2

x_i	The coordinate axis along the normal distance between joint axes from the previous joint to the next joint
z_i	The coordinate axis along the revolute axis of joints i
a_{ij}	The length of link ij
α_{ij}	The twist of link ij
R_i	The offset of joint i
θ_i	The revolute variable of joint i
$\mathbf{T}_{ij}$	The transformation matrix from joint i to joint j
Ro	The 3×3 rotational matrix
Tr	The 3×1 translational vector
I	The identity matrix
a/α	The link length and revolute variable of the link are a and α, respectively

Chapter 3

S1, S2, S3, G1, G2, G3

The symbols for different subtractive Goldberg 5*R* linkages and Goldberg 5*R* Linkages

m_i Symbols which represent different relationship between twist angles

H , P , Q The symbols for simplified mathematical relationship about θ_1

Chapter 4

$A_{2,3}$, $B_{2,3}$, …, $H_{2,3}$ and $L_{2,3}$

The symbols of simplified mathematical relationships, subscript 2 or 3 indicate the symbols for θ_2 or θ_3

$Aterm_{2,3}$, $Bterm_{2,3}$ and $Cterm_{2,3}$

The symbols for simplified mathematical relationship about θ_1, subscript 2 or 3 indicate the symbols for θ_2 or θ_3

$P_{I,II}$ Points on the paths of the line-symmetric octahedral Bricard linkage

$B_{I,II,III,IV}$ The bifurcation points on the kinematic paths

X and X′ The corresponding parameters in two types of general line-symmetric Bricard linkage, where X is for the parameters in the *original* linkage and X′ is for the parameters in the revised linkage

Chapter 5

P_{WDG}, Q_{WDG}, P_{DSG} and Q_{DSG}	The symbols for simplified mathematical relationship about θ_1 in the Wohlhart's double-Goldberg linkage and double-subtractive-Goldberg linkage
q	The symbol of simplified mathematical relationship
C	Random constant
Y_i'	The corresponding parameters of joint i in the spatial triangle
Y_i''	The corresponding parameters of joint i in the intermediate Bennett linkage
A, B, C, D	The symbols for different Bennett linkages
●	The joint in a link-pair that is going to be replaced
○	The joint in a link-pair that no actions will be performed

Appendix

$\Delta\theta_i$	A small increment of the revolute variable θ_i
$\mathbf{T}_i^{\theta}$	The transformation matrix about the revolute variable θ_i
$\mathbf{T}_{i(i+1)}^{L}$	The transformation matrix about the link length $a_{i(i+1)}$, twist $\alpha_{i(i+1)}$ and offset R_i
[**0**]	A zero matrix
E	The error matrix
$\mathbf{T}_i$	A simplified matrix representing the variable of $\Delta\theta_i$
$t_{i_{i,j}}$	A symbolic representation of the entry located at (i, j) of $\mathbf{T}_i$

$\Delta\theta_i^p$	A small finite predictor displacement which is proportional to the infinitesimal solution to the Jacobian matrix
$\Delta\theta_i^c$	A small corrector step added to the predictor displacement so that the linkage would move towards the corrected configuration

List of Figures

List of Tables

Abstract

This dissertation explores the possibilities to design reconfigurable mechanisms using the kinematic and geometric properties of existing overconstrained linkages with revolute joints. Despite the large number of overconstrained linkages reported in literatures, there lacks of a comprehensive study into the relationship among them, which limits the understanding of the overconstrained linkages and their potential applications.

The first part of this dissertation has been devoted to the systematic generalization of a series of double-Goldberg linkage families, in which the relationship between a number of existing linkages and their variational cases has been revealed. The common link-pair and common Bennett-linkage methods have been proposed to connect a Goldberg 5*R* linkage and a subtractive Goldberg 5*R* linkage to form six types of overconstrained linkage closures. Three sub-families, Wohlhart's double-Goldberg linkages, mixed double-Goldberg linkages and double-subtractive-Goldberg linkages, have been generalized to represent the original cases, variational cases and subtractive cases of double-Goldberg linkage family. A substantial source of design for reconfigurable mechanisms in the Bennett-based linkage family has been presented in this part. In the second part, the kinematic study has been focused on the general line-symmetric Bricard linkage. The closure equations of the original and revised general line-symmetric Bricard linkages have been derived in explicit forms. For the general line-symmetric Bricard linkage, two independent and distinct linkage closures have been discovered. It has also been revealed that the revised cases are equivalent to the original cases with different setups on joint-axis directions. The potential of designing the reconfigurable mechanism through kinematic singularity has been demonstrated with the bifurcation behavior of the special line-symmetric Bricard linkage with zero offsets.

The conceptual designs of reconfigurable mechanisms based on overconstrained linkages have been explored in the final part. Both the analytical and construct method have been presented to design morphing structures using overconstrained linkages. Based on the double-Goldberg linkage and the general line-symmetric Bricard linkage, reconfigurable mechanisms have been designed with multiple operation forms between 6*R* and 4*R* linkages. Furthermore, a generic method of link-pair replacement has been developed for reconfiguration purpose, which has been applied to reconfigure the topology of different Bennett linkage networks in order to obtain different overconstrained mechanisms.

Results in this dissertation could lead to the substantial advancement in the design of reconfigurable mechanism with kinematic singularities. In the future work, the methods could be applied to design advanced reconfigurable robotic platforms with less actuators but more structural support.

Chapter 1

Introduction

1.1 OVERVIEW

The initial research interest about the overconstrained linkages was driven by mathematicians like Pierre Frédéric Sarrus, Raoul Bricard, Geoffrey Thomas Bennett and Michael Goldberg in exploring the extension of planar geometries into three dimensional spaces. These pioneers' work did not receive so many attentions when they were firstly published. There were a lot of reasons for such situations. For instance, the original work by Sarrus (1853) and Bricard (1897; 1927) were published in French over a century ago. The original work done by Bricard (1897) was to answer a mathematical challenge posed by Stephanos (1894) that "Do there exist polyhedra with invariant facets that are susceptible to an infinite family of transformations that only alter solid angles and dihedrals?" As a result, three types of deformable octahedral were derived, which have only one degree of freedom in the present context. The engineering potentials of such deformable geometries was later noticed by other mathematicians, which open the doors of overconstrained linkages in kinematics and robotics. The most famous example is the Bennett linkage (Bennett, 1903; 1914), which is a four-bar mechanism moving in the 3D space. The Bennett linkage is later proved to be the only overconstrained linkage with four links connected by revolute joints whose axes are neither parallel nor concurrent (Delassus, 1922). The pioneering work by Goldberg (1943) is to use the Bennett linkage as the basic element to build more complex overconstrained five-bar and six-bar linkages. The topic of overconstrained linkages started to get noticed and researched in an engineering point of view. From the early 80s until now, J. Eddie Baker did the most work in the study and promotion of overconstrained mechanisms.

Kinematics is the study about the geometry of motion (Beggs, 1983). Generally, any chain of rigid bodies connected by certain movable joints could be considered as a *mechanism*. The *mobility* of a mechanism is the number of inputs required to determine the motion of all links with respect to a fixed reference frame. Once the motion is known, the forces which produced that motion may be found by means of dynamics. A *linkage* is a kinematic chain that consists of several rigid links connected by lower pair joints. There are six types of *lower pair joints*, which are defined by the type of surface contact between two members if the contact only occurs at the points on the contact surface, including revolute pair, prismatic pair, cylindrical pair, helical pair, spherical pair and planar pair. In this dissertation, the content is limited to revolute pair (*R*), or revolute joint, only. In 2D space, the mobility of a planar linkage could be correctly calculated by the *Kutzbach-Grubler's mobility criterion* (Hunt, 1990), which is a significant improvement in engineering applications. When the criterion is extended to the 3D space, according to this criterion, the mobility M for a linkage of n links connected by j joints can be determined by the following equation,

$$M = 6(n - j - 1) + \sum_{n=1}^{i} f_i \,, \tag{1.1.1}$$

where $f_i \ (i = 1, 2, ..., j)$ represents the mobility of joint i. For a single-loop spatial linkage with only revolute joints, the number of links and joints are equal, or $n = j$; and each revolute joint has mobility one, or $f_i = 1$. When a linkage has more degrees of freedom than the Kutzbach-Grubler's mobility criterion has predicted, this linkage is *overconstrained* in geometry conditions and therefore categorized as an *overconstrained linkage*. This definition of the overconstrained linkage will be used throughout this dissertation. From Eq. (1.1.1), at least seven links are required to construct a single-loop spatial linkage with only one degree of freedom. However, when certain geometry conditions are imposed, there exists a number

of overconstrained linkages with six, five or four revolute joints that has only mobility one during a full-cycle movement.

Besides the Kutzbach-Grubler's mobility criterion, there are a number of methods developed to determine a mechanism's mobility. Recently, a critical review on the calculation of mobility, the main structural and kinematic parameters of a mechanism, was made in (Gogu, 2005c) and 35 methods in literature during the past 150 years were summarized and analyzed in a systematic manner. Even though it is not the purpose of this dissertation to search for an optimal method for modern mechanism mobility calculation (Gogu, 2005a), it should be noticed that it remains one of the fundamental and critical problems for the advancement of mechanical engineering and there are still a lot of works to be done for a clearer method with broader applications in engineering and science. Examples of such effort could be found in (Gogu, 2005b), where a new formula for quick calculation of mobility has been proposed and demonstrated via the theory of linear transformation. The readers are encouraged to pursue advancements in this area in (Gogu, 2008), where new formulas of mobility calculations are applied to single- and multi-loop overconstrained linkages which do not obey the Kutzbach-Grubler's mobility criterion.

A *machine* is the assembly of certain components which consume the energy to perform certain intended actions. In mechanical engineering, such machine can be viewed as a *mechanism* which is designed to transform a set of input forces and motions to certain desired output forces and motions. The *configuration* of such mechanism is determined by the purpose of design, which is usually presented as certain physical arrangement of the mechanical components and parts. To meet the need of engineering applications, it is natural for the designer to integrate as many capabilities as possible into just one machine, which

could expand its application and reduce the cost of manufacturing. Such efforts usually require advanced design methods and control theories to make it work. In general, the concept of *reconfiguration* is to introduce the capability to a machine so that it could change its configurations according to the changing task requirements. In this research, efforts are made to explore the conceptual designs of such reconfigurable mechanisms using overconstrained linkages as the source of design. The motivation comes from the fact that such spatial motions generated from the overconstrained linkages could provide new possibilities for advanced mechanism designs.

In this dissertation, the exploration to the conceptual designs of reconfigurable mechanism using overconstrained linkages is achieved in two steps: 1) what method can be used to design and analyze the overconstrained linkages? 2) what kind of reconfigurable mechanism could be designed using the overconstrained linkage to achieve the change of configurations?

The first step requires the study about the kinematics of overconstrained linkage. Efforts have been made in literature to use different mathematical tools, including solid geometry (Bennett, 1903; 1914; Bricard, 1897; 1927; Goldberg, 1943), vectors (Dietmaier, 1995a; Wohlhart, 1987; 1991b), matrices (Denavit and Hartenberg, 1955), dual quaternion and dual number (Yang, 1963), and screw theory (Ball, 1876; Huang, 1992; Mavroidis, 1993). However, it is still not clear how the unique geometry conditions enable the mobility of these overconstrained linkages. Despite the various overconstrained linkages reported, there still lacks of a systematic organization about these linkages, which discourages the development for further applications. In this dissertation, the construct methods of common link-pair and common Bennett-linkage are used to find the relationship among a wide range of

overconstrained linkages in the Bennett-based family. Then, by making use of the geometric properties of the general line-symmetric Bricard linkage, a detailed analytical process is presented to study the linkage kinematics, where multiple operation forms are found.

The second step is the design of reconfigurable mechanisms using overconstrained linkages, where two different conceptual designs are explored in this dissertation. In the first conceptual design, the reconfiguration is achieved through kinematic bifurcations. Due to its special geometric constraints, certain linkage may present singular behavior on the kinematic paths, where the linkage could bifurcate into different operation forms on different kinematic paths. The design goal is to reconfigure the linkage by intentionally modifying an existing operation form or introducing a new operation form. Construct and analytical methods are presented in this dissertation to design a desired multiple operation form of a 4*R* linkage in certain overconstrained 6*R* linkage. In the second conceptual design, the reconfiguration is achieved through geometric reconstruction. In this design, the goal is to find a method that is generically applicable so that a wide range of linkage could be reconfigured. The method of link-pair replacement is proposed, which could be applied to different networks of Bennett linkage for the reconfiguration purposes. As a result, a wide range of overconstrained 6*R*, 5*R* and 4*R* linkages in the Bennett-based family are reconfigured from networks of Bennett linkages, which encourages the future work to find a suitable engineering application of such reconfigurable mechanism.

The remainder of this chapter is organized as follows. Section 1.2 reviews major overconstrained linkages that will be addressed in this dissertation. Section 1.3 reviews the development of reconfigurable mechanisms. Section 1.4 outlines the organization of the remaining chapters in this dissertation.

1.2 MAJOR OVERCONSTRAINED LINKAGE FAMILIES

The Bennett linkage is a spatial 4*R* linkage found in 1903 by a mathematician, Geoffrey Thomas Bennett (1903), from the University of Cambridge. Since then, it has received enormous attentions from kinematicians. Various research works has been devoted to the invention of single degree of freedom overconstrained linkages by combining two or more existing overconstrained linkages. Among them, the Bennett linkage has been a popular construct element. Myard (1931) was the first one to form 5*R* or 6*R* overconstrained linkages with two Bennett linkages. Later, Goldberg (1943) built a family of 5*R* and 6*R* linkages with two or three Bennett linkages. For the 5*R* linkage, Baker (1979) re-examined both the Myard's 5*R* linkages and the Goldberg's 5*R* linkages. He pointed out that the former one can be considered as a special case of the latter one. Wohlhart (1991a) derived the generalized Goldberg 5*R* linkage in detail, which was initially introduced by Goldberg (1943). The closure equations of the generalized Goldberg 5*R* linkage was also analyzed using screw theory by Baker (1983). Lee (2002) gave a comprehensive investigation to the kinematics of the generalized Goldberg 5*R* linkage. Recently, an extended Myard 5*R* linkage was proposed by Chen and You (2008a).

For the overconstrained 6*R* linkages, besides the 6*R* linkages proposed by Goldberg (1943) and Myard (1931), several linkages were published using construct methods. Waldron (1968) merged two Bennett linkages on a common joint and constrained the relative positioning of the links from these two Bennett linkages to build a hybrid 6*R* linkage. Yu and Baker (1981) reported a syncopation of Waldron's hybrid 6*R* linkage when the 6*R* linkage was degenerated into a Goldberg 5*R* linkage. Later, Baker (1993a) further utilized Goldberg's technique and derived two variants of the Goldberg 6*R* linkages. Wohlhart (1991a) found a new 6*R* linkage by firstly merging two Goldberg 5*R* linkages in a "face-to-face" configuration and then

removing the commonly shared links and joint. This 6*R* linkage was further combined with a Bennett linkage to form another 6*R* linkage with line symmetry (Wohlhart, 1991b). The term Bennett-based linkage family was firstly adopted by Baker (1993a) to identify the overconstrained linkages constructed with units of Bennett linkages. This was also to distinguish them with another important linkage family, the Bricard linkages, which are constructed in a different manner. Recently, Chen and You (2007) reported a 6*R* linkage based on the combination of two Goldberg 5*R* linkages in a "back-to-back" configuration. Similar to the Wohlhart's double-Goldberg 6*R* linkage, the linkage also can be isomerized with a Bennett linkage to form a line-symmetric 6*R* linkage, which becomes a special case of line-symmetric Bricard linkage.

The Bricard linkages form another important linkage family which comprises of three deformable octahedrons: the line-symmetric octahedral case, the plane-symmetric octahedral case and the doubly-collapsible octahedral case (Bricard, 1897); and three spatial linkages: the general line-symmetric case, the general plane-symmetric case and the trihedral case (Bricard, 1927). Bricard later pointed out that the line-symmetric octahedral case is a special case of the general line-symmetric linkage case (Baker, 1980; Bricard, 1927). Different from the Bennett-based linkages, the Bricard linkages were not originally constructed from the combination of smaller or simpler units. Instead, different symmetry properties are used in the geometry conditions, which enable mobility (Fowler and Guest, 2005; Guest and Fowler, 2005). Baker (1980) also reviewed the six cases of Bricard linkages. However, the closure equations derived by Baker (1980) are in implicit forms which make them impractical to conclude their kinematic properties. Phillips (1984; 1990) also reviewed the Bricard linkages and their relationship with other overconstrained linkages.

The three octahedral cases of Bricard linkages attracted a number of kinematic studies. A comprehensive analysis to the three octahedral cases was done by Bennett (1912). Baker (1986) noticed the relationship of a special line-symmetric octahedral Bricard linkage in stationary and linkage configurations with respect to the conformation of cyclohexane molecular in chair and boat forms. The closure equations of these three octahedral cases of Bricard linkages were derived analytically using matrix transformation method by Lee (1996). Recently, Chai and Chen (2010) found that the line-symmetric octahedral Bricard linkage with identical twist and offset always has a stationary structural configuration, which is independent from its mobile linkage form. In engineering applications, the octahedral cases of Bricard linkages are related to parallel manipulators such as the Stewart-Gough Manipulator (Husty, 2000; Husty and Karger, 1996; Husty and Zsombor-Murray, 1994) and Triangular Symmetric Simplified Manipulators (Nawratil, 2010; 2011), which are widely used as flight simulators and milling machines. The independent work by Nelson (2010; 2012) demonstrated the possibilities of building large network of polyhedral with the octahedral cases of Bricard linkages.

As for the three linkage cases, a plate-form model of the trihedral Bricard linkage was made and analyzed by Goldberg (1974). Yu (1981b) studied the geometry of the trihedral case with respect to its circumscribed sphere and associated hyperboloid. Wohlhart's early work (1993) shows that there are actually two distinct cases of the trihedral Bricard linkage. Due to their special geometry constraints, reciprocal screw system is extensively used for the analysis of Bricard linkages. Using this method, it was found that for any configuration of the general line-symmetric Bricard linkage, the central axis of the linear complex defined by the joint axes is orthogonally intersected to the linkage's line of symmetry (Baker and Wohlhart, 1994). This result was proved numerically by Lee (2000). The reciprocal screw system of the

general plane-symmetric six-screw linkage was also analyzed by Baker (1997), which covers the plane-symmetric case of Bricard linkage. A further numerical technique was developed using the direct elimination of the screw matrix to study the Bricard linkages (Lee, 2000). Recently, a threefold-symmetric Bricard linkage was proposed to explore the application of Bricard linkage in the design of deployable structures (Chen et al., 2005). A special line and plane symmetric Bricard linkage was analyzed with regards to its unique bifurcation behaviors (Chen and Chai, 2011). Besides the original cases of Bricard linkages, there are linkages found by other researchers that make use of certain symmetry properties to make the linkage mobile, such as the Altmann's linkage (Altmann, 1954), Schatz's linkage (Schatz, 1975) and Wohlhart's hybrid linkage (Wohlhart, 1987), which can be categorized into the Bricard linkage family.

1.3 RECONFIGURABLE MECHANISMS

Generally, reconfigurable mechanism is a mechanical system that can change its spatial configuration with different requirements or in different environments. Classical mechanism design is usually processed in two-dimensional space, which has proved its efficiency and accuracy in engineering applications. However, as the functionality of a designated mechanical system increases, the complexity of mechanism design grows. The overconstrained linkage provides a feasible source of design for mechanisms with reconfiguration capabilities. A number of research interests for the reconfigurable mechanism focused on applications in aircraft wing design. The reader is encouraged to pursuit the review article by Barbarino, Bilgen, Ajaj, Friswell and Inman (2011) for details. Research interests in reconfigurable mechanism design have also been extended to the design of multi-loop linkages. The mechanism developed by Stubbs, Whittier and Reinholtz (2004) exhibits high loading capacity and less actuators, which can be reconfigured between two desired air-

foil shapes. On the other hand, recent advancement promotes the concept of reconfigurable mechanism designs in a broader manner. Generally, three categories of reconfigurable mechanisms can be summarized.

The *first category* is based on the reassembly of identical or similar robotics modules, each of which is an integrated system of microprocessors, batteries, sensors and end-effectors etc. For the past two decades, research shows that such robotic systems are very adaptive and versatile to the changing environments (Fukuda and Ueyama, 1994; Kamimura et al., 2005; Yim, 1994). A comprehensive study into the development and applications of modular reconfigurable robotic system was done by Chen (1994). Development has been made to design a modular reconfigurable robot system for factory automation purpose (Chen and Burdick, 1995; Chen and Yang, 1996).

The *second category* is the metamorphic mechanism (Dai and Rees Jones, 1999; Dai and Zhang, 2009; Zhang et al., 2008), which can generate different topologies for reconfigurations. It is capable of changing its own shape by rearranging the connectivity of its parts. In the past decade, the metamorphic mechanism has been fast developed from conceptual study into physical implementation (Zhang and Dai, 2009a) and industry application (Dai and Rees Jones, 1999; Seffen et al., 2000).

The *third category* is based on the transformation among different kinematic paths using kinematic singularities (Kong and Huang, 2009; Wohlhart, 1996; 2010), such as kinematotropy mechanism (Wohlhart, 1996) and mechanism with bifurcations. The kinematotropy mechanism can change its global mobility with positional actuations at the transit positions. Galletti and Fanghella (2001) designed a series of kinematotropy

mechanisms using the displacement group method. With the group-algebraic approach, Lee and Hervé (2005) found that a closed-loop chain can be reconfigured when there are two or more subgroups involved in the mechanism. Conceptual designs of mechanisms with desired bifurcation paths have also been studied. Kong and Huang (2009) proposed a number of one degree of freedom single-loop mechanisms with two operation modes. Wohlhart (2010) also proposed a series of multifunctional 7*R* linkages by inserting an overconstrained 4*R*, 5*R* or 6*R* mobile chain into a closed-loop 7*R* linkage.

1.4 ORGANIZATION OF THE DISSERTATION

The remaining chapters of this dissertation are organized in the following way.

Chapter 2 reviews fundamentals of the overconstrained spatial linkages. It reviews the construction and geometry conditions of the major overconstrained linkages that will be addressed in this dissertation. It also reviews the reconfigurable mechanism that will be addressed in this dissertation.

Chapter 3 explores methods that can be used to build the double-Goldberg overconstrained linkages using two 5*R* linkages as the building blocks. It presents the detailed construction of a mixed double-Goldberg linkage family using a Goldberg 5*R* linkage and a subtractive Goldberg 5*R* linkage. The original cases, variational cases and subtractive cases of the double-Goldberg linkage family are achieved in a similar manner. It demonstrates the close relationship between the double-Goldberg linkage family and the Bennett-based linkage family, which provides a systematic organization of the Bennett-based overconstrained linkages. Works in this chapter provides a substantial source of design for reconfigurable mechanisms in the Bennett-based linkage family, which further motivates the design of the

multiple operation forms in the double-Goldberg linkages and reconfigurable Bennett network in chapter 5.

Chapter 4 derives the explicit closure equations of the original and revised general line-symmetric Bricard linkage through matrix method. The relationship between these two linkages is revealed in this chapter. It presents new linkage closures that were not mentioned in previous literatures. It also investigates the bifurcation behaviors of its special case with zero offsets. Works in this chapter offers the comprehensive understanding of the general line-symmetric Bricard linkage, which motivates the design of multiple operation forms in the general line-symmetric Bricard linkage in chapter 5.

Chapter 5 presents several conceptual designs of reconfigurable mechanisms based on overconstrained linkages. It firstly challenges the possibilities to introduce the operation form of a 4*R* linkage into a 6*R* linkage. Examples are demonstrated using the double-Goldberg 6*R* linkages in the Bennett-based linkage family and the general line-symmetric Bricard linkage in the Bricard linkage family to achieve this goal. The methods used in this chapter could be further applied to design reconfigurable mechanisms based on bifurcations. The second conceptual design is the reconfigurable Bennett network. A generic method of link-pair replacement is proposed to reconfigure the spatial configuration and mobility of the network. When different networks are applied, different types of overconstrained linkages are achieved. Results in this chapter demonstrate the potentials and methodologies of using overconstrained linkages to design reconfigurable mechanisms with kinematic singularities.

Chapter 6 summarizes the novel development presented in this dissertation. It also makes suggestions for possible future research based on this dissertation.

Chapter 2

Review of Overconstrained Linkages and Reconfigurable Mechanisms

2.1 OVERVIEW

Denavit and Hartenberg (1955) have established a minimum four-parameter system to solve the kinematics of spatial mechanisms. In this dissertation, the coordinate system in Fig. 2.1.1 is attached to each joint in such a way that z_i is along the axis of revolute joint i, and x_i is along the direction of link connected to joint i.

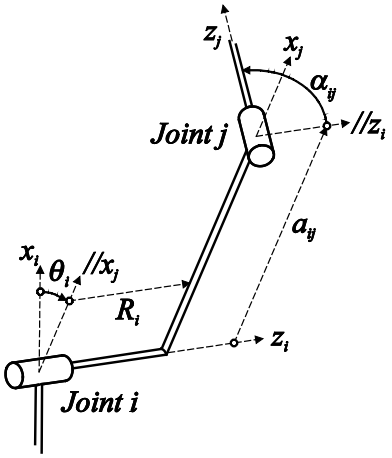

Fig. 2.1.1 The spatial setup of the parameters.

Thus, the relative position between two adjacent joints can be determined as follows:

- θ_i is the *revolute variable*, which is the positive angle of rotation from x_i to x_j about z_i, and usually defined in the range of $[-\pi, \pi)$;
- R_i is the *offset*, which is the normal distance from x_i to x_j along z_i, and usually defined in the range of $(-\infty, +\infty)$;

- α_{ij} is the *twist*, which is the positive angle of rotation from z_i to z_j about x_j, and usually defined in the range of $[-\pi, \pi)$;
- a_{ij} is the *length*, which is the normal distance from z_i to z_j along x_j, and usually defined in the range of $(-\infty, +\infty)$.

These four parameters are assembled into a 4×4 homogeneous transformation matrix $\mathbf{T}_{ij}$ for kinematic analysis, as shown in Eq. (2.1.1), where $\mathbf{Ro}_{3\times3}$ is the rotational matrix and $\mathbf{Tr}_{3\times1}$ is the translational vector.

$$\begin{aligned}\mathbf{T}_{ij} &= \begin{bmatrix} \mathbf{Ro}_{3\times3} & \mathbf{Tr}_{3\times1} \\ \mathbf{0}_{1\times3} & 1 \end{bmatrix} \\ &= \begin{bmatrix} \cos\theta_i & -\cos\alpha_{ij}\sin\theta_i & \sin\alpha_{ij}\sin\theta_i & a_{ij}\cos\theta_i \\ \sin\theta_i & \cos\alpha_{ij}\cos\theta_i & -\sin\alpha_{ij}\cos\theta_i & a_{ij}\sin\theta_i \\ 0 & \sin\alpha_{ij} & \cos\alpha_{ij} & R_i \\ 0 & 0 & 0 & 1 \end{bmatrix}\end{aligned} \quad . \tag{2.1.1}$$

The necessary condition for a closed loop of *n* links is that the successive product of the transformation matrices must be preserved as a unit matrix. The number of free revolute variables is equivalent to the degree of freedom (mobility) of the linkage.

$$\mathbf{T}_{12}\mathbf{T}_{23}\mathbf{T}_{34}\cdots\mathbf{T}_{n1} = \mathbf{I}\,. \tag{2.1.2}$$

2.2 OVERCONSTRAINED 4*R* LINKAGES

It is proved that at least four links are required to produce a linkage with only one degree of freedom (Phillips, 1984). The Bennett linkage is the only overconstrained 4*R* linkage having the axes of four revolute joints neither parallel nor concurrent (Bennett, 1903). This linkage was also found independently by Borel (Bennett, 1914). The geometry conditions and closure equations of the original Bennett linkage are

$$a_{12} = a_{34},\ \alpha_{12} = \alpha_{34},\ a_{23} = a_{41},\ \alpha_{23} = \alpha_{41},\ R_i = 0\ (i = 1, 2, 3 \text{ and } 4), \tag{2.2.1}$$

$$\frac{\sin\alpha_{12}}{a_{12}} = \frac{\sin\alpha_{23}}{a_{23}}; \tag{2.2.2}$$

and

$$\theta_1 + \theta_3 = 0,\ \theta_2 + \theta_4 = 0, \tag{2.2.3}$$

$$\tan\frac{\theta_1}{2}\tan\frac{\theta_2}{2} = \frac{\sin\dfrac{\alpha_{23}+\alpha_{12}}{2}}{\sin\dfrac{\alpha_{23}-\alpha_{12}}{2}}, \tag{2.2.4}$$

respectively. In other literatures, the relationship in Eq. (2.2.3) may be defined as follows.

$$\theta_1 + \theta_3 = 2\pi,\ \theta_2 + \theta_4 = 2\pi. \tag{2.2.5}$$

Here, constrained by the domain of definition of the revolute variables in section 2.1, we use the relationship in Eq. (2.2.3) to unify representations. The proportional relationship of sine of twist over link length is called the *Bennett ratio*, as shown in Eq. (2.2.2).

A lot of research has been done to study properties of the Bennett linkage. A complete set of four-bar linkages connected by cylinder, revolute and prismatic joints with only mobility one was given by Savage (1972), in which the Bennett linkage was proved to be the only overconstrained four-bar linkage connected by revolute joints. Through the use of tensor analysis, Ho (1978) provided the existence criteria of Bennett linkage in a different way. Using the screw algebra method, Baker (1978) analyzed the extreme motion in the Bennett linkage. Later, a comprehensive comparison analysis about the relationship between the Bennett, Goldberg and Myard linkages was given by Baker (1979). Yu (1981a) studied the associated tetrahedron and the hyperboloid axes of the Bennett linkage. Explorations on possible linkages that could be achieved from Bennett linkages have been conducted continuously (Baker and Min, 1986; Yu and Baker, 1981). Methods like axode analysis

(Baker, 2001) and screw theory (Perez and McCarthy, 2002) have been used to study the kinematics of the Bennett linkage. Extension has been made to create networks of Bennett linkages for deployable structures (Chen and Baker, 2005; Chen and You, 2005; 2008b).

Even though the geometry conditions of the Bennett linkage appear to be line-symmetric, the relationship in Eq. (2.2.3) indicates that the linkage moves in an asymmetric manner. The general line-symmetric geometry requires the geometry conditions and revolute variables on the opposite links and joints to be identical. In fact, there exists two solutions to the general line-symmetric overconstrained 4*R* linkage, which was already discussed in (Hervé and Dahan, 1983) and (Dalha, 1982). However, such conclusion did not draw the necessary attentions from kinematicians. In what follows, we are going to revisit this linkage by deriving the geometry conditions and closure equations of these two forms using the matrix method. Firstly, we only take the line-symmetric part of the geometry conditions that

$$\begin{gathered} a_{12} = a_{34},\ \alpha_{12} = \alpha_{34},\ a_{23} = a_{41},\ \alpha_{23} = \alpha_{41}, \\ R_i = 0\ (i = 1, 2, 3 \text{ and } 4), \end{gathered} \tag{2.2.6}$$

to re-examine the geometry constraints of the linkage. We substitute Eq. (2.2.6) into the transformation matrix of the Bennett linkage.

$$\mathbf{T}_{12}\mathbf{T}_{23}\mathbf{T}_{34}\mathbf{T}_{41} = \mathbf{I}. \tag{2.2.7}$$

With the homogeneous transformation matrix, we multiply $\mathbf{T}_{12}^{-1}\mathbf{T}_{23}^{-1}$ on both side of Eq. (2.2.7).

$$\mathbf{T}_{34}\mathbf{T}_{41} = \mathbf{T}_{12}^{-1}\mathbf{T}_{23}^{-1}. \tag{2.2.8}$$

The relationship for entries (1, 1), (3, 3) and (3, 4) in Eq. (2.2.8) are

$$\cos\theta_1\cos\theta_2 - \cos\alpha_{12}\sin\theta_1\sin\theta_2 = \cos\theta_3\cos\theta_4 - \cos\alpha_{12}\sin\theta_3\sin\theta_4, \tag{2.2.9}$$

$$\cos\alpha_{12}\cos\alpha_{23} - \sin\alpha_{12}\sin\alpha_{23}\cos\theta_2 = \cos\alpha_{12}\cos\alpha_{23} - \sin\alpha_{12}\sin\alpha_{23}\cos\theta_4, \tag{2.2.10}$$

$$a_{23}\sin\alpha_{12}\sin\theta_2 = -a_{12}\sin\alpha_{23}\sin\theta_4 . \tag{2.2.11}$$

For non-trivial solutions of a spatial linkage, we can derive from Eq. (2.2.10) that

$$\theta_2 = \theta_4 \text{ or } \theta_2 = -\theta_4 . \tag{2.2.12}$$

For the positive relationship that $\theta_2 = \theta_4$, the resultant Bennett linkage is found to be in line-symmetric setup. Substituting $\theta_2 = \theta_4$ into Eq. (2.2.11) gives

$$\frac{\sin\alpha_{12}}{a_{12}} = -\frac{\sin\alpha_{23}}{a_{23}} . \tag{2.2.13}$$

Substituting Eq. (2.2.13) into Eq. (2.2.9), we can derive the closure equation of the Bennett linkage in line-symmetric setup as

$$\theta_1 = \theta_3,\ \theta_2 = \theta_4,\ \tan\frac{\theta_1}{2}\tan\frac{\theta_2}{2} = \frac{\cos\dfrac{\alpha_{23}+\alpha_{12}}{2}}{\cos\dfrac{\alpha_{23}-\alpha_{12}}{2}} . \tag{2.2.14}$$

For the negative relationship that $\theta_2 = -\theta_4$, the resultant Bennett linkage is in asymmetric setup. Similarly, when substituting $\theta_2 = -\theta_4$ into Eq. (2.2.11), we will derive

$$\frac{\sin\alpha_{12}}{a_{12}} = \frac{\sin\alpha_{23}}{a_{23}} . \tag{2.2.15}$$

And the closure equations of the resultant linkage are the same as Eqs. (2.2.3) and (2.2.4). From the above derivations, we find that there are actually two setups of the Bennett linkage: one in line-symmetric setup, while the other in asymmetric setup. The one that appears in most literatures is the asymmetric setup of the Bennett linkage, which is the same as the original appearance of the linkage in (Bennett, 1903).

Since the opposite links in a Bennett linkage share the identical geometry conditions, there are actually two different links, link 12 and link 23, in the Bennett linkage defined in Eq. (2.2.6). According to Eqs. (2.2.13) and (2.2.15), the symmetric property of the Bennett

linkage is determined by the Bennett ratios of links 12 and 23. We prepare two sets of parameters a/α and b/β as follows to demonstrate the differences.

$$a = 1.0000,\ \alpha = 100.0000\pi/180,\ b = 0.6527,\ \beta = 40.0000\pi/180. \tag{2.2.16}$$

We assign the geometry condition of link 12 to be a/α. If we want to construct a Bennett linkage in line-symmetric setup, we can derive from Eq. (2.2.13) the following two sets of solutions for link 23.

$$a_{23} = b, \alpha_{23} = -\beta \text{ or } a_{23} = b, \alpha_{23} = \beta \pm \pi. \tag{2.2.17}$$

Similarly, for a Bennett linkage in asymmetric setup, we can derive from Eq. (2.2.15) the following two sets of solutions for link 23.

$$a_{23} = b, \alpha_{23} = \beta \text{ or } a_{23} = b, \alpha_{23} = -\beta \pm \pi. \tag{2.2.18}$$

Note that here, we constrain the solutions in domain that $a_{23} \in [0,+\infty)$ and $\alpha_{23} \in [-\pi, \pi)$. It is always mathematically possible to use length parameters, including link length and offset, with negative values for analytical derivations. However, for the physical setup of the linkage, it is recommended in this dissertation to use the solutions of length parameters in the domain of $[0,+\infty)$ to avoid duplicates, which comply with their physical meanings. The drawbacks of using negative length parameters will be addressed in chapter 4 when distinguishing the difference between the original and revised general line-symmetric Bricard linkages. The differences among the above four sets of solutions are illustrated in Fig. 2.2.1.

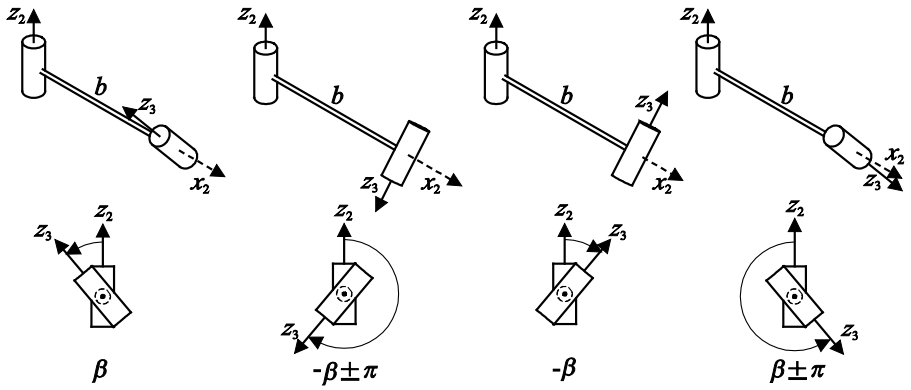

Fig. 2.2.1 The four configurations of link 23.

As a result, we can construct four Bennett linkages based on these four sets of solutions. In Fig. 2.2.2, there are two Bennett linkages in asymmetric setups: AB-1 and AB-2, which comprise of link-pair $a/\alpha \sim b/\beta$ and link-pair $a/\alpha \sim b/-\beta \pm \pi$, respectively. There are another two Bennett linkages in line-symmetric setups: LB-1 and LB-2, which comprise of link-pair $a/\alpha \sim b/-\beta$ and link-pair $a/\alpha \sim b/\beta \pm \pi$, respectively.

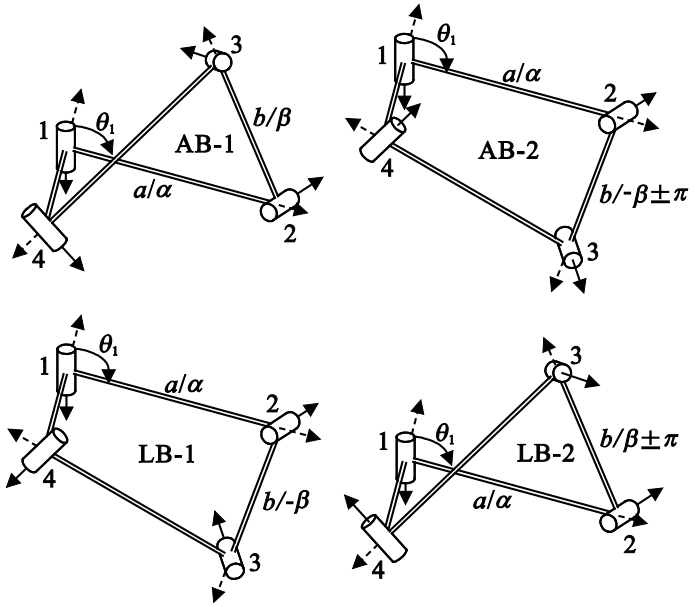

Fig. 2.2.2 The four different Bennett linkages in asymmetric and line-symmetric setups ($\theta_1 = 110.0000\pi/180$).

From Fig. 2.2.2, it is found that even though AB-1 and LB-2 have different symmetry properties, they share the same configurations in space if we ignore the joint axis directions. This is the same for AB-2 and LB-1. Therefore, we can summarize the geometry conditions of the Bennett linkage as follows,

$$\begin{aligned} &a_{12} = a_{34},\ \alpha_{12} = \alpha_{34},\ a_{23} = a_{41},\ \alpha_{23} = \alpha_{41}, \\ &R_i = 0\ (i = 1, 2, 3 \text{ and } 4),\ \frac{\sin\alpha_{12}}{a_{12}} = \pm\frac{\sin\alpha_{23}}{a_{23}}; \end{aligned} \tag{2.2.19}$$

in which the positively equaled Bennett ratios will produce a Bennett linkage in asymmetric setup while the negatively equaled Bennett ratios will produce a Bennett linkage in line-

symmetric setup. However, as demonstrated in Fig. 2.2.2, for the Bennett linkages in either asymmetric or line-symmetric setups, there are always two different configurations of the linkage with different joint axis directions. For two Bennett linkages with the same configurations in space, one of them is asymmetric while the other is line-symmetric and they differ to each other by π on one of the twists.

In the following context, the Bennett-based linkage family is based on the combination of Bennett linkage as the building block. Consider that these linkages only make use of the Bennett linkage as a construct unit, thus the above changes in the geometry conditions will not affect the configuration of the resultant linkages. But on the geometry conditions, the negatively equaled Bennett ratios could be added to generalize the representations. Due to the limited influence of this change, we will still use the classical geometry conditions of these linkages unless further explanation is required. However, when different symmetry properties of the Bennett linkage are taken into consideration, the detailed geometry conditions of the asymmetric and line-symmetric Bennett linkages shall be taken into consideration, which will be used in the multiple operation forms of the general line-symmetric Bricard linkage in chapter 5.

2.3 OVERCONSTRAINED 5*R* LINKAGES

2.3.1 Goldberg's 5*R* Linkages

Goldberg's remarkable work was based on the concept to build overconstrained 5*R* linkage by combining two Bennett linkages, or subtracting them from another primary loop (Goldberg, 1943). As shown in Fig. 2.3.1(a), the Goldberg 5*R* linkage is obtained through the summation of two Bennett linkages superposed on a common link b/β with two adjacent

links a/α and c/γ collinearly rigidified. After removing the common link and joints, the Goldberg 5*R* linkage will be formed. In Fig. 2.3.1(b), the syncopated Goldberg 5*R* linkage is formed by the subtraction of a Goldberg 5*R* linkage from a primary Bennett linkage. After removing the links and joints in the Goldberg 5*R* linkage that are overlapped with the primary Bennett linkage, the rest part will form the syncopated Goldberg 5*R* linkage. Here, the line and dot model is used to simplify the construct process, where the solid lines represent the links, the dots are the joints and the dash-lines are the links to be removed.

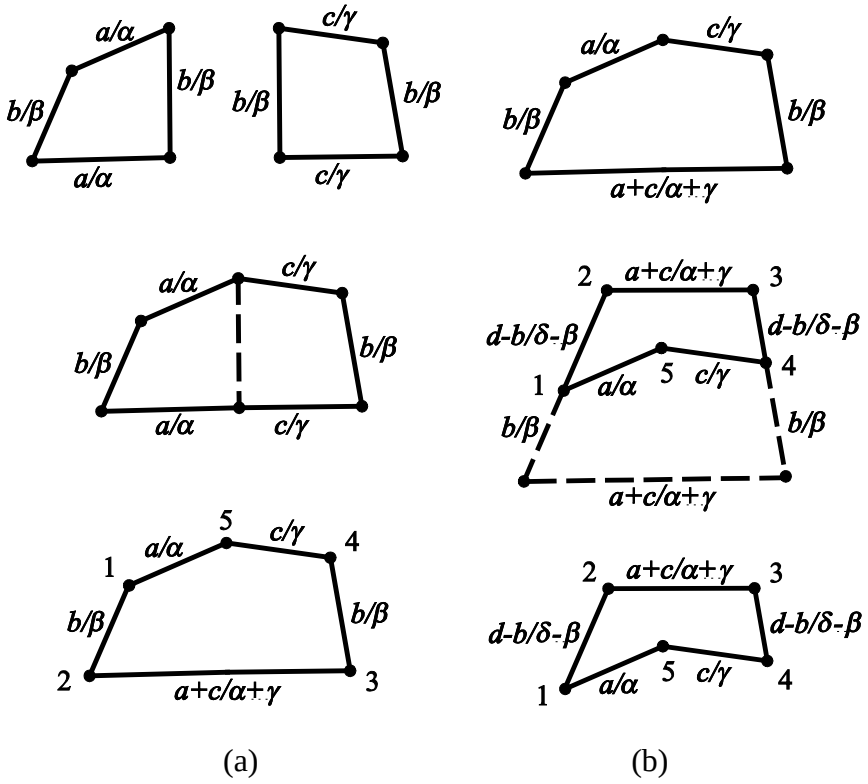

(a) (b)

Fig. 2.3.1 The construction of (a) Goldberg 5*R* linkage and (b) syncopated Goldberg 5*R* linkage.

The geometry conditions of the Goldberg 5*R* linkage and the syncopated Goldberg 5*R* linkage are

$$\begin{aligned} &a_{12} = a_{34} = b,\ a_{23} = a + c,\ a_{45} = c,\ a_{51} = a, \\ &\alpha_{12} = \alpha_{34} = \beta,\ \alpha_{23} = \alpha + \gamma,\ \alpha_{45} = \gamma,\ \alpha_{51} = \alpha, \end{aligned} \tag{2.3.1}$$

$$\frac{\sin\alpha}{a}=\frac{\sin\beta}{b}=\frac{\sin\gamma}{c},\ R_i=0\ (i=1,2,...,5);$$

and

$$\begin{aligned} &a_{12}=a_{34}=d-b,\ a_{23}=a+c,\ a_{45}=c,\ a_{51}=a,\\ &\alpha_{12}=\alpha_{34}=\delta-\beta,\ \alpha_{23}=\alpha+\gamma,\ \alpha_{45}=\gamma,\ \alpha_{51}=\alpha, \end{aligned} \tag{2.3.2a}$$

$$\frac{\sin\alpha}{a}=\frac{\sin\beta}{b}=\frac{\sin\gamma}{c}=\frac{\sin(\delta-\beta)}{d-b}, \tag{2.3.2b}$$

$$\frac{\sin\frac{\alpha+\beta}{2}}{\sin\frac{\alpha-\beta}{2}}\frac{\sin\frac{\gamma+\beta}{2}}{\sin\frac{\gamma-\beta}{2}}=\frac{\sin\frac{\delta+\alpha+\gamma}{2}}{\sin\frac{\delta-\alpha-\gamma}{2}},\ \frac{\sin\delta}{d}=\frac{\sin(\alpha+\gamma)}{a+c}, \tag{2.3.2c}$$

$$R_i=0\ (i=1,2,...,5), \tag{2.3.2d}$$

respectively. Goldberg (1943) tried to investigate relationship between these two linkages through numerical examples. He found the relationship in Eq. (2.3.2b) in the syncopated linkage shown in Fig. 2.3.1(b), from which he concluded that the syncopated Goldberg 5*R* linkage might be resolved into the combination of two Bennett linkages like the Goldberg 5*R* linkage. Later, this conclusion was proved by Baker (1979) that Eq. (2.3.2a) can be derived analytically from Eq. (2.3.2b) for any syncopated Goldberg 5*R* linkages. Therefore, the syncopated Goldberg 5*R* linkage is actually a special case of the Goldberg 5*R* linkage.

2.3.2 Generalized Goldberg 5*R* Linkage

Even the Goldberg 5*R* linkage is still a very special linkage with two links collinearly rigidified, which means that the "*kink angle*" between these two links is locked to zero. In Fig. 2.3.2, when the kink angle ε is locked at different values other than zero, a more generalized linkage can be obtained. Offsets will be introduced to corresponding links. This innovative method was firstly raised by Goldberg (1943) in a qualitative way. Baker (1983) also studied

the generalized case using the screw theory. An in-depth research into the kinematics of the generalized Goldberg 5*R* linkage was made by Wohlhart (1991a).

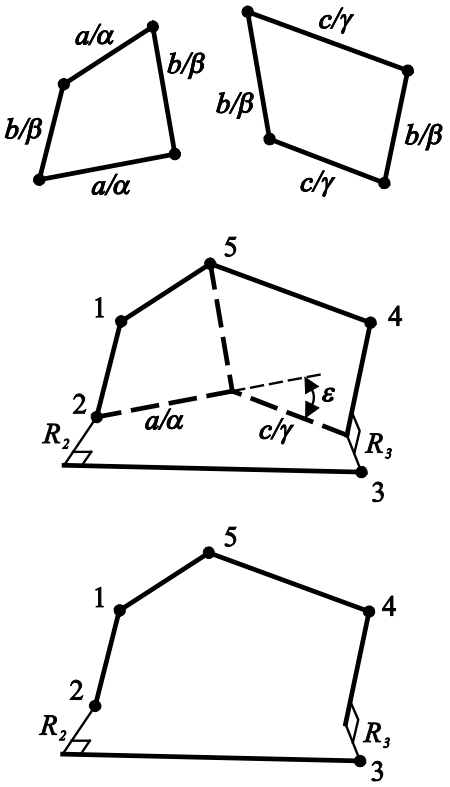

Fig. 2.3.2 The construction of the generalized Goldberg 5*R* linkage.

As shown in Fig. 2.3.2, when $\varepsilon \in [-\pi, \pi)$, the two links a/α and c/γ that are locked by the kink angle are then replaced by a new link 23. In the meanwhile, offsets R_2 and R_3 will be introduced to links 23 and 34 in the thin solid lines, respectively. This generalized linkage could also be explained using the link-pair replacement method developed in chapter 5. The geometry conditions of the generalized Goldberg 5*R* linkage are

$$\begin{aligned} &a_{12} = a_{34},\ \alpha_{12} = \alpha_{34},\ \frac{\sin\alpha_{12}}{a_{12}} = \frac{\sin\alpha_{45}}{a_{45}} = \frac{\sin\alpha_{51}}{a_{51}}, \\ &\cos\alpha_{23} = \cos\alpha_{45}\cos\alpha_{51} - \cos\varepsilon\sin\alpha_{45}\sin\alpha_{51}, \\ &a_{23} = \frac{a_{12}}{\sin\alpha_{12}}(\cos\alpha_{45} + \cos\alpha_{51})\tan\frac{\alpha_{23}}{2}, \end{aligned} \tag{2.3.3}$$

$$R_1 = R_4 = R_5 = 0,\ R_2 = R_3 = \frac{a_{12}}{\sin\alpha_{12}} \sin\varepsilon \frac{\sin\alpha_{45}\sin\alpha_{51}}{1+\cos\alpha_{23}}.$$

2.3.3 Myard's 5*R* Linkages

Prior to Goldberg, Myard (1931) also published two types of overconstrained 5*R* linkages, one in a plane-symmetric form and the other in an asymmetric form. It is the plane-symmetric Myard linkage that attracts the most attentions, as shown in Fig. 2.3.3. Its geometry conditions are listed in Eq. (2.3.4). The configuration of the asymmetric Myard 5*R* linkage is equivalent to the linkage shown in Fig. 2.3.1(a) when $a = c$ and $\alpha = \gamma$.

$$\begin{gathered} a_{12} = a_{51} = a,\ a_{23} = a_{45} = b,\ a_{34} = 0, \\ \alpha_{12} = \pi - \alpha_{51} = \alpha,\ \alpha_{23} = \alpha_{41} = \frac{\pi}{2},\ \alpha_{34} = \pi - 2\alpha, \\ \frac{\sin\alpha}{a} = \frac{1}{b},\ R_1 = R_2 = R_5 = 0,\ R_3 = R_4. \end{gathered} \tag{2.3.4}$$

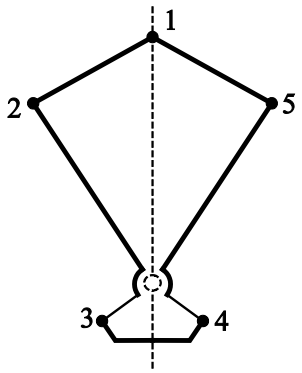

Fig. 2.3.3 The plane-symmetric Myard linkage.

However, Myard's work was mainly focused on the geometric properties of the linkage. It is found that the plane-symmetric Myard's 5*R* linkage could be interpreted as a special case of generalized Goldberg 5*R* linkage, and the asymmetric Myard's 5*R* linkage could be identified as a special case of the Goldberg 5*R* linkage (Baker, 1979). Thus, both of the two Myard 5*R* linkages in fact belong to the Goldberg's 5*R* linkages.

2.3.4 Extended Myard 5*R* Linkage

Recently, an extended Myard 5*R* linkage was proposed by Chen and You (2008a), in which the twists of two Bennett linkages that build this 5*R* linkage are unnecessary to be $\frac{\pi}{2}$. The geometry conditions of this linkage are listed as follows.

$$\begin{gathered} a_{12} = a_{51} = a\,,\ a_{23} = a_{45} = b\,,\ a_{34} = 0\,, \\ \alpha_{12} = \pi - \alpha_{51} = \alpha\,,\ \alpha_{23} = \alpha_{45} = \beta\,,\ \alpha_{34} = \pi - 2\alpha\,, \\ \frac{\sin\alpha}{a} = \frac{\sin\beta}{b},\ R_i = 0\ (i = 1, 2, ..., 5). \end{gathered} \tag{2.3.5}$$

Similar to the plane-symmetric Myard 5*R* linkage, a pair of equal offsets could be added to the extended Myard 5*R* linkage. Therefore, the geometry conditions of the offsets in Eq. (2.3.5) that $R_i = 0\ (i = 1, 2, ..., 5)$ could be improved as $R_3 = R_4$ and $R_1 = R_2 = R_5 = 0$. The same as Myard's plane-symmetric 5*R* linkage, the extended Myard 5*R* linkage still belongs to the Goldberg's 5*R* linkages.

2.3.5 Summary

A more general discussion on the overconstrained five-bar linkage with revolute, prismatic, cylindrical and helical pairs was conducted to find all cases of overconstrained five-bar mechanisms (Pamidi et al., 1973). However, when the joints are limited to revolute joint only, the linkages shown above are the only overconstrained 5*R* linkages published in literatures until now. From the above introduction, there is a clear view that all of the overconstrained 5*R* linkages belong to the family of Goldberg's 5*R* linkages. Similar to the overconstrained 4*R* linkage, there is still only one linkage family in the category of overconstrained 5*R* linkage with revolute joint only, which are the Goldberg's 5*R* linkages.

2.4 OVERCONSTRAINED 6*R* LINKAGES

There are several overconstrained 6*R* linkages that have been widely applied to industries for a long time. For example, the double-Hooke's joint linkage is widely used in the automobile industry for power transmission, and the Schatz linkage is applied in the design of food mixture machine (Baker et al., 1982). Another example is the Sarrus linkage (Sarrus, 1853), which is also well applied to the design of deployable structures (Gantes, 1989). A detailed study into the kinematics of various overconstrained 6*R* linkages was done by Dietmaier (1995a). A refined list of 28 overconstrained 6*R* linkages was recently made by Baker (2002). Most of these linkages belong to two major linkage families: the family of Bennett-based linkages and the family of Bricard linkages. Major linkages in these two families will be reviewed in what follows.

2.4.1 Goldberg's 6*R* Linkages

Similar to the Goldberg's 5*R* linkages, the Goldberg's 6*R* linkages can be summarized as the summation of one Goldberg 5*R* linkage (or its syncopation) with another Bennett linkage, as well as the subtraction of it from a primary Bennett linkage. Four types of overconstrained 6*R* linkages were developed by Goldberg (1943), which are the serial Goldberg 6*R* linkage in Fig. 2.4.1(a), the syncopated serial Goldberg 6*R* linkage in Fig. 2.4.1(b), the *L*-shape Goldberg 6*R* linkage in Fig. 2.4.2(a) and the syncopated *L*-shape Goldberg 6*R* linkage in Fig. 2.4.2(b).

As shown in Fig. 2.4.1(a), the serial Goldberg 6*R* linkage is obtained by three Bennett linkages connected in series on a common link b/β. In Fig. 2.4.1(b), its syncopation is the subtraction of a serial Goldberg 6*R* linkage from a primary Bennett linkage with two pairs of links, $a+c+d/\alpha+\gamma+\delta$ and e/ε, in a similar manner as the syncopated Goldberg 5*R* linkage.

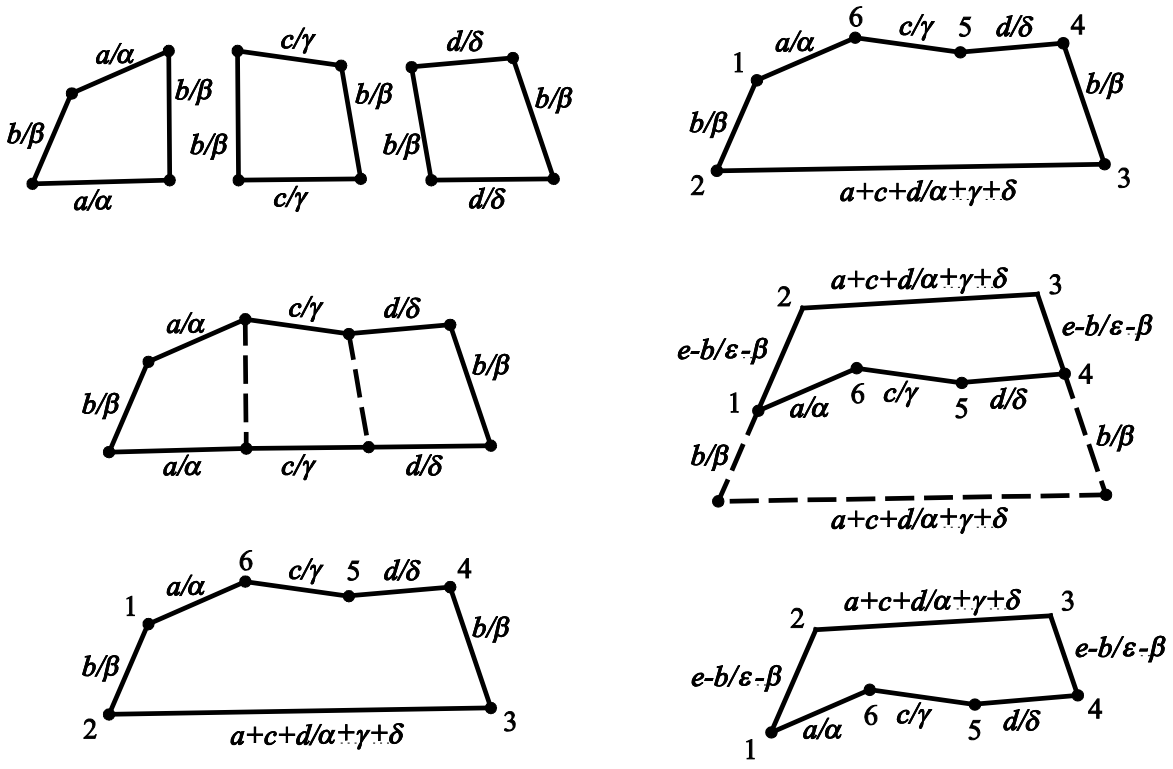

Fig. 2.4.1 The construction of (a) the serial Goldberg 6*R* linkage and (b) the syncopated serial Goldberg 6*R* linkage.

The geometry conditions of the serial Goldberg 6*R* linkage and the syncopated serial Goldberg 6*R* linkage are

$$\begin{gathered} a_{12} = a_{34} = b\,,\ a_{23} = a + c + d\,,\ a_{45} = d\,,\ a_{56} = c\,,\ a_{61} = a\,, \\ \alpha_{12} = \alpha_{34} = \beta\,,\ \alpha_{23} = \alpha + \gamma + \delta\,,\ \alpha_{45} = \delta\,,\ \alpha_{56} = \gamma\,,\ \alpha_{61} = \alpha\,, \\ \frac{\sin\alpha}{a} = \frac{\sin\beta}{b} = \frac{\sin\gamma}{c} = \frac{\sin\delta}{d}\,,\ R_i = 0\ (i = 1, 2, ..., 6)\,; \end{gathered} \tag{2.4.1}$$

and

$$\begin{gathered} a_{12} = a_{34} = e - b\,,\ a_{23} = a + c + d\,,\ a_{45} = d\,,\ a_{56} = c\,,\ a_{61} = a\,, \\ \alpha_{12} = \alpha_{34} = \varepsilon - \beta\,,\ \alpha_{23} = \alpha + \gamma + \delta\,,\ \alpha_{45} = \delta\,,\ \alpha_{56} = \gamma\,,\ \alpha_{61} = \alpha\,, \\ \frac{\sin\alpha}{a} = \frac{\sin\beta}{b} = \frac{\sin\gamma}{c} = \frac{\sin\delta}{d}\,,\ \frac{\sin\varepsilon}{e} = \frac{\sin(\alpha+\gamma+\delta)}{a+c+d}\,, \end{gathered} \tag{2.4.2}$$

$$\frac{\sin\frac{\alpha+\beta}{2}}{\sin\frac{\alpha-\beta}{2}}\frac{\sin\frac{\gamma+\beta}{2}}{\sin\frac{\gamma-\beta}{2}}\frac{\sin\frac{\delta+\beta}{2}}{\sin\frac{\delta-\beta}{2}}=\frac{\sin\frac{\varepsilon+\alpha+\gamma+\delta}{2}}{\sin\frac{\varepsilon-\alpha-\gamma-\delta}{2}},\ R_i=0\ (i=1,2,...,6),$$

respectively.

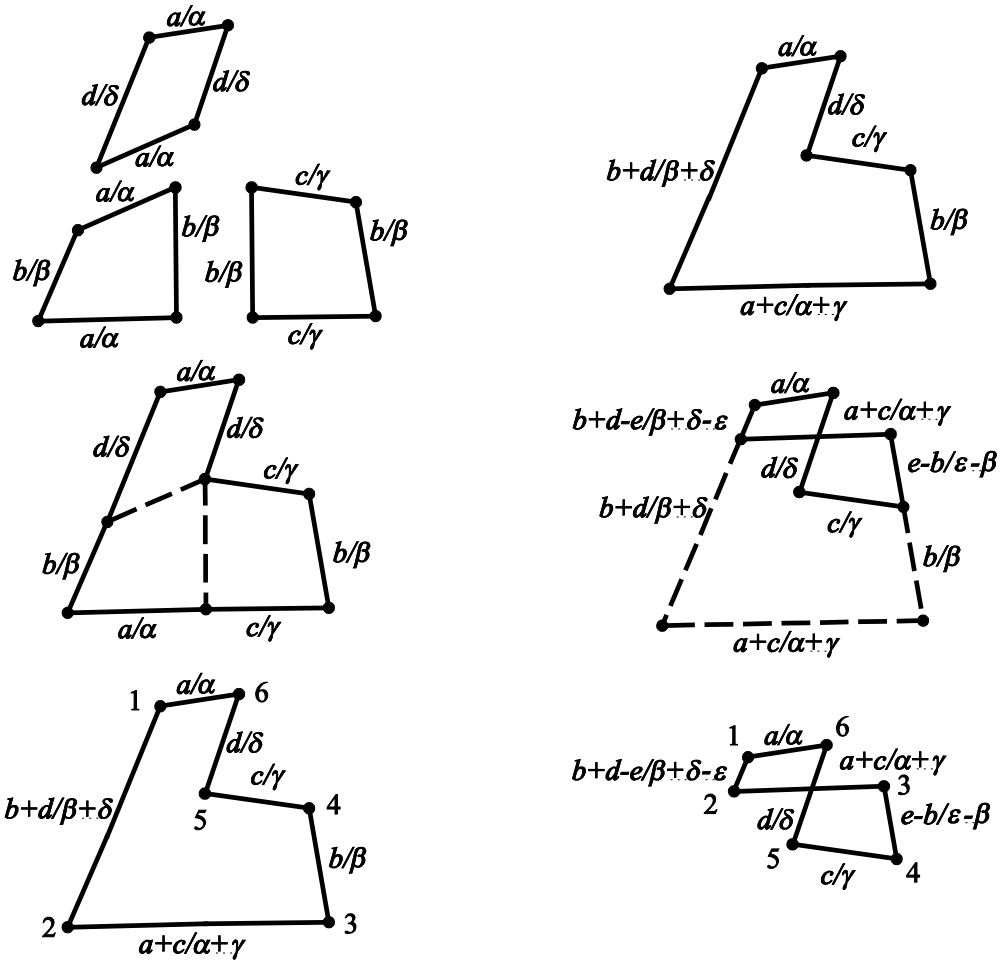

(a) (b)

Fig. 2.4.2 The construction of (a) the *L*-shape Goldberg 6*R* linkage and (b) the syncopated *L*-shape Goldberg 6*R* linkage.

In Fig. 2.4.2(a), the *L*-shape Goldberg 6*R* linkage is an extension of the Goldberg 5*R* linkage. However, the new Bennett linkage shares another common link a/α with the 5*R* linkage and is combined in a crossed direction, which forms an *L*-shape configuration. The syncopated *L*-shape Goldberg 6*R* linkage is shown in Fig. 2.4.2(b), which is obtained from the subtraction of an *L*-shape Goldberg 6*R* linkage from a primary Bennett linkage with link

$b+d-e/\beta+\delta-\varepsilon$ and $e-b/\varepsilon-\beta$. The geometry conditions of the *L*-shape Goldberg 6*R* linkage and the syncopated *L*-shape Goldberg 6*R* linkage are

$$\begin{gathered} a_{12}=b+d,\ a_{23}=a+c,\ a_{34}=b,\ a_{45}=c,\ a_{56}=d,\ a_{61}=a, \\ \alpha_{12}=\beta+\delta,\ \alpha_{23}=\alpha+\gamma,\ \alpha_{34}=\beta,\ \alpha_{45}=\gamma,\ \alpha_{56}=\delta,\ \alpha_{61}=\alpha, \\ \frac{\sin\alpha}{a}=\frac{\sin\beta}{b}=\frac{\sin\gamma}{c}=\frac{\sin\delta}{d},\ R_i=0\ (i=1,2,...,6); \end{gathered} \tag{2.4.3}$$

and

$$\begin{gathered} a_{12}=b+d-e,\ a_{23}=a+c,\ a_{34}=e-b,\ a_{45}=c,\ a_{56}=d,\ a_{61}=a, \\ \alpha_{12}=\beta+\delta-\varepsilon,\ \alpha_{23}=\alpha+\gamma,\ \alpha_{34}=\varepsilon-\beta,\ \alpha_{45}=\gamma,\ \alpha_{56}=\delta,\ \alpha_{61}=\alpha, \\ \frac{\sin\alpha}{a}=\frac{\sin\beta}{b}=\frac{\sin\gamma}{c}=\frac{\sin\delta}{d},\ \frac{\sin\varepsilon}{e}=\frac{\sin(\alpha+\gamma)}{a+c}, \\ \frac{\sin\frac{\alpha+\beta}{2}}{\sin\frac{\alpha-\beta}{2}}\cdot\frac{\sin\frac{\gamma+\beta}{2}}{\sin\frac{\gamma-\beta}{2}}=\frac{\sin\frac{\varepsilon+\alpha+\gamma}{2}}{\sin\frac{\varepsilon-\alpha-\gamma}{2}},\ R_i=0\ (i=1,2,...,6), \end{gathered} \tag{2.4.4}$$

respectively.

The same as the Goldberg's 5*R* linkages, during the construction of each Goldberg's 6*R* linkages, the kink angles are all locked to zero. A generalized case of each Goldberg's 6*R* linkages can be obtained in a similar way as the generalized Goldberg 5*R* linkage does. It should be pointed out that unlike the Goldberg 5*R* linkage and its syncopation, the Goldberg 6*R* linkage and its syncopation are different linkages.

2.4.2 Variants of Goldberg's 6*R* Linkages

By further utilizing Goldberg's technique in the choice of links to be locked in Goldberg's 6*R* linkages, two variants of Goldberg's 6*R* linkages were published by Baker (1993a).

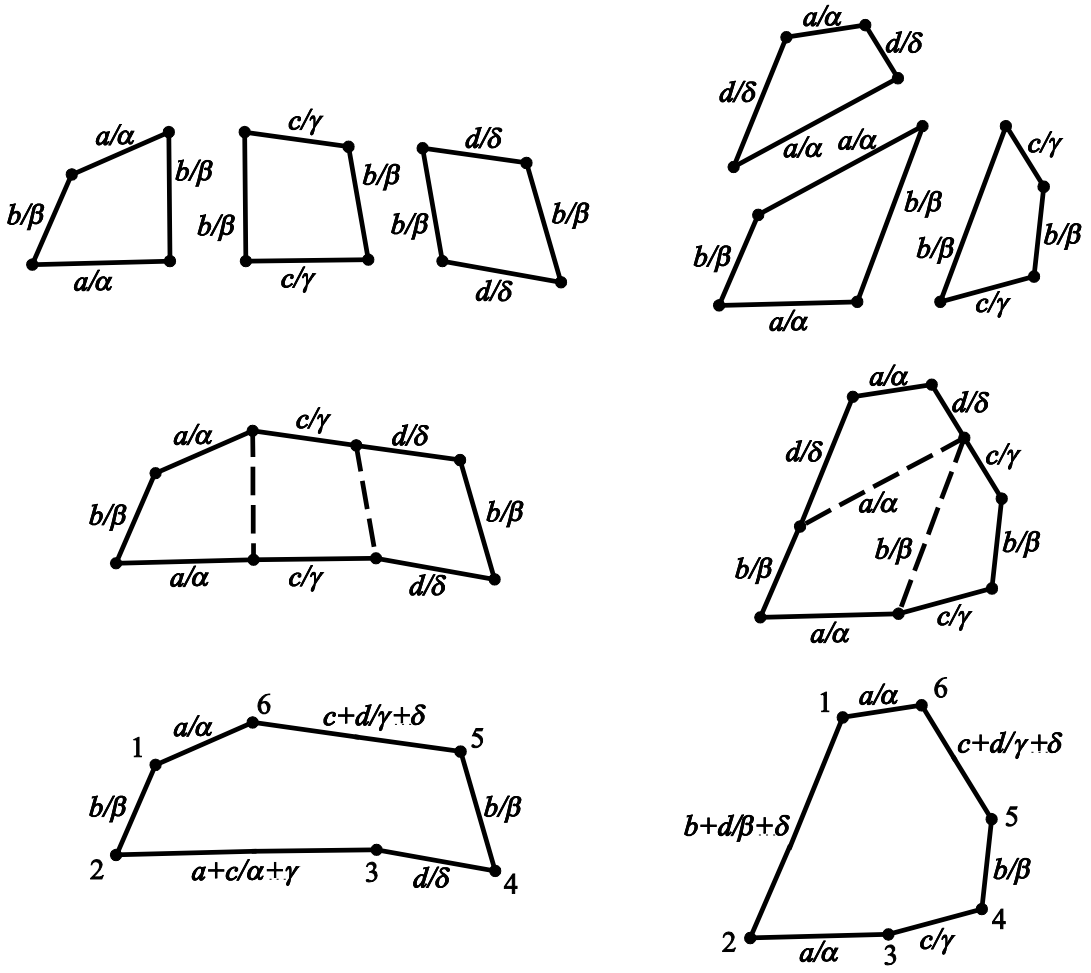

(a) (b)

Fig. 2.4.3 The construction of (a) the variant of serial Goldberg 6*R* linkage and (b) the variant of *L*-shape Goldberg 6*R* linkage.

The first variant is based on the serial Goldberg 6*R* linkage. As shown in Fig. 2.4.3(a), three Bennett linkages with a link b/β in common are placed in serial for combination. Different from the serial Goldberg 6*R* linkage, one kink angle of link-pair $a/\alpha \sim c/\gamma$ at the bottom left and another kink angle of link-pair $c/\gamma \sim d/\delta$ at the top right are locked to zeros. After removing the superposed links and joints, the variant of serial Goldberg 6*R* linkage will be formed. The second variant is based on the *L*-shape Goldberg 6*R* linkage. As shown in Fig. 2.4.3(b), three Bennett linkages A, B and C are carefully chosen so that the two linkages on the left share a common link a/α, and the two linkages at the bottom share a common link

b/β. After superposing the three linkages on the common links, one kink angle of link-pair $b/\beta \sim d/\delta$ on the left and another kink angle of link-pair $c/\gamma \sim d/\delta$ on the top right can be locked to zeros. Then, removing the superposed links and joints, the variant of *L*-shape Goldberg 6*R* linkage will be formed. The geometry conditions of the first and second variant of Goldberg's 6*R* linkages are

$$\begin{gathered} a_{12} = a_{45} = b,\ a_{23} = a + c,\ a_{34} = d,\ a_{56} = c + d,\ a_{61} = a, \\ \alpha_{12} = \alpha_{45} = \beta,\ \alpha_{23} = \alpha + \gamma,\ \alpha_{34} = \delta,\ \alpha_{56} = \gamma + \delta,\ \alpha_{61} = \alpha, \\ \frac{\sin\alpha}{a} = \frac{\sin\beta}{b} = \frac{\sin\gamma}{c} = \frac{\sin\delta}{d},\ R_i = 0\ (i = 1, 2, ..., 6); \end{gathered} \tag{2.4.5}$$

and

$$\begin{gathered} a_{12} = b + d,\ a_{23} = a,\ a_{34} = c,\ a_{45} = b,\ a_{56} = c + d,\ a_{61} = a, \\ \alpha_{12} = \beta + \delta,\ \alpha_{23} = \alpha,\ \alpha_{34} = \gamma,\ \alpha_{45} = \beta,\ \alpha_{56} = \gamma + \delta,\ \alpha_{61} = \alpha, \\ \frac{\sin\alpha}{a} = \frac{\sin\beta}{b} = \frac{\sin\gamma}{c} = \frac{\sin\delta}{d},\ R_i = 0\ (i = 1, 2, ..., 6). \end{gathered} \tag{2.4.6}$$

Both variants of the Goldberg's 6*R* linkages can be generalized in a similar way as the generalized Goldberg 5*R* linkage.

2.4.3 Wohlhart's Double-Goldberg 6*R* Linkage

Wohlhart's method could be viewed as an extension of Goldberg's technique (Wohlhart, 1991a). In Fig. 2.4.4, two Goldberg 5*R* linkages are carefully chosen so that they share the identical link-pair $a/\alpha \sim c/\gamma$. The Wohlhart's double-Goldberg 6*R* linkage is obtained by firstly merging these two Goldberg 5*R* linkages on the common link-pair $a/\alpha \sim c/\gamma$, and then removing it out. A generalized Wohlhart's double-Goldberg 6*R* linkage can be constructed when the two kink angles are not constrained to be zero. When the kink angle is zero, the geometry conditions of the Wohlhart's double-Goldberg 6*R* linkage are

$$a_{12} = a_{34} = b,\ a_{23} = a_{56} = a + c,\ a_{34} = a_{61} = d,$$
$$\alpha_{12} = \alpha_{34} = \beta,\ \alpha_{23} = \alpha_{56} = \alpha + \gamma,\ \alpha_{34} = \alpha_{61} = \delta, \tag{2.4.7}$$
$$\frac{\sin\alpha}{a} = \frac{\sin\beta}{b} = \frac{\sin\gamma}{c} = \frac{\sin\delta}{d},\ R_i = 0\ (i = 1, 2, ..., 6).$$

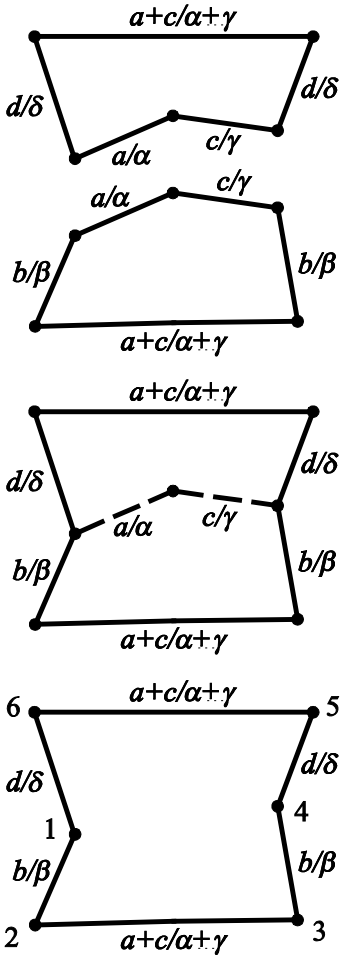

Fig. 2.4.4 The construction of the Wohlhart's double-Goldberg 6*R* linkage.

2.4.4 Back-to-back Double-Goldberg 6*R* Linkage

In the back-to-back double-Goldberg 6*R* linkage, the other three links 12, 23 and 34 are chosen for connection (Chen and You, 2007). When both Goldberg 5*R* linkages are identical in θ_2 and θ_3, they share the same kinematic paths on these two joints. A 6*R* linkage can be obtained by superposing on link-pair 12-23-34 and then removing the common links and joints, as shown in Fig. 2.4.5. The geometry conditions are listed as follows.

$$a_{12} = a_{34} = a\,,\ a_{23} = a_{56} = d - b\,,\ a_{45} = a_{61} = c\,,$$

$$\alpha_{12} = \alpha_{34} = \alpha\,,\ \alpha_{23} = \alpha_{56} = \delta - \beta\,,\ \alpha_{45} = \alpha_{61} = \gamma\,,$$

$$\frac{\sin\alpha}{a} = \frac{\sin\beta}{b} = \frac{\sin\gamma}{c} = \frac{\sin\delta}{d},\ \tan\frac{\alpha}{2}\cdot\tan\frac{\gamma}{2} = \tan\frac{\beta}{2}\cdot\tan\frac{\delta}{2}, \tag{2.4.8}$$

$$R_i = 0\ (i = 1, 2, ..., 6)\,.$$

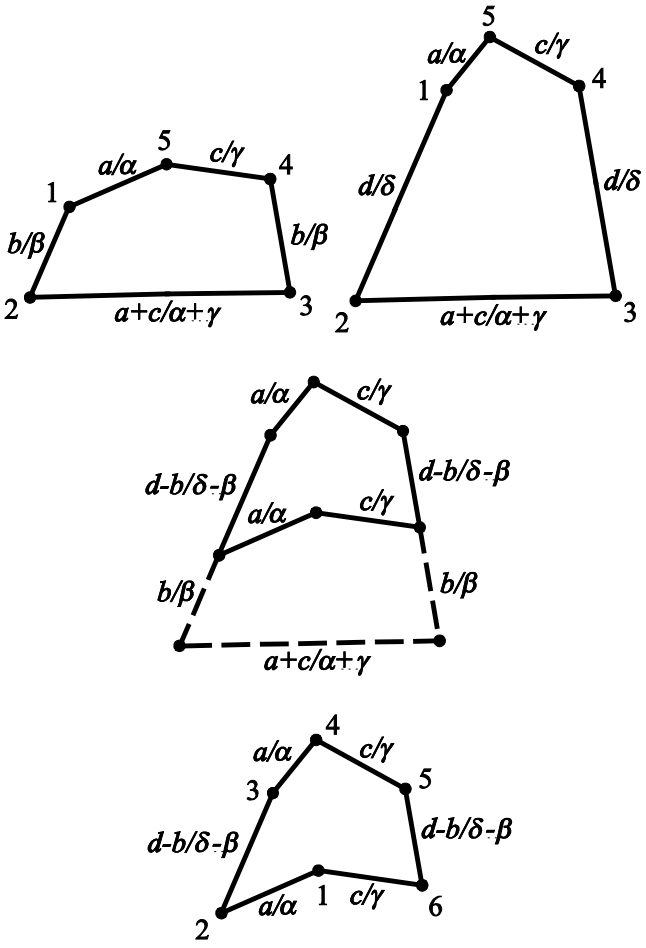

Fig. 2.4.5 The construction of the back-to-back double-Goldberg 6*R* linkage.

Results shown in section 5.2 demonstrate that this linkage is actually a special case of the Wohlhart's double-Goldberg 6*R* linkage with a special geometry constraint. A different case of the back-to-back double-Goldberg 6*R* linkage can be obtained by isomerizing link-pair 61-12 into link-pair 61'-1'2, as shown in Fig. 2.4.6.

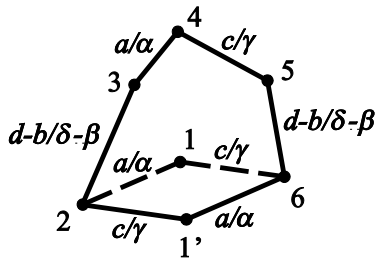

Fig. 2.4.6 The isomerization between two cases of the back-to-back double Goldberg 6*R* linkage.

Different from Wohlhart's result, a different geometry constraint on the offsets could be introduced in the back-to-back double-Goldberg 6*R* linkage, which is similar to the linkage found by Mavroidis and Roth (1995). The patterns of offsets are the same as in Mavroidis and Roth's 6*R* linkage, which are

$$\begin{aligned} &R_1 = R_4 = 0,\ R_2 = R_5,\ R_3 = R_6 \text{ for the original case,} \\ \text{or } &R_1 = R_4 = 0,\ R_2 = R_6,\ R_3 = R_5 \text{ for the isomerized case.} \end{aligned} \tag{2.4.9}$$

2.4.5 Waldron's Hybrid 6*R* Linkage

This linkage was proposed by Waldron (1968) which combines a pair of 4-bar linkages and only the case of two 4*R* linkages is useful for us. This linkage could be further degenerated into the Goldberg's 5*R* linkages (Baker, 1993a). In order to build this hybrid 6*R* linkage, two Bennett linkages are randomly chosen and collinearly placed in such a way that one joint from each Bennett linkages shares the same revolute axis in space, as shown in Fig. 2.4.7.

After defining the relative distance e between the two joints along the common axis and locking the two kink angles, ε_1 between the adjacent links b/δ and d/δ, and ε_2 between the adjacent links a/α and c/γ, to fixed values, a new link could be introduced to replace

each link-pair with offsets added to the corresponding links. However, the geometry conditions of this linkage were not given by Waldron, but later provided by Baker (1993a).

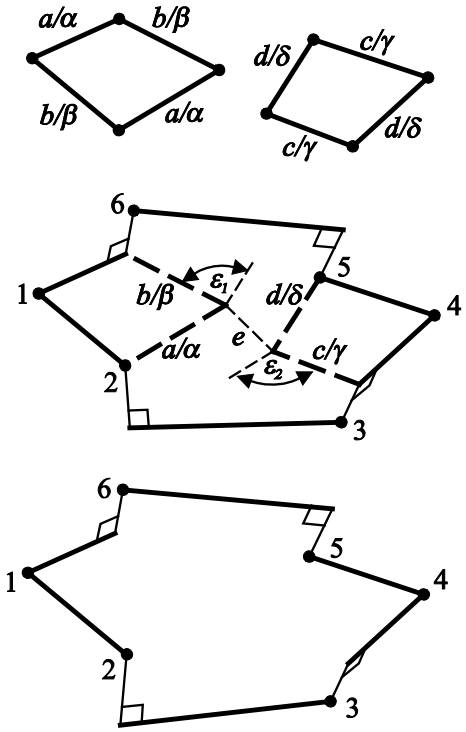

Fig. 2.4.7 The construction of the Waldron's hybrid 6*R* linkage.

2.4.6 Yu & Baker's Syncopated 6*R* Linkage

During the degeneration process from the Waldron's hybrid 6*R* linkage into the Goldberg 5*R* linkage, Yu and Baker (1981) noticed a special state of the Waldron's hybrid 6*R* linkage where syncopation can be formed using Goldberg's method. In the degeneration process shown in Fig. 2.4.8, two Bennett linkages are randomly chosen to be connected.

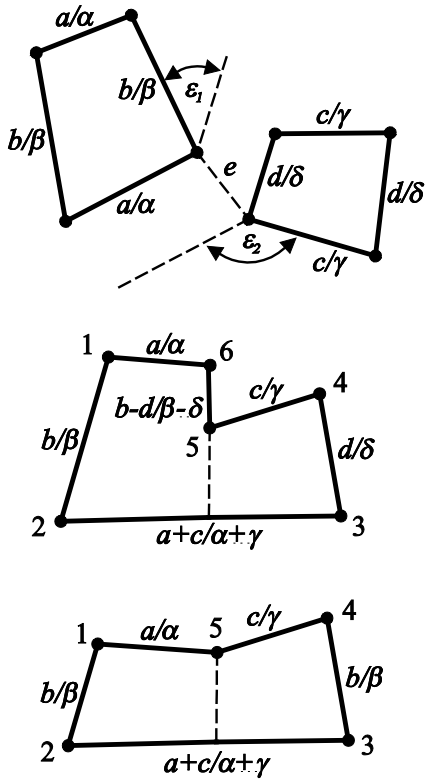

Fig. 2.4.8 The degeneration process from a Waldron's hybrid 6*R* linkage into a Goldberg 5*R* linkage.

They are placed in such a manner that the offset e along the common revolute axis shrinks to zero, the kink angle ε_1 is locked to 0 and another kink angle ε_2 is locked to π. Thus, the two links b/β and d/δ forming kink angle ε_1 are now overlapped while the other two links a/α and c/γ forming kink angle ε_2 are now collinearly posed. After firstly removing the overlapped part, and then combining the collinearly posed links, a special case of the Waldron's hybrid 6*R* linkage can be formed. When the two Bennett linkages are carefully chosen to share a common link on the overlapped part, or link b/β is chosen to be the same as link d/δ, a Goldberg 5*R* linkage can be obtained subsequently.

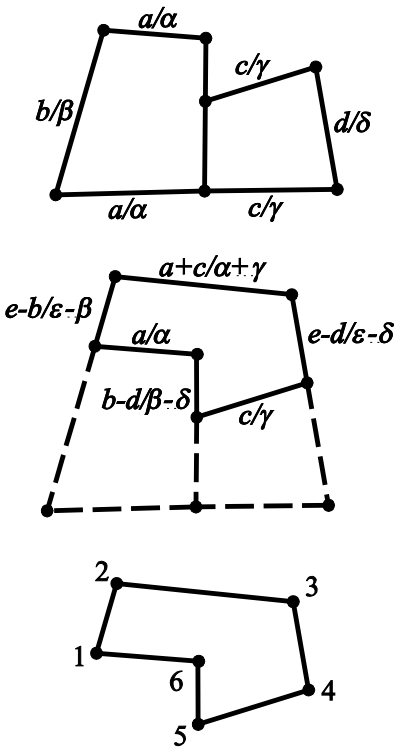

Fig. 2.4.9 The construction of the Yu & Baker's syncopated 6*R* linkage.

Following Goldberg's method of using a Goldberg 5*R* linkage to form a syncopated 5*R* linkage, Yu and Baker did the same operation to the special case of Waldron's hybrid 6*R* linkage to find a syncopated 6*R* linkage in Fig. 2.4.9. This linkage can be degenerated into the syncopated Goldberg 5*R* linkage when link b/δ shares the same geometry conditions as link d/δ. The geometry conditions of the Yu & Baker's syncopated 6*R* linkage are

$$a_{12}=e-b,\ a_{23}=a+c,\ a_{34}=e-d,\ a_{45}=c,\ a_{56}=b-d,\ a_{61}=a,$$

$$\alpha_{12}=\varepsilon-\beta,\ \alpha_{23}=\alpha+\gamma,\ \alpha_{34}=\varepsilon-\delta,\ \alpha_{45}=\gamma,\ \alpha_{56}=\beta-\delta,\ \alpha_{61}=\alpha,$$

$$\frac{\sin\alpha}{a}=\frac{\sin\beta}{b}=\frac{\sin\gamma}{c}=\frac{\sin\delta}{d},\ \frac{\sin\frac{\alpha+\beta}{2}}{\sin\frac{\alpha-\beta}{2}}\frac{\sin\frac{\gamma+\delta}{2}}{\sin\frac{\gamma-\delta}{2}}=\frac{\sin\frac{\varepsilon+\alpha+\gamma}{2}}{\sin\frac{\varepsilon-\alpha-\gamma}{2}}, \tag{2.4.10}$$

$$\frac{\sin\varepsilon}{e}=\frac{\sin(\alpha+\gamma)}{a+c},\ R_i=0\ (i=1,2,...,6).$$

2.4.7 Mavroidis & Roth's 6*R* Linkage and Dietmaier's 6*R* Linkage

The methods adopted in finding the above overconstrained 6*R* linkages are mainly geometry based, which only give parts of the solutions to the family of overconstrained 6*R* linkages. As the development in inverse kinematics goes broader and deeper, numerical based methods have been developed which utilize the power of computers to find the solutions in a different way. Mavroidis, Roth and Dietmaier are the pioneers in utilizing the inverse kinematics methods to find new overconstrained 6*R* linkages.

The linkage found by Mavroidis and Roth (1995) is based on a numerical scheme developed by Raghavan and Roth (1990). The purpose of this scheme is to solve the inverse kinematics for general 6*R* manipulators. Any close-loop mechanism can be viewed as a serial robot arm with its end-effector attached to its base frame. By solving the inverse kinematics of a closed-loop 6*R* mechanism, an overconstrained 6*R* linkage was proposed by Mavroidis and Roth with the following geometry conditions

$$\begin{gathered} a_{12} = a_{34},\ a_{23} = a_{56},\ a_{45} = a_{61}, \\ \alpha_{12} = \alpha_{34},\ \alpha_{23} = \alpha_{56},\ \alpha_{45} = \alpha_{61}, \\ \frac{\sin\alpha_{12}}{a_{12}} = \frac{\sin\alpha_{34}}{a_{34}} = \frac{\sin\alpha_{45}}{a_{45}} = \frac{\sin\alpha_{61}}{a_{61}}, \\ R_1 = R_4 = 0,\ R_2 = R_5,\ R_3 = R_6 \text{ or } R_1 = R_4 = 0,\ R_2 = R_6,\ R_3 = R_5. \end{gathered} \tag{2.4.11}$$

The geometry conditions in Eq. (2.4.11) share certain similarities to the Wohlhart's double-Goldberg 6*R* linkage in Eq. (2.4.7). In terms of generosity, the geometry conditions in Eq. (2.4.11) cover the generalized Wohlhart's double-Goldberg 6*R* linkage in the choice of lengths and twists on links 23 and 56. On the other hand, there is another case of the Mavroidis & Roth's 6*R* linkage when the geometry conditions on links 34 and 45 are exchanged, which is the same as in the back-to-back double-Goldberg 6*R* linkage. Even

though the Mavroidis & Roth's 6*R* linkage is found using numerical method, we can still find its correlation with other existing linkages found using construct methods, which is an interesting phenomenon that worth attentions. Later, another overconstrained 6*R* linkage was found by Dietmaier (1995b) using the numerical scheme developed by Lee and Liang (1988). After trying to solve the same inverse kinematics problem and observing the results, a new linkage was proposed with the following geometry conditions.

$$\frac{\sin\alpha_{12}}{a_{12}}=\frac{\sin\alpha_{61}}{a_{61}},\ \frac{\sin\alpha_{34}}{a_{34}}=\frac{\sin\alpha_{45}}{a_{45}},\ a_{23}=a_{56},\ \alpha_{23}=\alpha_{56},$$

$$\frac{\sin\alpha_{12}}{a_{12}}\cdot(\cos\alpha_{12}+\cos\alpha_{61})=\frac{\sin\alpha_{34}}{a_{34}}\cdot(\cos\alpha_{34}+\cos\alpha_{45}), \tag{2.4.12}$$

$$R_1=R_5,\ R_2=R_4,\ R_3=R_6=0.$$

The geometry conditions shown above were summarized by Dietmaier through observation of the raw data. In the meanwhile, he claimed that when further constraints are added to Eq. (2.4.12) so that $a_{12}=a_{34}$, $a_{45}=a_{61}$, $\alpha_{12}=\alpha_{34}$ and $\alpha_{45}=\alpha_{61}$, the Mavroidis & Roth's 6*R* linkage could be obtained, apart from the part that offsets are interchangeable in Mavroidis & Roth's 6*R* linkage. Recently, the mobility of Dietmaier's linkage is confirmed by Baker (2010) using single reciprocal screw method. The discovery of both linkages set a good example in the application of inverse kinematics methods in finding new overconstrained 6*R* linkage. Despite the fact that different methods are used, these two linkages indeed share some similarities in geometry conditions which worth attentions.

2.4.8 Bricard Linkages

One of the most fascinating and remarkable linkage families in the overconstrained 6*R* linkages is the family of Bricard linkages (Bricard, 1897; 1927). Review to the Bricard linkages was included in section 1.2. There are six cases in the original family, including:

(1) The general line-symmetric case,

$$\begin{gathered} a_{12}=a_{45},\ a_{23}=a_{56},\ a_{34}=a_{61}, \\ \alpha_{12}=\alpha_{45},\ \alpha_{23}=\alpha_{56},\ \alpha_{34}=\alpha_{61}, \\ R_1=R_4,\ R_2=R_5,\ R_3=R_6; \end{gathered} \tag{2.4.13}$$

(2) The general plane-symmetric case,

$$\begin{gathered} a_{12}=a_{61},\ a_{23}=a_{56},\ a_{34}=a_{45}, \\ \alpha_{12}+\alpha_{61}=\pi,\ \alpha_{23}+\alpha_{56}=\pi,\ \alpha_{34}+\alpha_{45}=\pi, \\ R_1=R_4=0,\ R_2=R_6,\ R_3=R_5; \end{gathered} \tag{2.4.14}$$

(3) The trihedral case,

$$\begin{gathered} a_{12}^2+a_{34}^2+a_{56}^2=a_{23}^2+a_{45}^2+a_{61}^2, \\ \alpha_{12}=\alpha_{34}=\alpha_{56}=\frac{\pi}{2},\ \alpha_{23}=\alpha_{45}=\alpha_{61}=-\frac{\pi}{2}, \\ R_i=0\ (i=1,2,...,6); \end{gathered} \tag{2.4.15}$$

(4) The line-symmetric octahedral case,

$$a_{12}=a_{23}=a_{34}=a_{45}=a_{56}=a_{61}=0,\ R_1=R_4,\ R_2=R_5,\ R_3=R_6; \tag{2.4.16}$$

(5) The plane-symmetric octahedral case,

$$\begin{gathered} a_{12}=a_{23}=a_{34}=a_{45}=a_{56}=a_{61}=0, \\ R_1+R_4=0,\ R_2=-R_1\cdot\frac{\sin\alpha_{34}}{\sin(\alpha_{12}+\alpha_{34})},\ R_3=R_1\cdot\frac{\sin\alpha_{12}}{\sin(\alpha_{12}+\alpha_{34})}, \\ R_5=R_1\cdot\frac{\sin\alpha_{61}}{\sin(\alpha_{45}+\alpha_{61})},\ R_6=-R_1\cdot\frac{\sin\alpha_{45}}{\sin(\alpha_{45}+\alpha_{61})}; \end{gathered} \tag{2.4.17}$$

(6) The doubly collapsible octahedral case,

$$a_{12}=a_{23}=a_{34}=a_{45}=a_{56}=a_{61}=0,\ R_1\cdot R_3\cdot R_5+R_2\cdot R_4\cdot R_6=0. \tag{2.4.18}$$

2.4.9 The Revised General Line-symmetric and Plane-symmetric Bricard Linkages

During the numerical search of new and revised overconstrained linkages, Mavroidis and Roth (1995) found additional linkage closures which are similar to the original general line-symmetric and plane-symmetric Bricard linkages. The geometry conditions of the revised general line-symmetric Bricard linkage are

$$\begin{aligned} &a_{12} = a_{45},\ a_{23} = a_{56},\ a_{34} = a_{61}, \\ &\alpha_{12} = \alpha_{45},\ \alpha_{23} = \alpha_{56},\ \alpha_{34} = \alpha_{61}, \\ &R_1 = -R_4,\ R_2 = -R_5,\ R_3 = -R_6. \end{aligned} \tag{2.4.19}$$

Note that in this revised case, the offsets on the opposite links are set as negatively equaled, which is different from the original case, where the offset on the opposite links are positively equaled in Eq. (2.4.13). Further analysis about the differences between the original and revised general line-symmetric Bricard linkage is addressed in chapter 4.

In the revised general plane-symmetric Bricard linkage, the geometry conditions are

$$\begin{aligned} &a_{12} = a_{61},\ a_{23} = a_{56},\ a_{34} = a_{45}, \\ &\alpha_{12} + \alpha_{61} = 0,\ \alpha_{23} + \alpha_{56} = 0,\ \alpha_{34} + \alpha_{45} = 0, \\ &R_1 = R_4 = 0,\ R_2 = -R_6,\ R_3 = -R_5. \end{aligned} \tag{2.4.20}$$

Note that in this revised case, the twists and offsets are set in a different manner compared to Eq. (2.4.14).

2.4.10 Altmann's 6*R* Linkage

A 6*R* linkage was published by Altmann (1954) and was later identified as a simplified case of Bricard's general line-symmetric 6*R* linkage. It was studied by Phillips (1984; 1990), and

re-examined by Baker (1993b) using the screw system algebra. Its geometry conditions are listed as follows.

$$a_{12} = a_{45},\ a_{23} = a_{56} = 0,\ a_{34} = a_{61},$$

$$\alpha_{12} = \alpha_{23} = \alpha_{34} = \alpha_{56} = \frac{\pi}{2},\ \alpha_{45} = \alpha_{61} = -\frac{\pi}{2}, \tag{2.4.21}$$

$$R_i = 0\ (i = 1, 2, ..., 6).$$

2.4.11 Wohlhart's Hybrid 6*R* Linkage

It was noticed that in some linkages there exist a transversal line that intersects all revolute axes during the linkage's full-cycle movement. Such characteristic exists in general plane-symmetric Bricard linkages, trihedral Bricard linkages, Bennett linkage, plane-symmetric Myard 5*R* linkage and double-Hooke's linkage. Based on this observation, an overconstrained 6*R* linkage was proposed by Wohlhart (1987) with three link-pairs of partial symmetry. In Fig. 2.4.10, the three link-pairs with partial symmetry are 61-12, 23-34 and 45-56.

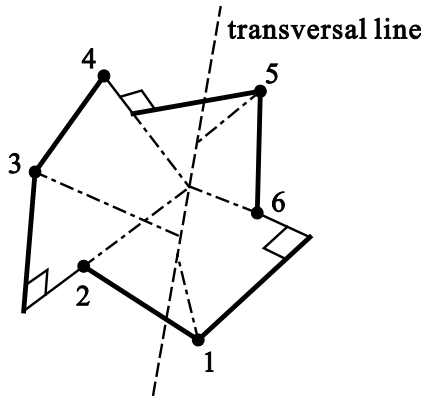

Fig. 2.4.10 The Wohlhart's 6*R* linkage with partial symmetry and a transversal axis in common.

The geometry conditions of Wohlhart's hybrid 6*R* linkage are

$$a_{12} = a_{23},\ a_{34} = a_{45},\ a_{56} = a_{61},$$

$$\alpha_{12} = -\alpha_{23},\ \alpha_{34} = -\alpha_{45},\ \alpha_{56} = -\alpha_{61}, \tag{2.4.22}$$

$$R_1 = R_3 = R_5 = R_2 + R_4 + R_6 = 0.$$

2.4.12 Summary

The purpose of this review is not meant to include all the linkages in the category of overconstrained 6*R* linkages, but to review the major linkages in this category and summarize the historical relationship among them. The reader is encouraged to refer to the work by Dietmaier (1995a) for a detailed study into the kinematics of various overconstrained 6*R* linkages and Baker (2002) for a refined list of 28 overconstrained 6*R* linkages that have been published in literatures. The overconstrained 6*R* linkages could not be easily classified into a single linkage family like the overconstrained 5*R* and 4*R* linkages. Among them, two major linkage families could be generalized, which are the Bennett-based linkage family and the Bricard linkage family. Linkages in the Bennett-based linkage family are constructed from the combination and subtraction from the basic linkages, such as the Bennett linkage and the Goldberg linkages. Linkage in the Bricard linkage family makes use of special geometry constraint in line-symmetry, plane-symmetry, common transversal and etc. to form overconstrained 6*R* linkages. Even though for linkages like the Mavroidis & Roth's 6*R* linkage and Dietmaier's 6*R* linkage, which were found through inverse kinematics methods, they still share similarities in the geometry conditions and spatial configurations with other existing linkages in the Bennett-based and Bricard families.

2.5 RECONFIGURABLE MECHANISMS

Recent advance in mechanism design promotes the development of a class of mechanisms which are reconfigurable with multiple operation forms. Such reconfigurable mechanisms are based on solely one mechanism and are capable of fulfilling multiple tasks in different operation forms. A comprehensive review about the current development, principles and strategies of the reconfigurable mechanisms was discussed in (Kuo et al., 2009). Several mechanisms found in the past two decades exhibit the property of reconfiguration during operation. The kinematotropic mechanisms (Wohlhart, 1996) can change its global mobility with positional parameter actuations at the bifurcation points. A number of single- and multi-loop kinematotropic mechanisms are found recently (Galletti and Fanghella, 1999; 2001; Galletti and Giannotti, 2002). The metamorphic mechanism (Dai and Rees Jones, 1999) has received wide recognition during the past decade, which has variable topology and mobility during operation. Theoretical studies in (Dai and Rees Jones, 2005; Lan and Du, 2008; Zhang and Dai, 2009b) discussed the topological changes in the metamorphic mechanisms. Application of the metamorphic mechanisms can be found in robotics design (Dai and Wang, 2007), biological modeling (Zhang et al., 2008) and genome reconfigurations (Zhang and Dai, 2008). Mechanism with variable topologies also draws attentions for its reconfigurable potentials (Yan and Kang, 2009; Yan and Kuo, 2006a; 2006b).

This dissertation focuses on the reconfigurable mechanism that is based on the transformation among different kinematic paths using kinematic singularities (Kong and Huang, 2009; Wohlhart, 1996; 2010), such as kinematotropy mechanism (Wohlhart, 1996) and mechanism with bifurcations. The kinematotropy mechanism can change their global mobility with positional actuations at the transit positions. Galletti and Fanghella (2001) designed a series of kinematotropy mechanisms using the displacement group method. With

the group-algebraic approach, Lee and Hervé (2005) found that a closed-loop chain can be reconfigured when there are two or more subgroups involved in the mechanism. Another type of singularity is applied to design linkages with desired bifurcated paths. Recently, Kong and Huang (2009) proposed a number of one degree of freedom single-loop mechanisms with two operation modes. Wohlhart (2010) also proposed a series of multifunctional 7*R* linkages by inserting an overconstrained 4*R*, 5*R* or 6*R* mobile chain into a closed-loop 7*R* linkage.

Chapter 3

The Double-Goldberg Linkage Family

3.1 OVERVIEW

In this chapter, the double-Goldberg linkage family is presented by using the Goldberg 5*R* linkages or the subtractive Goldberg 5*R* linkages as the building blocks to construct overconstrained 6*R* linkages. A large number of linkages are covered under this linkage family. A family of mixed double-Goldberg 6*R* linkage is used as an example to explain the construct details of this linkage family.

The layout of this chapter is as follows. Section 3.2 reviews the Goldberg 5*R* linkage and the subtractive Goldberg 5*R* linkage. Two construct methods and all the possible resultant 6*R* linkages are listed in section 3.3. In section 3.4, the six distinct types of the mixed double-Goldberg linkages are analyzed individually with closure equations. The properties and extensions of this new linkage family are discussed in section 3.5, which concludes this chapter.

3.2 THE GOLDBERG AND SUBTRACTIVE GOLDBERG 5*R* LINKAGES

When superposing two Bennett linkages on a common link a/α and locking the two adjacent links b/β and c/γ collinearly as shown in Fig. 3.2.1, a Goldberg 5*R* linkage can be obtained after removing the common link and joints (Baker, 1979; Goldberg, 1943). Its geometry conditions and closure equations are reproduced as follows.

$$a_{12}=a_{34},\ a_{23}=a_{45}+a_{51},\ \alpha_{12}=\alpha_{34},\ \alpha_{23}=\alpha_{45}+\alpha_{51},$$
$$\frac{\sin\alpha_{12}}{a_{12}}=\frac{\sin\alpha_{12}}{a_{12}}=\frac{\sin\alpha_{12}}{a_{12}},\ R_i=0\ (i=1,2,...,5); \tag{3.2.1}$$

and

$$\tan\frac{\theta_2}{2}=\frac{\sin\frac{\alpha_{51}+\alpha_{12}}{2}}{\tan\frac{\theta_1}{2}\sin\frac{\alpha_{51}-\alpha_{12}}{2}},\ \tan\frac{\theta_3}{2}=\frac{\tan\frac{\theta_1}{2}\sin\frac{\alpha_{45}+\alpha_{12}}{2}}{\sin\frac{\alpha_{45}-\alpha_{12}}{2}}, \tag{3.2.2}$$
$$\theta_1+\theta_4=\pi,\ \theta_2+\theta_3+\theta_5=\pi.$$

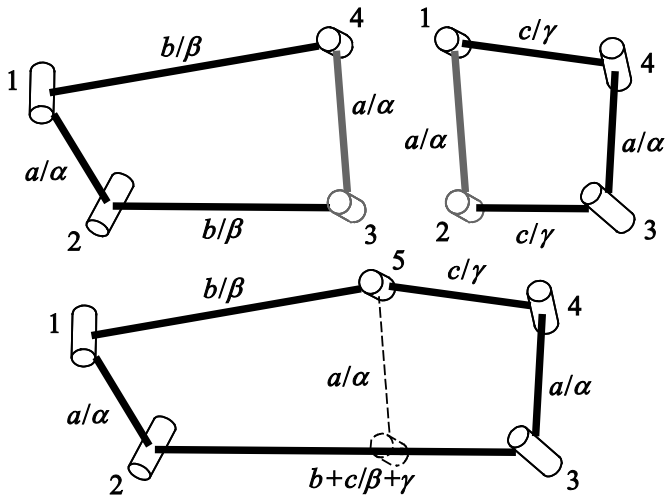

Fig. 3.2.1 The construction of the Goldberg 5*R* linkage.

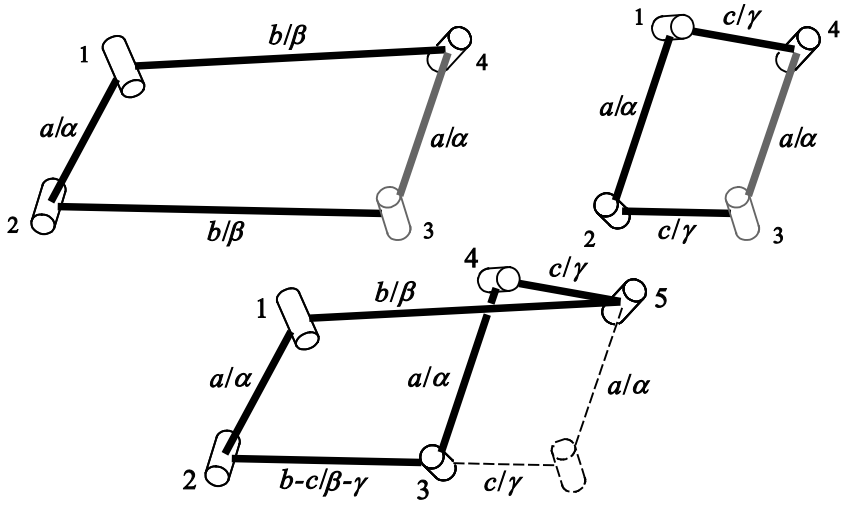

Fig. 3.2.2 The construction of the subtractive Goldberg 5*R* linkage.

Similarly, with the same two Bennett linkages used in the construction of Goldberg 5*R* linkage, a subtractive Goldberg 5*R* linkage can be obtained when links b/β and c/γ are inversely posed as shown in Fig. 3.2.2. The corresponding geometry conditions and closure equations are

$$\begin{gathered} a_{12}=a_{34},\ a_{23}=a_{45}-a_{51},\ \alpha_{12}=\alpha_{34},\ \alpha_{23}=\alpha_{45}-\alpha_{51}, \\ \frac{\sin\alpha_{12}}{a_{12}}=\frac{\sin\alpha_{45}}{a_{45}}=\frac{\sin\alpha_{51}}{a_{51}},\ R_i=0\ (i=1,2,...,5); \end{gathered} \tag{3.2.3}$$

and

$$\begin{gathered} \tan\frac{\theta_2}{2}=\frac{\sin\dfrac{\alpha_{51}+\alpha_{12}}{2}}{\tan\dfrac{\theta_1}{2}\cdot\sin\dfrac{\alpha_{51}-\alpha_{12}}{2}},\ \tan\frac{\theta_3}{2}=\frac{\tan\dfrac{\theta_1}{2}\cdot\sin\dfrac{\alpha_{45}+\alpha_{12}}{2}}{\sin\dfrac{\alpha_{45}-\alpha_{12}}{2}}, \\ \theta_1+\theta_4=0,\ \theta_2+\theta_3+\theta_5=0. \end{gathered} \tag{3.2.4}$$

respectively.

3.3 THE CONSTRUCT METHODS

The *Bennett ratio* is defined to characterize the Bennett linkage as a proportional relationship between the sine of twist and length of the link. Four basic links, a/α, b/β, c/γ and d/δ with the same Bennett ratios,

$$\frac{\sin\alpha}{a}=\frac{\sin\beta}{b}=\frac{\sin\gamma}{c}=\frac{\sin\delta}{d}, \tag{3.3.1}$$

will be used in the following construct methods. There are two construct methods to combine two 5*R* linkages into a 6*R* linkage. Here, we name a *link-pair* as two adjacent links connected by a shared joint. Wohlhart (1991a) proposed the first construction method when forming his double-Goldberg 6*R* linkage. In detail, two linkages with the identical link-pairs are connected together by superposing on this common link-pair as shown in Fig. 3.3.1(a). After

removing the commonly shared link-pair, the rest part will form a single-loop overconstrained linkage. We call such method the *common link-pair* (CLP). For the second construct method, instead of making the identical link-pairs superposed, we can connect them into a Bennett linkage, as shown in Fig. 3.3.1(b) in dash lines. Removing this commonly shared Bennett linkage will also produce a single-loop overconstrained linkage. And this method is called the *common Bennett-linkage* (CBL).

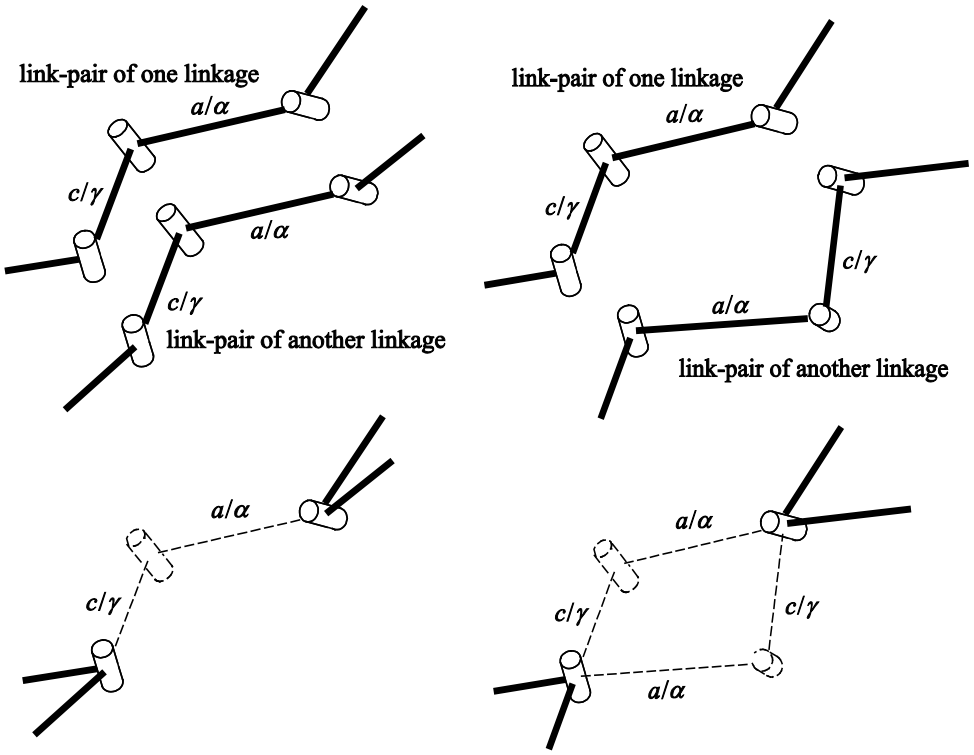

(a) (b)

Fig. 3.3.1 The methods of (a) common link-pair and (b) common Bennett-linkage.

Here, two different 5*R* linkages will be used as the construct elements of the new linkage family, including a subtractive Goldberg 5*R* linkage S and a Goldberg 5*R* linkage G. In order to form the common link-pair and common Bennett-linkage, linkages S and G both comprise of links a/α and c/γ. When the link-pair $a/\alpha \sim c/\gamma$ is located at different parts of the 5*R* linkage, three possible configurations of the Goldberg 5*R* linkage can be formed. So does the subtractive Goldberg 5*R* linkage, as listed in Fig. 3.3.2.

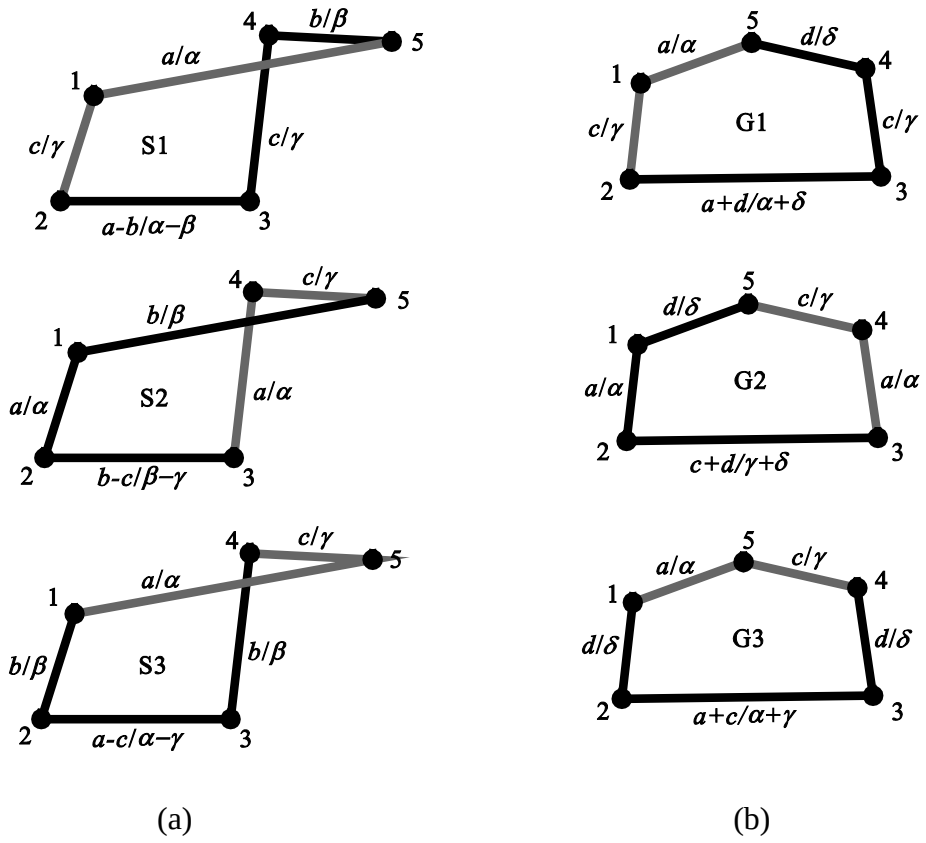

(a) (b)

Fig. 3.3.2 The schematics of (a) the subtractive Goldberg 5*R* linkage S and (b) the Goldberg 5*R* linkage G that could be used for connection.

As we are going to construct 6*R* linkage by combining one subtractive Goldberg 5*R* linkage and one Goldberg 5*R* linkage through common link-pair and common Bennett-linkage, there are totally 18 ($=3\times3\times2$) possible combinations. However, after careful examination, duplicates are identified and removed. Thus, only six distinct types of linkages can be constructed with proposed linkages and methods, which are listed in Table 3.3.1.

Table 3.3.1 All possible constructions of the mixed double-Goldberg 6*R* linkages.

Type	Linkage		Construct Method	Schematics
	S	G		
I	S3	G3	CLP&CBL	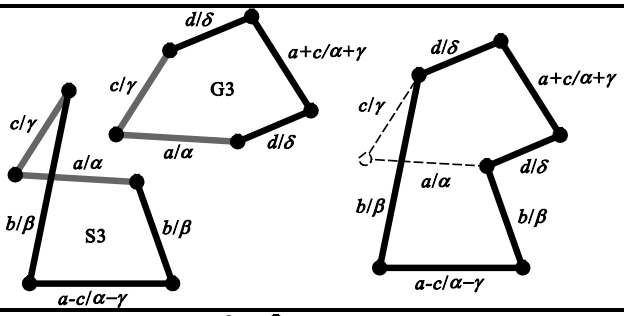
II	S3	G1	CLP&CBL	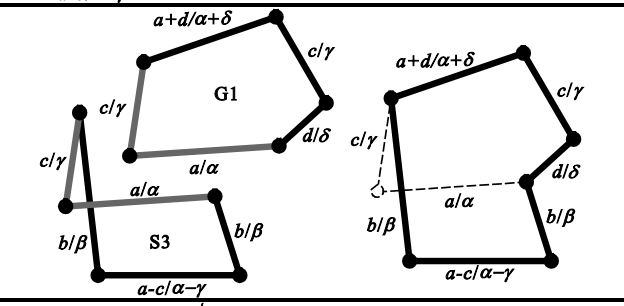
	S3	G2		
	S1	G3		
	S2	G3		
III	S1	G1	CLP	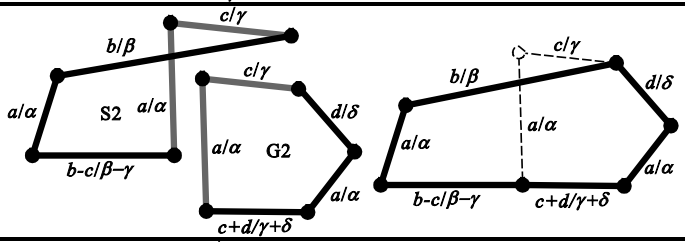
	S2	G2		
IV	S1	G1	CBL	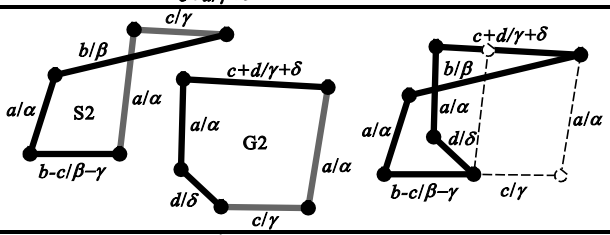
	S2	G2		
V	S1	G2	CLP	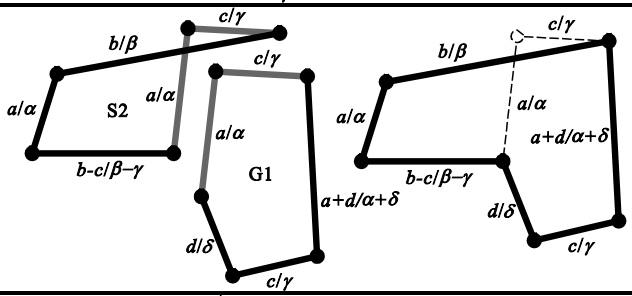
	S2	G1		
VI	S1	G2	CBL	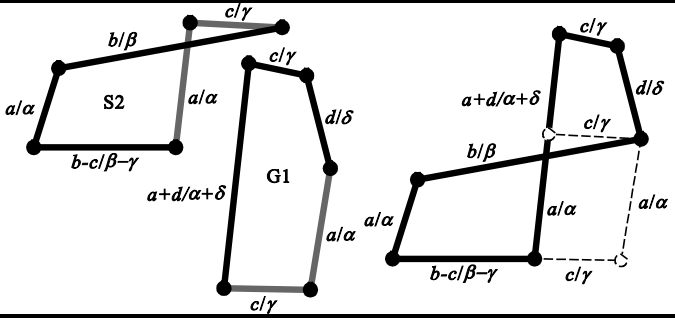
	S2	G1		

3.4 SIX TYPES OF MIXED DOUBLE-GOLDBERG 6*R* LINKAGES

Because all of the six distinct linkages listed in Table 3.3.1 are built from two different types of 5*R* linkages, we name them as a family of mixed double-Goldberg 6*R* linkages. To simplify the representation, six sets of mathematical relationships are defined as below.

$$\begin{aligned} m_1 &= \frac{\sin\frac{\beta+\alpha}{2}}{\sin\frac{\beta-\alpha}{2}},\ m_2 = \frac{\sin\frac{\gamma+\alpha}{2}}{\sin\frac{\gamma-\alpha}{2}},\ m_3 = \frac{\sin\frac{\delta+\alpha}{2}}{\sin\frac{\delta-\alpha}{2}}, \\ m_4 &= \frac{\sin\frac{\delta+\gamma}{2}}{\sin\frac{\delta-\gamma}{2}},\ m_5 = \frac{\sin\frac{\delta+\beta}{2}}{\sin\frac{\delta-\beta}{2}},\ m_6 = \frac{\sin\frac{\beta+\gamma}{2}}{\sin\frac{\beta-\gamma}{2}}. \end{aligned} \tag{3.4.1}$$

Here, only Type I linkage is presented with detailed derivation process. The rest linkage types can be derived in a similar manner.

3.4.1 Type I

Linkages S3 and G3 are selected to build the Type I mixed double-Goldberg 6*R* linkage. As shown in Fig. 3.4.1, link-pair 51-45 of linkages S3 and G3 share the same geometry conditions so that they can be merged to form a common link-pair connection. After removing the connection, a single-loop 6*R* linkage can be obtained. The geometry conditions of linkages S3 and G3 are

$$\begin{aligned} &a_{12}^{\mathrm{S3}} = a_{34}^{\mathrm{S3}} = b,\ a_{23}^{\mathrm{S3}} = a - c,\ a_{45}^{\mathrm{S3}} = c,\ a_{51}^{\mathrm{S3}} = a, \\ &\alpha_{12}^{\mathrm{S3}} = \alpha_{34}^{\mathrm{S3}} = \beta,\ \alpha_{23}^{\mathrm{S3}} = \alpha - \gamma,\ \alpha_{45}^{\mathrm{S3}} = \gamma,\ \alpha_{51}^{\mathrm{S3}} = \alpha, \\ &a_{12}^{\mathrm{G3}} = a_{34}^{\mathrm{G3}} = d,\ a_{23}^{\mathrm{G3}} = a + c,\ a_{45}^{\mathrm{G3}} = c,\ a_{51}^{\mathrm{G3}} = a, \\ &\alpha_{12}^{\mathrm{G3}} = \alpha_{34}^{\mathrm{G3}} = \delta,\ \alpha_{23}^{\mathrm{G3}} = \alpha + \gamma,\ \alpha_{45}^{\mathrm{G3}} = \gamma,\ \alpha_{51}^{\mathrm{G3}} = \alpha. \end{aligned} \tag{3.4.2}$$

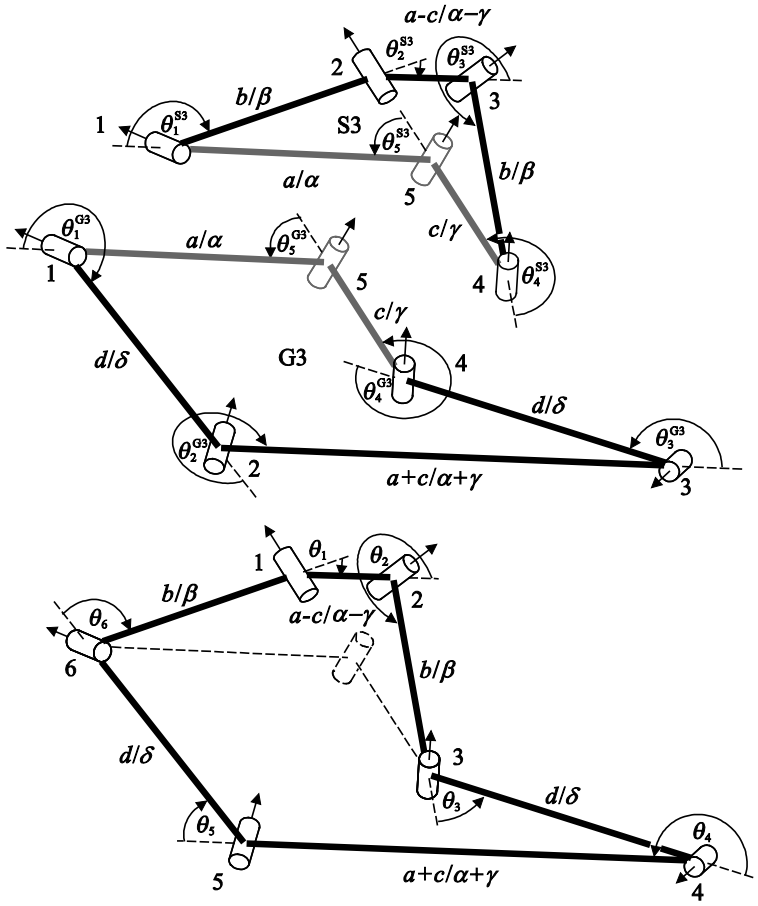

Fig. 3.4.1 The construction of the Type I mixed double-Goldberg 6*R* linkage.

From Fig. 3.4.1, the geometry conditions of the resultant 6*R* linkage can be obtained.

$$\begin{gathered} a_{12} = a - c\,,\ a_{23} = a_{61} = b\,,\ a_{34} = a_{56} = d\,,\ a_{45} = a + c\,, \\ \alpha_{12} = \alpha - \gamma\,,\ \alpha_{23} = \alpha_{61} = \beta\,,\ \alpha_{34} = \alpha_{56} = \delta\,,\ \alpha_{45} = \alpha + \gamma\,, \\ \frac{\sin\alpha}{a} = \frac{\sin\beta}{b} = \frac{\sin\gamma}{c} = \frac{\sin\delta}{d}\,,\ R_i = 0\ (i = 1, 2, ..., 6)\,. \end{gathered} \tag{3.4.3}$$

According to Eqs. (3.2.2) and (3.2.4), the closure equations of linkages S3 and G3 can be written as

$$\tan\frac{\theta_2^{S3}}{2} = -\frac{m_2}{\tan\dfrac{\theta_1^{S3}}{2}}\,,\ \tan\frac{\theta_3^{S3}}{2} = \frac{\tan\dfrac{\theta_1^{S3}}{2}}{m_6}\,,\ \theta_1^{S3} + \theta_4^{S3} = 0\,,\ \theta_2^{S3} + \theta_3^{S3} + \theta_5^{S3} = 0\,; \tag{3.4.4}$$

and

$$\tan\frac{\theta_2^{G3}}{2}=-\frac{m_2}{\tan\dfrac{\theta_1^{G3}}{2}},\ \tan\frac{\theta_3^{G3}}{2}=m_4\tan\frac{\theta_1^{G3}}{2},\ \theta_1^{G3}+\theta_4^{G3}=\pi,\ \theta_2^{G3}+\theta_3^{G3}+\theta_5^{G3}=\pi, \tag{3.4.5}$$

respectively. The compatibility relationship between revolute variables of the resultant 6*R* linkage and linkages S3 and G3 are

$$\begin{gathered}\theta_1=\theta_2^{S3},\ \theta_2=\theta_3^{S3},\ \theta_3=\theta_4^{S3}-\theta_4^{G3}+\pi,\\ \theta_4=2\pi-\theta_3^{G3},\ \theta_5=2\pi-\theta_2^{G3},\ \theta_3=\theta_1^{S3}-\theta_1^{G3}+\pi.\end{gathered} \tag{3.4.6}$$

In addition, the compatibility relationship,

$$\theta_5^{S3}=\theta_5^{G3}, \tag{3.4.7}$$

must be held to build a successful connection. The closure equations of the Type I mixed double-Goldberg 6*R* linkage are derived by substituting Eqs. (3.4.6) and (3.4.7) into Eqs. (3.4.4) and (3.4.5) as follows. The kinematic paths of the Type I linkage are plotted in Fig. 3.4.2.

$$\begin{gathered}\tan\frac{\theta_2}{2}=-\frac{m_2}{m_6\tan\dfrac{\theta_1}{2}},\ \theta_3=\pi+2\tan^{-1}Q-2\tan^{-1}\left(\frac{m_2}{\tan\dfrac{\theta_1}{2}}\right),\ \tan\frac{\theta_4}{2}=-\frac{m_2}{Q},\\ \tan\frac{\theta_5}{2}=m_4\tan\frac{\theta_1}{2},\ \theta_6=2\tan^{-1}\left(\frac{m_2}{\tan\dfrac{\theta_1}{2}}\right)-2\tan^{-1}Q,\end{gathered} \tag{3.4.8}$$

in which

$$Q=\begin{cases}\dfrac{1}{2H}\left[-\left(\dfrac{1}{m_2}+m_4\right)+\sqrt{\left(\dfrac{1}{m_2}+m_4\right)^2+4H^2\dfrac{m_2}{m_4}}\right] & (\theta_1\in[0,\pi))\\ \dfrac{1}{2H}\left[-\left(\dfrac{1}{m_2}+m_4\right)-\sqrt{\left(\dfrac{1}{m_2}+m_4\right)^2+4H^2\dfrac{m_2}{m_4}}\right] & (\theta_1\in[-\pi,0))\end{cases}, \tag{3.4.9}$$

$$H=\frac{m_2-m_6\tan^2\dfrac{\theta_1}{2}}{(m_2+m_6)\tan\dfrac{\theta_1}{2}}.$$

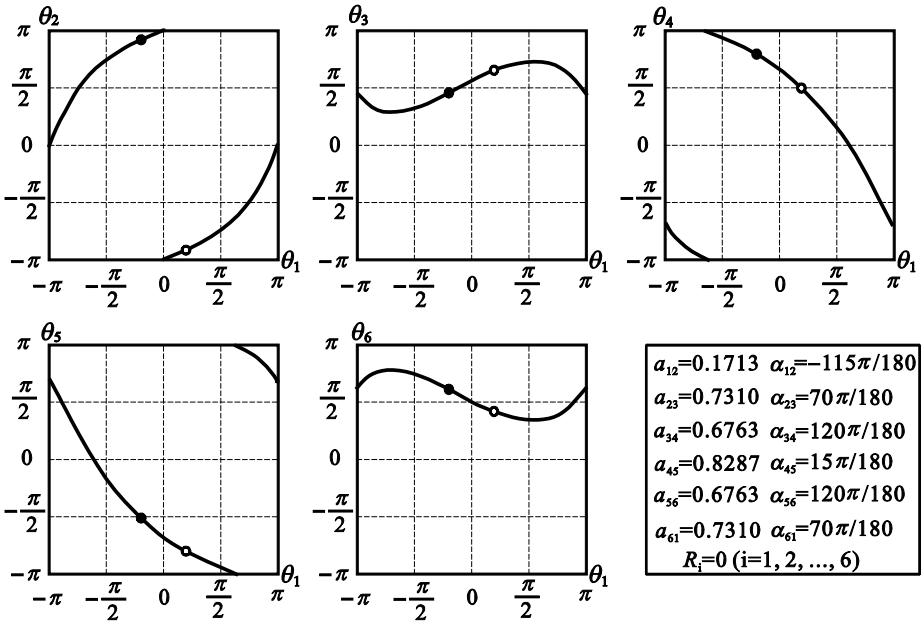

Fig. 3.4.2 The kinematic paths of the Type I mixed double-Goldberg 6*R* linkage.

It should be pointed out that using common Bennett-linkage method with the same linkages S3 and G3, the same linkage could be formed in a different configuration. In Fig. 3.4.2 for example, the hollow dots represent the configuration of the 6*R* linkage from common link-pair method $\theta_1 = \theta_1^{\mathrm{CLP}}$, and the solid dots represent the configuration from common Bennett-linkage method $\theta_1 = -\theta_1^{\mathrm{CBL}}$, then $\theta_1^{\mathrm{CLP}} = -\theta_1^{\mathrm{CBL}}$. When we replace linkage S3 with Goldberg 5*R* linkage G3 and follow the same construction as shown above, the Wohlhart's double-Goldberg 6*R* linkage will be obtained. However, in Wohlhart's linkage, bifurcations are later detected which will transform the linkage into non-constructive forms (Song and Chen, 2011); while in the Type I linkage derived above, no bifurcation has been found. Therefore, the Type I mixed double-Goldberg 6*R* linkage could be considered as a variant of Wohlhart's double-Goldberg 6*R* linkage.

3.4.2 Type II

Linkages S2 and G3 are selected to build the Type II mixed double-Goldberg 6*R* linkage. As shown in Fig. 3.4.3, link-pair 34-45 of linkage S2 and link-pair 51-45 of linkage G3 share the same geometry conditions so that they can be merged to form a common link-pair. After removing the connection, a single-loop 6*R* linkage can be obtained. The geometry conditions of linkages S2 and G3 are

$$\begin{aligned}
&a_{12}^{\mathrm{S2}} = a_{34}^{\mathrm{S2}} = a\,,\ a_{23}^{\mathrm{S2}} = b-c\,,\ a_{45}^{\mathrm{S2}} = c\,,\ a_{51}^{\mathrm{S2}} = b\,,\\
&\alpha_{12}^{\mathrm{S2}} = \alpha_{34}^{\mathrm{S2}} = \alpha\,,\ \alpha_{23}^{\mathrm{S2}} = \beta-\gamma\,,\ \alpha_{45}^{\mathrm{S2}} = \gamma\,,\ \alpha_{51}^{\mathrm{S2}} = \beta\,;\\
&a_{12}^{\mathrm{G3}} = a_{34}^{\mathrm{G3}} = d\,,\ a_{23}^{\mathrm{G3}} = a+c\,,\ a_{45}^{\mathrm{G3}} = c\,,\ a_{51}^{\mathrm{G3}} = a\,,\\
&\alpha_{12}^{\mathrm{G3}} = \alpha_{34}^{\mathrm{G3}} = \delta\,,\ \alpha_{23}^{\mathrm{G3}} = \alpha+\gamma\,,\ \alpha_{45}^{\mathrm{G3}} = \gamma\,,\ \alpha_{51}^{\mathrm{G3}} = \alpha\,.
\end{aligned} \tag{3.4.10}$$

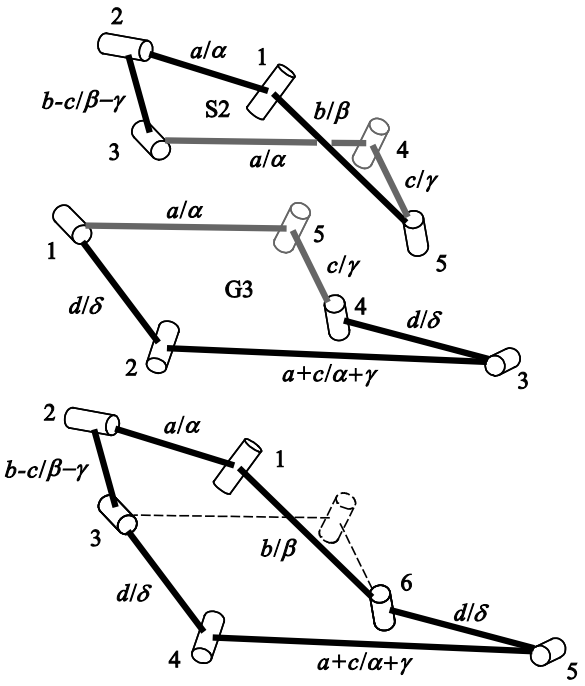

Fig. 3.4.3 The construction of the Type II mixed double-Goldberg 6*R* linkage.

Thus the geometry conditions of the resultant 6*R* linkage are

$$\begin{aligned}
&a_{12} = a\,,\ a_{23} = b-c\,,\ a_{34} = a_{56} = d\,,\ a_{45} = a+c\,,\ a_{61} = b\,,\\
&\alpha_{12} = \alpha\,,\ \alpha_{23} = \beta-\gamma\,,\ \alpha_{34} = \alpha_{56} = \delta\,,\ \alpha_{34} = \alpha+\gamma\,,\ \alpha_{61} = \beta\,,
\end{aligned} \tag{3.4.11}$$

$$\frac{\sin\alpha}{a}=\frac{\sin\beta}{b}=\frac{\sin\gamma}{c}=\frac{\sin\delta}{d},\ R_i=0\ (i=1,2,...,6)\ .$$

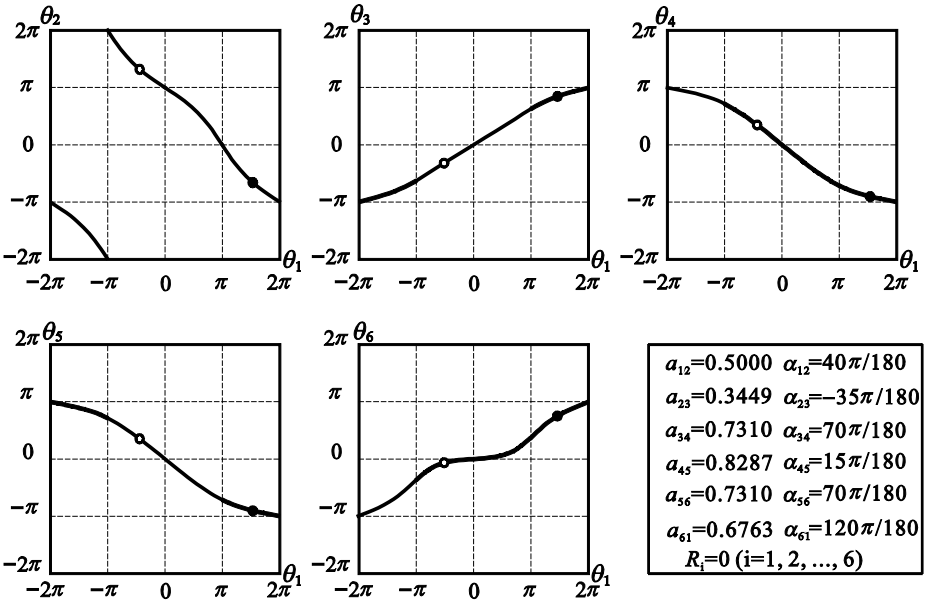

Fig. 3.4.4 The kinematic paths of the Type II mixed double-Goldberg 6*R* linkage.

The closure equations of the Type II 6*R* linkage can be derived as follows and its kinematic paths are plotted in Fig. 3.4.4.

$$\begin{gathered}\tan\frac{\theta_2}{2}=\frac{m_1}{\tan\dfrac{\theta_1}{2}},\ \tan\frac{\theta_3}{2}=\frac{P\cdot\tan\dfrac{\theta_1}{2}-m_2}{\tan\dfrac{\theta_1}{2}+P\cdot m_2},\ \tan\frac{\theta_4}{2}=-\frac{m_3}{P},\\ \tan\frac{\theta_5}{2}=-P\cdot m_4,\ \tan\frac{\theta_6}{2}=\frac{\tan^2\dfrac{\theta_1}{2}+m_1m_2-P\cdot(m_1-m_2)\tan\dfrac{\theta_1}{2}}{(m_1-m_2)\tan\dfrac{\theta_1}{2}+P\cdot\left(m_1m_2+\tan^2\dfrac{\theta_1}{2}\right)},\end{gathered}\tag{3.4.12}$$

in which

$$P=\frac{1}{2m_4\tan\dfrac{\theta_1}{2}}\left[\left(m_3m_4-1\right)\pm\sqrt{\left(m_3m_4-1\right)^2-4m_3m_4\tan^2\frac{\theta_1}{2}}\right].$$

As shown in Table 3.3.1, the same linkage will be obtained when using the common Bennett-linkage method. On the kinematic paths, the linkage obtained from common link-

pair (hollow dots in Fig. 3.4.4) has a phase delay of 2π when comparing to the linkage obtained from common Bennett-linkage (solid dots in Fig. 3.4.4). Due to the similarity of 5*R* linkages, S3+G1, S3+G2 and S1+G3 will also give the same 6*R* linkages. From the kinematic paths, it is interesting to note that θ_1 needs to rotate two full cycles, or variate in the range of $\left[-2\pi, 2\pi\right)$, so that θ_3, θ_4, θ_5 and θ_6 have one full cycle of movement while θ_2 follows with two cycles of motion. When the linkage S2 is replaced by Goldberg 5*R* linkage G2, the Type II linkage will be the second variant of Goldberg 6*R* linkage proposed by Baker (1993a). Therefore, the Type II is viewed as a variant of Baker's second variant of Goldberg 6*R* linkage.

3.4.3 Types III and IV

Linkages S2 and G2 are selected to build the Types III and IV mixed double-Goldberg 6*R* linkage. Link-pair 34-45 of these two linkages share the same geometry conditions so that they can be merged to form a common link-pair. After removing the connection, a Type II linkage can be obtained as shown in Fig. 3.4.5. The geometry conditions of linkages S2 and G2 are

$$\begin{aligned}
&a_{12}^{\mathrm{S2}} = a_{34}^{\mathrm{S2}} = a\,,\ a_{23}^{\mathrm{S2}} = b - c\,,\ a_{45}^{\mathrm{S2}} = c\,,\ a_{51}^{\mathrm{S2}} = b\,,\\
&\alpha_{12}^{\mathrm{S2}} = \alpha_{34}^{\mathrm{S2}} = \alpha\,,\ \alpha_{23}^{\mathrm{S2}} = \beta - \gamma\,,\ \alpha_{45}^{\mathrm{S2}} = \gamma\,,\ \alpha_{51}^{\mathrm{S2}} = \beta\,;\\
&a_{12}^{\mathrm{G2}} = a_{34}^{\mathrm{G2}} = a\,,\ a_{23}^{\mathrm{G2}} = c + d\,,\ a_{45}^{\mathrm{G2}} = c\,,\ a_{51}^{\mathrm{G2}} = d\,,\\
&\alpha_{12}^{\mathrm{G2}} = \alpha_{34}^{\mathrm{G2}} = \alpha\,,\ \alpha_{23}^{\mathrm{G2}} = \gamma + \delta\,,\ \alpha_{45}^{\mathrm{G2}} = \gamma\,,\ \alpha_{51}^{\mathrm{G2}} = \delta\,.
\end{aligned} \tag{3.4.13}$$

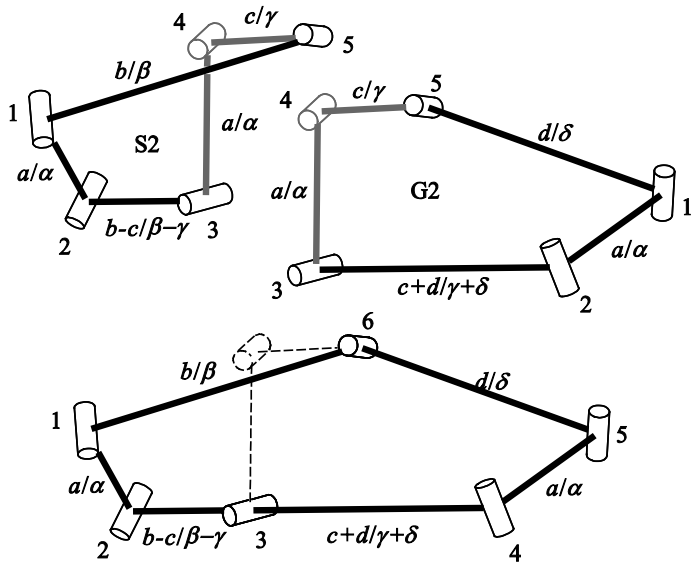

Fig. 3.4.5 The construction of the Type III mixed double-Goldberg 6*R* linkage.

From Fig. 3.4.5, the geometry conditions of the Type III linkage can be obtained.

$$\begin{gathered} a_{12}=a_{45}=a,\ a_{23}=b-c,\ a_{34}=c+d,\ a_{56}=d,\ a_{61}=b, \\ \alpha_{12}=\alpha_{45}=\alpha,\ \alpha_{23}=\beta-\gamma,\ \alpha_{34}=\gamma+\delta,\ \alpha_{56}=\delta,\ \alpha_{61}=\beta, \\ \frac{\sin\alpha}{a}=\frac{\sin\beta}{b}=\frac{\sin\gamma}{c}=\frac{\sin\delta}{d}, \\ R_i=0\ (i=1,2,...,6). \end{gathered} \tag{3.4.14}$$

When we change the construction method to the common Bennett-linkage to connect linkages S2 and G2, the Type IV linkage will be obtained, see Fig. 3.4.6. Therefore, the geometry conditions of the Type IV linkage are

$$\begin{gathered} a_{12}=a_{45}=a,\ a_{23}=b-c,\ a_{34}=d,\ a_{56}=c+d,\ a_{61}=b, \\ \alpha_{12}=\alpha_{45}=\alpha,\ \alpha_{23}=\beta-\gamma,\ \alpha_{34}=\delta,\ \alpha_{56}=\gamma+\delta,\ \alpha_{61}=\beta, \\ \frac{\sin\alpha}{a}=\frac{\sin\beta}{b}=\frac{\sin\gamma}{c}=\frac{\sin\delta}{d}, \\ R_i=0\ (i=1,2,...,6). \end{gathered} \tag{3.4.15}$$

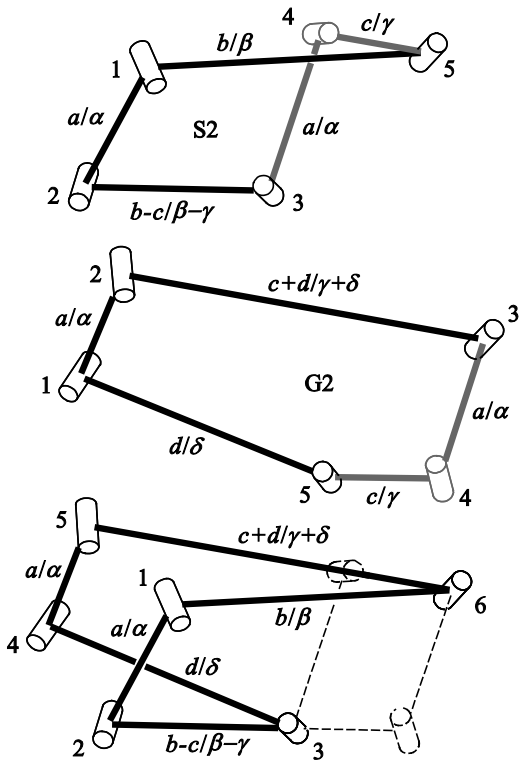

Fig. 3.4.6 The construction of the Type IV mixed double-Goldberg 6*R* linkage.

The closure equations of Types III and IV mixed double-Goldberg 6*R* linkages are derived as

$$\tan\frac{\theta_2}{2}=\frac{m_1}{\tan\frac{\theta_1}{2}},\ \theta_3=0,\ \tan\frac{\theta_4}{2}=-m_3\tan\frac{\theta_1}{2},$$
$$\theta_5=\pm\pi-\theta_1,\ \tan\frac{\theta_6}{2}=\frac{\left(1-m_1m_3\right)\tan\frac{\theta_1}{2}}{m_1+m_3\tan^2\frac{\theta_1}{2}};\tag{3.4.16}$$

and

$$\tan\frac{\theta_2}{2}=\frac{m_1}{\tan\frac{\theta_1}{2}},\ \tan\frac{\theta_3}{2}=\frac{m_2+m_3\tan^2\frac{\theta_1}{2}}{(m_2m_3-1)\tan\frac{\theta_1}{2}},\ \theta_4=\pm\pi-\theta_1,$$
$$\tan\frac{\theta_5}{2}=m_3\tan\frac{\theta_1}{2},\ \tan\frac{\theta_6}{2}=\frac{m_1m_2+\tan^2\frac{\theta_1}{2}}{\left(m_1-m_2\right)\tan\frac{\theta_1}{2}},\tag{3.4.17}$$

respectively. Their kinematic paths are plotted in Fig. 3.4.7 and Fig. 3.4.8.

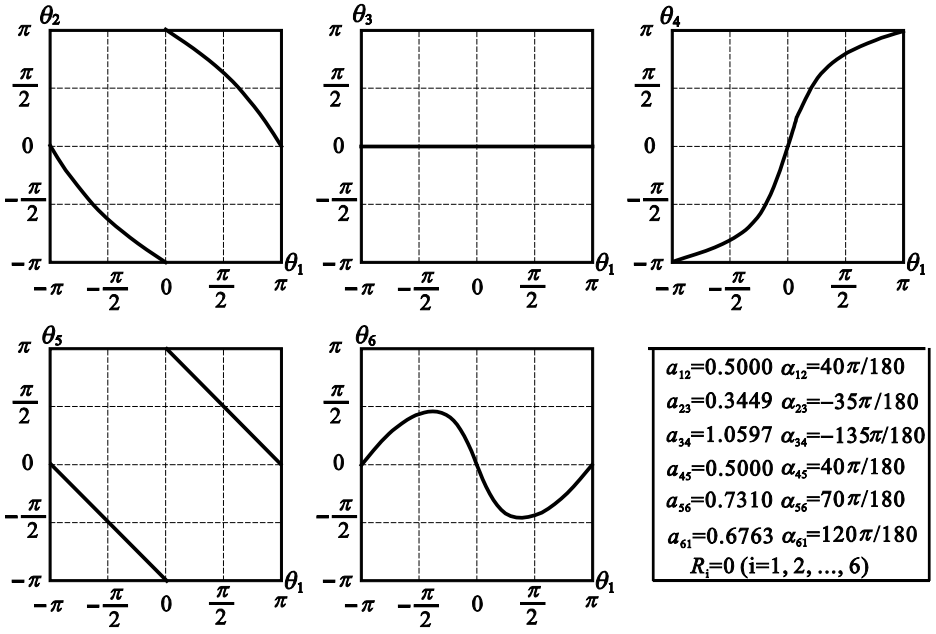

Fig. 3.4.7 The kinematic paths of the Type III mixed double-Goldberg 6*R* linkage.

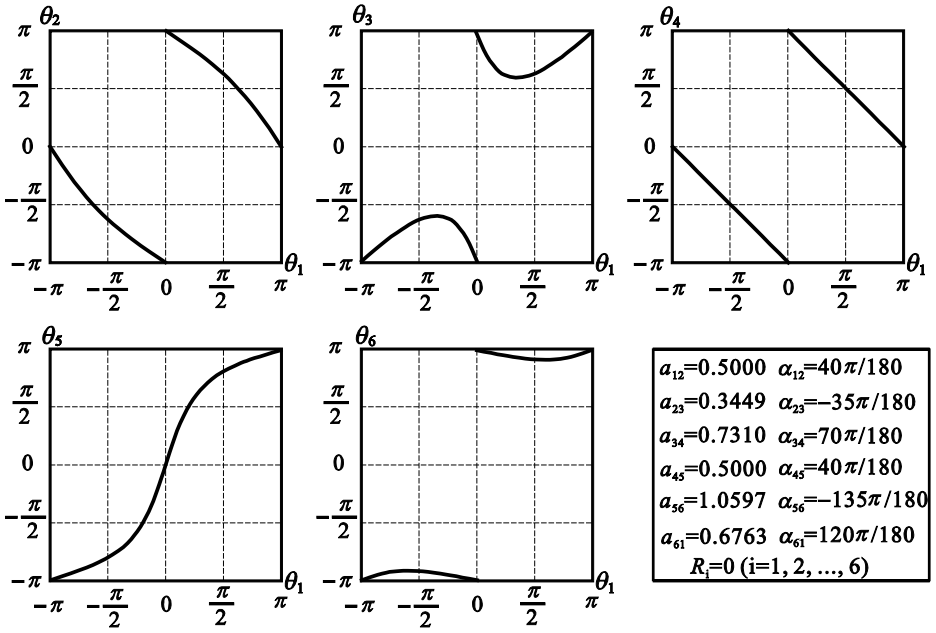

Fig. 3.4.8 The kinematic paths of the Type IV mixed double-Goldberg 6*R* linkage.

For Type III linkage, it is obvious that θ_3 is constrained to zero during the full cycle movement. The instantaneous mobility of joint 3 is locked to zero for the whole domain. Thus, the link-pair 23-34 could be viewed as a composite link 24 of $b+d\,/\,\beta+\delta$. Therefore, the Type III is equivalent to a Goldberg 5*R* linkage. For Type IV linkage, from the construct

method and geometry conditions, the Type IV can be considered as a variant of Baker's first variant of Goldberg 6*R* linkage (Baker, 1993a). As demonstrated in Table 3.3.1, the connection between S1 and G1 gives the same 6*R* linkages.

3.4.4 Types V and VI

Linkages S2 and G1 are selected to build the Types V and VI mixed double-Goldberg 6*R* linkage. Link-pair 34-45 of linkage S2 and link-pair 51-12 of linkage G1 share the same geometry conditions. They can be merged to form a common link-pair connection. After removing the connection, a Type V linkage can be obtained in Fig. 3.4.9. The geometry conditions of linkages S2 and G1 are

$$\begin{aligned}
&a_{12}^{\mathrm{S2}} = a_{34}^{\mathrm{S2}} = a\,,\ a_{23}^{\mathrm{S2}} = b - c\,,\ a_{45}^{\mathrm{S2}} = c\,,\ a_{51}^{\mathrm{S2}} = b\,,\\
&\alpha_{12}^{\mathrm{S2}} = \alpha_{34}^{\mathrm{S2}} = \alpha\,,\ \alpha_{23}^{\mathrm{S2}} = \beta - \gamma\,,\ \alpha_{45}^{\mathrm{S2}} = \gamma\,,\ \alpha_{51}^{\mathrm{S2}} = \beta\,;\\
&a_{12}^{\mathrm{G1}} = a_{34}^{\mathrm{G1}} = c\,,\ a_{23}^{\mathrm{G1}} = a + d\,,\ a_{45}^{\mathrm{G1}} = d\,,\ a_{51}^{\mathrm{G1}} = a\,,\\
&\alpha_{12}^{\mathrm{G1}} = \alpha_{34}^{\mathrm{G1}} = \gamma\,,\ \alpha_{23}^{\mathrm{G1}} = \alpha + \delta\,,\ \alpha_{45}^{\mathrm{G1}} = \delta\,,\ \alpha_{51}^{\mathrm{G1}} = \alpha\,.
\end{aligned} \tag{3.4.18}$$

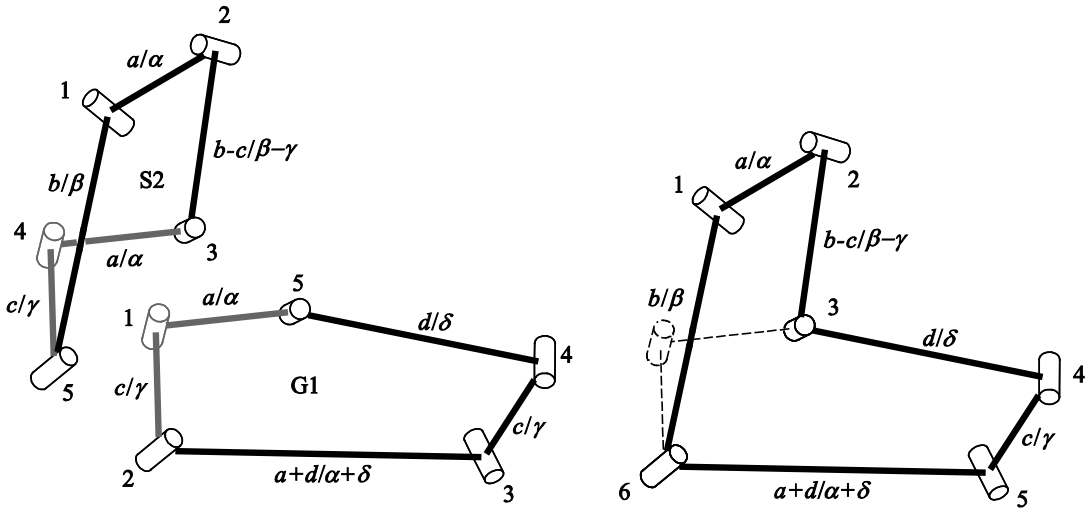

Fig. 3.4.9 The construction of the Type V mixed double-Goldberg 6*R* linkage.

Thus, the geometry conditions of the resultant 6*R* linkage can be obtained.

$$\begin{aligned} &a_{12}=a,\ a_{23}=b-c,\ a_{34}=d,\ a_{45}=c,\ a_{56}=a+d,\ a_{61}=b,\\ &\alpha_{12}=\alpha,\ \alpha_{23}=\beta-\gamma,\ \alpha_{34}=\delta,\ \alpha_{45}=\gamma,\ \alpha_{56}=\alpha+\delta,\ \alpha_{61}=\beta,\\ &\frac{\sin\alpha}{a}=\frac{\sin\beta}{b}=\frac{\sin\gamma}{c}=\frac{\sin\delta}{d},\ R_i=0\ (i=1,2,...,6). \end{aligned} \tag{3.4.19}$$

Similar to Types III and IV, we can change the connection method to the common Bennett-linkage to connect linkages S2 and G1 to obtain the Type VI linkage, see Fig. 3.4.10. The geometry conditions of the Type VI linkage are

$$\begin{aligned} &a_{12}=a,\ a_{23}=b-c,\ a_{34}=a+d,\ a_{45}=c,\ a_{56}=d,\ a_{61}=b,\\ &\alpha_{12}=\alpha,\ \alpha_{23}=\beta-\gamma,\ \alpha_{34}=\alpha+\delta,\ \alpha_{45}=\gamma,\ \alpha_{56}=\delta,\ \alpha_{61}=\beta,\\ &\frac{\sin\alpha}{a}=\frac{\sin\beta}{b}=\frac{\sin\gamma}{c}=\frac{\sin\delta}{d},\ R_i=0\ (i=1,2,...,6). \end{aligned} \tag{3.4.20}$$

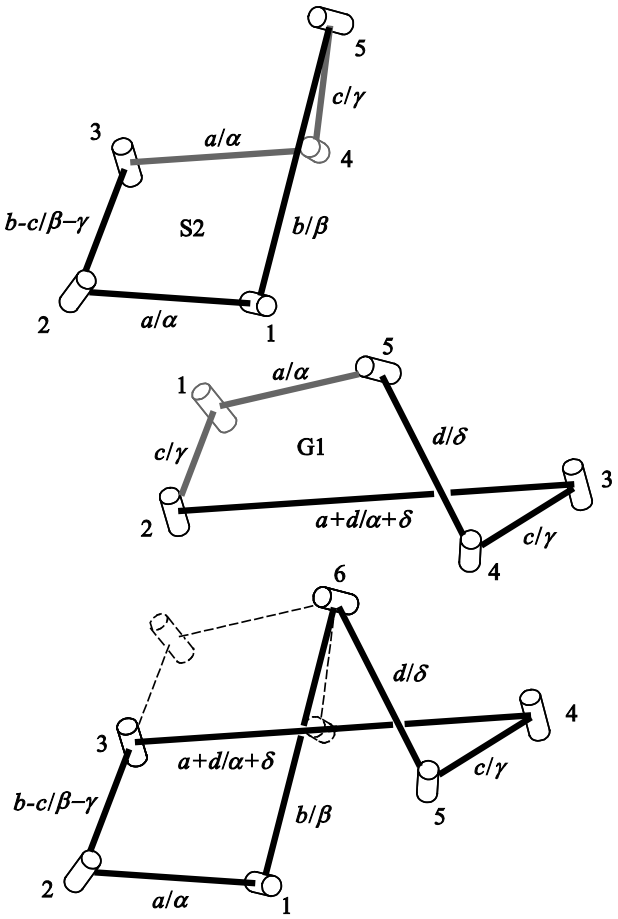

Fig. 3.4.10 The construction of the Type VI mixed double-Goldberg 6*R* linkage.

The closure equations of Types V and VI mixed double-Goldberg 6*R* linkages are derived as

$$\begin{gathered}\tan\frac{\theta_2}{2}=\frac{m_1}{\tan\dfrac{\theta_1}{2}},\ \tan\frac{\theta_3}{2}=\frac{1}{m_4\tan\dfrac{\theta_1}{2}},\\ \theta_4=\pm\pi-\theta_1,\ \theta_5=\pm\pi-\theta_3,\ \tan\frac{\theta_6}{2}=-\frac{m_1}{\tan\dfrac{\theta_1}{2}};\end{gathered}\tag{3.4.21}$$

and

$$\begin{gathered}\tan\frac{\theta_2}{2}=\frac{m_1}{\tan\dfrac{\theta_1}{2}},\ \tan\frac{\theta_3}{2}=\frac{\tan\dfrac{\theta_1}{2}}{m_2},\ \tan\frac{\theta_4}{2}=m_4\tan\frac{\theta_1}{2},\\ \theta_5=\pm\pi-\theta_1,\ \tan\frac{\theta_6}{2}=\frac{(m_4\tan^2\dfrac{\theta_1}{2}+m_1m_2m_4+m_1-m_2)\tan\dfrac{\theta_1}{2}}{(m_1m_4-m_2m_4-1)\tan^2\dfrac{\theta_1}{2}-m_1m_2},\end{gathered}\tag{3.4.22}$$

respectively. Their kinematic paths are plotted in Fig. 3.4.11 and Fig. 3.4.12.

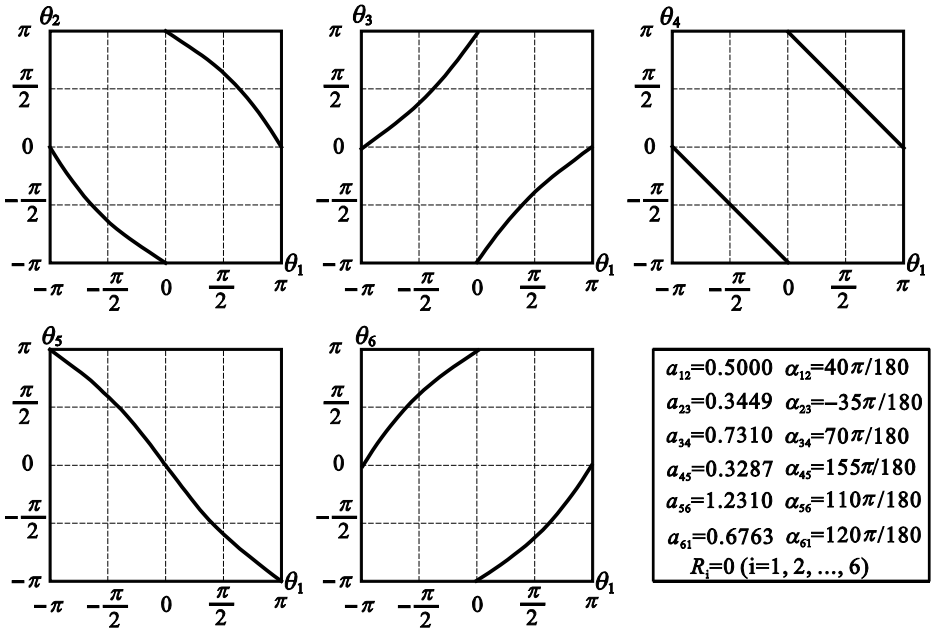

Fig. 3.4.11 The kinematic paths of the Type V mixed double-Goldberg 6*R* linkage.

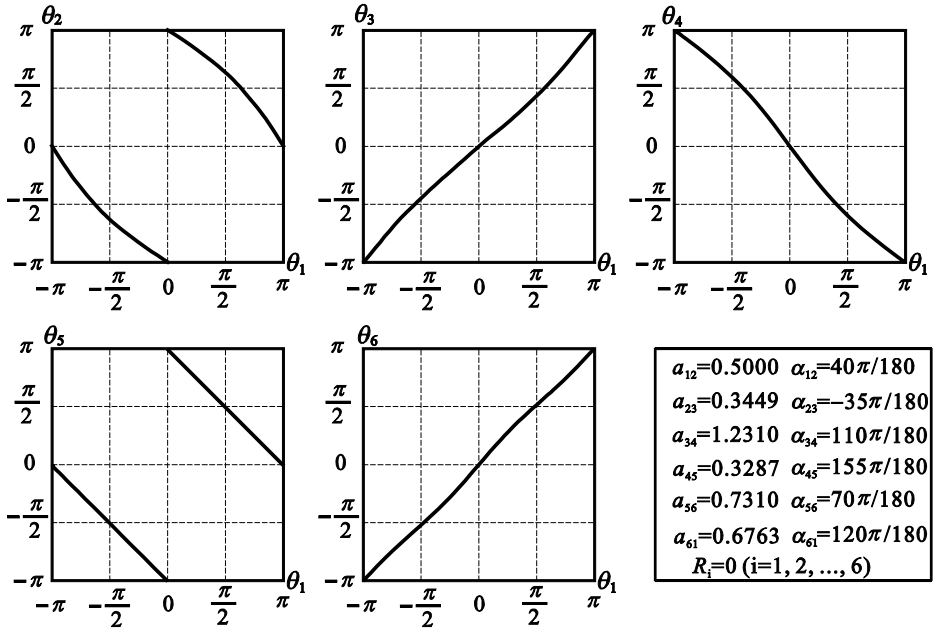

Fig. 3.4.12 The kinematic paths of the Type VI mixed double-Goldberg 6*R* linkage.

From the geometry conditions, Type V linkage is in fact a variant of Waldron's hybrid 6*R* linkage comprising of one Bennett linkage with links a/α and b/β, and another Bennett linkage with links c/γ and d/δ. And from the geometry conditions shown above, it is obvious that the Type VI is related to the *L*-shape Goldberg 6*R* linkage (Goldberg, 1943) where link 23 is in negative length (Chen and You, 2005; 2008b). Therefore, we can view the Type VI as a variant of the *L*-shape Goldberg 6*R* linkage.

3.5 SUMMARY

A new family of mixed double-Goldberg 6*R* linkages is built from the combination of a subtractive Goldberg 5*R* linkage and a Goldberg 5*R* linkage through either a common link-pair or a common Bennett-linkage. The six resultant linkages are summarized in Table 3.5.1. All of them have single mobility. Physical model of the Type V linkage is shown in Fig. 3.5.1.

Table 3.5.1 The linkage identifications of the mixed double-Goldberg linkage family.

Type	**Linkage Identification**
I	Variant of the Wohlhart's double-Goldberg 6*R* linkage
II	Variant of the Baker's first variant of Goldberg 6*R* linkage
III	The Goldberg 5*R* linkage (equivalent)
IV	Variant of the Baker's second variant of Goldberg 6*R* linkage
V	Variant of the Waldron's hybrid 6*R* linkage
VI	Variant of the *L*-shape Goldberg 6*R* linkage

(a) (b) (c)

Fig. 3.5.1 The motion segments of Type V linkage model.

All the linkages in the family of mixed double-Goldberg 6*R* linkages are built from four basic links a/α, b/β, c/γ and d/δ. After comparing the geometry conditions of each linkage type, an *extra link* c/γ is identified which plays a different role when comparing to the other three links a/α, b/β and d/δ. In the Types V and VI linkages, link c/γ is one of the six individual links in the linkage; while in Types I, II, III and IV linkages, link c/γ is not directly existed in the linkage but hidden in links such as $a+c/\alpha+\gamma$ or $b-c/\beta-\gamma$. In order to identify this extra link, we can shrink the geometry conditions of the link to zeros. When link c/γ is shrunk to none, all the linkages above will preserve a similar configuration as before. Take Type I linkage in Eq. (3.4.3) for example, when c/γ is shrunk to none, links 12 and 45 will be link a/α at the same time. In this case, Type I linkage could be identified as a Mavroidis & Roth's 6*R* linkage with zero offsets instead of a variant of Wohlhart's double-Goldberg 6*R* linkage. Similar observations could be made in other linkage types.

Here, two different types of 5*R* linkages are used to build a family of mixed double-Goldberg 6*R* linkages. As shown in Table 3.5.1, all linkages derived above belong to the Bennett-based overconstrained linkage family. Through the use of common Bennett-linkage and common link-pair between different 5*R* linkages, the relationship among a number of Bennett-based overconstrained linkages has been revealed. Alternatively, we can change our construction elements into two Goldberg 5*R* linkages or two subtractive Goldberg 5*R* linkages. All possible linkages constructed from two 5*R* linkages through either common link-pair or common Bennett-linkage are listed in Table 3.5.2 and Table 3.5.3.

Table 3.5.2 The linkages in the double-Goldberg linkage family.

<table>
<tr><td>Double-Goldberg linkage family</td><td>Wohlhart's Double-Goldberg linkage family (WDG)</td><td>Mixed Double-Goldberg linkage family (MDG)</td><td>Double-Subtractive-Goldberg linkage family (DSG)</td></tr>
<tr><td>Construct unit</td><td>2 Goldberg 5R linkages</td><td>1 Goldberg 5R linkage
and
1 subtractive-Goldberg 5R linkage</td><td>2 subtractive-Goldberg 5R linkages</td></tr>
<tr><td>Link-pair for connection</td><td colspan="2">Link-pairs 51-12 and 12-51
Link-pairs 34-45 and 45-34
Link-pairs 45-51 and 51-45</td><td> 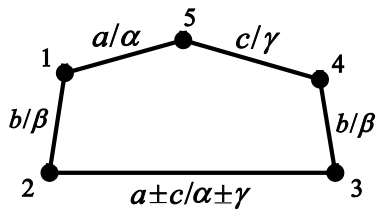
</td></tr>
<tr><td>Construct method</td><td colspan="3">Common link-pair method (CLP)
Common Bennett-linkage method (CBL)</td></tr>
<tr><td>Resultant linkage case</td><td>The original cases</td><td>The variational cases</td><td>The subtractive cases</td></tr>
<tr><td>Resultant linkage type</td><td colspan="3">Type I: the Wohlhart's double-Goldberg 6R linkage
Type II: the Baker's second variant of Goldberg 6R linkage
Type III: the (subtractive) Goldberg 5R linkage
Type IV: the Baker's first variant of Goldberg 6R linkage
Type V: the Waldron's hybrid 6R linkage
Type VI: the L-shape Goldberg 6R linkage</td></tr>
</table>

Table 3.5.3 The complete families of the double-Goldberg 6*R* linkages.

Type	**W**ohlhart's **D**ouble-**G**oldberg linkage family (***WDG***)	**M**ixed **D**ouble-**G**oldberg linkage family (***MDG***)	**D**ouble-**S**ubtractive-**G**oldberg linkage family (***DSG***)
I	Three cases of the Wohlhart's double-Goldberg 6*R* linkages		
	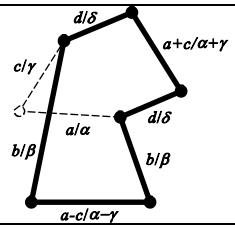	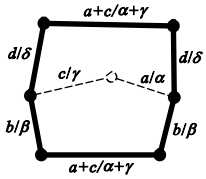	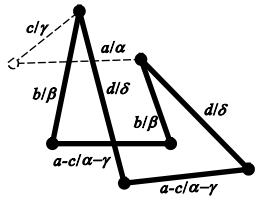
II	Three cases of the Baker's second variant of Goldberg 6*R* linkages		
	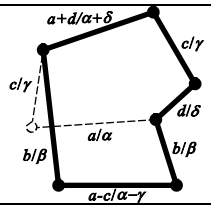	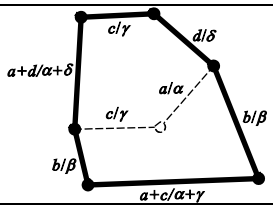	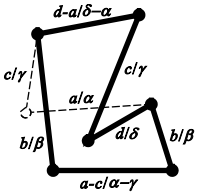
III	Three cases of the (subtractive) Goldberg 5*R* linkages		
	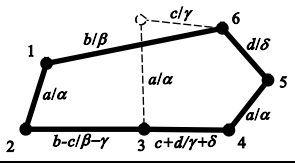	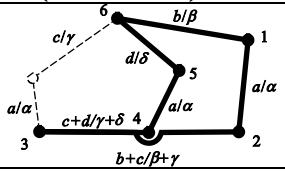	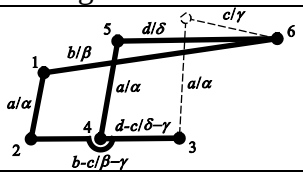
IV	Three cases of the Baker's first variant of Goldberg 6*R* linkages		
	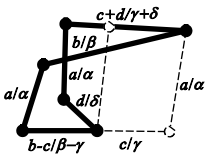	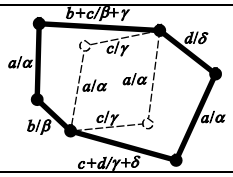	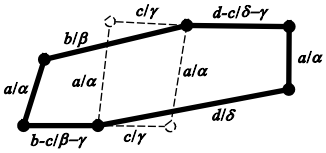
V	Three cases of the Waldron's hybrid 6*R* linkages		
	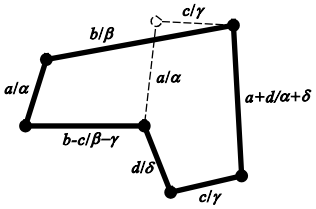	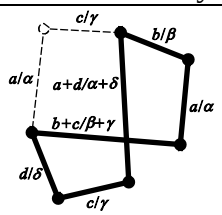	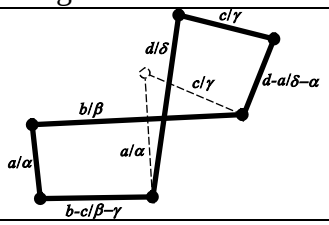
VI	Three cases of the *L*-shape Goldberg 6*R* linkages		
	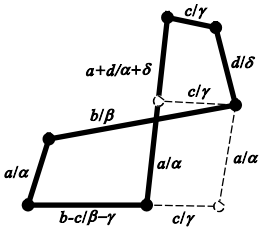	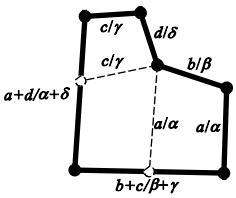	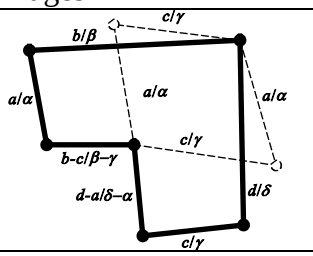

Chapter 4

The General Line-symmetric Bricard Linkage

4.1 OVERVIEW

Although the closure equations of the *original* general line-symmetric Bricard linkage have been provided by Baker (1980) in implicit form, it requires further study into its kinematics for a better understanding about the linkage. The numerical work by Mavroidis and Roth (1995) reported a *revised* general line-symmetric Bricard linkage with negatively equaled offsets on the opposite joints, whose revolute variables are also negatively equaled. In this chapter, we study the kinematics of the general line-symmetric Bricard linkage and explore the relationship between the *original* and *revised* general line-symmetric Bricard linkages. Results in this chapter motivate the design of multiple operation forms for the general line-symmetric Bricard linkage in chapter 5.

The layout of this chapter is as follows. Derivations of the explicit closure equations of the *original* and *revised* general line-symmetric Bricard linkages are included in sections 4.2 and 4.3. Discussions about the relationship between the original and revised linkages, relationship between the general line-symmetric Bricard linkage and octahedral Bricard linkage and the bifurcation behavior of the line-symmetric Bricard without zero offsets are included in section 4.4. Final remarks are drawn in section 4.5, which concludes the chapter.

4.2 THE EXPLICIT CLOSURE EQUATIONS OF THE ORIGINAL GENERAL LINE-SYMMETRIC BRICARD LINKAGE

The geometry conditions of the *original* general line-symmetric Bricard linkage are

$$\begin{gathered} a_{12}=a_{45},\ a_{23}=a_{56},\ a_{34}=a_{61}, \\ \alpha_{12}=\alpha_{45},\ \alpha_{23}=\alpha_{56},\ \alpha_{34}=\alpha_{61}, \\ R_1=R_4,\ R_2=R_5,\ R_3=R_6. \end{gathered} \tag{4.2.1}$$

Due to the line-symmetric geometry, the revolute variables of the original general line-symmetric Bricard linkage are positively equaled on the opposite joints $\theta_1=\theta_3$, $\theta_2=\theta_4$ and $\theta_3=\theta_6$ (Baker, 1980). The simplified geometry conditions of the *original* general line-symmetric Bricard linkage are

$$a_{i(i+1)}=a_{(i+3)(i+4)},\alpha_{i(i+1)}=\alpha_{(i+3)(i+4)},\ R_i=R_{(i+3)}\ \ (i=1,2,3). \tag{4.2.2}$$

Note that to ensure this is a closed-loop 6*R* mechanism, the subscripts must be the remainder of 6 in positive numbers. The closure condition is

$$\mathbf{T}_{12}\mathbf{T}_{23}\cdots\mathbf{T}_{61}=\mathbf{I}, \tag{4.2.3}$$

which could be generalized into the following form.

$$\mathbf{T}_{i(i+1)}\mathbf{T}_{(i+1)(i+2)}\mathbf{T}_{(i+2)(i+3)}=\mathbf{T}_{(i+5)i}^{-1}\mathbf{T}_{(i+4)(i+5)}^{-1}\mathbf{T}_{(i+3)(i+4)}^{-1}. \tag{4.2.4}$$

In the transformation matrix in Eq. (2.1.1), the angular parameters, including twist and revolute variable, are stored in both rotational matrix $\mathbf{Ro}_{3\times3}$ and translational vector $\mathbf{Tr}_{3\times1}$. The length parameters, including link length and offset, are stored only in the translational vector $\mathbf{Tr}_{3\times1}$. Therefore, we may firstly use the rotational matrix $\mathbf{Ro}_{3\times3}$ only to derive the relationship among the angular parameters, and then introduce the length parameters using the translational vector $\mathbf{Tr}_{3\times1}$ to derive the explicit closure equations. Here, entry (1, 1) in Eq. (4.2.4) is extracted and reformed as follows.

$$\begin{aligned}&\left(\cos\theta_i\cos\theta_{i+1}\cos\theta_{i+2}-\cos\theta_{i+3}\cos\theta_{i+4}\cos\theta_{i+5}\right)\\&-\left(\sin\theta_i\sin\theta_{i+1}\cos\theta_{i+2}-\sin\theta_{i+3}\sin\theta_{i+4}\cos\theta_{i+5}\right)\cos\alpha_{i(i+1)}\\&-\left(\cos\theta_i\sin\theta_{i+1}\sin\theta_{i+2}-\cos\theta_{i+3}\sin\theta_{i+4}\sin\theta_{i+5}\right)\cos\alpha_{(i+1)(i+2)}\\&+\left(\sin\theta_i\sin\theta_{i+2}-\sin\theta_{i+3}\sin\theta_{i+5}\right)\sin\alpha_{i(i+1)}\sin\alpha_{(i+1)(i+2)}\\&-\left(\sin\theta_i\cos\theta_{i+1}\sin\theta_{i+2}-\sin\theta_{i+3}\cos\theta_{i+4}\sin\theta_{i+5}\right)\cos\alpha_{i(i+1)}\cos\alpha_{(i+1)(i+2)}=0.\end{aligned}\tag{4.2.5}$$

Eq. (4.2.5) always holds no matter what the values of twist angles are. Thus, one non-trivial solution is when the items in every bracket of Eq. (4.2.5) are zeros, i.e.

$$\cos\theta_i\cos\theta_{i+1}\cos\theta_{i+2}-\cos\theta_{i+3}\cos\theta_{i+4}\cos\theta_{i+5}=0,\tag{4.2.6a}$$

$$\sin\theta_i\sin\theta_{i+1}\cos\theta_{i+2}-\sin\theta_{i+3}\sin\theta_{i+4}\cos\theta_{i+5}=0,\tag{4.2.6b}$$

$$\cos\theta_i\sin\theta_{i+1}\sin\theta_{i+2}-\cos\theta_{i+3}\sin\theta_{i+4}\sin\theta_{i+5}=0,\tag{4.2.6c}$$

$$\sin\theta_i\sin\theta_{i+2}-\sin\theta_{i+3}\sin\theta_{i+5}=0,\tag{4.2.6d}$$

$$\sin\theta_i\cos\theta_{i+1}\sin\theta_{i+2}-\sin\theta_{i+3}\cos\theta_{i+4}\sin\theta_{i+5}=0.\tag{4.2.6e}$$

Substituting Eq. (4.2.6d) into Eq. (4.2.6e) gives

$$\cos\theta_{i+1}=\cos\theta_{i+4}.\tag{4.2.7}$$

From Eq. (4.2.6d), we have

$$\frac{\sin\theta_{\mathrm{i}}}{\sin\theta_{i+3}}=\frac{\sin\theta_{i+5}}{\sin\theta_{i+2}}.\tag{4.2.8}$$

By substituting $i=1,2,3$ into Eqs. (4.2.7) and (4.2.8), we have

$$\cos\theta_2=\cos\theta_5,\cos\theta_3=\cos\theta_6,\cos\theta_4=\cos\theta_1,\tag{4.2.9}$$

and

$$\frac{\sin\theta_1}{\sin\theta_4}=\frac{\sin\theta_6}{\sin\theta_3}=\frac{\sin\theta_5}{\sin\theta_2}.\tag{4.2.10}$$

Considering the domain of definition that $\theta_i\in[-\pi,\pi)$ and Eqs. (4.2.6a)-(4.2.6c), the following relationships can be concluded as the solutions to Eqs. (4.2.9) and (4.2.10).

$$\text{positive relationship, } \theta_i = \theta_{i+3}; \tag{4.2.11a}$$

$$\text{and negative relationship, } \theta_i = -\theta_{i+3}. \tag{4.2.11b}$$

In the above process, entry (1, 1) of Eq. (4.2.4) is selected for the derivation of the relationships shown in Eq. (4.2.11). Alternatively, we can also use entries (2, 2) and (3, 3) in Eq. (4.2.4) to derive the same relationships in Eq. (4.2.11). Note that these entries are all located in the rotational matrix, which contains only the rotational information during coordinate transformation of the links and joints. Then, one can consider link length and offset located in the translational vector to derive the closure equations in explicit forms. Among the simplified expressions of the translational vectors shown in Eq. (4.2.12), it is clear that entry (3, 4) consists of the least unknown variables.

$$\mathbf{T}_{(1,\,4)}\left(\theta_i, \theta_{i+1}, \theta_{i+2}, \theta_{i+4}, \theta_{i+5}\right) = 0, \tag{4.2.12a}$$

$$\mathbf{T}_{(2,\,4)}\left(\theta_i, \theta_{i+1}, \theta_{i+2}, \theta_{i+4}, \theta_{i+5}\right) = 0, \tag{4.2.12b}$$

$$\mathbf{T}_{(3,\,4)}\left(\theta_{i+1}, \theta_{i+2}, \theta_{i+4}, \theta_{i+5}\right) = 0. \tag{4.2.12c}$$

By substituting the relationship in Eq. (4.2.11) into Eq. (4.2.12c), for different subscript numbers, we have that

- when $i = 1$, the relationship between θ_2 and θ_3 can be derived;
- when $i = 2$, the relationship between θ_1 and θ_3 can be derived;
- when $i = 3$, the relationship between θ_1 and θ_2 can be derived.

To derive the closure equations, θ_1 is taken as the input. Then, only the relationship between θ_1 and $\theta_{2,3}$ will be obtained in the following process. Together with Eq. (4.2.11), the complete set of closure equations for the *original* general line-symmetric Bricard linkage will be obtained in explicit forms.

4.2.1 Positive Relationship: $\theta_i = \theta_{i+3}$

Firstly, we consider the case of positive relationship in Eq. (4.2.11a) that $\theta_i = \theta_{i+3}$, where the revolute variables follow the property of line-symmetry. When $i = 3$, substituting Eq. (4.2.11a) into Eq. (4.2.12c) gives

$$\begin{aligned}
&(a_{12}\sin\alpha_{34} + a_{34}\sin\alpha_{12}\cos\alpha_{23})\sin\theta_1 \\
&-(R_2\sin\alpha_{12}\sin\alpha_{34} + R_3\sin\alpha_{12}\cos\alpha_{23}\sin\alpha_{34})\cos\theta_1 \\
&+(a_{12}\sin\alpha_{23} + a_{23}\cos\alpha_{34}\sin\alpha_{12})\sin\theta_2 \\
&-(R_1\sin\alpha_{12}\sin\alpha_{23} + R_3\sin\alpha_{12}\sin\alpha_{23}\cos\alpha_{34})\cos\theta_2 \\
&+R_3\sin\alpha_{23}\sin\alpha_{34}\sin\theta_1\sin\theta_2 \\
&+(a_{34}\cos\alpha_{12}\sin\alpha_{23} + a_{23}\sin\alpha_{34})\sin\theta_1\cos\theta_2 \\
&+(a_{23}\cos\alpha_{12}\sin\alpha_{34} + a_{34}\sin\alpha_{23})\cos\theta_1\sin\theta_2 \\
&-R_3\cos\alpha_{12}\sin\alpha_{23}\sin\alpha_{34}\cos\theta_1\cos\theta_2 \\
&+R_1(\cos\alpha_{12}\cos\alpha_{23} + \cos\alpha_{34}) + R_2(\cos\alpha_{23} + \cos\alpha_{12}\cos\alpha_{34}) \\
&+R_3(1 + \cos\alpha_{12}\cos\alpha_{23}\cos\alpha_{34}) = 0.
\end{aligned} \tag{4.2.13}$$

The above equation can be simplified as

$$\begin{aligned}
&A_2\sin\theta_1 + B_2\cos\theta_1 + C_2\sin\theta_2 + D_2\cos\theta_2 \\
&+E_2\sin\theta_1\sin\theta_2 + F_2\sin\theta_1\cos\theta_2 + G_2\cos\theta_1\sin\theta_2 + H_2\cos\theta_1\cos\theta_2 + L_2 = 0,
\end{aligned} \tag{4.2.14}$$

in which

$$\begin{cases}
A_2 = +(a_{34}\sin\alpha_{12}\cos\alpha_{23} + a_{12}\sin\alpha_{34}) \\
B_2 = -(R_3\sin\alpha_{12}\cos\alpha_{23}\sin\alpha_{34} + R_2\sin\alpha_{12}\sin\alpha_{34}) \\
C_2 = +(a_{23}\sin\alpha_{12}\cos\alpha_{34} + a_{12}\sin\alpha_{23}) \\
D_2 = -(R_3\sin\alpha_{12}\sin\alpha_{23}\cos\alpha_{34} + R_1\sin\alpha_{12}\sin\alpha_{23}) \\
E_2 = +R_3\sin\alpha_{23}\sin\alpha_{34} \\
F_2 = +(a_{34}\cos\alpha_{12}\sin\alpha_{23} + a_{23}\sin\alpha_{34}) \\
G_2 = +(a_{23}\cos\alpha_{12}\sin\alpha_{34} + a_{34}\sin\alpha_{23}) \\
H_2 = -R_3\cos\alpha_{12}\sin\alpha_{23}\sin\alpha_{34} \\
L_2 = +R_1(\cos\alpha_{12}\cos\alpha_{23} + \cos\alpha_{34}) + R_2(\cos\alpha_{23} + \cos\alpha_{12}\cos\alpha_{34}) \\
\qquad + R_3(1 + \cos\alpha_{12}\cos\alpha_{23}\cos\alpha_{34}).
\end{cases} \tag{4.2.15}$$

After tangent half-angle substitution of $\sin\theta_2$ and $\cos\theta_2$, Eq. (4.2.14) can be rewritten into

$$\begin{aligned}&\left[\left(A_2\sin\theta_1+B_2\cos\theta_1+L_2\right)-\left(D_2+F_2\sin\theta_1+H_2\cos\theta_1\right)\right]\tan^2\frac{\theta_2}{2}\\&+2\left(C_2+E_2\sin\theta_1+G_2\cos\theta_1\right)\tan\frac{\theta_2}{2}\\&+\left[\left(A_2\sin\theta_1+B_2\cos\theta_1+L_2\right)+\left(D_2+F_2\sin\theta_1+H_2\cos\theta_1\right)\right]=0.\end{aligned}\tag{4.2.16}$$

Again, Eq. (4.2.16) can be simplified as

$$Aterm_2\cdot\tan^2\frac{\theta_2}{2}+Bterm_2\cdot\tan\frac{\theta_2}{2}+Cterm_2=0,\tag{4.2.17}$$

in which θ_1 is represented in

$$\begin{cases}Aterm_2=\left(A_2\sin\theta_1+B_2\cos\theta_1+L_2\right)-\left(D_2+F_2\sin\theta_1+H_2\cos\theta_1\right)\\Bterm_2=2\left(C_2+E_2\sin\theta_1+G_2\cos\theta_1\right)\\Cterm_2=\left(A_2\sin\theta_1+B_2\cos\theta_1+L_2\right)+\left(D_2+F_2\sin\theta_1+H_2\cos\theta_1\right).\end{cases}\tag{4.2.18}$$

Solutions to Eq. (4.2.17) are

$$\tan\frac{\theta_2}{2}=\frac{-Bterm_2\pm\sqrt{Bterm_2^2-4Aterm_2\cdot Cterm_2}}{2Aterm_2},\tag{4.2.19}$$

in which all symbols are defined in Eqs. (4.2.15) and (4.2.18). The explicit relationship between θ_1 and θ_2 is therefore obtained. Similarly, by analyzing the case when $i=2$, the relationship between θ_1 and θ_3 can be derived as

$$\tan\frac{\theta_3}{2}=\frac{-Bterm_3\pm\sqrt{Bterm_3^2-4Aterm_3\cdot Cterm_3}}{2Aterm_3},\tag{4.2.20}$$

where

$$\begin{cases}Aterm_3=\left(A_3\sin\theta_1+B_3\cos\theta_1+L_3\right)-\left(D_3+F_3\sin\theta_1+H_3\cos\theta_1\right)\\Bterm_3=2\left(C_3+E_3\sin\theta_1+G_3\cos\theta_1\right)\\Cterm_3=\left(A_3\sin\theta_1+B_3\cos\theta_1+L_3\right)+\left(D_3+F_3\sin\theta_1+H_3\cos\theta_1\right).\end{cases}\tag{4.2.21}$$

and

$$\begin{cases} A_3 = +\left(a_{12}\cos\alpha_{23}\sin\alpha_{34} + a_{34}\sin\alpha_{12}\right) \\ B_3 = -\left(R_2\sin\alpha_{12}\cos\alpha_{23}\sin\alpha_{34} + R_3\sin\alpha_{12}\sin\alpha_{34}\right) \\ C_3 = +\left(a_{23}\cos\alpha_{12}\sin\alpha_{34} + a_{34}\sin\alpha_{23}\right) \\ D_3 = -\left(R_2\cos\alpha_{12}\sin\alpha_{23}\sin\alpha_{34} + R_1\sin\alpha_{23}\sin\alpha_{34}\right) \\ E_3 = +R_2\sin\alpha_{12}\sin\alpha_{23} \\ F_3 = +\left(a_{12}\sin\alpha_{23}\cos\alpha_{34} + a_{23}\sin\alpha_{12}\right) \\ G_3 = +\left(a_{23}\sin\alpha_{12}\cos\alpha_{34} + a_{12}\sin\alpha_{23}\right) \\ H_3 = -R_2\sin\alpha_{12}\sin\alpha_{23}\cos\alpha_{34} \\ L_3 = +R_1\left(\cos\alpha_{12} + \cos\alpha_{23}\cos\alpha_{34}\right) + R_2\left(1 + \cos\alpha_{12}\cos\alpha_{23}\cos\alpha_{34}\right) \\ \qquad + R_3\left(\cos\alpha_{23} + \cos\alpha_{12}\cos\alpha_{34}\right). \end{cases} \tag{4.2.22}$$

Because not all entries in the transformation matrix are used in the derivation process, the above results only demonstrate the necessary conditions for the closure relationship among the revolute variables. To ensure the closure, Eqs. (4.2.11a), (4.2.19) and (4.2.20) have been substituted back into the transformation matrix to check whether Eq. (4.2.3) is held for the geometry conditions. In such a way, two sets of closure equations are concluded to achieve different linkage closures as follows.

$$\begin{cases} \theta_2 = 2\tan^{-1}\left(\dfrac{-Bterm_2 + \sqrt{Bterm_2^2 - 4Aterm_2\cdot Cterm_2}}{2Aterm_2}\right) \\ \theta_3 = 2\tan^{-1}\left(\dfrac{-Bterm_3 - \sqrt{Bterm_3^2 - 4Aterm_3\cdot Cterm_3}}{2Aterm_3}\right), \\ \theta_4 = \theta_1 \\ \theta_5 = \theta_2 \\ \theta_6 = \theta_3 \end{cases} \tag{4.2.23}$$

and

$$\begin{cases} \theta_2 = 2\tan^{-1}\left(\dfrac{-Bterm_2 - \sqrt{Bterm_2^2 - 4Aterm_2 \cdot Cterm_2}}{2Aterm_2}\right) \\ \theta_3 = 2\tan^{-1}\left(\dfrac{-Bterm_3 + \sqrt{Bterm_3^2 - 4Aterm_3 \cdot Cterm_3}}{2Aterm_3}\right) \\ \theta_4 = \theta_1 \\ \theta_5 = \theta_2 \\ \theta_6 = \theta_3 \end{cases}. \tag{4.2.24}$$

Results in Eqs. (4.2.23) and (4.2.24) indicate that there are two distinct forms of the *original* general line-symmetric Bricard linkage, both with the property of line-symmetry, named as *Form I linkage* and *Form II linkage*, respectively. Their kinematic paths are plotted in Fig. 4.2.1 and Fig. 4.2.2. Their spatial configurations are illustrated in Fig. 4.2.3 and Fig. 4.2.4, in which the lines of symmetry are identified as the central lines in front views and dash cycles in top views. The geometry conditions of the *original* general line-symmetric Bricard linkage are set as follows.

$$a_{12} = a_{45} = 2.4000,\ a_{23} = a_{56} = 2.9000,\ a_{34} = a_{61} = 1.5000; \tag{4.2.25a}$$

$$\alpha_{12} = \alpha_{45} = 40\pi/180,\ \alpha_{23} = \alpha_{56} = 80\pi/180,\ \alpha_{34} = \alpha_{61} = 130\pi/180; \tag{4.2.25b}$$

$$R_1 = R_4 = 0.5000,\ R_2 = R_5 = 0.5500,\ R_3 = R_6 = 0.4200. \tag{4.2.25c}$$

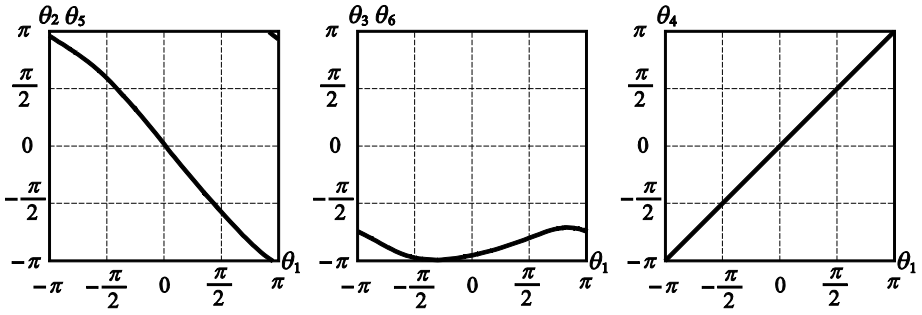

Fig. 4.2.1 The kinematic paths of the *original* Form I general line-symmetric Bricard linkage.

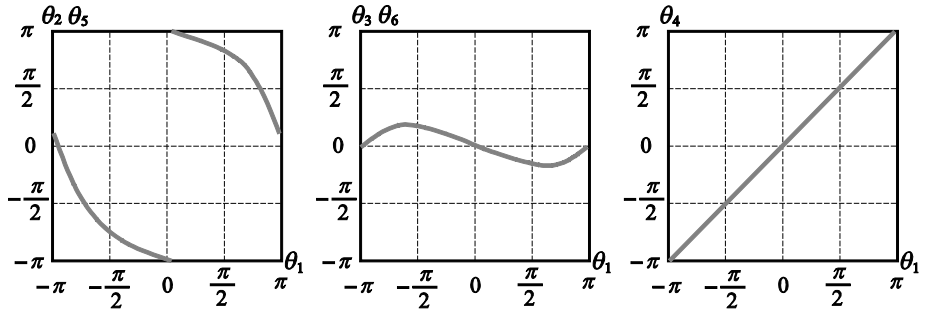

Fig. 4.2.2 The kinematic paths of the *original* Form II general line-symmetric Bricard linkage.

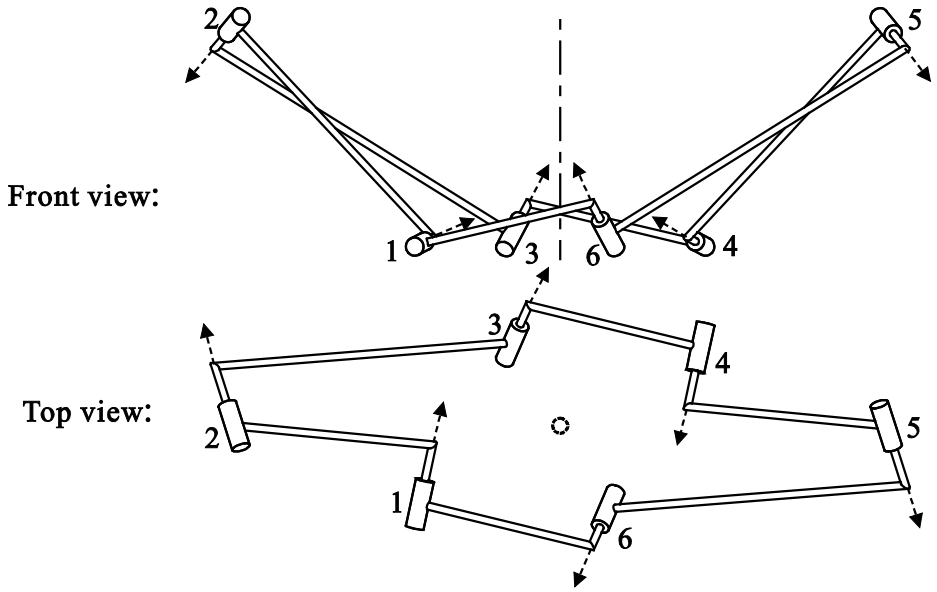

Fig. 4.2.3 The spatial configuration of the *original* Form I general line-symmetric Bricard linkage when $\theta_1^{\mathrm{I}} = 60.0000\pi/180$

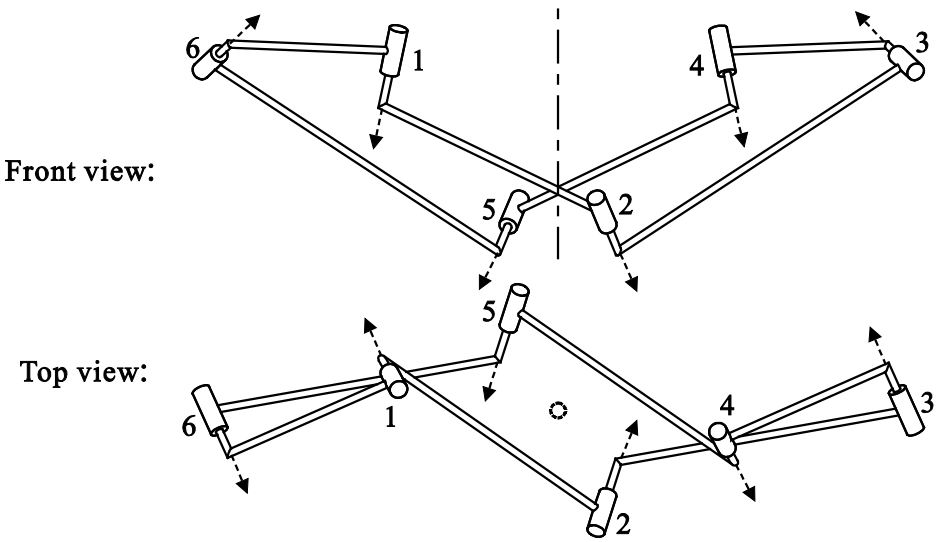

Fig. 4.2.4 The spatial configuration of the *original* Form II general line-symmetric Bricard linkage when $\theta_1^{\mathrm{II}} = 60.0000\pi/180$.

The singularity behaviors of these two linkage forms are examined with the Singular Value Decomposition method (Gan and Pellegrino, 2006; Pellegrino, 1993), which is reviewed in the Appendix A. It is found that these two kinematic paths are solely existed without any bifurcation points. As shown in Fig. 4.2.5, these two linkage forms are independent with no common configurations under the same geometry conditions.

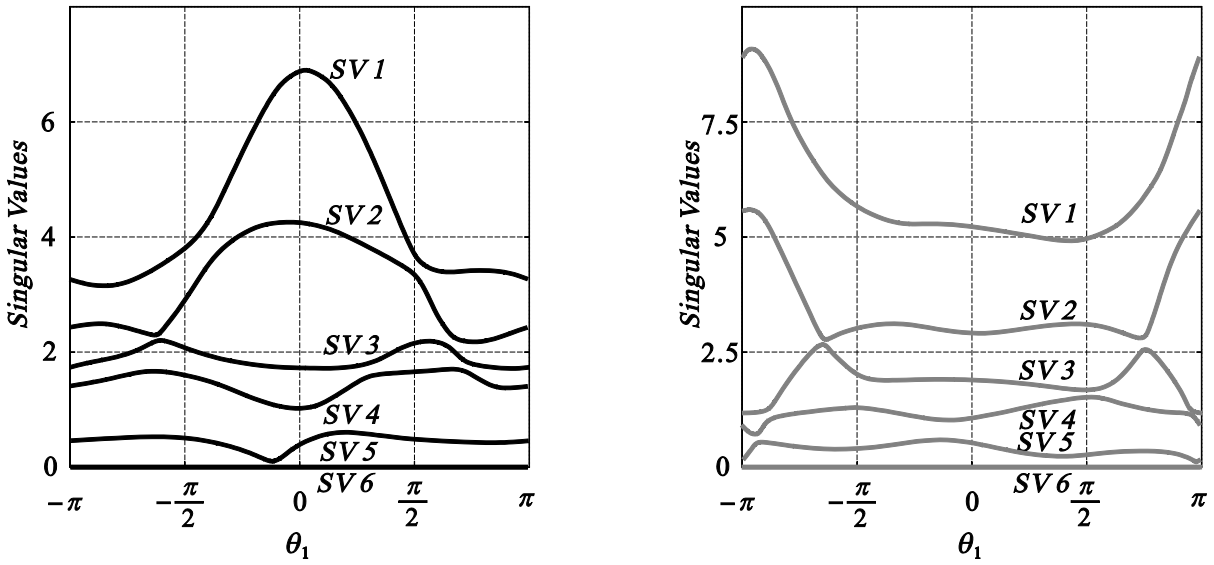

Fig. 4.2.5 The SVD results of the *original* general line-symmetric Bricard linkages: (a) Form I linkage; (b) Form II linkage.

4.2.2 Negative Relationship: $\theta_i = -\theta_{i+3}$

For the case of negative relationship, the revolute variables do not follow the line-symmetry property. We can follow the same procedure as the positive relationship to derive the closure equations. However, when substituting the results into the transformation matrix, the closure condition in Eq. (4.2.3) is not held. Thus, no linkage closure could be achieved with $\theta_i = -\theta_{i+3}$, which means that the negative relationship of $\theta_i = -\theta_{i+3}$ is just a trivial relationship for the *original* general line-symmetric Bricard linkage.

4.3 THE EXPLICIT CLOSURE EQUATIONS OF THE REVISED GENERAL LINE-SYMMETRIC BRICARD LINKAGE

Besides the *original* case, a numerical search of new and revised overconstrained linkages was conducted in (Mavroidis and Roth, 1995), where a *revised* closure of the general line-symmetric Bricard linkage was found with negatively equaled offsets on the opposite joints as below.

$$\begin{aligned} &a'_{12} = a'_{45},\ a'_{23} = a'_{56},\ a'_{34} = a'_{61}, \\ &\alpha'_{12} = \alpha'_{45},\ \alpha'_{23} = \alpha'_{56},\ \alpha'_{34} = \alpha'_{61}, \\ &R'_1 = -R'_4,\ R'_2 = -R'_5,\ R'_3 = -R'_6. \end{aligned} \tag{4.3.1}$$

The simplified geometry conditions of the *revised* general line-symmetric Bricard linkage are

$$a'_{i(i+1)} = a'_{(i+3)(i+4)}, \alpha'_{i(i+1)} = \alpha'_{(i+3)(i+4)},\ R'_i = -R'_{(i+3)}\ \ (i = 1, 2, 3). \tag{4.3.2}$$

On the geometry conditions, the only difference between the *original* and *revised* linkages is the offsets. Similar as the process in section 4.2, where entry (1, 1) is in the rotational matrix, Eq. (4.2.5) applies for both the *original* and *revised* linkages. Therefore, Eq. (4.2.11) can be obtained for the *revised* general line-symmetric Bricard linkage as well.

4.3.1 Positive Relationship: $\theta'_i = \theta'_{i+3}$

For the case of positive relationship, the revolute variables follow the line-symmetry property. We can follow the same procedure as section 4.2.1 to derive the closure equations. However, when substituting the results back into the transformation matrix, the closure condition in Eq. (4.2.3) is not held. Thus, no linkage closure could be achieved with $\theta'_i = \theta'_{i+3}$, which means the positive relationship of $\theta'_i = \theta'_{i+3}$ is just a trivial relationship for the *revised* general line-symmetric Bricard linkage.

4.3.2 Negative Relationship: $\theta_i' = -\theta_{i+3}'$

For the case of negative relationship, the same procedure could be carried out to derive the explicit closure equations. As a result, the following two sets of closure equations are concluded to produce two different linkage closures, which are called the *Form* I' and *Form* II' of the *revised* general line-symmetric Bricard linkages.

$$\begin{cases} \theta_2' = 2\tan^{-1}\left(\dfrac{-Bterm_2' + \sqrt{Bterm_2'^2 - 4Aterm_2' \cdot Cterm_2'}}{2Aterm_2'}\right) \\ \theta_3' = 2\tan^{-1}\left(\dfrac{-Bterm_3' - \sqrt{Bterm_3'^2 - 4Aterm_3' \cdot Cterm_3'}}{2Aterm_3'}\right), \\ \theta_4' = -\theta_1' \\ \theta_5' = -\theta_2' \\ \theta_6' = -\theta_3' \end{cases} \tag{4.3.3}$$

and

$$\begin{cases} \theta_2' = 2\tan^{-1}\left(\dfrac{-Bterm_2' - \sqrt{Bterm_2'^2 - 4Aterm_2' \cdot Cterm_2'}}{2Aterm_2'}\right) \\ \theta_3' = 2\tan^{-1}\left(\dfrac{-Bterm_3' + \sqrt{Bterm_3'^2 - 4Aterm_3' \cdot Cterm_3'}}{2Aterm_3'}\right), \\ \theta_4' = -\theta_1' \\ \theta_5' = -\theta_2' \\ \theta_6' = -\theta_3' \end{cases} \tag{4.3.4}$$

where

$$\begin{cases} Aterm_2' = \left(A_2' \sin\theta_1' + B_2' \cos\theta_1' + L_2'\right) - \left(D_2' + F_2' \sin\theta_1' + H_2' \cos\theta_1'\right) \\ Bterm_2' = 2\left(C_2' + E_2' \sin\theta_1' + G_2' \cos\theta_1'\right) \\ Cterm_2' = \left(A_2' \sin\theta_1' + B_2' \cos\theta_1' + L_2'\right) + \left(D_2' + F_2' \sin\theta_1' + H_2' \cos\theta_1'\right), \end{cases} \tag{4.3.5}$$

$$\begin{cases} A'_2 = +\left(a'_{34}\sin\alpha'_{12}\cos\alpha'_{23} - a'_{12}\sin\alpha'_{34}\right) \\ B'_2 = +\left(R'_3\sin\alpha'_{12}\cos\alpha'_{23}\sin\alpha'_{34} + R'_2\sin\alpha'_{12}\sin\alpha'_{34}\right) \\ C'_2 = -\left(a'_{23}\sin\alpha'_{12}\cos\alpha'_{34} - a'_{12}\sin\alpha'_{23}\right) \\ D'_2 = +\left(R'_3\sin\alpha'_{12}\sin\alpha'_{23}\cos\alpha'_{34} - R'_1\sin\alpha'_{12}\sin\alpha'_{23}\right) \\ E'_2 = -R'_3\sin\alpha'_{23}\sin\alpha'_{34} \\ F'_2 = +\left(a'_{34}\cos\alpha'_{12}\sin\alpha'_{23} - a'_{23}\sin\alpha'_{34}\right) \\ G'_2 = -\left(a'_{23}\cos\alpha'_{12}\sin\alpha'_{34} - a'_{34}\sin\alpha'_{23}\right) \\ H'_2 = +R'_3\cos\alpha'_{12}\sin\alpha'_{23}\sin\alpha'_{34} \\ L'_2 = +R'_1\left(\cos\alpha'_{12}\cos\alpha'_{23} - \cos\alpha'_{34}\right) + R'_2\left(\cos\alpha'_{23} - \cos\alpha'_{12}\cos\alpha'_{34}\right) \\ \qquad + R'_3\left(1 - \cos\alpha'_{12}\cos\alpha'_{23}\cos\alpha'_{34}\right), \end{cases} \tag{4.3.6}$$

and

$$\begin{cases} Aterm'_3 = \left(A'_3\sin\theta'_1 + B'_3\cos\theta'_1 + L'_3\right) - \left(D'_3 + F'_3\sin\theta'_1 + H'_3\cos\theta'_1\right) \\ Bterm'_3 = 2\left(C'_3 + E'_3\sin\theta'_1 + G'_3\cos\theta'_1\right) \\ Cterm'_3 = \left(A'_3\sin\theta'_1 + B'_3\cos\theta'_1 + L'_3\right) + \left(D'_3 + F'_3\sin\theta'_1 + H'_3\cos\theta'_1\right), \end{cases} \tag{4.3.7}$$

$$\begin{cases} A'_3 = -\left(a'_{12}\cos\alpha'_{23}\sin\alpha'_{34} - a'_{34}\sin\alpha'_{12}\right) \\ B'_3 = +\left(R'_2\sin\alpha'_{12}\cos\alpha'_{23}\sin\alpha'_{34} + R'_3\sin\alpha'_{12}\sin\alpha'_{34}\right) \\ C'_3 = -\left(a'_{23}\cos\alpha'_{12}\sin\alpha'_{34} - a'_{34}\sin\alpha'_{23}\right) \\ D'_3 = +\left(R'_2\cos\alpha'_{12}\sin\alpha'_{23}\sin\alpha'_{34} + R'_1\sin\alpha'_{23}\sin\alpha'_{34}\right) \\ E'_3 = +R'_2\sin\alpha'_{12}\sin\alpha'_{23} \\ F'_3 = -\left(a'_{12}\sin\alpha'_{23}\cos\alpha'_{34} - a'_{23}\sin\alpha'_{12}\right) \\ G'_3 = -\left(a'_{23}\sin\alpha'_{12}\cos\alpha'_{34} - a'_{12}\sin\alpha'_{23}\right) \\ H'_3 = +R'_2\sin\alpha'_{12}\sin\alpha'_{23}\cos\alpha'_{34} \\ L'_3 = +R'_1\left(\cos\alpha'_{12} - \cos\alpha'_{23}\cos\alpha'_{34}\right) + R'_2\left(1 - \cos\alpha'_{12}\cos\alpha'_{23}\cos\alpha'_{34}\right) \\ \qquad + R'_3\left(\cos\alpha'_{23} - \cos\alpha'_{12}\cos\alpha'_{34}\right). \end{cases} \tag{4.3.8}$$

The following geometry conditions are used to plot the kinematic paths in Fig. 4.3.1 and Fig. 4.3.2 using Eqs. (4.3.3) and (4.3.4), respectively. The spatial configurations of these two linkage closures are plotted in Fig. 4.3.3 and Fig. 4.3.4, respectively. Note that the twists on links 34 and 61 in Eq. (4.2.25) differ from the twists on links $3'4'$ and $6'1'$ in Eq. (4.3.9) by π. And the offsets are negatively equaled in Eq. (4.3.9c).

$$a'_{12} = a'_{45} = 2.40,\ a'_{23} = a'_{56} = 2.90,\ a'_{34} = a'_{61} = 1.50\,; \tag{4.3.9a}$$

$$\alpha'_{12} = \alpha'_{45} = 40\pi/180,\ \alpha'_{23} = \alpha'_{56} = 80\pi/180,\ \alpha'_{34} = \alpha'_{61} = -50\pi/180\,; \tag{4.3.9b}$$

$$R'_1 = -R'_4 = 0.50,\ R'_2 = -R'_5 = 0.55,\ R'_3 = -R'_6 = 0.42\,. \tag{4.3.9c}$$

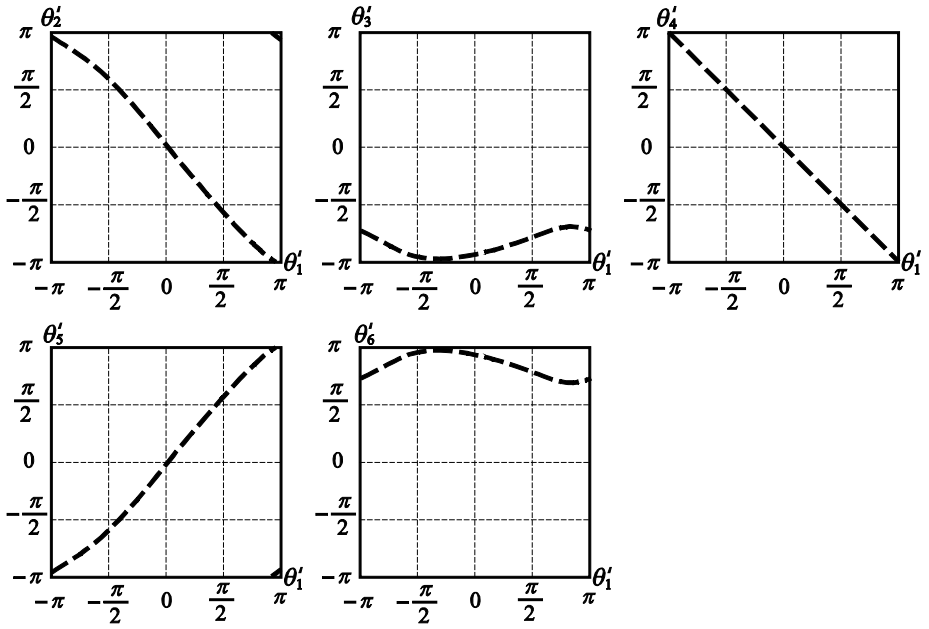

Fig. 4.3.1 The kinematic paths of the *revised* Form I′ general line-symmetric Bricard linkage.

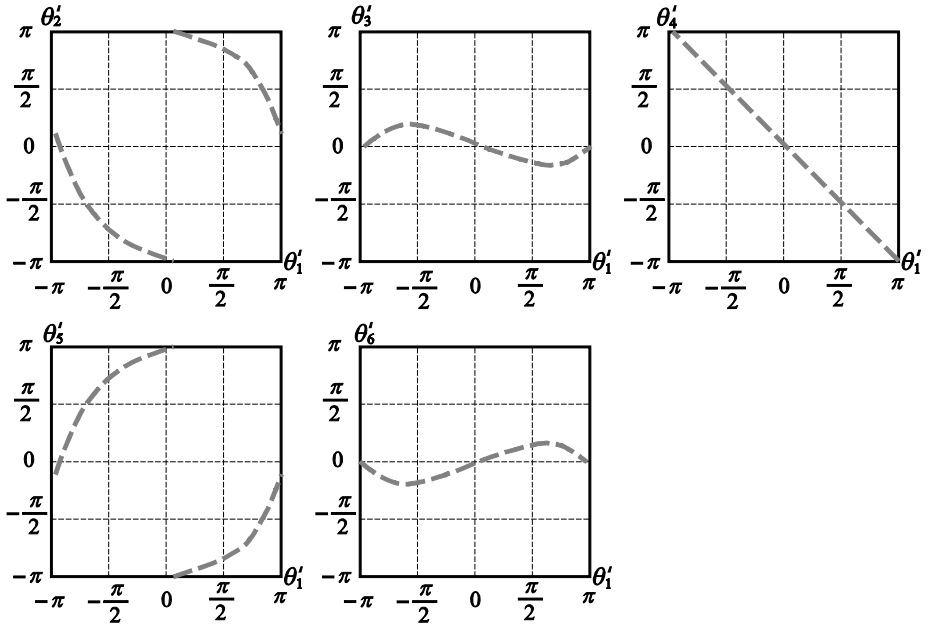

Fig. 4.3.2 The kinematic paths of the *revised* Form II′ general line-symmetric Bricard linkage.

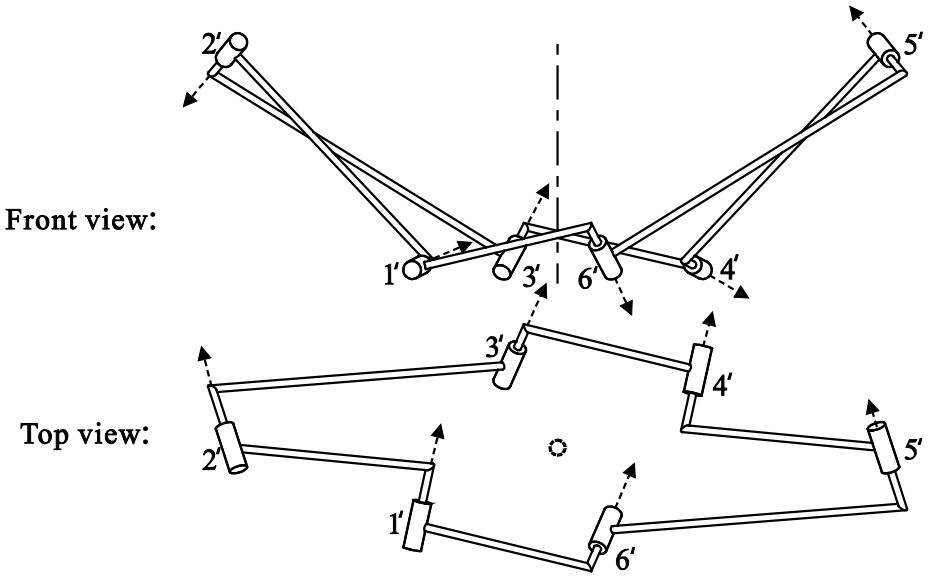

Fig. 4.3.3 The spatial configuration of the *revised* Form I′ general line-symmetric Bricard linkage when $\theta_1^{\mathrm{I}'} = 60.0000\pi/180$

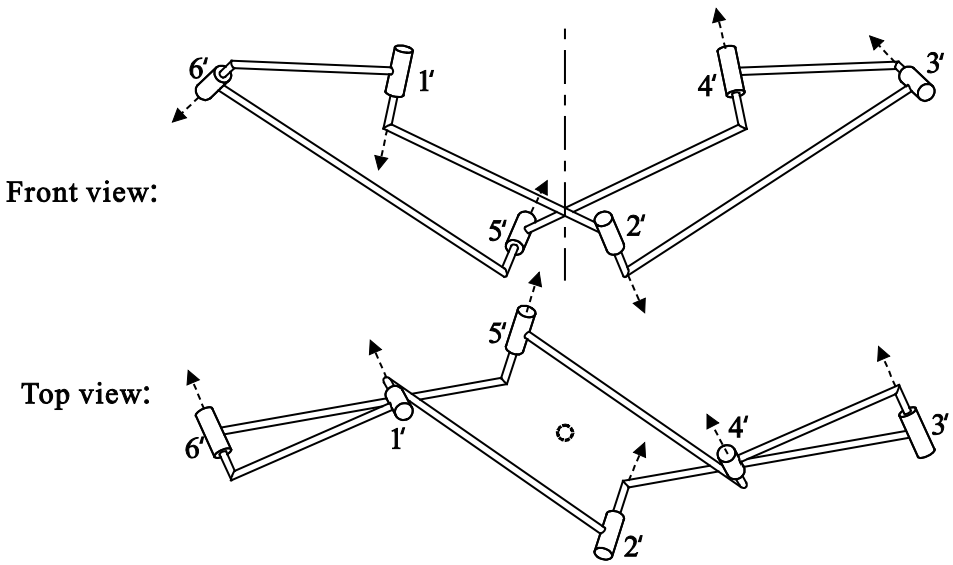

Fig. 4.3.4 The spatial configuration of the *revised* Form II′ general line-symmetric Bricard linkage when $\theta_1^{\mathrm{II}'} = 60.0000\pi/180$.

4.4 DISCUSSIONS

4.4.1 Relationship between the Original and Revised General Line-symmetric Bricard Linkages

By comparing the explicit closure equations of the *original* general line-symmetric Bricard linkage in Eqs. (4.2.23) and (4.2.24) with the *revised* general line-symmetric Bricard linkage's in Eqs. (4.3.3) and (4.3.4), it can be found that when

$$\begin{gathered} a_{12}=a'_{12}=a_{45}=a'_{45},\ a_{23}=a'_{23}=a_{56}=a'_{56},\ a_{34}=a'_{34}=a_{61}=a'_{61}, \\ \alpha_{12}=\alpha'_{12}=\alpha_{45}=\alpha'_{45},\ \alpha_{23}=\alpha'_{23}=\alpha_{56}=\alpha'_{56},\ \alpha_{34}=\alpha'_{34}\pm\pi=\alpha_{61}=\alpha'_{61}\pm\pi, \\ R_1=R'_1=R_4=-R'_4,\ R_2=R'_2=R_5=-R'_5,\ R_3=R'_3=R_6=-R'_6, \end{gathered} \tag{4.4.1}$$

we will have

$$\theta_1=\theta'_1,\theta_2=\theta'_2,\theta_3=\theta'_3,\theta_4=-\theta'_4,\theta_5=-\theta'_5,\theta_6=-\theta'_6\ , \tag{4.4.2}$$

for both linkage forms, which has been confirmed by the kinematic paths in Fig. 4.2.1, Fig. 4.2.2, Fig. 4.3.1 and Fig. 4.3.2. Even though the geometry conditions and revolute variables in the *revised* general line-symmetric Bricard linkage are not line-symmetric, the spatial configurations of the resultant linkages in Fig. 4.3.3 and Fig. 4.3.4 are still in a line-symmetric manner. In fact, with the geometric parameters in Eqs. (4.2.25) and (4.3.9) which satisfies Eq. (4.4.1), the spatial configurations of the *revised* Forms I′ and II′ linkages in Fig. 4.3.3 and Fig. 4.3.4 are the same as the *original* Forms I and II linkages' in Fig. 4.2.3 and Fig. 4.2.4.

Take the Form I of the *original* and *revised* general line-symmetric Bricard linkages for example, the joints 4, 5, 6 in Fig. 4.4.1(a) and (b) are in opposite directions due to $\alpha_{34}=\alpha'_{34}\pm\pi=\alpha_{61}=\alpha'_{61}\pm\pi$. As a result, $\theta_4=-\theta'_4,\theta_5=-\theta'_5,\theta_6=-\theta'_6$. The same analysis could be carried out for the relationship between the Form II *original* and *revised* linkages.

The *original* and *revised* linkages are actually equivalent to each other with different setups on joint axis directions.

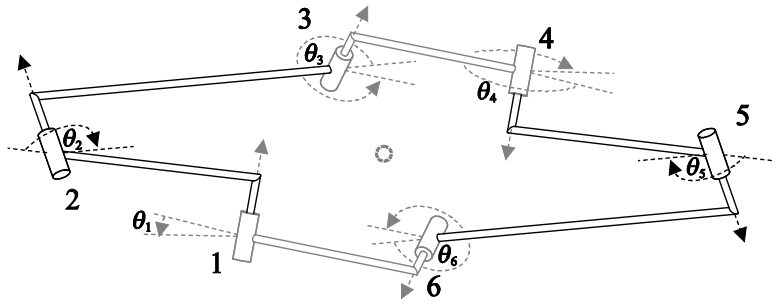

(a)

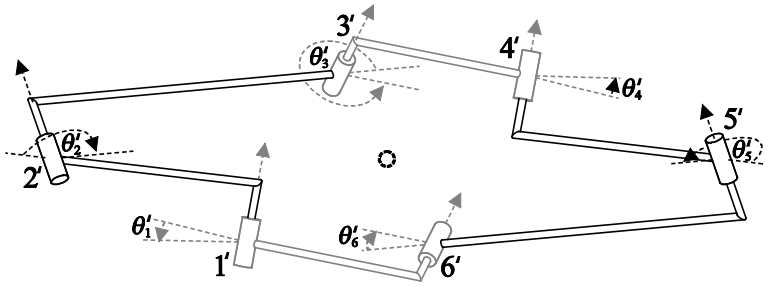

(b)

Fig. 4.4.1 The illustrations of the general line-symmetric Bricard linkage: (a) the *original* Form I linkage; (b) the *revised* Form I′ linkage.

4.4.2 Relationship with the General Line-symmetric Octahedral Bricard Linkage

For the general line-symmetric octahedral Bricard linkage as a special case of the general line-symmetric Bricard linkage, we can substitute $a_{i(i+1)} = 0 \ \left(i = 1, 2, ..., 6\right)$ into the two sets of closure equations of the general line-symmetric Bricard linkage to give the closure equations of the line-symmetric octahedral Bricard linkage. As shown in Fig. 4.4.2, it is found that the closure equations of each linkage form can only produce half of the kinematic paths in the line-symmetric octahedral Bricard linkage, which can be joined together to form a full-cycle movement at points $\mathrm{P_I}$ and $\mathrm{P_{II}}$. When the revolute variables are in negative relationship, no closure can be achieved for the line-symmetric octahedral Bricard linkage. The results in Fig. 4.4.2 comply with previous results in (Chai and Chen, 2010; Lee, 1996).

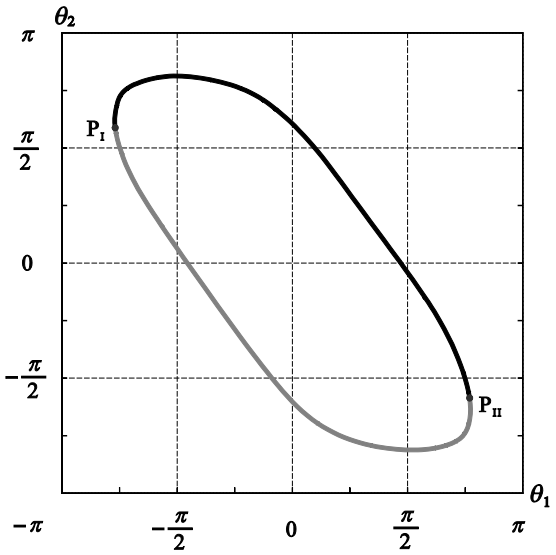

Fig. 4.4.2 The kinematic paths of the line-symmetric octahedral Bricard linkage, where the geometry conditions are the same as Eq. (4.2.25) with $a_{i(i+1)} = 0$. The black solid line is from the closure equations of the Form I linkage; the grey solid line is from those of the Form II linkage.

4.4.3 Special Case of the Line-symmetric Bricard Linkage with Zero Offsets

One case of special interests is the linkage with all zero offsets in Eqs. (4.2.2) and (4.3.2), whose closure equations can be obtained by substituting $R_i = 0$ $(i = 1, 2, ..., 6)$ into the closure equations derived above. The geometry conditions of the resultant linkages become

$$a_{i(i+1)} = a_{(i+3)(i+4)}, \alpha_{i(i+1)} = \alpha_{(i+3)(i+4)}, \ R_i = 0 \ (i = 1, 2, ..., 6). \tag{4.4.3}$$

In this case, the *original* and *revised* general line-symmetric Bricard linkages have the same geometry conditions as Eq. (4.4.3). The kinematic paths of the Forms I and II of the *original* and *revised* line-symmetric Bricard linkages are plotted in Fig. 4.4.3~Fig. 4.4.6, where the parameters are the same as Eq. (4.2.25) with $R_i = 0$. From the conclusion in section 4.4.1, the *revised* linkages in Fig. 4.4.5 and Fig. 4.4.6 are equivalent to another *original* linkage with $\alpha_{34} = \alpha_{61} = -50\pi/180$.

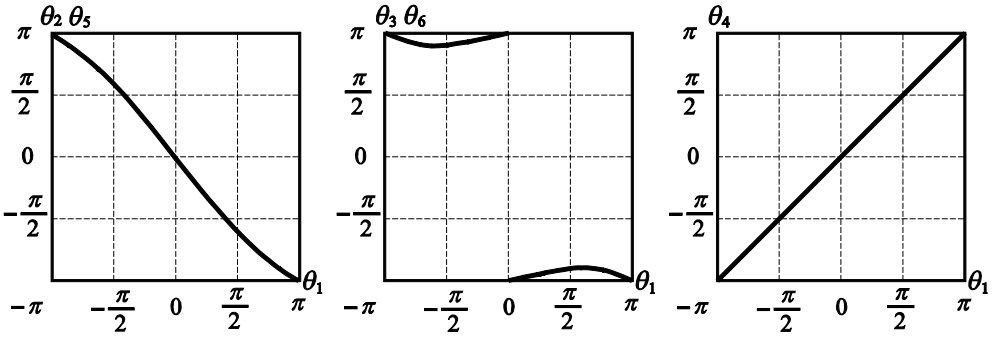

Fig. 4.4.3 The kinematic paths of the *original* Form I line-symmetric Bricard linkage with zero offset.

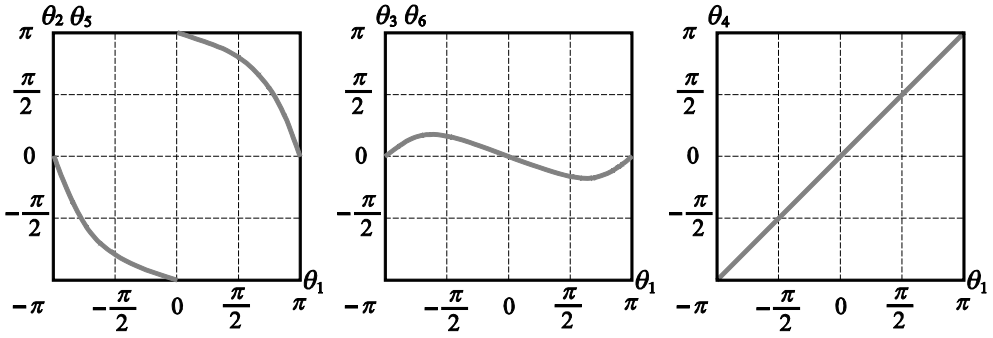

Fig. 4.4.4 The kinematic paths of the *original* Form II line-symmetric Bricard linkage with zero offset.

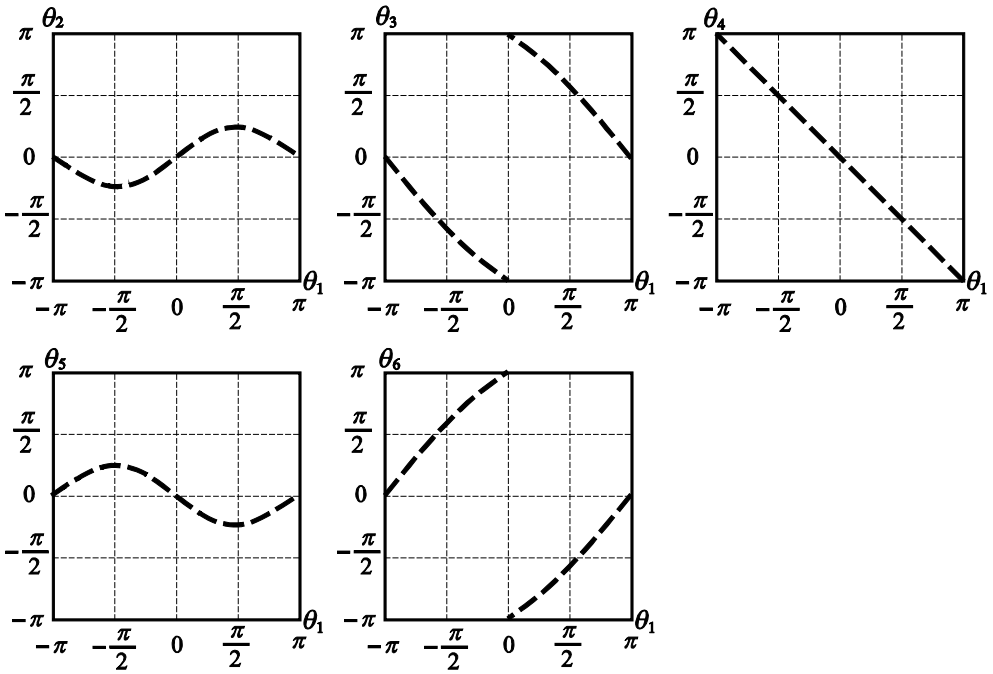

Fig. 4.4.5 The kinematic paths of the *revised* Form I′ line-symmetric Bricard linkage with zero offset.

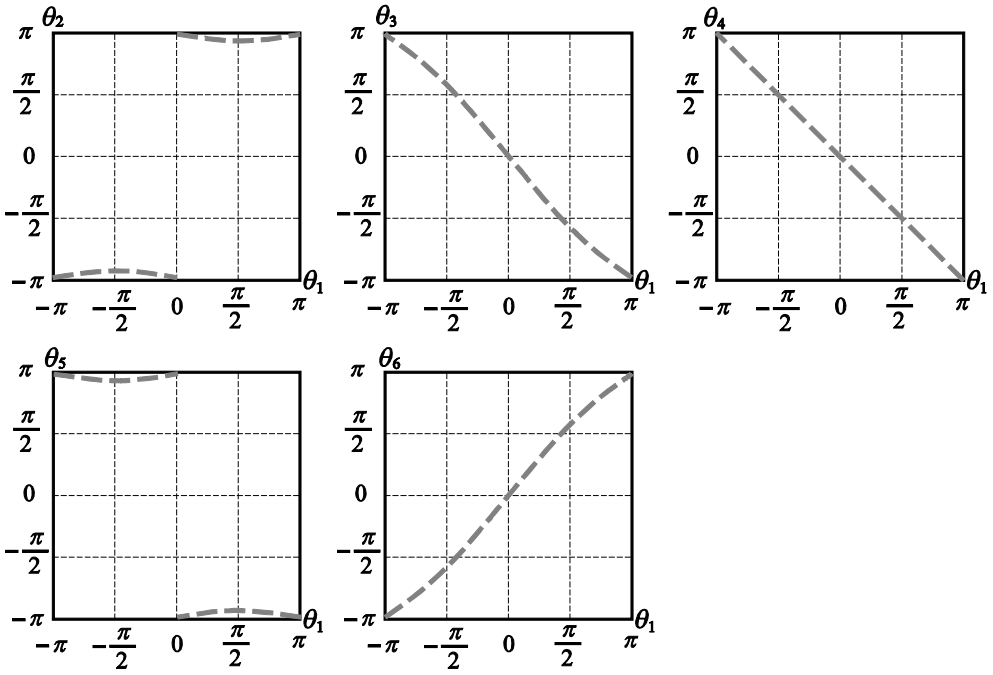

Fig. 4.4.6 The kinematic paths of the *revised* Form II′ line-symmetric Bricard linkage with zero offset.

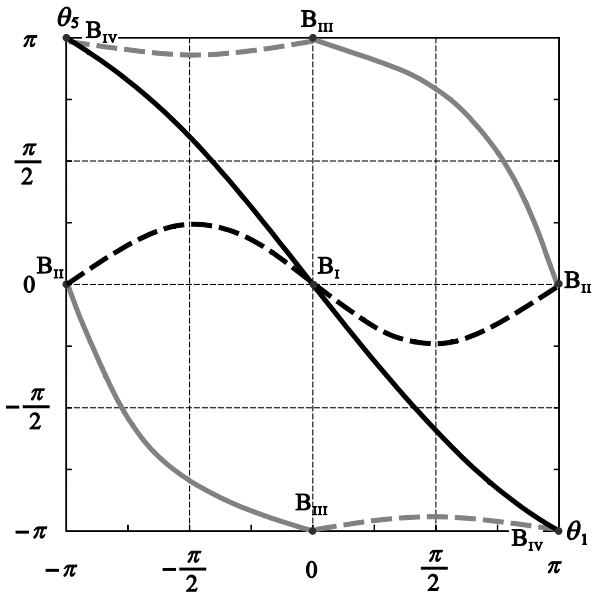

Fig. 4.4.7 The transformation among the four forms of the line-symmetric Bricard 6*R* linkage with zero offsets. The black and grey solid lines are the *original* Forms I and II line-symmetric Bricard linkages; while the black and grey dash lines are the *revised* Forms I′ and II′ line-symmetric Bricard linkages.

From the above kinematic paths, certain common configurations of the linkage are found which enable bifurcations between the *original* and *revised* linkage forms. As shown in Fig. 4.4.7, bifurcation points B_I, B_{II}, B_{III} and B_{IV}, are identified on the kinematic paths of these

four linkage forms. The relationship between θ_1 and θ_5 is used in Fig. 4.4.7 to demonstrate the transformation among different linkage forms.

As shown in Fig. 4.4.7, when the *original* Form I linkage in black solid line moves to $\theta_1 = 0$ at B_I, it can bifurcate into the kinematic paths of *revised* Form I′ linkage in black dash line. Then, when the *revised* Form I′ linkage in black dash line moves to $\theta_1 = \pi$ at B_{II}, it can bifurcate into the kinematic paths of *original* Form II linkage in grey solid lines. When the *original* Form II linkage in grey solid lines moves to $\theta_1 = 0$ at B_{III}, it can bifurcate into the kinematic paths of *revised* Form II′ linkage in grey dash lines. Finally, when the *revised* Form II′ linkage in grey dash lines moves to $\theta_1 = -\pi$ at B_{IV}, it can bifurcate back to the kinematic paths of *original* Form I linkage in black solid lines. As a result, a full map of bifurcation among these four linkage forms with the identical geometry conditions is obtained. Such bifurcation behavior in the line-symmetric Bricard linkage without offsets makes it a good source of design for reconfigurable mechanisms.

4.5 SUMMARY

In this chapter, the kinematics of the general line-symmetric Bricard linkage is investigated through the algebraic derivation of its explicit closure equations. It is found that there are two independent linkage forms of the *original* general line-symmetric Bricard linkage, which are called the Form I linkage and Form II linkage under the same geometry conditions. A *revised* general line-symmetric Bricard linkage is also investigated with negatively equaled offsets on the opposite joints. Further analysis shows that the *original* and *revised* linkages are equivalent with different setups on the joint axis directions. The closure equations of the general line-symmetric Bricard linkage could also be used to analyze the line-symmetric

octahedral Bricard linkage, whose link lengths are zeros. The result for the line-symmetric octahedral Bricard linkage comply with the result in (Chai and Chen, 2010; Lee, 1996), which verifies that the line-symmetric octahedral Bricard linkage is a special case of the general line-symmetric Bricard linkage. Investigations are made to the line-symmetric Bricard linkage with zero offsets. Since there are no offsets, the geometry conditions of the *original* and *revised* linkages become identical. When substituted with the same geometry conditions, these four linkage forms, two forms from the *original* linkage closure and two forms from the *revised* linkage closure, could transform into each other through bifurcation points. Such bifurcation behavior makes this linkage a good source of design for reconfigurable mechanism. In fact, this property explains the multiple forms and bifurcation behaviors of the Wohlhart's double-Goldberg 6*R* linkage and the double-subtractive-Goldberg 6*R* linkages (Song and Chen, 2011; Wohlhart, 1991a), which can be isomerized into a line-symmetric Bricard linkage with zero offsets (Wohlhart, 1991b). The results found here provide an in-depth understanding to the kinematics of the general line-symmetric Bricard linkage, which will be used in chapter 5 for the design of general line-symmetric Bricard linkage with multiple operation forms.

Chapter 5

Reconfigurable Mechanism Design

5.1 OVERVIEW

This chapter explores the possibilities and methodologies to design reconfigurable mechanisms based on overconstrained linkages. The layout of this chapter is as follows. Section 5.2 focuses on the design of double-Goldberg linkages with multiple operation forms using analytical method. Section 5.3 focuses on the design of general line-symmetric Bricard linkage with multiple operation forms using construct method. Section 5.4 presents a network of Bennett linkages with reconfiguration potentials using generic method.

5.2 MULTIPLE OPERATION FORMS OF THE DOUBLE-GOLDBERG LINKAGES

5.2.1 Two Cases of Double-Goldberg 6*R* Linkages

In the Goldberg 5*R* linkage and the subtractive Goldberg 5*R* linkage shown in Fig. 5.2.1, the link-pair $a/\alpha \sim c/\gamma$ in grey color are referred to as the *roof-links*, which is opposite to the composite links $a+c/\alpha+\gamma$ or $a-c/\alpha-\gamma$. The Bennett ratios of links a/α, b/β and c/γ are equal.

(a) (b)

Fig. 5.2.1 Two types of 5*R* linkages: (a) the Goldberg 5*R* linkage, (b) the subtractive Goldberg 5*R* linkage.

A closed loop overconstrained 6*R* linkage can be obtained when merging two 5*R* linkages on the common roof-links. The geometry conditions of this 6*R* linkage are

$$\begin{gathered} a_{12} = a_{45} = a \pm c\,,\ a_{23} = a_{61} = d\,,\ a_{34} = a_{56} = b\,, \\ \alpha_{12} = \alpha_{45} = \alpha \pm \gamma\,,\ \alpha_{23} = \alpha_{61} = \delta\,,\ \alpha_{34} = \alpha_{56} = \beta\,, \\ \frac{\sin\alpha}{a} = \frac{\sin\beta}{b} = \frac{\sin\gamma}{c} = \frac{\sin\delta}{d}, \\ R_i = 0\ (i = 1, 2, ..., 6). \end{gathered} \tag{5.2.1}$$

in which, '+' is for Wohlhart's double-Goldberg 6*R* linkage (Wohlhart, 1991a) and '-' is for the double-subtractive-Goldberg 6*R* linkage. Recent study found that both linkages have two different constructive forms, namely Forms I and II linkages (Song and Chen, 2011), see Fig. 5.2.2 and Fig. 5.2.3 .

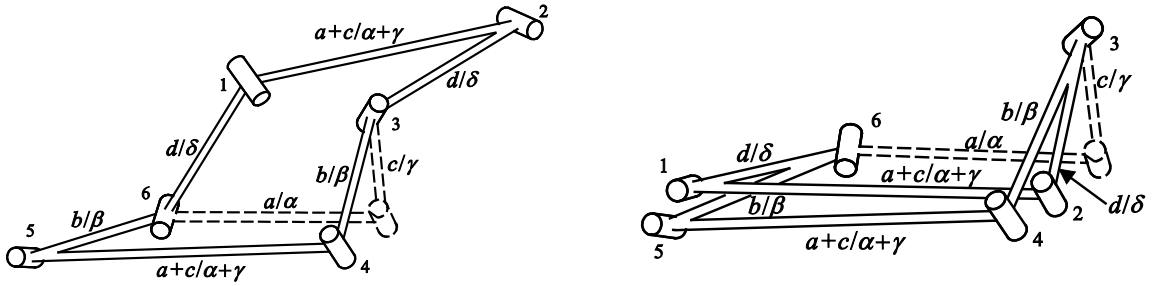

Fig. 5.2.2 The constructive forms of the Wohlhart's double Goldberg 6*R* linkage: (a) Form I linkage; (b) Form II linkage.

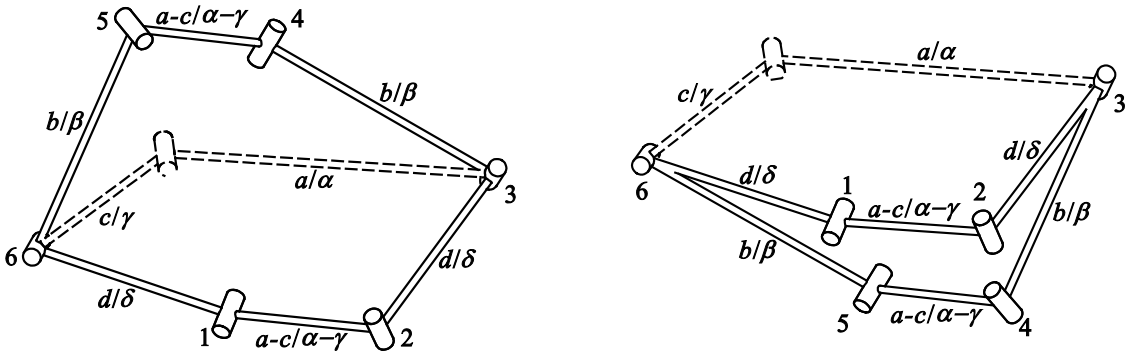

Fig. 5.2.3 The constructive forms of the double-subtractive-Goldberg 6*R* linkage: (a) Form I linkage; (b) Form II linkage.

The closure equations of the Forms I and II Wohlhart's double-Goldberg 6*R* linkage are

$$\theta_2 = 2\tan^{-1}\left(\frac{m_3 m_4}{\tan\frac{\theta_1}{2}}\right),\ \theta_3 = \pi + 2\tan^{-1}\left(\frac{m_3}{\tan\frac{\theta_1}{2}}\right) + 2\tan^{-1}\left(P_{\mathrm{WDG}}\right),$$
$$\theta_4 = 2\tan^{-1}\left(m_6 P_{\mathrm{WDG}}\right),\ \theta_5 = 2\tan^{-1}\left(\frac{m_1}{P_{\mathrm{WDG}}}\right),\ \theta_6 = -\theta_3, \tag{5.2.2}$$

where $m_i\,(i = 1, 3, 4, 6)$ were defined in Eq. (3.4.1) and are reproduced as below.

$$m_1 = \frac{\sin\frac{\beta+\alpha}{2}}{\sin\frac{\beta-\alpha}{2}},\ m_3 = \frac{\sin\frac{\delta+\alpha}{2}}{\sin\frac{\delta-\alpha}{2}},\ m_4 = \frac{\sin\frac{\delta+\gamma}{2}}{\sin\frac{\delta-\gamma}{2}},\ m_6 = \frac{\sin\frac{\beta+\gamma}{2}}{\sin\frac{\beta-\gamma}{2}}. \tag{5.2.3}$$

For Form I linkage,

$$q = \sqrt{m_3 m_4},\ Q_{\mathrm{WDG}} = \frac{\left(q^2-1\right)\tan\frac{\theta_1}{2}}{q^2 + \tan^2\frac{\theta_1}{2}},$$
$$P_{\mathrm{WDG}} = \begin{cases} \dfrac{\left(1-m_1 m_2\right) + \sqrt{\left(1-m_1 m_6\right)^2 - 4m_1 m_6 Q_{\mathrm{WDG}}^2}}{2m_6 Q_{\mathrm{WDG}}} & \begin{pmatrix} -\pi \le \theta_1 < 2\tan^{-1} q \\ -2\tan^{-1} q \le \theta_1 < \pi \end{pmatrix} \\ \dfrac{\left(1-m_1 m_6\right) - \sqrt{\left(1-m_1 m_6\right)^2 - 4m_1 m_6 Q_{\mathrm{WDG}}^2}}{2m_6 Q_{\mathrm{WDG}}} & \left(-2\tan^{-1} q \le \theta_1 < 2\tan^{-1} q\right) \end{cases}; \tag{5.2.4}$$

and for Form II linkage,

$$P_{\mathrm{WDG}} = \begin{cases} \dfrac{\left(1-m_1 m_6\right) + \sqrt{\left(1-m_1 m_6\right)^2 - 4m_1 m_6 Q_{\mathrm{WDG}}^2}}{2m_2 Q_{\mathrm{WDG}}} & \left(-2\tan^{-1} q \le \theta_1 < 2\tan^{-1} q\right) \\ \dfrac{\left(1-m_1 m_6\right) - \sqrt{\left(1-m_1 m_6\right)^2 - 4m_1 m_6 Q_{\mathrm{WDG}}^2}}{2m_6 Q_{\mathrm{WDG}}} & \begin{pmatrix} -\pi \le \theta_1 < 2\tan^{-1} q \\ -2\tan^{-1} q \le \theta_1 < \pi \end{pmatrix} \end{cases}. \tag{5.2.5}$$

And the closure equations for Forms I and II double-subtractive-Goldberg 6*R* linkage are

$$\theta_2 = 2\tan^{-1}\left(\frac{m_3}{m_4\tan\frac{\theta_1}{2}}\right),\ \theta_3 = \pi + 2\tan^{-1}\left(P_{\mathrm{DSG}}\right) - 2\tan^{-1}\left(m_4\tan\frac{\theta_1}{2}\right), \tag{5.2.6}$$

$$\theta_4 = -2\tan^{-1}\left(\frac{m_1}{P_{\mathrm{DSG}}}\right),\ \theta_5 = -2\tan^{-1}\left(\frac{P_{\mathrm{DSG}}}{m_6}\right),\ \theta_6 = -\theta_3 .$$

For Form I linkage,

$$Q_{\mathrm{DSG}} = \frac{m_3 + m_4\tan^2\dfrac{\theta_1}{2}}{(m_4 - m_3)\tan\dfrac{\theta_1}{2}},$$

$$P_{\mathrm{DSG}} = \begin{cases} \dfrac{1}{2}\left[(m_6 - m_1)Q_{\mathrm{DSG}} + \sqrt{(m_6 - m_1)^2 Q_{\mathrm{DSG}}^2 - 4m_1 m_6}\right] & (-\pi \le \theta_1 < 0) \\ \dfrac{1}{2}\left[(m_6 - m_1)Q_{\mathrm{DSG}} - \sqrt{(m_6 - m_1)^2 Q_{\mathrm{DSG}}^2 - 4m_1 m_6}\right] & (0 \le \theta_1 < \pi) \end{cases}; \tag{5.2.7}$$

and for Form II linkage,

$$P_{\mathrm{DSG}} = \begin{cases} \dfrac{1}{2}\left[(m_6 - m_1)Q_{\mathrm{DSG}} + \sqrt{(m_6 - m_1)^2 Q_{\mathrm{DSG}}^2 - 4m_1 m_6}\right] & (0 \le \theta_1 < \pi) \\ \dfrac{1}{2}\left[(m_6 - m_1)Q_{\mathrm{DSG}} - \sqrt{(m_6 - m_1)^2 Q_{\mathrm{DSG}}^2 - 4m_1 m_6}\right] & (-\pi \le \theta_1 < 0) \end{cases}. \tag{5.2.8}$$

Through bifurcation analysis (Song and Chen, 2011), two non-constructive forms are detected in both linkages using the Singular Value Decomposition method (Gan and Pellegrino, 2006; Pellegrino, 1993), namely the Forms III and IV linkages. All four linkage forms can bifurcate into each other through bifurcation points.

5.2.2 Investigations on the Multiple Operation Forms

Our objective is to achieve a 4*R* operation form for both double-Goldberg linkages. Generally, there are three types of 4*R* linkages, the planar 4*R* linkage, the spherical 4*R* linkage and the Bennett linkage. Considering the construction process and geometry conditions in both double-Goldberg linkages, it is only possible to achieve the reconfiguration between the double-Goldberg linkages and Bennett linkage. Due to the symmetry property of the Bennett linkage, only joints 3 and 6 on the double-Goldberg 6*R* linkage can be selected for possible 4*R* linkages with joints 1, 2, 4 and 5. From Eqs. (5.2.2) and (5.2.6), since $\theta_3 = -\theta_6$ for both

linkages, joints 3 and 6 will be inactive only when $d\theta_3/d\theta_1 = d\theta_6/d\theta_1 = 0$. Here, the double-subtractive-Goldberg 6*R* linkage is taken as an example for derivation. Following a similar procedure, we can also derive the same result from the closure equations in Wohlhart's double-Goldberg 6*R* linkage. From Eq. (5.2.6), we setup the condition that

$$\frac{d\theta_3}{d\theta_1} = \frac{d\left[\pi + 2\tan^{-1}\left(P_{\mathrm{DSG}}\right) - 2\tan^{-1}\left(m_4 \tan\frac{\theta_1}{2}\right)\right]}{d\theta_1} = 0, \tag{5.2.9}$$

The general solution to Eq. (5.2.9) should meet the following condition that

$$\tan^{-1}\left(P_{\mathrm{DSG}}\right) - \tan^{-1}\left(m_4 \tan\frac{\theta_1}{2}\right) + C = 0 \ (C \text{ is a constant}). \tag{5.2.10}$$

Rearranging Eq. (5.2.10) to derive the tangent on both sides of the equation that

$$P_{\mathrm{DSG}} = \frac{m_4 \tan\frac{\theta_1}{2} - \tan C}{1 + m_4 \tan\frac{\theta_1}{2}\tan C}, \tag{5.2.11}$$

which can be simplified as

$$\tan C = \frac{m_4 \tan\frac{\theta_1}{2} - P_{\mathrm{DSG}}}{P_{\mathrm{DSG}} m_4 \tan\frac{\theta_1}{2} + 1}. \tag{5.2.12}$$

When substituting Eq. (5.2.7) into Eq. (5.2.12), the square root of the variables in the Eq. (5.2.12) makes it too complex to solve for the general solution of C. However, since C could be any random constant value that works for all solutions to Eq. (5.2.10), we may consider the case when Eq. (5.2.12) is free of θ_1 to meet this condition. One of the simplest solutions is when $\tan C = 0$, so that

$$\begin{aligned} & m_4 \tan\frac{\theta_1}{2} - P_{\mathrm{DSG}} \\ &= m_4 \tan\frac{\theta_1}{2} - \frac{1}{2}\left[(m_2 - m_1)Q_{\mathrm{DSG}} \pm \sqrt{(m_2 - m_1)^2 Q_{\mathrm{DSG}}^2 - 4m_1 m_2}\right] \\ &= 0, \end{aligned} \tag{5.2.13}$$

which can be simplified as

$$m_4^2\left[(m_2 - m_1) - (m_4 - m_3)\right]\tan^2\frac{\theta_1}{2} + \left[m_3 m_4 (m_2 - m_1) - m_1 m_2 (m_4 - m_3)\right] = 0\,. \tag{5.2.14}$$

As θ_1 is a free input in Eq. (5.2.14), the following relationship must hold.

$$\begin{cases} m_4^2\left[(m_2 - m_1) - (m_4 - m_3)\right] = 0 \\ m_3 m_4 (m_2 - m_1) - m_1 m_2 (m_4 - m_3) = 0\,. \end{cases} \tag{5.2.15}$$

Solutions to Eq. (5.2.15) are

$$\begin{cases} m_3 = m_1 \\ m_4 = m_2 \end{cases}, \tag{5.2.16}$$

and

$$\begin{cases} m_3 = -m_2 \\ m_4 = -m_1 \end{cases}. \tag{5.2.17}$$

When substituting Eq. (5.2.3) into Eq. (5.2.16), the following relationship will be obtained.

$$\begin{cases} \dfrac{\sin\dfrac{\delta+\gamma}{2}}{\sin\dfrac{\delta-\gamma}{2}} = \dfrac{\sin\dfrac{\beta+\gamma}{2}}{\sin\dfrac{\beta-\gamma}{2}} \\ \dfrac{\sin\dfrac{\delta+\alpha}{2}}{\sin\dfrac{\delta-\alpha}{2}} = \dfrac{\sin\dfrac{\beta+\alpha}{2}}{\sin\dfrac{\beta-\alpha}{2}} \end{cases}. \tag{5.2.18}$$

Solution to Eq. (5.2.18) gives that

$$\delta = \beta\,. \tag{5.2.19}$$

When the condition in Eq. (5.2.19) is satisfied, consider the geometry condition that links b/β and d/δ share the same Bennett ratio of $\sin\beta/b=\sin\delta/d$, we shall have that links b/β and d/δ become identical to each other. Therefore, the two subtractive-Goldberg 5*R* linkages forming the double-subtractive-Goldberg 6*R* linkage also become identical. In this case, for the Form II linkage in Fig. 5.2.3(b), links 56 and 61 (and links 23 and 34) will be identical to each other. As a result, no loop closure could be formed in the Form II linkage, which makes the Eq. (5.2.16) a trivial solution to Eq. (5.2.15).

When substituting Eq. (5.2.3) into Eq. (5.2.17), the following relationship can be obtained.

$$\begin{cases} \dfrac{\sin\dfrac{\delta+\gamma}{2}}{\sin\dfrac{\delta-\gamma}{2}}=-\dfrac{\sin\dfrac{\beta+\alpha}{2}}{\sin\dfrac{\beta-\alpha}{2}} & \text{(5.2.20a)} \\ \dfrac{\sin\dfrac{\delta+\alpha}{2}}{\sin\dfrac{\delta-\alpha}{2}}=-\dfrac{\sin\dfrac{\beta+\gamma}{2}}{\sin\dfrac{\beta-\gamma}{2}} & \text{(5.2.20b)} \end{cases}.$$

Take Eq. (5.2.20a) for example, multiplying $\dfrac{2\cos\dfrac{\delta-\gamma}{2}}{2\cos\dfrac{\delta-\gamma}{2}}$ on the left hand side and $\dfrac{2\cos\dfrac{\beta-\alpha}{2}}{2\cos\dfrac{\beta-\alpha}{2}}$ on the right hand side gives

$$\frac{2\sin\dfrac{\delta+\gamma}{2}\cos\dfrac{\delta-\gamma}{2}}{2\sin\dfrac{\delta-\gamma}{2}\cos\dfrac{\delta-\gamma}{2}}=-\frac{2\sin\dfrac{\beta+\alpha}{2}\cos\dfrac{\beta-\alpha}{2}}{2\sin\dfrac{\beta-\alpha}{2}\cos\dfrac{\beta-\alpha}{2}}, \tag{5.2.21}$$

which can be written into

$$\frac{\sin(\delta+\gamma)}{\sin\delta-\cos\gamma}=-\frac{\sin(\beta+\alpha)}{\sin\beta-\cos\alpha}, \tag{5.2.22}$$

or

$$\frac{\sin\delta\cos\gamma+\cos\delta\sin\gamma}{\sin\delta-\cos\gamma}=-\frac{\sin\beta\cos\alpha+\cos\beta\sin\alpha}{\sin\beta-\cos\alpha}. \tag{5.2.23}$$

Using the half-angle tangent formulas on Eq. (5.2.23) gives

$$\frac{\tan\frac{\delta}{2}+\tan\frac{\gamma}{2}}{\tan\frac{\delta}{2}-\tan\frac{\gamma}{2}}=-\frac{\tan\frac{\beta}{2}+\tan\frac{\alpha}{2}}{\tan\frac{\beta}{2}-\tan\frac{\alpha}{2}}, \tag{5.2.24}$$

which can be simplified into

$$\tan\frac{\alpha}{2}\tan\frac{\gamma}{2}=\tan\frac{\beta}{2}\tan\frac{\delta}{2}. \tag{5.2.25}$$

By using the same method as above, we can also derive Eq. (5.2.25) from the Eq. (5.2.20b). Following the above steps, the relationship in Eq. (5.2.25) can be derived from the closure equations of the Wohlhart's double-Goldberg 6*R* linkage in Eq. (5.2.2). Eq. (5.2.25) is a special relationship additional to the geometry conditions of these two types of double-Goldberg 6*R* linkages, which is equivalent to

$$\frac{\tan\frac{\alpha}{2}\pm\tan\frac{\gamma}{2}}{\tan\frac{\alpha\pm\gamma}{2}}=\frac{\tan\frac{\beta}{2}\pm\tan\frac{\delta}{2}}{\tan\frac{\beta\pm\delta}{2}}, \tag{5.2.26}$$

i.e.,

$$\frac{\tan\frac{\alpha}{2}\pm\tan\frac{\gamma}{2}}{\tan\frac{\beta}{2}\pm\tan\frac{\delta}{2}}=\frac{\tan\frac{\alpha\pm\gamma}{2}}{\tan\frac{\beta\pm\delta}{2}}. \tag{5.2.27}$$

Expanding the left and right hand sides of Eq. (5.2.27) gives

$$\frac{\sin\frac{\alpha}{2}\cos\frac{\gamma}{2}\pm\cos\frac{\alpha}{2}\sin\frac{\gamma}{2}}{\cos\frac{\alpha}{2}\cos\frac{\gamma}{2}}\cdot\frac{\cos\frac{\beta}{2}\cos\frac{\delta}{2}}{\sin\frac{\beta}{2}\cos\frac{\delta}{2}\pm\cos\frac{\beta}{2}\sin\frac{\delta}{2}}=\frac{\sin\frac{\alpha\pm\gamma}{2}}{\cos\frac{\alpha\pm\gamma}{2}}\cdot\frac{\cos\frac{\beta\pm\delta}{2}}{\sin\frac{\beta\pm\delta}{2}},\tag{5.2.28}$$

or

$$\frac{\cos\frac{\beta}{2}\cos\frac{\delta}{2}}{\cos\frac{\alpha}{2}\cos\frac{\gamma}{2}}=\frac{\cos\frac{\beta\pm\delta}{2}}{\cos\frac{\alpha\pm\gamma}{2}}.\tag{5.2.29}$$

From Eq. (5.2.29), we come to the relationship that

$$\frac{\cos\frac{\alpha+\gamma}{2}}{\cos\frac{\beta+\delta}{2}}=\frac{\cos\frac{\alpha-\gamma}{2}}{\cos\frac{\beta-\delta}{2}},\tag{5.2.30}$$

Multiplying $\dfrac{2\sin\frac{\alpha\pm\gamma}{2}}{2\sin\frac{\beta\pm\delta}{2}}$ on both sides of Eq. (5.2.30) gives

$$\frac{\sin(\alpha\pm\gamma)}{\sin\alpha\pm\sin\gamma}=\frac{\sin(\beta\pm\delta)}{\sin\beta\pm\sin\delta}.\tag{5.2.31}$$

Note that these double-Goldberg 6*R* linkages are constructed by four basic links a/α, b/β, c/γ and d/δ with the same Bennett ratios that,

$$\frac{\sin\alpha}{a}=\frac{\sin\beta}{b}=\frac{\sin\gamma}{c}=\frac{\sin\delta}{d}.\tag{5.2.32}$$

By substituting Eq. (5.2.32) into Eq. (5.2.31), we come to the result that

$$\frac{\sin(\alpha\pm\gamma)}{a\pm c}=\frac{\sin(\beta\pm\delta)}{b\pm d}.\tag{5.2.33}$$

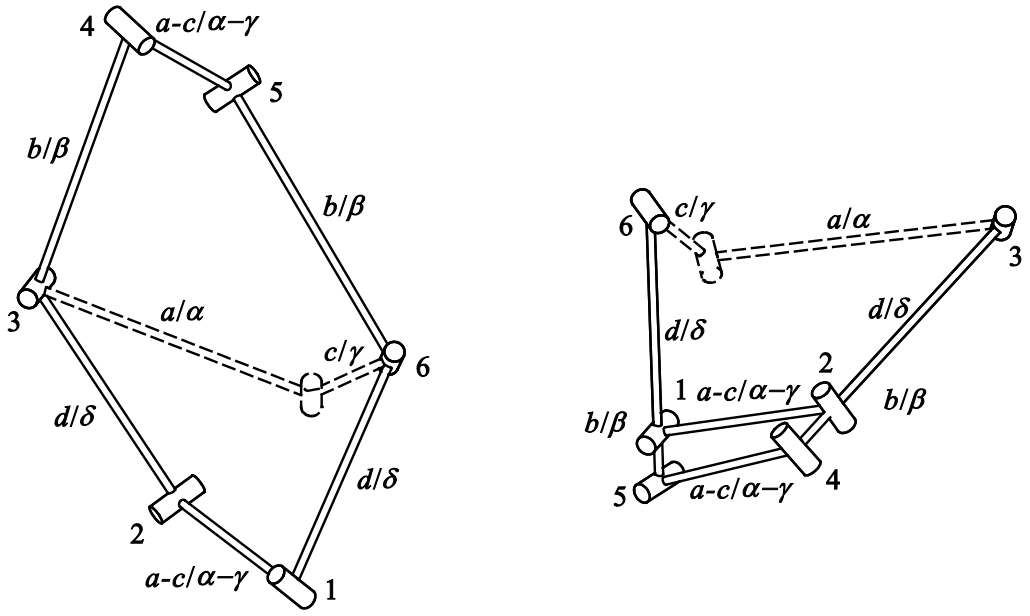

Fig. 5.2.4 The constructive forms of the double-subtractive-Goldberg 6*R* linkage with multiple operation forms: (a) Form I linkage (constructive 6*R* form); (b) Form II linkage (Bennett 4*R* form)

When introducing Eq. (5.2.25) into the double-subtractive-Goldberg 6*R* linkage, as shown in Fig. 5.2.4(a), the Form I linkage is still a constructive 6*R* linkage with six movable links and joints. However, in the Form II linkage in Fig. 5.2.4(b), the revolute variables on joints 3 and 6 are constrained to be $\theta_3 = -\theta_6 = \pi$ and the link-pairs 23-34 and 56-61 become collinear in a negatively collinear manner. Consider Eq. (5.2.33) with '-' sign, the closed-loop enclosed by joints 1, 2, 4 and 5 can be viewed as a Bennett 4*R* linkage constructed by link-pair $a-c/\alpha-\gamma \sim b-d/\beta-\delta$. Therefore, the operation form of a constructive 6*R* linkage is degenerated into a Bennett 4*R* linkage. In the following modeling, the geometry conditions for the four basic links are as follows.

$$\begin{aligned} a &= 1.0000,\ \alpha = 125.0000\pi/180; \\ b &= 1.5072,\ \beta = 60.0000\pi/180; \\ c &= 0.2993,\ \gamma = 14.1927\pi/180; \\ d &= 0.8632,\ \delta = 45.0000\pi/180. \end{aligned} \tag{5.2.34}$$

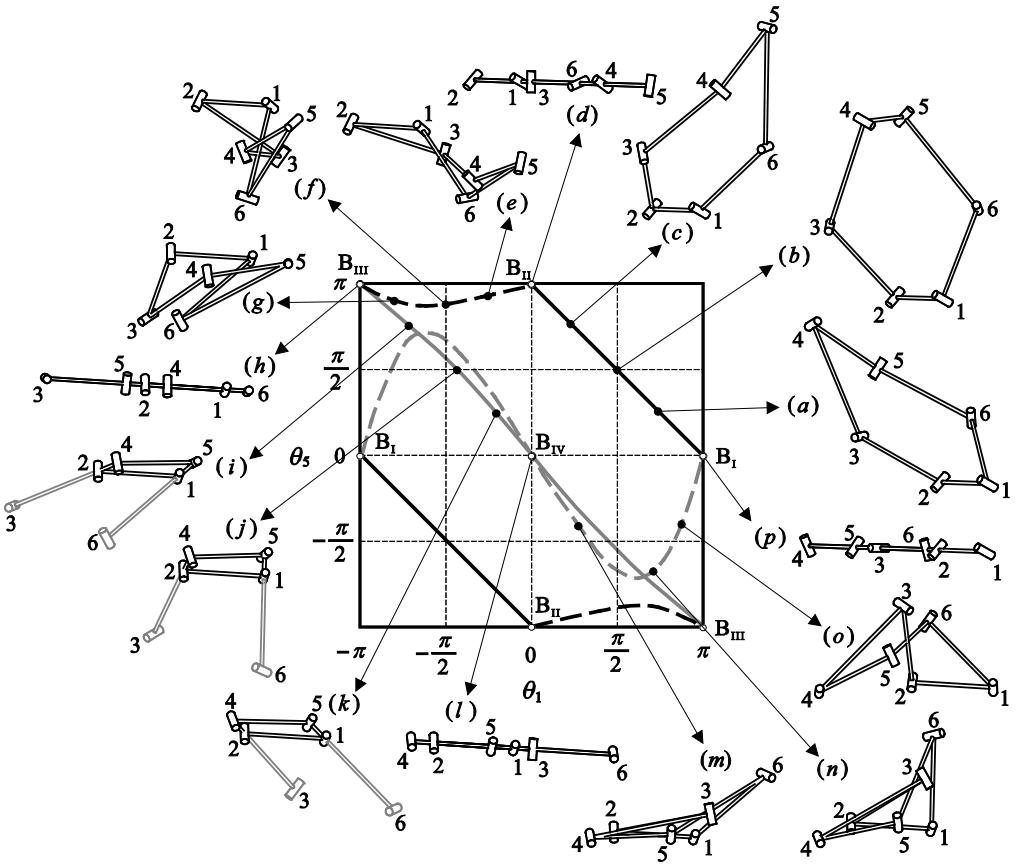

Fig. 5.2.5 The bifurcation behavior of the double-subtractive-Goldberg 6*R* linkage with multiple operation forms. (a)-(c) are the motion sequences of the Form I linkage; (d) is the bifurcation configuration between Forms I and III linkages; (e)-(g) are the motion sequences of Form III linkage; (h) is the bifurcation configuration between Forms III and II linkages; (i)-(k) are the motion sequences of the Form II linkage; (l) is the bifurcation configuration between Forms II and IV linkages; (m)-(o) are the motion sequences of Form IV linkage; and (p) is the bifurcation configuration between Forms I and IV linkages.

By using the SVD method, we can detect the non-constructive Forms III and IV linkages, which are still 6*R* linkages, and plot the transitions of the double-subtractive-Goldberg 6*R* linkage with multiple operation forms in Fig. 5.2.5. The relationship between θ_1 and θ_5 is used to demonstrate the bifurcation paths. Different linkage forms can transform into each other through bifurcation points $B_{I,II,III,IV}$. Note that at the bifurcation points, all six links become collinear to each other at configurations (d), (h), (l) and (p) in Fig. 5.2.5. It is proved in the Appendix B that between θ_1 and θ_5 we shall have

$$\tan\frac{\theta_1}{2}\cdot\tan\frac{\theta_5}{2}=1 \text{ or } \theta_1+\theta_5=\pm\pi, \tag{5.2.35}$$

which makes the curve of the Form I linkage straight lines in Fig. 5.2.5. It is unavoidable to have part of the kinematic paths present as a straight line.

When introducing Eq. (5.2.25) to the Wohlhart's double-Goldberg 6*R* linkage, in the Form I linkage in Fig. 5.2.6(a), the revolute variables on joints 3 and 6 become $\theta_3=\theta_6=0$. From Eq. (5.2.33) with '+' sign, the loop enclosed by joints 1, 2, 4 and 5 can be viewed as a Bennett 4*R* linkage constructed by link-pair $a+c/\alpha+\gamma \sim b+d/\beta+\delta$. The Form II linkage is still a constructive 6*R* linkage as shown in Fig. 5.2.6(b).

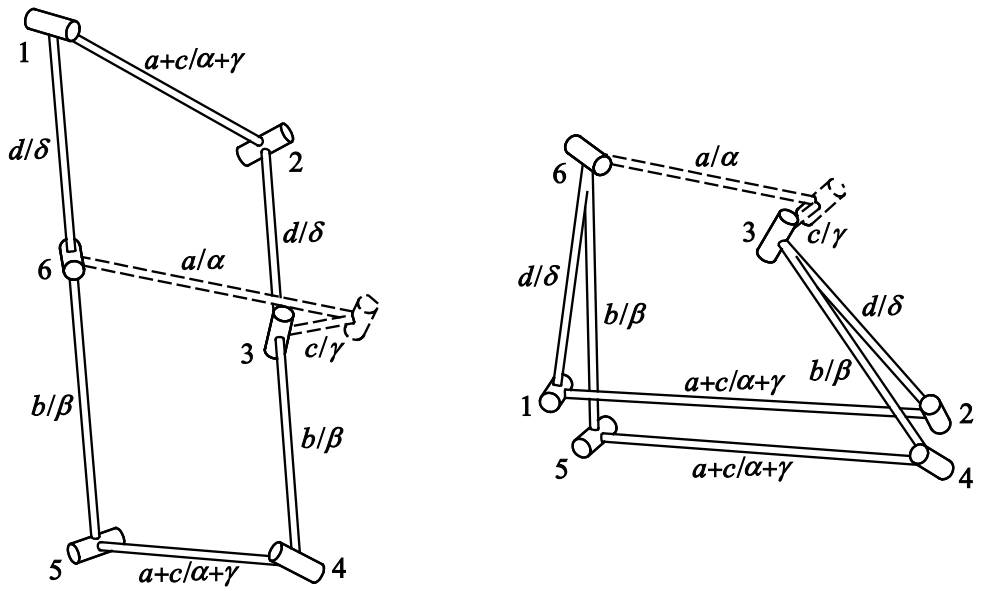

(a) (b)

Fig. 5.2.6 The constructive forms of the Wohlhart's double-Goldberg 6*R* linkage with multiple operation forms: (a) Form I linkage (Bennett 4*R* form); (b) Form II linkage (constructive 6*R* form)

By using SVD method, we can detect the non-constructive Forms III and IV linkages, which are still 6*R* linkages, and plot the transitions of the Wohlhart's double-Goldberg 6*R* linkage with multiple operation forms in Fig. 5.2.7. Different linkage forms can transform

into each other through bifurcation points $B_{I,II,III,IV}$. At the bifurcation points, all six links also become collinear to each other at configurations (d), (h), (l) and (p) in Fig. 5.2.7. Note that in this case, it can be derived that $\theta_1 + \theta_5 = 0$ for the Form II linkage, and therefore the curves of the Form II linkage will appear as a straight line in Fig. 5.2.7.

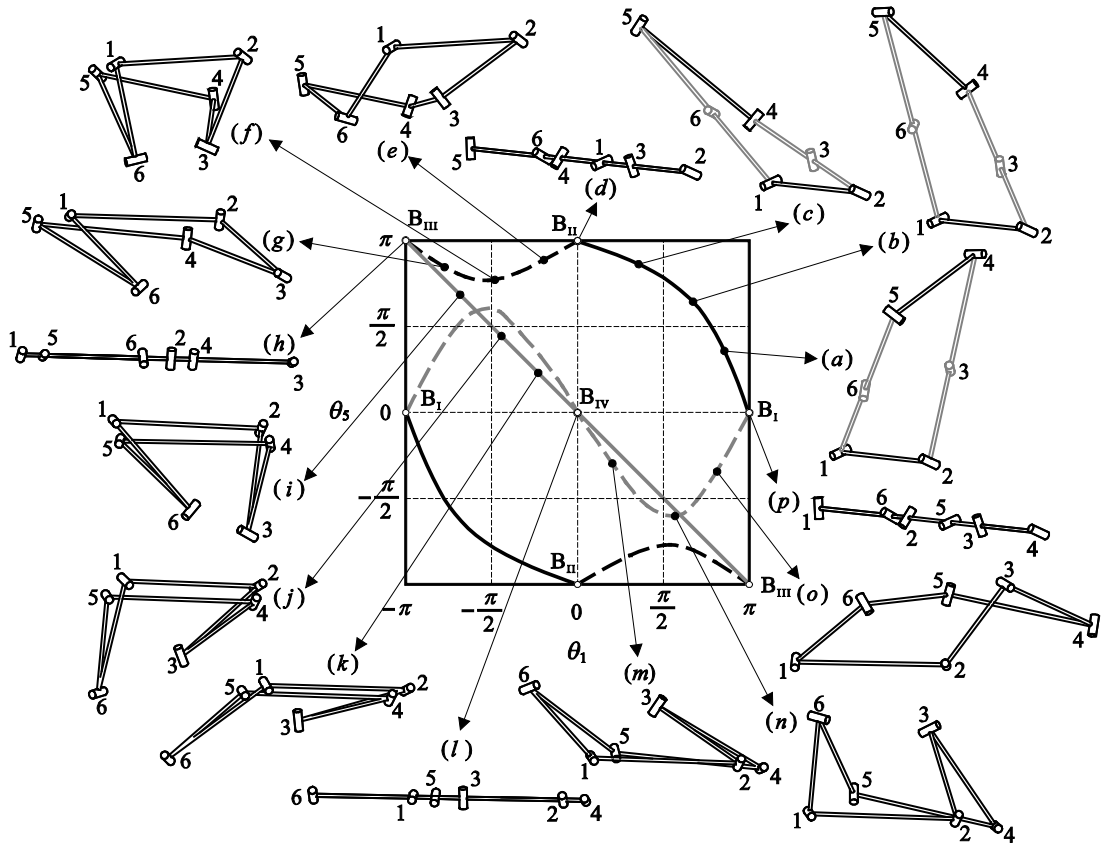

Fig. 5.2.7 The transitions of the Wohlhart's double-Goldberg 6*R* linkage with multiple operation forms. (a)-(c) are the motion sequences of the Form I linkage; (d) is the bifurcation configuration between Forms I and III linkages; (e)-(g) are the motion sequences of Form III linkage; (h) is the bifurcation configuration between Forms III and II linkages; (i)-(k) are the motion sequences of the Form II linkage; (l) is the bifurcation configuration between Forms II and IV linkages; (m)-(o) are the motion sequences of Form IV linkage; and (p) is the bifurcation configuration between Forms I and IV linkages.

5.2.3 Summary

In both of the Wohlhart's double-Goldberg 6*R* linkage and the double-subtractive-Goldberg 6*R* linkage, there are four operation forms, which include two constructive 6*R* linkage forms

and two non-constructive 6*R* linkage forms. In Eq. (5.2.36), a special geometric relationship that $\tan\frac{\alpha}{2}\tan\frac{\gamma}{2}=\tan\frac{\beta}{2}\tan\frac{\delta}{2}$ is introduced to the general double-Goldberg 6*R* linkage.

$$
\begin{gathered}
a_{12}=a_{45}=a\pm c\,,\ a_{23}=a_{61}=d\,,\ a_{34}=a_{56}=b\,,\\
\alpha_{12}=\alpha_{45}=\alpha\pm\gamma\,,\ \alpha_{23}=\alpha_{61}=\delta\,,\ \alpha_{34}=\alpha_{56}=\beta\,,\\
\frac{\sin\alpha}{a}=\frac{\sin\beta}{b}=\frac{\sin\gamma}{c}=\frac{\sin\delta}{d}\,,\\
\tan\frac{\alpha}{2}\cdot\tan\frac{\gamma}{2}=\tan\frac{\beta}{2}\cdot\tan\frac{\delta}{2}\,,\\
R_i=0\ (i=1,2,...,6)\,.
\end{gathered}
\tag{5.2.36}
$$

As a result, one constructive 6*R* linkage form of the double-Goldberg 6*R* linkages is degenerated into a Bennett linkage. The resultant double-Goldberg 6*R* linkages have multiple operation forms among a constructive 6*R* linkage form, two non-constructive 6*R* linkage forms and a Bennett 4*R* linkage form. Different linkage forms can transform into each other through bifurcation points.

5.3 MULTIPLE OPERATION FORMS OF THE LINE-SYMMETRIC BRICARD LINKAGE

5.3.1 The Spatial Triangle

A spatial triangle is enclosed by three spatial lines and their common perpendiculars. Its kinematics was firstly investigated using dual quaternion method (Yang, 1963). Fig. 5.3.1 illustrates a spatial triangle with revolute joints connecting the adjacent links. Later, its geometry properties were revisited by Mavroidis and Roth (1997) using transformation matrix. Recently, the importance of the spatial triangle was discussed in (Huang, 2003; Huang and Chen, 1995; Zarrouk and Shoham, 2011).

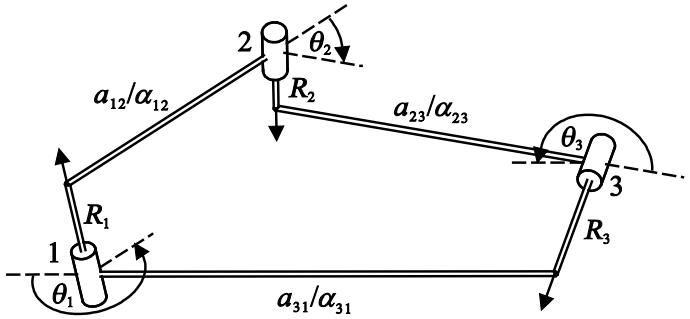

Fig. 5.3.1 The spatial configuration of the spatial triangle.

The geometry conditions of the spatial triangle could be determined using the transformation matrix that

$$\mathbf{T}_{12}\mathbf{T}_{23}\mathbf{T}_{31} = \mathbf{I}\,. \tag{5.3.1}$$

By solving Eq. (5.3.1), the geometry conditions of any one of the three links could be determined by the other two links (Mavroidis and Roth, 1997). For example, when the geometry conditions on links 12 and 23 are known, then the geometric parameters related to link 31 could be determined by the following equations.

$$\tan\theta_1 = -\frac{\sin\alpha_{23}\sin\theta_2}{\sin\alpha_{12}\cos\alpha_{23} + \cos\alpha_{12}\sin\alpha_{23}\cos\theta_2}, \tag{5.3.2}$$

$$\tan\theta_3 = -\frac{\sin\alpha_{12}\sin\theta_2}{\sin\alpha_{23}\cos\alpha_{12}+\cos\alpha_{23}\sin\alpha_{12}\cos\theta_2},$$

$$\tan\alpha_{31} = -\frac{\sin\alpha_{12}\sin\theta_2}{\sin\theta_1\cos\theta_2+\cos\alpha_{12}\sin\theta_2\cos\theta_1},$$

$$a_{31} = a_{23}\left(\cos\alpha_{12}\sin\theta_1\sin\theta_2-\cos\theta_1\cos\theta_2\right)-a_{12}\cos\theta_1-R_2\sin\alpha_{12}\sin\theta_1,$$

$$R_1 = \frac{a_{12}\left(\cos\alpha_{31}\sin\theta_1\sin\theta_3-\cos\theta_1\cos\theta_3\right)-a_{23}-a_{31}\cos\theta_3}{\sin\alpha_{31}\sin\theta_3},$$

$$R_3 = \frac{a_{31}\left(\cos\alpha_{23}\sin\theta_2\sin\theta_3-\cos\theta_2\cos\theta_3\right)-a_{12}-a_{23}\cos\theta_2}{\sin\alpha_{31}\sin\theta_3}.$$

5.3.2 The Bennett Linkages with Two Different Setups

As discussed in section 2.2, there are two setups of Bennett linkage: one in asymmetric setup with positively equaled Bennett ratios, and the other in line-symmetric setup with negatively equaled Bennett ratios, as reproduced in Fig. 5.3.2.

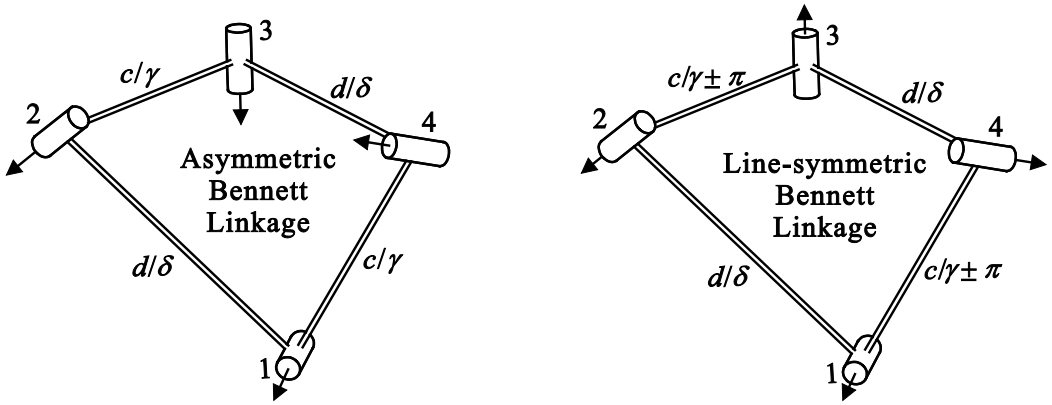

(a) (b)

Fig. 5.3.2 The Bennett linkage in different setups: (a) in asymmetric setup; (b) in line-symmetric serup

The geometry conditions of the Bennett linkage in asymmetric setup are set as follows.

$$a_{12} = a_{34} = d,\ \alpha_{12} = \alpha_{34} = \delta,\ a_{23} = a_{41} = c,\ \alpha_{23} = \alpha_{41} = \gamma, \tag{5.3.3}$$

$$\frac{\sin\alpha_{12}}{a_{12}}=\frac{\sin\alpha_{23}}{a_{23}},\ R_i=0\ (i=1,2,3\text{ and }4).$$

Therefore, its closure equations are

$$\theta_1+\theta_3=0,\ \theta_2+\theta_4=0,\ \tan\frac{\theta_1}{2}\tan\frac{\theta_2}{2}=\frac{\sin\dfrac{\gamma+\delta}{2}}{\sin\dfrac{\gamma-\delta}{2}}. \tag{5.3.4}$$

Then, the geometry conditions of the corresponding Bennett linkage in line-symmetric setup will be as follows.

$$\begin{gathered}a_{12}=a_{34}=d,\ \alpha_{12}=\alpha_{34}=\delta,\ a_{23}=a_{41}=c,\ \alpha_{23}=\alpha_{41}=\gamma\pm\pi,\\ \frac{\sin\alpha_{12}}{a_{12}}=-\frac{\sin\alpha_{23}}{a_{23}},\ R_i=0\ (i=1,2,3\text{ and }4).\end{gathered} \tag{5.3.5}$$

And its closure equations are

$$\theta_1=\theta_3,\ \theta_2=\theta_4,\ \tan\frac{\theta_1}{2}\tan\frac{\theta_2}{2}=\frac{\cos\dfrac{\gamma+\delta}{2}}{\cos\dfrac{\gamma-\delta}{2}}. \tag{5.3.6}$$

5.3.3 Reconfigurable Line-symmetric Bricard Linkages

In what follows, we are going to use the Bennett linkage with different setups as an intermediate bridge to connect two identical spatial triangles to form different assemblies. After removing the links in the center, the rest part exhibits as a general line-symmetric Bricard linkage. Since the joint axes shall be kept along the same directions during construction, both setups of the Bennett linkage can be used for construction. In Fig. 5.3.3, we firstly use a Bennett linkage $1''3''4''6''$ in asymmetric setup as the intermediate bridge to connect two identical spatial triangles $1'2'3'$ and $4'5'6'$. Note that the geometry conditions on link $1''3''$ ($4''6''$) shall be the same as link $1'3'$ ($4'6'$) except that its offset is zero. The

intermediate Bennett linkage is then merged with these two spatial triangles on the links in grey color.

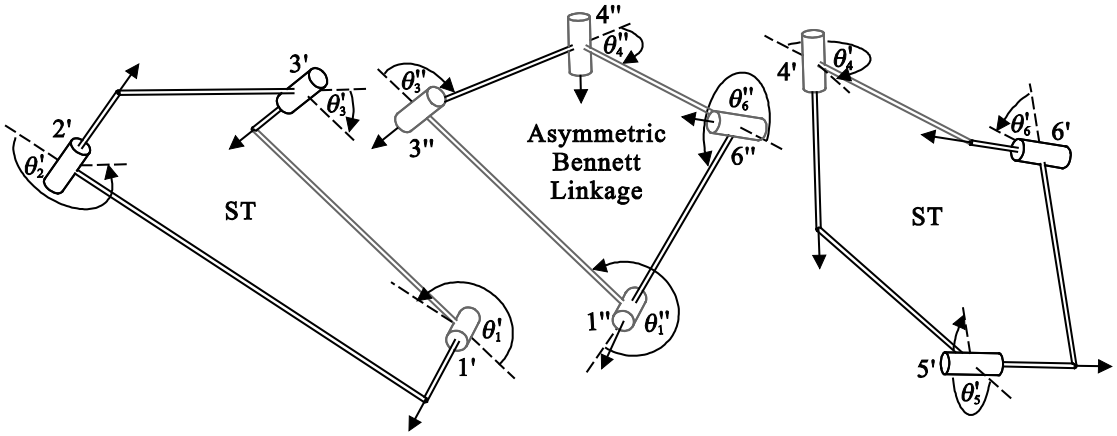

Fig. 5.3.3 The construction of the first reconfigurable line-symmetric Bricard linkage.

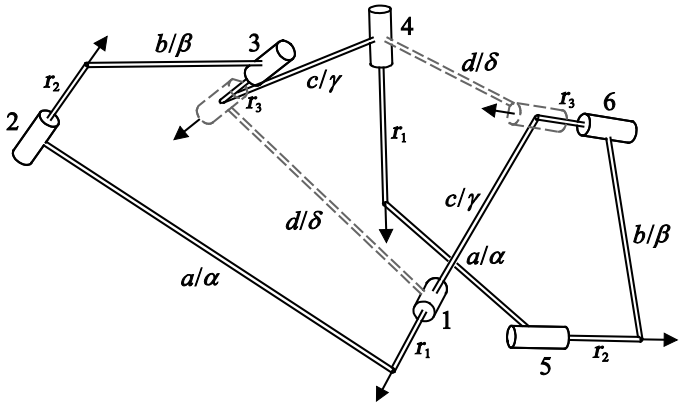

Fig. 5.3.4 The resultant configuration of the first reconfigurable line-symmetric Bricard linkage.

As shown in Fig. 5.3.4, after removing the common links and joints marked in dash lines, the rest part will form a single-loop overconstrained 6*R* linkage, which is the first reconfigurable line-symmetric Bricard linkage. Note that after construction, the offset on link $3'1'$ is transferred to new link 34, and this is the same for links $4'6'$ and 61.

For spatial triangle $1'2'3'$, the geometry conditions on links $1'2'$ and $2'3'$ are

$$a'_{12} = a,\ \alpha'_{12} = \alpha,\ a'_{23} = b,\ \alpha'_{23} = \beta, \tag{5.3.7}$$

and the revolute variable θ_2' on joint $2'$ is a fixed design parameter. Then, the geometry conditions related to link $3'1'$ could be determined by Eq. (5.3.2). Here, the representations are simplified as follows.

$$a_{31}' = d,\ \alpha_{31}' = \delta,\ R_1' = r_1,\ R_3' = r_3, \tag{5.3.8}$$

where

$$\begin{aligned}
\tan\theta_1' &= -\frac{\sin\beta\sin\theta_2'}{\sin\alpha\cos\beta+\cos\alpha\sin\beta\cos\theta_2'},\\
\tan\theta_3' &= -\frac{\sin\alpha\sin\theta_2'}{\cos\alpha\sin\beta+\sin\alpha\cos\beta\cos\theta_2'},\\
\tan\delta &= -\frac{\sin\alpha\sin\theta_2'}{\sin\theta_1'\cos\theta_2'+\cos\alpha\cos\theta_1'\sin\theta_2'},\\
d &= b\left(\cos\alpha\sin\theta_1'\sin\theta_2' - \cos\theta_1'\cos\theta_2'\right) - a\cos\theta_1' - r_2\sin\alpha\sin\theta_1',\\
r_1 &= \frac{a\left(\cos\delta\sin\theta_1'\sin\theta_3' - \cos\theta_1'\cos\theta_3'\right) - b - d\cos\theta_3'}{\sin\delta\sin\theta_3'},\\
r_3 &= \frac{d\left(\cos\beta\sin\theta_2'\sin\theta_3' - \cos\theta_2'\cos\theta_3'\right) - a - b\cos\theta_2'}{\sin\delta\sin\theta_3'}.
\end{aligned} \tag{5.3.9}$$

The geometry conditions of spatial triangle $4'5'6'$ is identical to spatial triangle $1'2'3'$, where

$$\begin{aligned}
&a_{45}' = a_{12}' = a,\ \alpha_{45}' = \alpha_{12}' = \alpha,\ R_4' = R_1' = r_1,\ \theta_4' = \theta_1',\\
&a_{56}' = a_{23}' = b,\ \alpha_{56}' = \alpha_{23}' = \beta,\ R_5' = R_2' = r_2,\ \theta_5' = \theta_2',\\
&a_{64}' = a_{31}' = d,\ \alpha_{64}' = \alpha_{31}' = \delta,\ R_6' = R_3' = r_3,\ \theta_6' = \theta_3'.
\end{aligned} \tag{5.3.10}$$

During the construction, link $3'1'$ in the spatial triangle shares the same link length and twist with link $3''1''$ in the Bennett linkage in asymmetric setup, except that link $3''1''$ has zero offset. Therefore, we can use link $3''1''$ to design the geometry of link $3''4''$ to form a Bennett linkage in asymmetric setup, whose geometry conditions and closure equations are the same as Eqs. (5.3.3) and (5.3.4). According to the above setups, we can write the geometry conditions of the first reconfigurable line-symmetric Bricard linkage as follows.

$$
\begin{aligned}
&a_{12} = a_{45} = a,\ \alpha_{12} = \alpha_{45} = \alpha,\ R_1 = R_4 = r_1,\\
&a_{23} = a_{56} = b,\ \alpha_{23} = \alpha_{56} = \beta,\ R_2 = R_5 = r_2,\\
&a_{34} = a_{61} = c,\ \alpha_{34} = \alpha_{61} = \gamma,\ R_3 = R_6 = r_3.
\end{aligned}
\tag{5.3.11}
$$

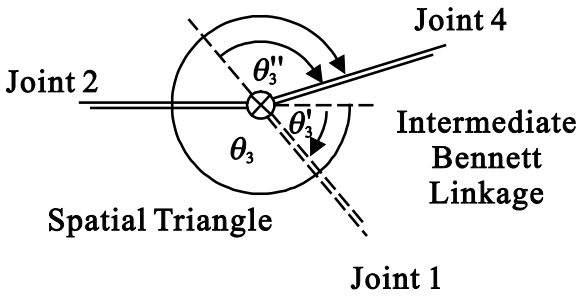

Fig. 5.3.5 The compatibility condition of joint 3 in the first reconfigurable line-symmetric Bricard linkage.

From the relationship between θ_3' in the spatial triangle, θ_3'' in the intermediate Bennett linkage and θ_3 in the first reconfigurable line-symmetric Bricard linkage, we may derive the compatibility condition for joint 3 that,

$$\theta_3 = \theta_3' + \theta_3'' + \pi\,. \tag{5.3.12}$$

The detailed relationship between θ_i, θ_i' and θ_i'' could be given following the process in Fig. 5.3.5. Therefore, we can derive the compatibility conditions for the first reconfigurable line-symmetric Bricard linkage in Eq. (5.3.13), from which we can summarize that $\theta_1 \neq \theta_4$, $\theta_2 = \theta_5$ and $\theta_3 \neq \theta_6$. Even though the geometry conditions of the first reconfigurable line-symmetric Bricard linkage are line-symmetric in Eq. (5.3.11), the resultant linkage is still an asymmetric linkage during movement in Eq. (5.3.13). This is caused by the asymmetric Bennett linkage used as the intermediate bridge during the construction.

$$
\begin{aligned}
&\theta_1 = \theta_1' + \theta_1'' - \pi\,,\ \theta_2 = \theta_2'\,,\ \theta_3 = \theta_3' + \theta_3'' + \pi\,,\\
&\theta_4 = \theta_4' + \theta_4'' - \pi = \theta_1' - \theta_1'' - \pi\,,\ \theta_5 = \theta_5' = \theta_2'\,,\ \theta_6 = \theta_6' + \theta_6'' - \pi = \theta_3' - \theta_3'' - \pi\,.
\end{aligned}
\tag{5.3.13}
$$

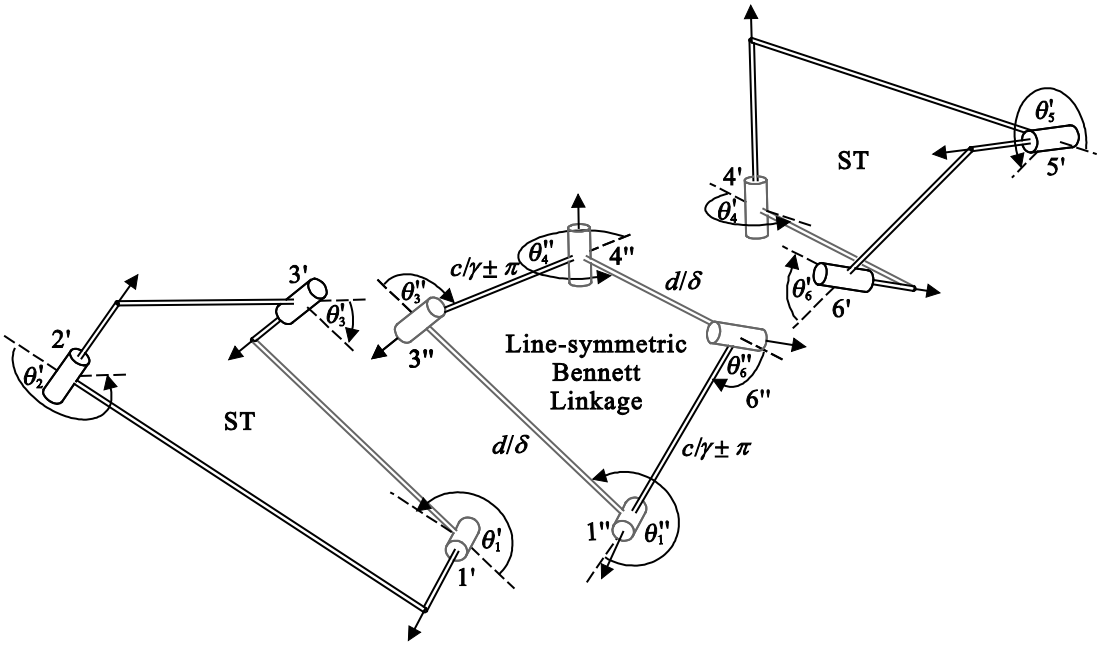

Fig. 5.3.6 The construct of the second reconfigurable line-symmetric Bricard linkage.

As illustrated in Fig. 5.3.6, a different linkage can be achieved by replacing the intermediate bridge in the first reconfigurable line-symmetric Bricard linkage with a Bennett linkage in line-symmetric setup, whose geometry conditions and closure equations are the same as Eqs. (5.3.5) and (5.3.6). In Fig. 5.3.7, after removing the common links and joints marked in dash lines, the rest part will form the second reconfigurable line-symmetric Bricard linkage. The offset on link $3'1'$ is transferred to new link 34, and this is the same for links $4'6'$ and 61. The geometry conditions of the second reconfigurable line-symmetric Bricard linkage could be summarized as follows.

$$\begin{aligned} &a_{12} = a_{45} = a,\ \alpha_{12} = \alpha_{45} = \alpha,\ R_1 = R_4 = r_1, \\ &a_{23} = a_{56} = b,\ \alpha_{23} = \alpha_{56} = \beta,\ R_2 = R_5 = r_2, \\ &a_{34} = a_{61} = c,\ \alpha_{34} = \alpha_{61} = \gamma \pm \pi,\ R_3 = R_6 = r_3. \end{aligned} \tag{5.3.14}$$

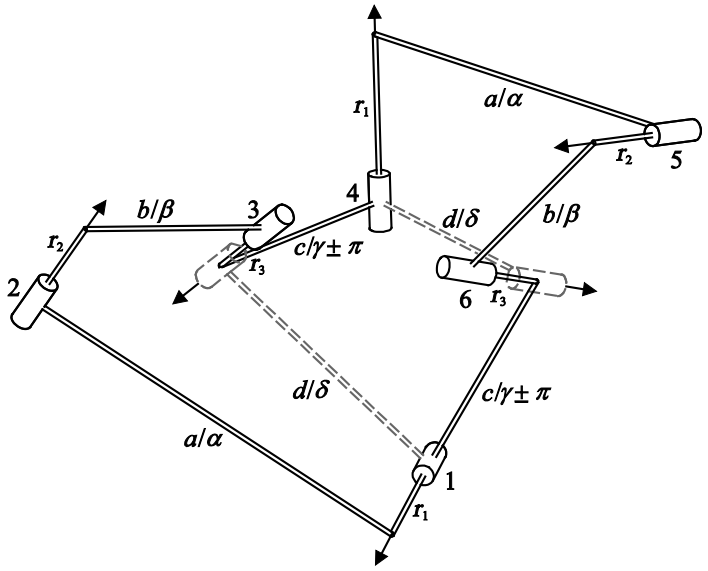

Fig. 5.3.7 The resultant configuration of the second reconfigurable line-symmetric Bricard linkage.

Similarly, we can derive the compatibility conditions for the second reconfigurable line-symmetric Bricard linkage as follows,

$$\begin{gathered}\theta_1 = \theta_1' + \theta_1'' - \pi\,,\ \theta_2 = \theta_2'\,,\ \theta_3 = \theta_3' + \theta_3'' + \pi\,, \\ \theta_4 = \theta_4' + \theta_4'' - \pi = \theta_1' + \theta_1'' - \pi\,,\ \theta_5 = \theta_5' = \theta_2'\,,\ \theta_6 = \theta_6' + \theta_6'' + \pi = \theta_3' + \theta_3'' + \pi\,.\end{gathered} \tag{5.3.15}$$

From the above equation, we can summarize that $\theta_1 = \theta_4$, $\theta_2 = \theta_5$ and $\theta_3 = \theta_6$ for the resultant linkage. Since the linkage is line-symmetric in both geometry conditions and revolute variables, the second reconfigurable line-symmetric Bricard linkage is indeed a line-symmetric linkage. This is caused by the line-symmetric Bennett linkage used as the intermediate bridge during construction.

5.3.4 Bifurcation Analysis of the Reconfigurable Line-symmetric Bricard Linkages

Possible reconfiguration potentials of the resultant linkages could be analyzed by investigating their bifurcation behaviors. Since the twist angles on links 34 and 61 are different in the first and second reconfigurable line-symmetric Bricard linkages when comparing Eqs. (5.3.11) and (5.3.14), it is important to treat these two linkages as different

linkages. For the first reconfigurable line-symmetric Bricard linkage, we can plot its kinematic paths in Fig. 5.3.8 and its singular value variations in Fig. 5.3.9 using the Singular Value Decomposition method. Further examination shows that the kinematic paths in Fig. 5.3.8 comply with the result in Eq. (5.3.13), and therefore the resultant linkage is confirmed to be asymmetric. $\theta_{2,5}$ are constrained to a fixed value of $-\tan^{-1}\left(\dfrac{\sin\delta\sin\theta_3'}{\sin\beta\cos\delta+\cos\beta\sin\delta\cos\theta_3'}\right)$ during the full cycle movement, which corresponds to the configuration on joints $2'$ and $5'$ in the spatial triangle.

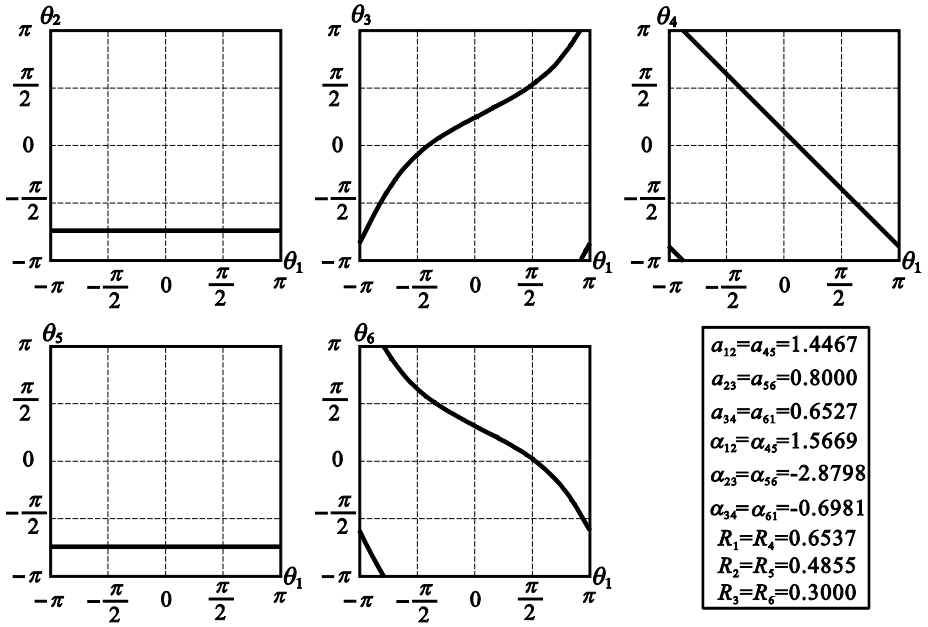

Fig. 5.3.8 The kinematic paths of the first reconfigurable Bricard linkage.

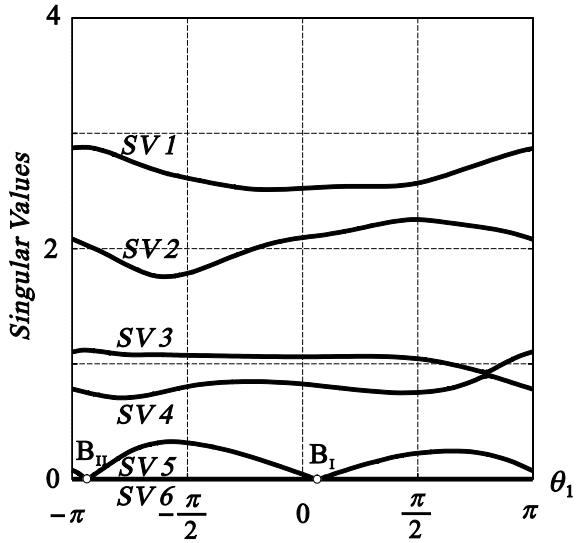

Fig. 5.3.9 The SVD results of the first reconfigurable Bricard linkage.

From the SVD results in Fig. 5.3.9, the fifth singular value falls to near zero at B_I and B_{II}. It is worth investigating possible bifurcation behaviors near these points. At point B_I, it is found that the first reconfigurable line-symmetric Bricard linkage could bifurcate into an operation form with six active joints of revolute in Fig. 5.3.10. The central line in the front view is the line of symmetry of the linkage, which is represented as the dashed dot in the top view.

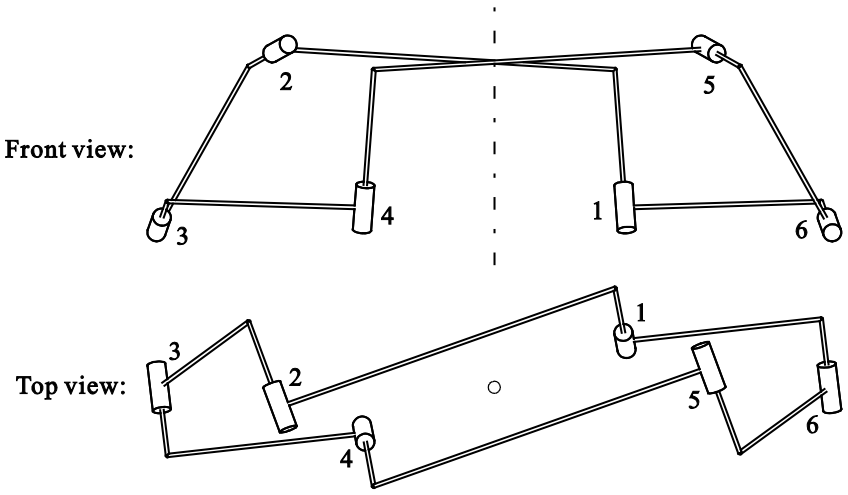

Fig. 5.3.10 The configuration of the Form I of the first reconfigurable line-symmetric Bricard linkage when $\theta_2 = -70.0000\pi/180$, which is a 6*R* linkage.

By using the SVD method, we can plot the linkage's kinematic paths in Fig. 5.3.11 and the singular value variations in Fig. 5.3.12. It is found that this linkage form is in correspondence to the closure equations of the Form I general line-symmetric Bricard linkage derived in Eq. (4.2.23). To differentiate different linkages, we name the linkage in Fig. 5.3.4 as the Bennett form of the first reconfigurable Bricard linkage; and the linkage in Fig. 5.3.10 as the Form I of the first reconfigurable line-symmetric Bricard linkage. In Fig. 5.3.12, the fifth singular value falls to zero at B_I, which is in accordance with the SVD results in Fig. 5.3.9. The location of B_I can be determined analytically by substituting the fixed revolute parameter on joint 2 in Bennett form into the closure equations of the Form I general line-

symmetric Bricard linkage in Eq. (4.2.23) as follows, where $Aterm_2$, $Bterm_2$ and $Cterm_2$ are functions of θ_1. The solution to Eq. (5.3.16) is derived in the Appendix C.

$$-\tan^{-1}\left(\frac{\sin\delta\sin\theta_3'}{\sin\beta\cos\delta+\cos\beta\sin\delta\cos\theta_3'}\right)= 2\tan^{-1}\left(\frac{-Bterm_2+\sqrt{Bterm_2^2-4Aterm_2\cdot Cterm_2}}{2Aterm_2}\right) \tag{5.3.16}$$

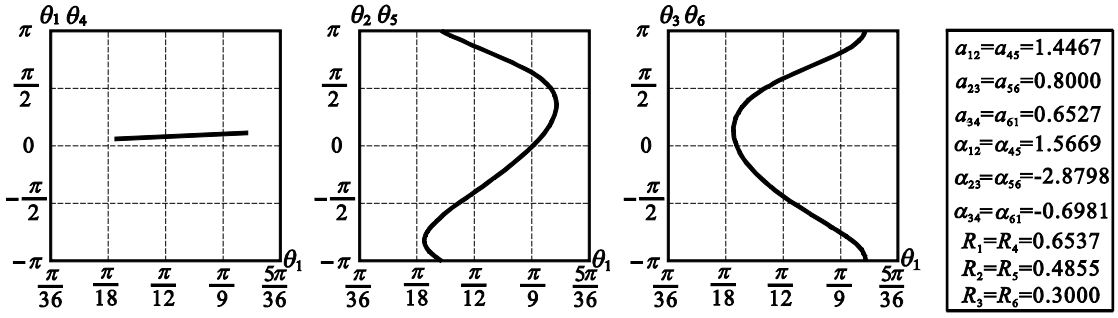

Fig. 5.3.11 The kinematic paths of Form I of the first reconfigurable line-symmetric Bricard linkage.

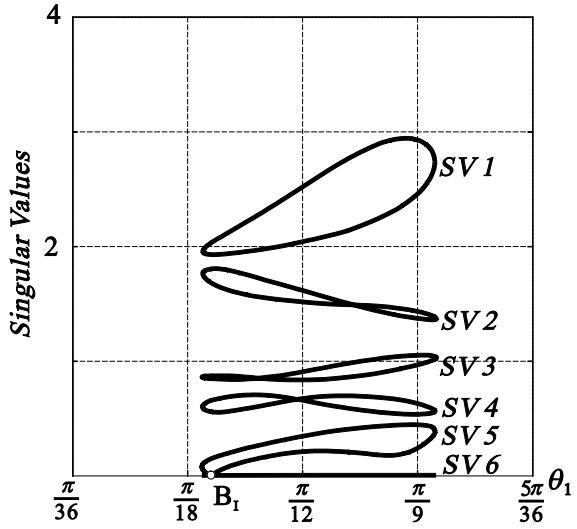

Fig. 5.3.12 The SVD results of Form I of the first reconfigurable line-symmetric Bricard linkage.

On the other hand, the Bennett form of the first reconfigurable line-symmetric Bricard linkage could bifurcate into another operation form with six active joints of revolute at B_{II} in Fig. 5.3.13. By using the SVD method, we can plot its kinematic paths in Fig. 5.3.14 and its singular value variations in Fig. 5.3.15. It is found that this linkage form is in correspondence

to the closure equations of the Form II general line-symmetric Bricard linkage in Eq. (4.2.24). Therefore, the resultant linkage is called the Form II of first reconfigurable line-symmetric Bricard linkage. In Fig. 5.3.15, the fifth singular value falls to zero at B_{II}, which is in accordance with the SVD results in Fig. 5.3.9. The location of B_{II} can be determined in the same way as B_I by solving Eq. (5.3.17), whose solution is derived in the Appendix C.

$$-\tan^{-1}\left(\frac{\sin\delta\sin\theta_3'}{\sin\beta\cos\delta+\cos\beta\sin\delta\cos\theta_3'}\right)= 2\tan^{-1}\left(\frac{-Bterm_2-\sqrt{Bterm_2^2-4Aterm_2\cdot Cterm_2}}{2Aterm_2}\right) \tag{5.3.17}$$

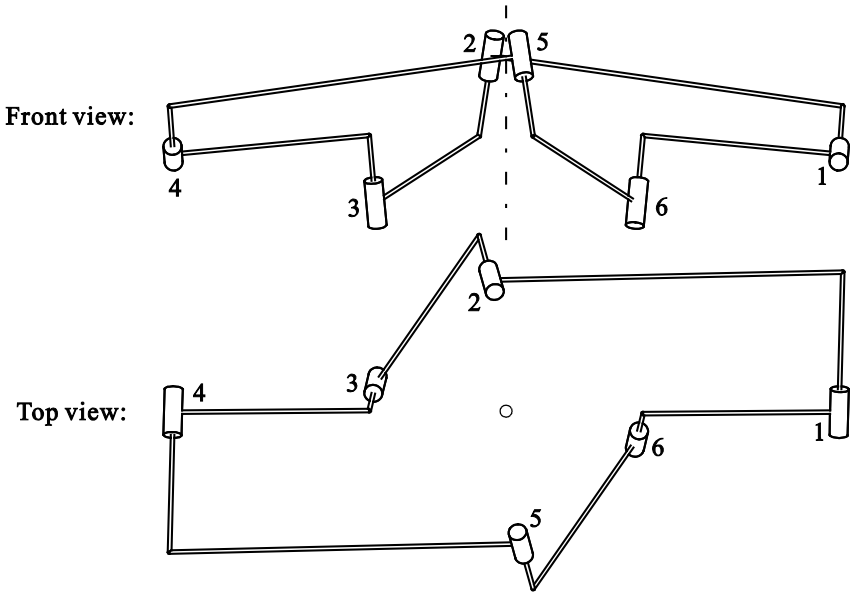

Fig. 5.3.13 The configuration of Form II of the first reconfigurable line-symmetric Bricard linkage when $\theta_2 = -70.0000\pi/180$, which is a 6*R* linkage.

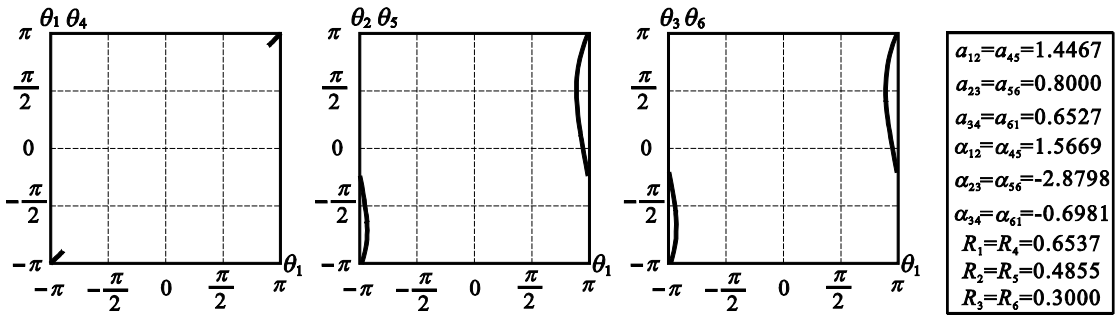

Fig. 5.3.14 The kinematic paths of Form II of the first reconfigurable line-symmetric Bricard linkage.

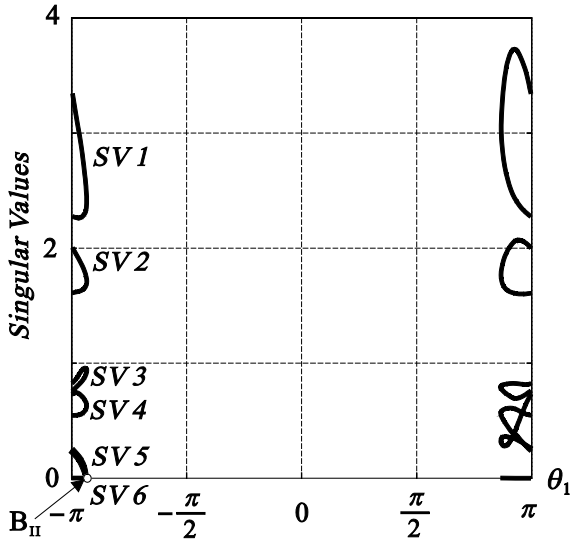

Fig. 5.3.15 The SVD results of Form II of the first reconfigurable line-symmetric Bricard linkage.

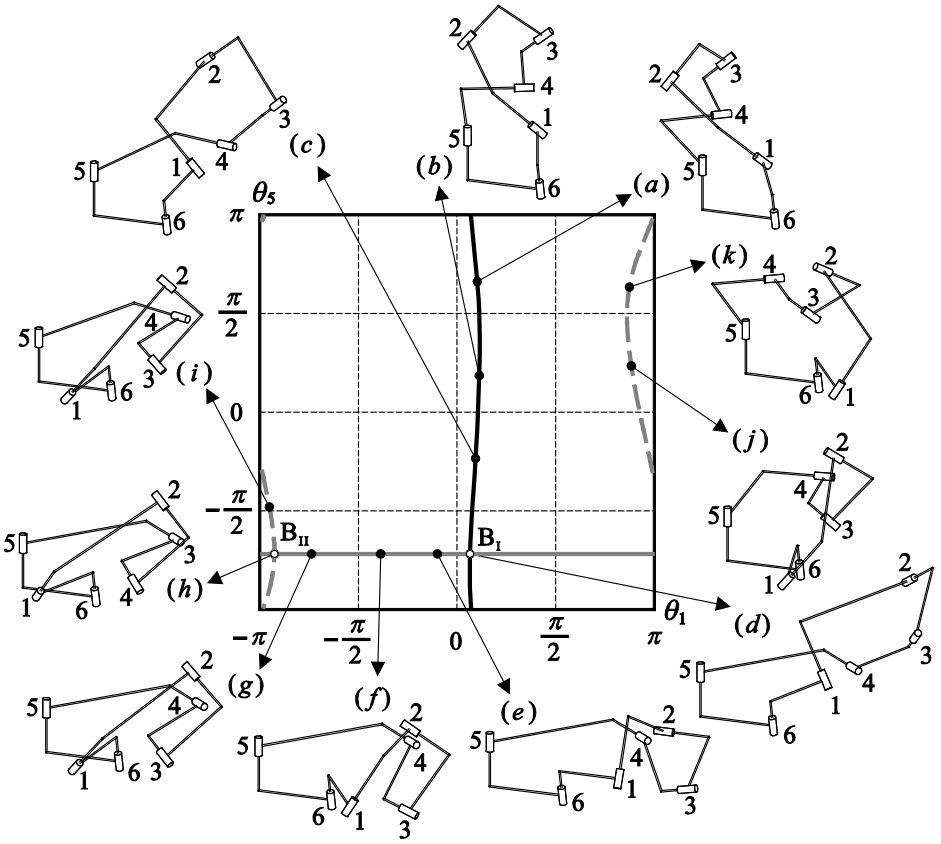

Fig. 5.3.16 The transformations of the first reconfigurable line-symmetric Bricard assembly with multiple operation forms. (a)-(c) are the motion sequences of the Form I linkage; (d) is the bifurcation configuration between Form I linkage and the Bennett form linkage; (e)-(g) are the motion sequences of the Bennett form linkage; (h) is the bifurcation configuration between the Bennett form linkage and the Form II linkage; (i)-(k) are the motion sequences of the Form II linkage. The Forms I and II linkages have 6 active joints of revolute while the the Bennett form linkage only have 4 active joints of revolute, which makes the Bennett form linkage function like a Bennett linkage.

Therefore, we can plot the full map of bifurcation for the first reconfigurable line-symmetric Bricard linkage in Fig. 5.3.16. The Bennett form linkage can bifurcation into the Form I or Form II linkages on different bifurcation points, but the Forms I and II linkages cannot bifurcation into each other directly. As a result, we successfully introduced the operation form of a Bennett linkage with only 4 active joints of revolute to bridge the two forms of the general line-symmetric Bricard linkage. The reconfiguration potential of the first reconfigurable line-symmetric Bricard linkage is enabled by the Bennett linkage in asymmetric setup used to connect the two identical spatial triangles. This asymmetric property is different from the original line-symmetric property, which triggers the reconfiguration.

For the second reconfigurable line-symmetric Bricard linkage, a Bennett linkage in line-symmetric setup is used for the connection between the two identical spatial triangles. We can plot the singular value variations in Fig. 5.3.17 and its kinematic paths in Fig. 5.3.18 using SVD method. As shown in Fig. 5.3.17, no bifurcation points can be found in the second reconfigurable line-symmetric Bricard linkage, which is different from the first reconfigurable line-symmetric Bricard linkage.

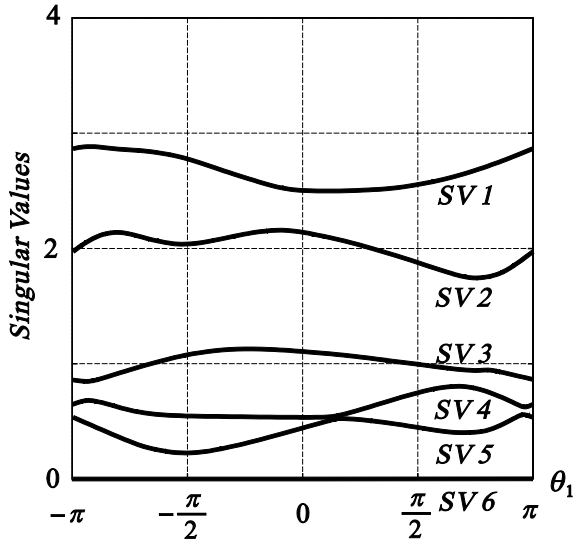

Fig. 5.3.17 The SVD results of the second reconfigurable line-symmetric Bricard linkage.

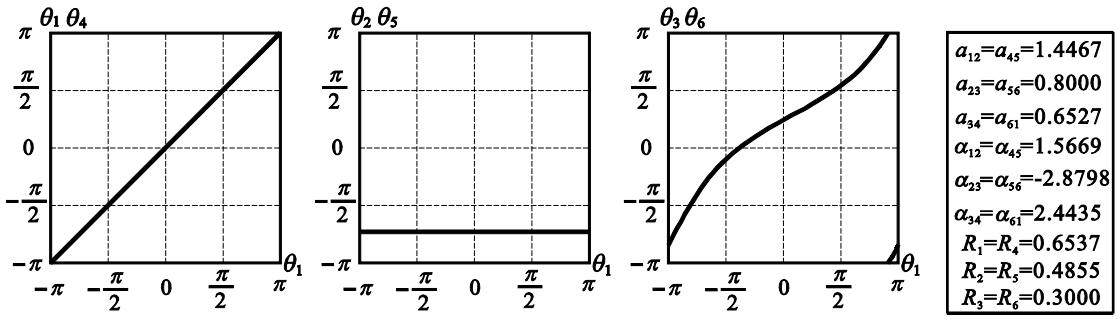

Fig. 5.3.18 The kinematic paths of the second reconfigurable line-symmetric Bricard linkage.

The kinematic paths of the second reconfigurable line-symmetric Bricard linkage in Fig. 5.3.18 comply with the relationship in Eq. (5.3.15). Therefore, the resultant linkage is indeed a line-symmetric linkage. On the kinematic paths, $\theta_{2,5}$ are constrained to a fixed value of $-\tan^{-1}\left(\frac{\sin\delta\sin\theta_3'}{\sin\beta\cos\delta+\cos\beta\sin\delta\cos\theta_3'}\right)$ during the full cycle movement, which is the same as the Bennett form of the first reconfigurable line-symmetric Bricard linkage. Further investigation shows that the kinematic paths in Fig. 5.3.18 are in correspondence with the closure equations of the Form II general line-symmetric Bricard linkage in Eq. (4.2.24). Therefore, the Bennett form of the second reconfigurable line-symmetric Bricard linkage is actually the Form II of the general line-symmetric Bricard linkage. Such result is caused by the Bennett linkage with line-symmetric setup used in the second reconfigurable line-symmetric Bricard linkage. After construction, the symmetry property of the resultant linkage is exactly the same as the original line-symmetric Bricard linkage. As a result, the second reconfigurable line-symmetric Bricard linkage essentially shares the same kinematic properties and bifurcation behaviors as the original general line-symmetric Bricard linkage.

5.3.5 Summary

In section 5.3, the feasibility to design a reconfigurable linkage is demonstrated by constructing basic elements, i.e. spatial triangles and Bennett linkages, in different symmetric

manners. From the above investigations, we successfully introduced the operation form of a Bennett linkage into the general line-symmetric Bricard linkage using construct method. By using spatial triangles and Bennett linkages with different symmetry setups as the building blocks, two reconfigurable line-symmetric Bricard linkages are formed which can be identified as general line-symmetric Bricard linkages from their geometry conditions.

A summary of the two reconfigurable line-symmetric Bricard linkages could be listed in Table 5.3.1. The first reconfigurable line-symmetric Bricard linkage is achieved by firstly connecting two identical spatial triangles with a Bennett linkage in asymmetric setup, and then removing the redundant links inside to form a closed-loop overconstrained 6*R* linkage. The use of a Bennett linkage in asymmetric setup disrupts the line-symmetric relationship among the kinematic variables in the resultant linkage. As a result, the first reconfigurable line-symmetric Bricard linkage forms a new asymmetric linkage form with only four active joints of revolute. In the first reconfigurable line-symmetric Bricard linkage, the reconfiguration between 4*R* and 6*R* linkage is achieved through bifurcation points. The second reconfigurable line-symmetric Bricard linkage can be obtained by replacing the Bennett linkage in asymmetric setup in the first reconfigurable line-symmetric Bricard linkage with a Bennett linkage in line-symmetric setup. Since the symmetry property among the kinematic variables is preserved during the construction, the resultant linkage is still the same as the general line-symmetric Bricard linkage. The construct method used makes the 6*R* linkage form of the general line-symmetric Bricard linkage reaching its limiting position and behaving like a 4*R* linkage. The second reconfigurable line-symmetric Bricard linkage shares the same kinematic properties with the general line-symmetric Bricard linkage and it is not reconfigurable between the two resultant linkage forms.

Table 5.3.1 Summary of the two reconfigurable line-symmetric Bricard linkages.

Reconfigurable Line-symmetric Bricard Linkages	The first reconfigurable line-symmetric Bricard linkage	The second reconfigurable line-symmetric Bricard linkage
Construct Units	Spatial Triangle + Bennett linkage in asymmetric setup + Spatial Triangle	Spatial Triangle + Bennett linkage in line-symmetric setup + Spatial Triangle
Resultant linkage forms	Form I linkage in 6*R* Form II linkage in 6*R* *Bennett linkage form* in 4*R*	Form I linkage in 6*R* Form II linkage in 4*R*
Reconfiguration Potential	Reconfigurable through bifurcation points	Not reconfigurable as the resultant linkages forms are still independent and distinct to each other

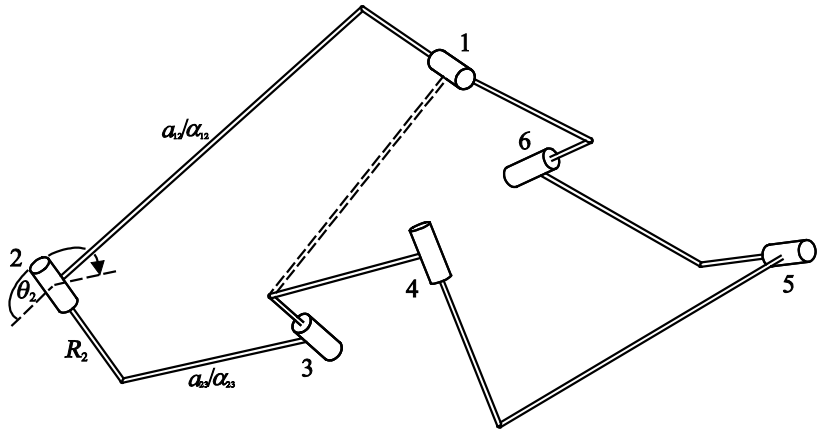

Fig. 5.3.19 The illustration of a general line-symmetric Bricard linkage with reconfiguration potentials.

In order to design a general line-symmetric Bricard linkage with reconfiguration capability, we need to make sure that the resultant linkage can be disassembled into two identical spatial triangles and an asymmetric Bennett linkage. Take the illustration in Fig. 5.3.19 for example, the known parameters on links 12 and 23 are a_{12}, α_{12}, a_{23}, α_{23}, R_2 and the fixed kink angle θ_2. By using these parameters, we could form a spatial triangle 123 with a new *virtual* link 13. Using the closure equations of the spatial triangle in Eq. (5.3.2), we can

determine the geometry condition on the *virtual* link 13 (a_{13} and α_{13}), the offsets on links 12 and 34 (R_1 and R_3), the kink angle between links 23 and 31 on joint 3 (θ_3') and the kink angle between links 31 and 12 on joint 1 (θ_1'). When the Bennett ratio of link 13 is *negatively* equal to the Bennett ratio of link 34, an asymmetric Bennett linkage could be formed by these two links. In this case, the resultant linkage is equivalent to the first reconfigurable line-symmetric Bricard linkage and therefore it can be reconfigured between 4*R* and 6*R* linkages through bifurcation points. The geometry conditions for the resultant linkage with reconfiguration capability are

$$\begin{gathered}
a_{12}=a_{45},\ \alpha_{12}=\alpha_{45},\ a_{23}=a_{56},\ \alpha_{23}=\alpha_{56},\ a_{34}=a_{61},\ \alpha_{34}=\alpha_{61},\\
-\frac{\sin\alpha_{34}}{a_{34}}=\frac{\sin\alpha_{23}\sin\theta_2\sin\theta_1'-\cos\alpha_{23}\sin\alpha_{12}\cos\theta_1'-\cos\alpha_{12}\cos\theta_2\sin\alpha_{23}\cos\theta_1'}{a_{23}\left(\cos\alpha_{12}\sin\theta_1'\sin\theta_2-\cos\theta_1'\cos\theta_2\right)-a_{12}\cos\theta_1'-R_2\sin\alpha_{12}\sin\theta_1'},\\
R_1=R_4=\frac{a_{12}\left(\cos\alpha_{31}\sin\theta_1'\sin\theta_3'-\cos\theta_1'\cos\theta_3'\right)-a_{23}-a_{31}\cos\theta_3'}{\sin\alpha_{31}\sin\theta_3'},\\
R_2=R_5,\ R_3=R_6=\frac{a_{31}\left(\cos\alpha_{23}\sin\theta_2\sin\theta_3'-\cos\theta_2\cos\theta_3'\right)-a_{12}-a_{23}\cos\theta_2}{\sin\alpha_{31}\sin\theta_3'}.
\end{gathered}\tag{5.3.18}$$

where $\theta_{2,5}$ and $R_{2,5}$ are design parameters for the kink angles and offsets on joints 2 and 5 when the linkage is in 4*R* form and

$$\begin{aligned}
\tan\theta_1'&=-\frac{\sin\alpha_{23}\sin\theta_2}{\sin\alpha_{12}\cos\alpha_{23}+\cos\alpha_{12}\sin\alpha_{23}\cos\theta_2},\\
\tan\theta_3'&=-\frac{\sin\alpha_{12}\sin\theta_2}{\sin\alpha_{23}\cos\alpha_{12}+\cos\alpha_{23}\sin\alpha_{12}\cos\theta_2}.
\end{aligned}\tag{5.3.19}$$

On the other hand, when the Bennett ratio of link 13 is *positively* equal to the Bennett ratio of link 34, a line-symmetric Bennett linkage will be formed. In this case, the resultant linkage is equivalent to the second reconfigurable line-symmetric Bricard linkage, which cannot bifurcate at all.

5.4 RECONFIGURABLE BENNETT NETWORK

5.4.1 The Method of Link-pair Replacement

As shown in Fig. 5.4.1(a), random links $1'2'$ and $2''3''$ are placed in space in such a manner that they share a common revolute axis on joints $2'$ and $2''$. Once the normal distance between joints $2'$ and $2''$ is fixed to e and the revolution from link $1'2'$ to link $2''3''$ is fixed to ε, the relative position between joints $1'$ and $3''$ can be determined by the link-pair $1'2' \sim 2'3''$ in Fig. 5.4.1(b).

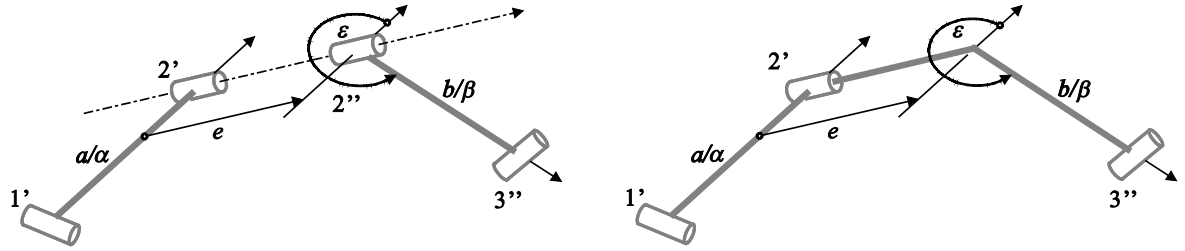

(a) (b)

Fig. 5.4.1 The spatial setup of link-pair replacement: (a) two links in space share a common revolute axis on joints $2'$ and $2''$; (b) a link-pair that determines joints $1'$ and $3''$ in space.

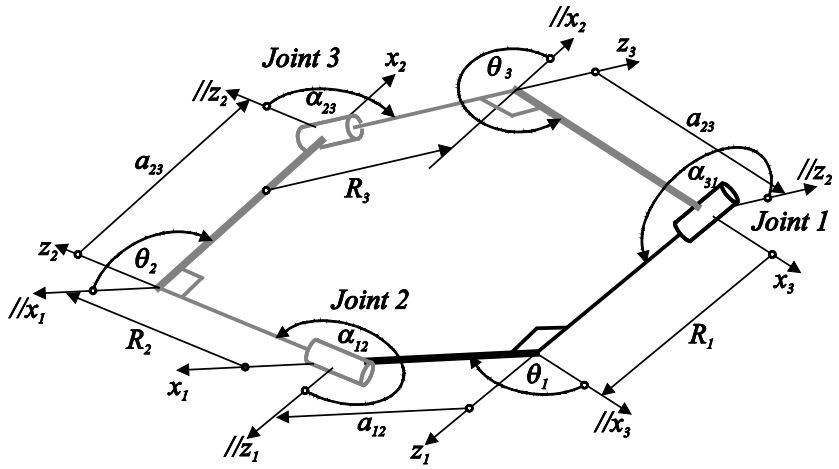

Fig. 5.4.2 The link-pair replacement of link-pair $23 \sim 31$ (grey) replaced by link 12 (black).

Since the relative position between joints $1'$ and $3''$ is already fixed by link-pair $1'2' \sim 2'3''$, we may introduce a new link to replace this link-pair to represent the relative position between joints $1'$ and $3''$, which is called *the link-pair replacement method*. The loop

enclosed by the existing link-pair and the new link forms a spatial triangle. In Fig. 5.4.2, link-pair $1'2' \sim 2'3''$ in Fig. 5.4.1 is equivalent to link-pair $12 \sim 23$ in Fig. 5.4.2. As a result, the relative position between joints 1 and 3 was originally represented by link-pair $12 \sim 23$, and is now represented by link 31. The known parameters on link-pair $12 \sim 23$ are a_{12}, α_{12}, R_2, θ_2, a_{23} and α_{23}. The parameters to be determined are related to link 31, including a_{31}, α_{31}, R_1, R_3, θ_1 and θ_3, which can be solved from the transformation matrix of the spatial triangle in Eq. (5.3.2).

5.4.2 Reconfigurable Bennett Network

By using the link-pair replacement method, the spatial configuration of a fixed link-pair could be replaced by a new link to simplify the representations. We could use this link-pair replacement to reconfigure the spatial configuration of a given linkage, especially for linkages in the Bennett-based linkage family. Shown in Fig. 5.4.3 is a network of four Bennett linkages A, B, C and D, which are made of links a/α, b/β, c/γ and d/δ with the same Bennett ratios. Such spatial network of four Bennett linkages was firstly discussed by Goldberg (1946) when he was investigating the Kempe's planar mechanism in three-dimensional space. Later, Baker (1983) re-examined the same network, but the discussion was still limited to the Kempe's planar mechanism. In this network of four Bennett linkages, each pair of adjacent Bennett linkages share a common link as the connection, i.e., linkages A and B share a common link c/γ, linkages B and C share a common link b/β, linkages C and D share a common link d/δ and linkages D and A share a common link a/α.

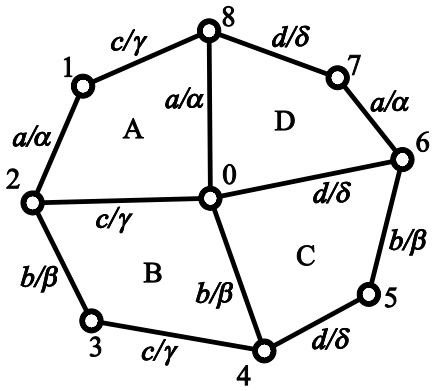

Fig. 5.4.3 The network of four Bennett linkages A, B, C and D.

The mobility of this network can be determined by inspecting linkages A, B and C with their connections shown in Fig. 5.4.4(a). The mobility of each Bennett linkage is determined by only one revolute variable, and the revolute variables of each Bennett linkage are independent to each other. Therefore, the kinematic property of this network with only linkages A, B and C is determined by three independent revolute variables, i.e. this network has three degrees of freedom. On the other hand, since all the links in this network share the same Bennett ratios, we can isomerize the link-pair $a/\alpha \sim d/\delta$ with a new link-pair to form a Bennett linkage D in Fig. 5.4.4(b), and the mobility of the resultant network will not be affected (Wohlhart, 1991b), which makes the resultant network the same as in Fig. 5.4.3. Therefore, the network of four Bennett linkages has three degrees of freedom in general.

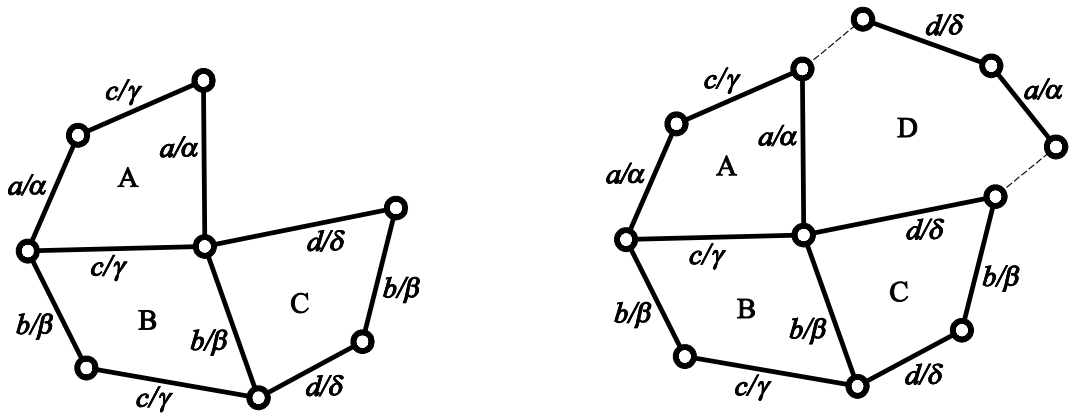

Fig. 5.4.4 The reconstruction of the network of four Bennett linkages: (a) the network with only Bennett linkages A, B and C; (b) isomerize link-pair $a/\alpha \sim d/\delta$ to form Bennett linkage D.

When the relative positions of certain joints on the peripheral loop of the network are fixed, the mobility of the network will be reduced accordingly. In the meanwhile, we can use the link-pair replacement method to reduce the number of links on the peripheral loop and then remove the four links in the center to form a single-loop overconstrained linkage. The resultant linkages will be investigated individually for identification. Since the original network has three degrees of freedom, we shall at least apply the link-pair replacement twice on the peripheral loop to reduce the mobility of the network to only one. The following procedures are designed to reconfigure the network of four Bennett linkages:

- Firstly, select any two link-pairs on the peripheral loop of the Bennett network to perform link-pair replacements;
- Then, remove the four links and joint 0 at the center to make it single loop;
- Finally, identify the mobility and property of the resultant linkage.

Note that a solid dot "●" is used to represent the joint that is going to be replaced and a hollow dot "○" is used to represent the joint where no actions are performed.

5.4.3 6*R* Linkages Achieved From the Reconfigurable Bennett Network

(1) Case 1: Joints 1 and 5 are selected

As shown in Fig. 5.4.5(a), link-pair replacement is performed on selected joints 1 and 5. The original link-pairs 81-12 and 45-56 are replaced by new links 82 and 46, respectively. After replacement, the relative position between joints 8 and 2 is rigidified by link 82, which is the same for joints 4 and 6. The number of joints and links on the peripheral loop is reduced from eight to six. A single-loop overconstrained 6*R* linkage can be obtained after removing the four links and joint 0 at the center.

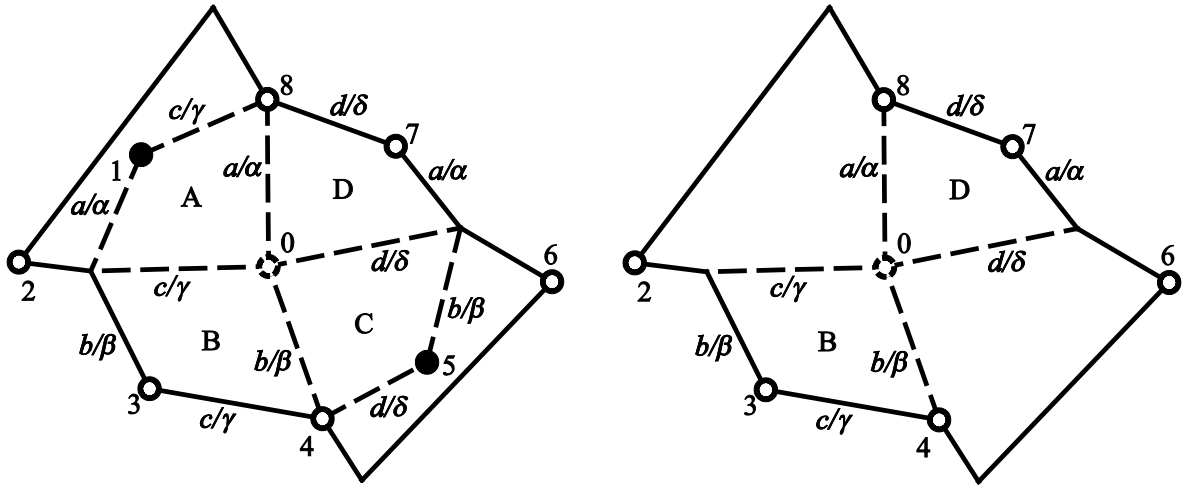

(a) (b)

Fig. 5.4.5 The construct illustration of the case 1 linkage: (a) the schematics of the reconfiguration process for case 1 linkage; (b) linkage identification of the case 1 linkage after reconfiguration.

As shown in Fig. 5.4.5(b), Bennett linkages B and D are superposed on joint 0 and they share the same Bennett ratios on each link, the resultant linkage in case 1 can be identified as the Waldron's hybrid 6*R* linkage with zero offset on joint 0 (Waldron, 1979), which has one degree of freedom. Alternatively, we can perform the link-pair replacement on joints 3 and 7 to achieve the same resultant linkage.

(2) Case 2: Joints 2 and 5 are selected

As shown in Fig. 5.4.6(a), link-pair replacement is performed on selected joints 2 and 5. The original link-pairs 12-23 and 45-56 are replaced by new links 13 and 46, respectively. After replacement, the relative position between joints 1 and 3 is rigidified by link 13, which is the same for joints 4 and 6. The number of joints and links on the peripheral loop is reduced from eight to six. A single-loop overconstrained 6*R* linkage can be achieved after removing the four links and joint 0 at the center.

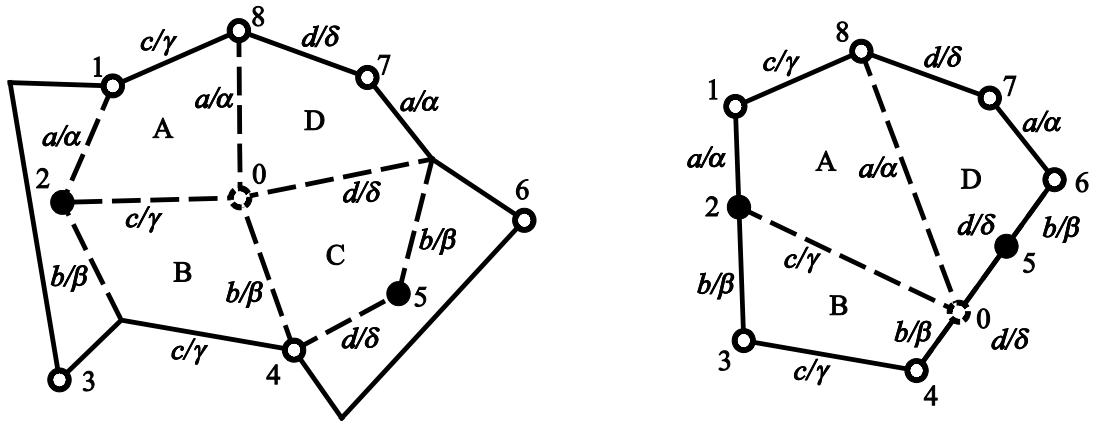

(a) (b)

Fig. 5.4.6 The reconfiguration of the Bennett network into the case 2 linkage: (a) the schematics of the reconfiguration process of case 2 linkage; (b) linkage identification of the case 2 linkage after reconfiguration.

We can identify the resultant linkage by inspecting its special case when link-pairs 12-23 and 45-56 are collinearly rigidified in Fig. 5.4.6(b). When link-pair 45-56 is collinearly rigidified, Bennett linkage C will contract into a straight line and therefore joints 0 and 5 are constrained along this line. From the combination between Bennett linkages A, B and D, we can identify the linkage in Fig. 5.4.6(b) as a variant of the *L*-shape Goldberg 6*R* linkage proposed by Baker (1993a). A more generalized case will be obtained when link-pairs 12-23 and 45-56 are not collinearly rigidified. Thus, the resultant linkage in case 2 is a generalized variant of the *L*-shape Goldberg 6*R* linkage and it has one degree of freedom. Alternatively, we can perform link-pair replacement on joint n and the third joint before or after joint n to achieve the same resultant linkage.

(3) Case 3: Joints 2 and 4 are selected

As shown in Fig. 5.4.7(a), link-pair replacement is performed on selected joints 2 and 4. The original link-pairs 12-23 and 34-45 are replaced by new links 13 and 35, respectively. After replacement, the relative position between joints 1 and 3 is rigidified by link 13, which is the

same for joints 3 and 5. The number of joints and links on the peripheral loop is reduced from eight to six. A single-loop overconstrained 6*R* linkage will be achieved after removing the four links and joint 0 at the center.

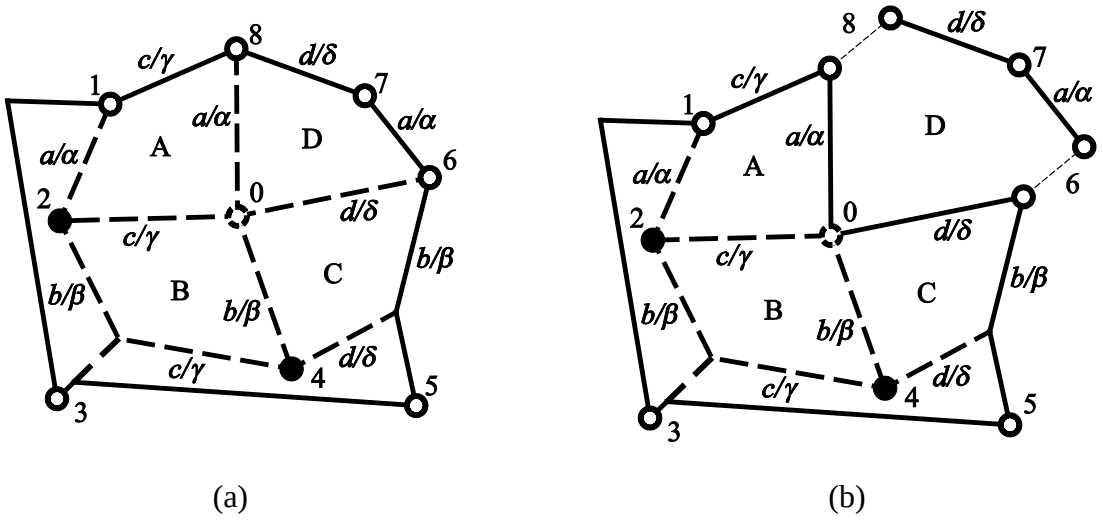

(a) (b)

Fig. 5.4.7 The reconfiguration of the Bennett network into the case 3 linkage: (a) the schematics of the reconfiguration process of case 3 linkage; (b) linkage identification of the case 3 linkage after reconfiguration.

To identify the resultant linkage, we can inspect the loop connected by joints 1, 3, 5, 6, 0 and 8, which is a generalized *L*-shape Goldberg 6*R* linkage (Goldberg, 1943). As shown in Fig. 5.4.7(b), when replacing link-pair 60-08 by link-pair 67-78, an isomerized case of the linkage will be obtained (Wohlhart, 1991b). Therefore, the resultant linkage in case 3 is an isomerized case of the generalized *L*-shape Goldberg 6*R* linkage which has only one degree of freedom. Alternatively, we can perform link-pair replacement on joints 4 and 6, 6 and 8 or 8 and 2 to achieve the same resultant linkage.

(4) Case 4: Joints 2 and 6 are selected

As shown in Fig. 5.4.8(a), link-pair replacement is performed on selected joints 2 and 6. The original link-pairs 12-23 and 56-67 are replaced by new links 13 and 57, respectively. After replacement, the relative position between joints 1 and 3 is rigidified by link 13, which is the

same for joints 5 and 7. The number of joints and links on the peripheral loop is reduced from eight to six. A single-loop overconstrained 6*R* linkage will be achieved after removing the four links and joint 0 at the center.

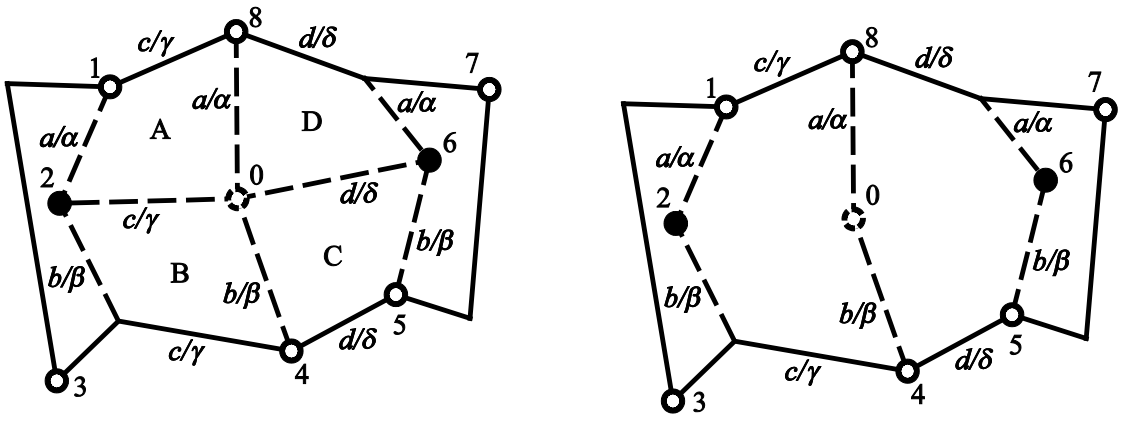

Fig. 5.4.8 The reconfiguration of the Bennett network into the case 4 linkage: (a) the schematics of the reconfiguration process of case 4 linkage; (b) linkage identification of the case 4 linkage after reconfiguration.

The resultant linkage can be identified as a generalized Wohlhart's double-Goldberg 6*R* linkage (Wohlhart, 1991a), see Fig. 5.4.8(b), which has only one degree of freedom. Alternatively, we can perform link-pair replacement on joints 4 and 8 to achieve the same resultant linkage.

(5) Reconfiguration among Different Cases

The link-pair replacement method could also be used to reconfigure the resultant linkage from one case to another. Take the example of the reconfiguration from case 4 to case 3 of the 6*R* linkage, as shown in Fig. 5.4.9. The only difference between these two cases is that joint 6 is selected for link-pair replacement in the case 4 linkage; while joint 4 is selected for link-pair replacement in the case 3 linkage. Therefore, we start by performing link-pair replacement on joint 4 in the case 4 linkage in Fig. 5.4.9(b). Then in Fig. 5.4.9(c), the link-pair replacement on joint 6 will be removed to release the constraint on joint 6. As a result,

the reconfiguration from case 4 into case 3 is achieved. This procedure can be extended to the reconfiguration between other cases following a similar procedure.

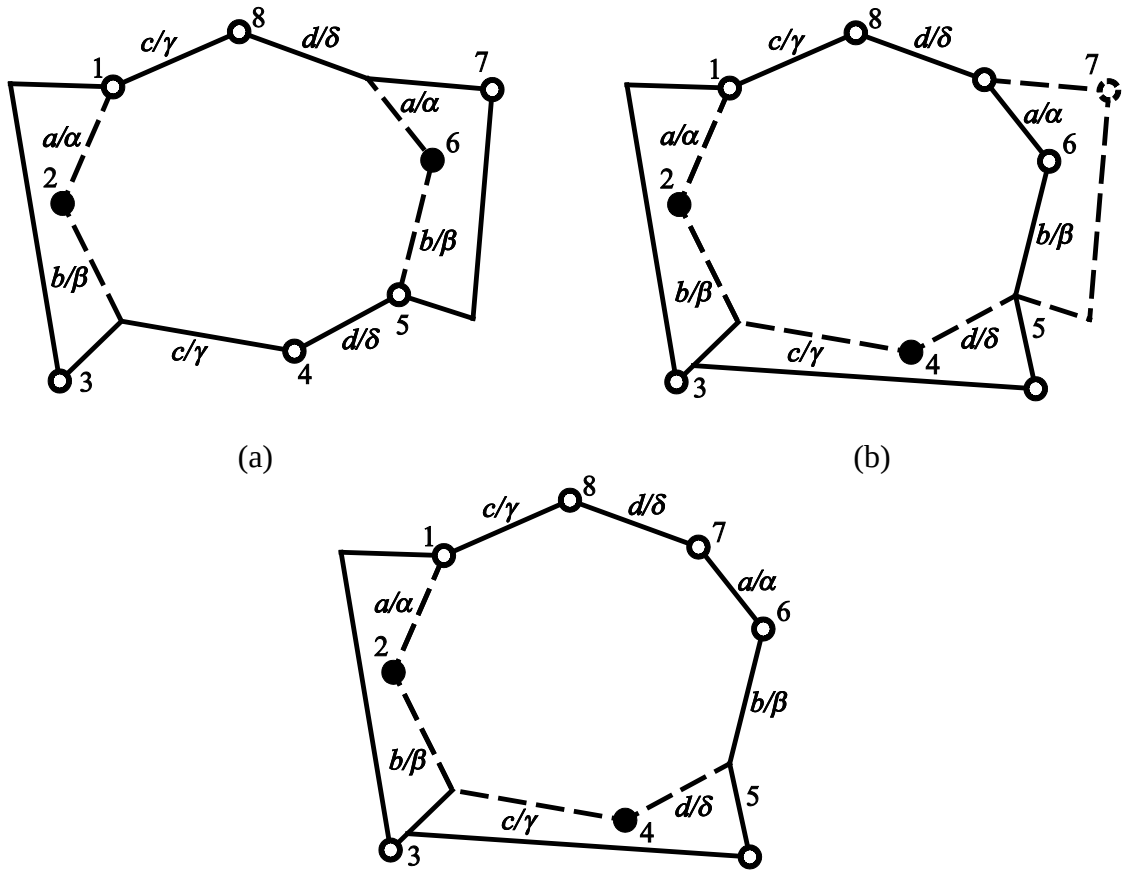

Fig. 5.4.9 The reconfiguration process from case 4 to case 3: (a) the case 4 linkage where joints 2 and 6 are selected for link-pair replacement; (b) reconfiguration process from case 4 linkage into case 3 linkage; (c) the case 3 linkage where joints 2 and 4 are selected for link-pair replacement.

5.4.4 5*R* Linkages Achieved From the Reconfigurable Bennett Network

There are some special cases that a 5*R* linkage can be obtained after the link-pair replacement of this Bennett network. As shown in Fig. 5.4.10(a), link-pair replacement is performed on selected joints 1 and 2. Since these two joints are adjacent to each other, we need to firstly replace link-pair 81-12 by a new link 82 and then replace the new link-pair 82-23 by another new link 83. After doing so, the relative position between joints 8 and 3 is rigidified by the new link 83.

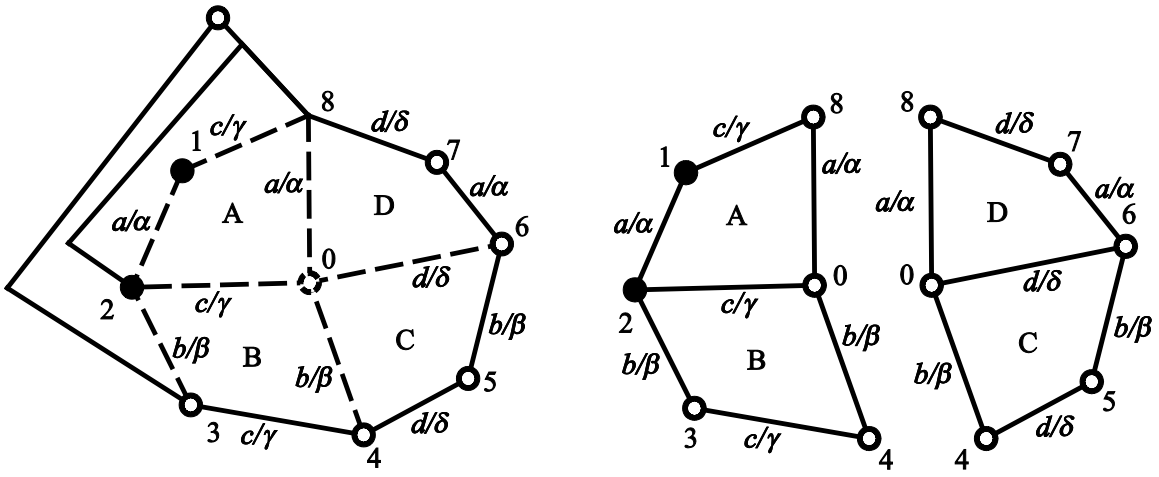

Fig. 5.4.10 The reconfiguration of the Bennett network into a 5*R* linkage: (a) the schematics of the link-pair replacement on joints 1 and 2; (b) the schematics of the network divided into two halves.

To find out the mobility of the resultant network, the original network is split into two halves in Fig. 5.4.10(b). When the link-pair replacement is performed on joints 1 and 2, the left half of the network comprising of Bennett linkages A and B becomes immobile. As a result, link-pair 80-04 on the left half of the network is fixed, i.e., the relative position between joints 8 and 4 is fixed. From the construction of the generalized Goldberg 5*R* linkage, we can conclude that only the right half of the network will be mobile and it is actually a generalized Goldberg 5*R* linkage with mobility one. By combining the two halves back together and removing the four links inside the loop, the resultant linkage is a generalized Goldberg 5*R* linkage with mobility one.

The serial combination between two Bennett linkages shown in Fig. 5.4.11 is comprised of two Bennett linkages superposed on a commonly shared link 05. Since each Bennett linkage has one independent revolute variable, this network has two degrees of freedom in total. To rigidify this network, both revolute variables must be fixed, i.e., one link-pair from each Bennett linkage must be fixed. This is why the left side of network in Fig. 5.4.10(b)

becomes immobile when performing link-pair replacement on joints 1 and 2 simultaneously. As a result, there will be only 5 movable joints in the resultant linkage, including joints 4, 5, 6, 7 and 8. In fact, a generalized Goldberg 5*R* linkage will be obtained when perform link-pair replacement on any two adjacent joints of the peripheral loop.

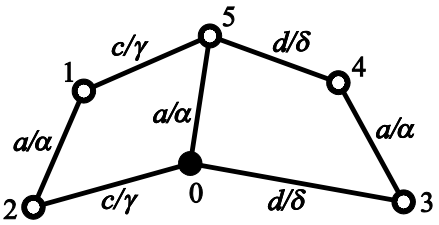

Fig. 5.4.11 The serial combination between two Bennett linkages.

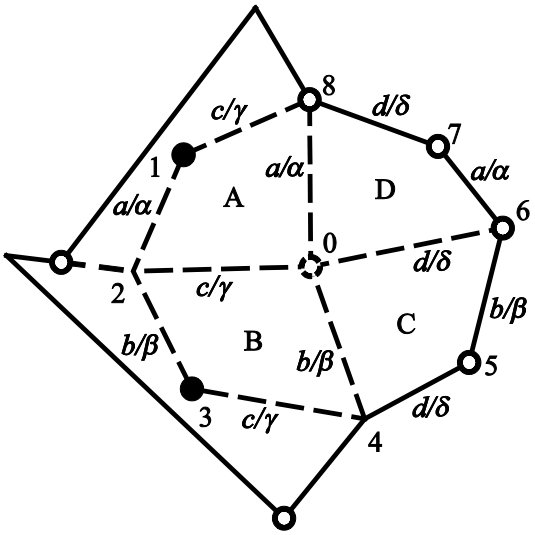

Fig. 5.4.12 The schematics of the case when joints 1 and 3 are selected for link-pair replacement.

Similar conclusion can be drawn when joints 1 and 3 are selected for link-pair replacement in Fig. 5.4.12. The left half of the network will be immobile after the link-pair replacement, including the link-pair on joint 2. The right half of the network is essentially a generalized Goldberg 5*R* linkage with only mobility one after removing the four links inside the loop. The same resultant linkage will be obtained when selecting joints 3 and 5, 5 and 7 or 7 and 1 for link-pair replacement. We can use the same method in section 5.4.3 to reconfigure between the 5*R* and 6*R* linkages achieved from the network.

5.4.5 4*R* Linkage Achieved From the Reconfigurable Bennett Network

It is worth discussing the possibilities to achieve a Bennett linkage, which is the only single-loop overconstrained 4*R* linkage, out of this reconfigurable Bennett network. As shown in the above cases, after performing the link-pair replacements twice on the peripheral loop of the reconfigurable Bennett network, the resultant linkage becomes a single-loop overconstrained 6*R* or 5*R* linkages with mobility one. By further applying the link-pair replacement on this network, the number of links and joints can be reduced to four. However, this operation is equivalent to adding another constraint to the 5*R* and 6*R* linkages obtained in sections 5.4.3 and 5.4.4, which will make the resultant linkage immobile.

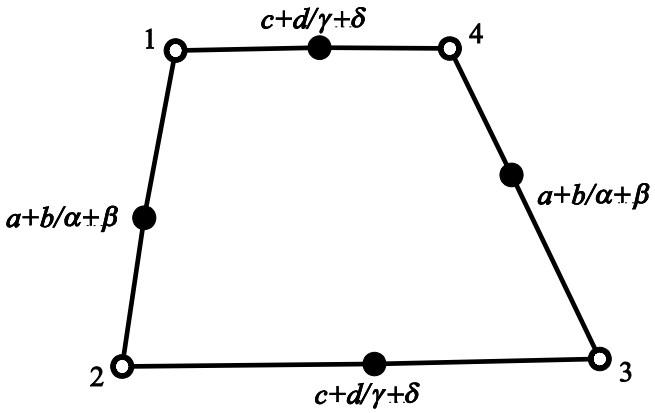

Fig. 5.4.13 A special case of the link-pair replacement on the reconfigurable Bennett network.

There are two special cases of the network that are worth noticing. One case is when the link-pairs on joints 1, 3, 5 and 7 are constrained into a line, and therefore the resultant network will contract into a line, which is a trivial configuration. The other case is when the link-pairs on joints 2, 4, 6 and 8 are constrained into a line as shown in Fig. 5.4.13. In this case, the resultant network will have only four movable joints and a single-loop mechanism can be achieved after removing the four links at the center. Such operation requires the geometry conditions of links a/α, b/β, c/γ and d/δ to meet the requirement of Bennett ratios on the composite links as follows,

$$\frac{\sin(\alpha+\beta)}{a+b}=\frac{\sin(\gamma+\delta)}{c+d}, \tag{5.4.1}$$

so that the Bennett linkage can be achieved. This 4*R* linkage achieved from this reconfigurable Bennett network is actually a special case of the Kempe's planar mechanism. Research about this part was already discussed in detail by Goldberg (1946). Overall, it is possible to obtain a 4*R* linkage from the proposed reconfigurable Bennett network in an indirect way by changing the geometry conditions, which is different from the link-pair replacement method proposed above.

5.4.6 Summary

In section 5.4, the method of link-pair replacement is proposed and applied to a designated reconfigurable Bennett network to change its topological structure. The effective number of links and joints on the Bennett network is reconfigured after link-pair replacement, which leads to different types of single-loop overconstrained 6*R* and 5*R* linkages. On the other hand, we can also use the link-pair replacement method to reconfigure the resultant linkages into different cases of the 6*R* and 5*R* linkages. The 4*R* linkage obtained from the network requires further modifications in geometry conditions and therefore cannot be reconfigured directly using the line-pair replacement method. The proposed Bennett network demonstrates the capability of fulfilling multiple tasks in different operation modes based on solely one mechanism and therefore can be categorized as reconfigurable mechanism (Kuo et al., 2009).

Since the sequence of joints is circular in Fig. 5.4.3, we only need to cover the choices of joints n/n+1, joints n/n+2, joints n/n+3 and joints n/n+4, which are summarized in Table 5.4.1. For example, when selecting joints n/n+1 to perform the link-pair replacement, all of the resultant linkages will be generalized Goldberg 5*R* linkages. When selecting joints n/n+2 to

perform the link-pair replacement, if starting from odd number like odd/odd+2, the resultant linkages will be generalized Goldberg 5*R* linkages; if starting from even number like even/even+2, the resultant linkages will be isomerized case of the generalized *L*-shape Goldberg 6*R* linkages. The rest cases could be summarized in a similar manner in Table 5.4.1. These linkages were originally derived using different methods. Now, we can conveniently correlate them under a common construction basis using the same method.

Table 5.4.1 The linkages reconfigured from the network of four Bennett linkages.

General linkage type	**Joints to be selected for link-pair replacement**		**Specific linkage type**
	Original sequence	**Generalized sequence**	
6*R* linkages	1/5, 3/7	odd/odd+4	Waldron's hybrid 6*R* linkage with zero common offset
	1/4, 2/5, 3/6, 4/7, 5/8	n/n+3	Generalized variant of the *L*-shape Goldberg 6*R* linkage
	2/4, 4/6, 6/8, 8/2	even/even+2	Isomerized case of the generalized *L*-shape Goldberg 6*R* linkage
	2/6, 4/8	even/even+4	Generalized Wohlhart's double-Goldberg 6*R* linkage
5*R* linkages	1/2, 2/3, 3/4, 4/5, 5/6, 6/7, 7/8, 8/1	n/n+1	Generalized Goldberg 5*R* linkage
	1/3, 4/5, 5/7, 7/1	odd/odd+2	
4*R* linkages	2/4/6/8	even joints	Bennett linkage (Special geometry constraint is required)
Trivial configuration	1/3/5/7	odd joints	N/A

Besides the proposed network with four Bennett linkages, this link-pair replacement method can be applied to other networks as well. Two such examples are presented in Fig. 5.4.14. When the link-pair replacement method is applied to the network in Fig. 5.4.14(a), the *L*-shape Goldberg 6*R* linkage and its variant can be derived subsequently. When the link-pair replacement method is applied to the network in Fig. 5.4.14(b), the serial Goldberg 6*R* linkage and its variant can be derived in a similar manner.

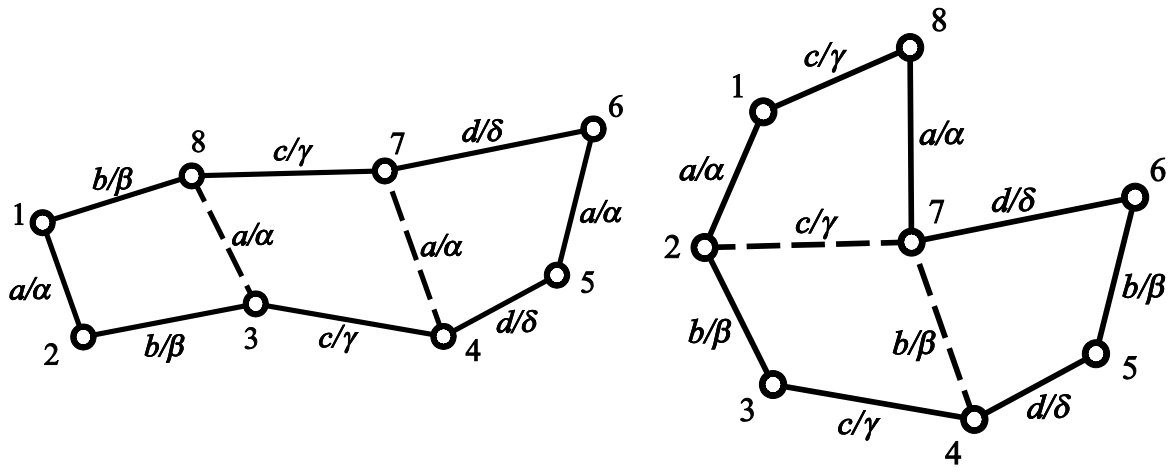

Fig. 5.4.14 Two different types of reconfigurable Bennett network: (a) the serial three-Bennett network; (b) the *L*-shape three-Bennett network.

Chapter 6

Conclusions and Future Work

6.1 CONCLUSIONS

Research works in previous literatures demonstrated continued interests in the topic of overconstrained linkages. However, there lacks of a systematic study into the relationship among the large number of linkages found, which hinders the potential applications of such advanced mechanisms. This dissertation set out from this goal to provide a substantial advancement in the systematic organizations of existing overconstrained linkages and conceptual designs of reconfigurable mechanisms.

In the study of overconstrained 4*R* linkage, this dissertation used the special geometries of Bennett linkages with different setups to construct different types of overconstrained 6*R* linkages. The existence of these two setups is caused by the trigonometric relationship and the linear closure conditions of the revolute variables. However, the existence of the line-symmetric setup and the asymmetric setup of the Bennett linkage did not draw the necessary attentions from researchers in related fields. When the number of links increases, the complexity of the problem increases. As demonstrated in this dissertation, this result is important not only in using the Bennett linkage as a construct unit to build linkages in the Bennett-based family, but also in using its symmetric geometry to construct linkages in the Bricard linkage family. Fundamental research work into the Bennett linkage and its extensions is of great importance to the future applications of overconstrained linkages.

In the study of overconstrained 5*R* linkage, this dissertation explores different methods to use such 5*R* linkages as the building block to construct overconstrained 6*R* linkages. The method of common link-pair, which was developed by Wohlhart; and the method of common Bennett-linkage, which is developed in this dissertation, are used to find all possible overconstrained 6*R* linkages that could be constructed using two overconstrained 5*R* linkages as the building blocks. As a result, a series of double-Goldberg linkage families are systematically organized. Three sub families of Wohlhart's double-Goldberg linkage family, mixed double-Goldberg linkage family and double-subtractive-Goldberg linkage family are obtained when different combinations of Goldberg 5*R* linkage and subtractive Goldberg 5*R* linkage are used. The most generalized form of the double-Goldberg linkage family is the case when two generalized Goldberg 5*R* linkages are used. As a result, a large number of linkages are covered under this linkage family, which provides a sufficient source of design for reconfigurable mechanisms.

In study of overconstrained 6*R* linkage, this dissertation contributes in a few aspects. *Firstly* in the Bennett-based linkage family, this dissertation systematically organized all possible linkages in the double-Goldberg linkage family, whose relationship were previously unclear in literatures. Furthermore, the existence of an extra link is identified in the geometry conditions of the double-Goldberg linkage families, which could be useful in reconfiguring the spatial configuration of the resultant linkages in future applications. *Secondly* in the Bricard linkage family, this dissertation explicitly derived the closure equations of the original and revised general line-symmetric Bricard linkages. The revised general line-symmetric Bricard linkage has negatively equaled offsets on the opposite joints, which shares certain similarity with the original linkage but lack of the analytical investigation into its explicit kinematics. It is found in this dissertation that there are two different linkage forms

for both the original and revised linkages, and the revised case is actually equivalent to the original case with different setups on the joint axis directions. This is caused by the limitation of DH parameters, which failed to distinguish the identities of such special geometries. The result about the general line-symmetric Bricard linkage also provides the analytical proof that the line-symmetric octahedral Bricard linkage is just its special case. For the special case of the line-symmetric Bricard linkage with no offset, the geometry conditions of the original and revised general line-symmetric Bricard linkage become identical. As a result, the resultant four linkage forms, two from the original linkage closure and two from the revised linkage closure, could transform into each other through bifurcations, which makes them a good source of design for reconfigurable mechanisms. However, the two revised linkage closures could be alternatively represented using the original linkages by adding or deducting π on the twists of one pair of opposite links.

In this dissertation, several conceptual designs of the reconfigurable mechanisms are proposed using the overconstrained linkages. The *first* reconfigurable mechanism is based on an overconstrained 6*R* linkage which can be reconfigured into a 4*R* linkage through bifurcations. The results in chapters 3 and 4 demonstrate the close connection between overconstrained 6*R* and 4*R* linkages. By using the original and subtractive cases of Type I double-Goldberg linkage as the source of design, the operation form of a 4*R* linkage is introduced to the existing bifurcation loop of these 6*R* linkages using analytical method. By using the general line-symmetric Bricard linkage as the source of design, the same goal is achieved using geometric method. A reconfigurable line-symmetric Bricard linkage is formed by using a Bennett linkage in different setups to bridge two identical spatial triangles. When the line-symmetric Bennett linkage is used, the resultant linkage shares the same geometry properties of the original line-symmetric Bricard linkage with one pair of revolute variables

reaching their limiting positions. When the asymmetric Bennett linkage is used, the original line-symmetric geometry of the linkage is disrupted. As a result, a new kinematic path is introduced to the resultant linkage's bifurcation loop, which makes this linkage capable of reconfiguration between 4*R* and 6*R* linkages through bifurcation points.

The *second* design is aimed at reconfiguring the topology of a designated network of Bennett linkages with different operation forms. Based on the geometry of the spatial triangle, a generic method of link-pair replacement is developed to determine and simplify the relative position of a fixed link-pair with a new link. A network of four Bennett linkages is taken as an example to demonstrate two different reconfiguration processes. The first process is to reconfigure the designated Bennett network into different cases of single-loop overconstrained linkages with only one degree of freedom. As a result, five cases of overconstrained linkages are obtained from this network using this method. The second process is to reconfigure the resultant linkage from one case into another, which is applicable for all resultant linkages. By changing the Bennett network into other topologies, i.e., the *L*-shape network of three Bennett linkages or the serial network of three Bennett linkages, different overconstrained linkages could be achieved. The result in this part provides a significant design methodology for reconfigurable mechanisms.

6.2 CONTRIBUTIONS

In this dissertation, a number of mechanism design issues are addressed to use the overconstrained linkages in the conceptual designs of reconfigurable mechanisms. The framework developed here provides a comprehensive understanding of overconstrained linkages, as well as the analytical, construct and generic methods that could be used to design reconfigurable mechanism using overconstrained linkages. Throughout this dissertation, the

focus is to explore the kinematics of the overconstrained linkage for a systematical understanding of its topology and to apply them in reconfigurable mechanism conceptual designs. The key to achieve this goal is to formulate the correlation among various types of the overconstrained linkages, and then to investigate methods that could be used to design and reconfigure desired linkages. The ultimate goal is to apply overconstrained spatial linkages in reconfigurable mechanism designs, so that certain sophisticated and complex engineering applications could be accomplished. The contributions of this research are as listed:

Chapter 3

i. Based on the combination between two overconstrained 5*R* linkages, a systematic organization of all possible linkages in the double-Goldberg linkage family is made, which includes a large number of linkages in the Bennett-based linkage family;
ii. A new mixed double-Goldberg 6*R* linkage family is built and analyzed using the common link-pair and common Bennett linkage methods to combine a Goldberg 5*R* linkage and a subtractive Goldberg 5*R* linkage;

Chapter 4

iii. The kinematic analysis to the original and revised general line-symmetric Bricard linkages is performed, where new linkage closures are analyzed and derived;
iv. The kinematic bifurcations among the four forms of the original and revised line-symmetric Bricard linkage without offsets are studied;

Chapter 5

v. Multiple operation forms and bifurcation behaviors of the double-subtractive-Goldberg 6*R* linkage, Wohlhart's double-Goldberg 6*R* linkage and the first reconfigurable line-symmetric Bricard linkage are studied using analytical and construct methods;

vi. The innovative construction of the reconfigurable line-symmetric Bricard linkage using two spatial triangles bridged by a Bennett linkage in asymmetric setup;

vii. A new generic method of link-pair replacement is proposed to reconfigure the topology of a network of Bennett linkages. The resultant linkages have only one degree of freedom and can be reconfigured into each other using this generic method;

viii. Based on the reconfiguration of a network of Bennett linkages, the relationship among a number of linkages in the Bennett-based linkage family is systematically organized;

6.3 FUTURE WORK

There are still a number of topics to be explored in the area of overconstrained linkage kinematics and its applications in advanced mechanism design. Besides the linkages listed in chapter 2, there are overconstrained linkages that are not included in this dissertation, such as the syncopated linkages. Research activities about the overconstrained linkage should not be limited to the kinematics of each specific linkage individually. As demonstrated in this dissertation, there is certain relationship among the overconstrained linkages which could be useful in applying such advanced mechanism in reconfigurable mechanism designs. Future research could focus on the applications of the overconstrained linkage in engineering designs.

The families of Bennett-based linkages and Bricard linkages are just a general description to generalize overconstrained linkages with similar characteristics. Such categorization could never be complete and accurate as new linkages and methods will be discovered and developed. Further research into the specific characteristics of certain linkage groups would be beneficial in novel mechanism design. On the other hand, solutions to the overconstrained linkages would be of great value for computational kinematics in robotics applications. The

increasing sophistication and complexity in current robotic applications requires further breakthroughs in mathematical tools for efficiency and accuracy. Research work in overconstrained linkages provides the theory and engineering foundations to develop such mathematical tools in the past decades, and will continue to contribute its value in the future.

It is already demonstrated in this dissertation that the overconstrained linkages could be a significant source of advanced mechanism designs with sophisticated or complex functions. In the reconfigurable mechanism with multiple operation forms presented in this dissertation, the bifurcation behavior is emphasized with great attentions to enable the reconfiguration between a 4*R* linkage and a 6*R* linkage. Limited by current technology in manufacturing and control, such bifurcation behavior is usually avoided in classical mechanism design. The result in this dissertation demonstrates the potential of designing overconstrained linkages with desired bifurcation behaviors. One possible solution with engineering practicability is to design the linkage in its alternative forms, where the complexity of machining each links and joints could be largely reduced, and it could be much easier to attach actuator on the links for control. Further research shall be explored in such areas to apply reconfigurable mechanisms in solving certain engineering problems.

The result in the reconfigurable Bennett network explores a different way of reconfigurable mechanism design based on overconstrained linkage. It is a generic method to reconfigure the spatial configuration of a designated network of Bennett linkages. Future research could be addressed on the special cases of such Bennett network, such as the case when all Bennett linkages are identical to each other or the case when all Bennett linkages share the same length to each other and etc. From historical experience, it is usually the special cases of such designs that provide the most functionality and flexibility in

applications. In future application-wise, we would like to see the reconfigurable mechanism deployed in novel modular robotic design. In such a system, each modular mimics the function of the basic link in the reconfigurable Bennett network, where the geometry conditions of each modular could change on its own. The connection of these modular robots could be reconfigured into different configurations to provide the necessary motion and structural support for the sophisticated tasks in engineering applications and space missions.

Appendix A:

The Singular Value Decomposition (SVD) Method

The SVD method tries to solve a linkage's Jacobian matrix with a predictor and corrector step (Gan and Pellegrino, 2006). To conduct this numerical scheme, the transformation matrix in (A1) is decomposed into two matrices, one matrix contains only the information about the revolute variable θ_i, marked as $\mathbf{T}_i^{\theta}$; while the other matrix contains information about the link length $a_{i(i+1)}$, twist angle $\alpha_{i(i+1)}$ and offset R_i in the transformation, marked as $\mathbf{T}_{i(i+1)}^{L}$. Thus,

$$\mathbf{T}_{i(i+1)} = \begin{bmatrix} \cos\theta_i & -\cos\alpha_{i(i+1)}\sin\theta_i & \sin\alpha_{i(i+1)}\sin\theta_i & a_{i(i+1)}\cos\theta_i \\ \sin\theta_i & \cos\alpha_{i(i+1)}\cos\theta_i & -\sin\alpha_{i(i+1)}\cos\theta_i & a_{i(i+1)}\sin\theta_i \\ 0 & \sin\alpha_{i(i+1)} & \cos\alpha_{i(i+1)} & R_i \\ 0 & 0 & 0 & 1 \end{bmatrix}, \tag{A1}$$

$$\mathbf{T}_{i(i+1)} = \mathbf{T}_{i(i+1)}^{L}\mathbf{T}_i^{\theta}, \tag{A2}$$

where

$$\mathbf{T}_{i(i+1)}^{L} = \begin{bmatrix} 1 & 0 & 0 & a_{i(i+1)} \\ 0 & \cos\alpha_{i(i+1)} & -\sin\alpha_{i(i+1)} & 0 \\ 0 & \sin\alpha_{i(i+1)} & \cos\alpha_{i(i+1)} & R_i \\ 0 & 0 & 0 & 1 \end{bmatrix}, \tag{A3}$$

and

$$\mathbf{T}_i^{\theta} = \begin{bmatrix} \cos\theta_i & -\sin\theta_i & 0 & 0 \\ \sin\theta_i & \cos\theta_i & 0 & 0 \\ 0 & 0 & 1 & 0 \\ 0 & 0 & 0 & 1 \end{bmatrix}. \tag{A4}$$

The closure equation below

$$\mathbf{T}_{12}\mathbf{T}_{23}\mathbf{T}_{34}\mathbf{T}_{45}\mathbf{T}_{56}\mathbf{T}_{61}=\mathbf{I}\,, \tag{A5}$$

becomes

$$\left(\mathbf{T}_{12}^{L}\mathbf{T}_{1}^{\theta}\right)\left(\mathbf{T}_{23}^{L}\mathbf{T}_{2}^{\theta}\right)\left(\mathbf{T}_{34}^{L}\mathbf{T}_{3}^{\theta}\right)\left(\mathbf{T}_{45}^{L}\mathbf{T}_{4}^{\theta}\right)\left(\mathbf{T}_{56}^{L}\mathbf{T}_{5}^{\theta}\right)\left(\mathbf{T}_{61}^{L}\mathbf{T}_{6}^{\theta}\right)=\mathbf{I}\,. \tag{A6}$$

Consider small geometry changes of the linkages configurations from θ_i to $\theta_i+\Delta\theta_i$ ($i=1,2,...,6$) with no deformation on any link. The linkage closure must also satisfy in the new configurations

$$\left(\mathbf{T}_{12}^{L}\mathbf{T}_{1}^{\theta+\Delta\theta}\right)\left(\mathbf{T}_{23}^{L}\mathbf{T}_{2}^{\theta+\Delta\theta}\right)\left(\mathbf{T}_{34}^{L}\mathbf{T}_{3}^{\theta+\Delta\theta}\right)\left(\mathbf{T}_{45}^{L}\mathbf{T}_{4}^{\theta+\Delta\theta}\right)\left(\mathbf{T}_{56}^{L}\mathbf{T}_{5}^{\theta+\Delta\theta}\right)\left(\mathbf{T}_{61}^{L}\mathbf{T}_{6}^{\theta+\Delta\theta}\right)=\mathbf{I}\,. \tag{A7}$$

If $\Delta\theta_i$ is very small, after operating Taylor expansion of the revolute variables and eliminating the higher-order terms, the transformation matrix of the revolute joint is

$$\begin{aligned}\mathbf{T}_{i}^{\theta+\Delta\theta}&=\begin{bmatrix}\cos(\theta_i+\Delta\theta_i) & -\sin(\theta_i+\Delta\theta_i) & 0 & 0\\ \sin(\theta_i+\Delta\theta_i) & \cos(\theta_i+\Delta\theta_i) & 0 & 0\\ 0 & 0 & 1 & 0\\ 0 & 0 & 0 & 1\end{bmatrix}\\ &=\begin{bmatrix}-\sin\theta_i & -\cos\theta_i & 0 & 0\\ \cos\theta_i & -\sin\theta_i & 0 & 0\\ 0 & 0 & 1 & 0\\ 0 & 0 & 0 & 1\end{bmatrix}\Delta\theta_i\\ &=\mathbf{T}_{i}^{\theta}+\mathbf{T}_{i}'^{\theta}\Delta\theta_i.\end{aligned} \tag{A8}$$

Substituting (A8) into (A7) will get

$$\begin{aligned}&\mathbf{T}_{12}^{L}\left(\mathbf{T}_{1}^{\theta}+\mathbf{T}_{1}'^{\theta}\Delta\theta_1\right)\mathbf{T}_{23}^{L}\left(\mathbf{T}_{2}^{\theta}+\mathbf{T}_{2}'^{\theta}\Delta\theta_2\right)\mathbf{T}_{34}^{L}\left(\mathbf{T}_{3}^{\theta}+\mathbf{T}_{3}'^{\theta}\Delta\theta_3\right)...\\ &\quad\mathbf{T}_{45}^{L}\left(\mathbf{T}_{4}^{\theta}+\mathbf{T}_{4}'^{\theta}\Delta\theta_4\right)\mathbf{T}_{56}^{L}\left(\mathbf{T}_{5}^{\theta}+\mathbf{T}_{5}'^{\theta}\Delta\theta_5\right)\mathbf{T}_{61}^{L}\left(\mathbf{T}_{6}^{\theta}+\mathbf{T}_{6}'^{\theta}\Delta\theta_6\right)=\mathbf{I},\end{aligned} \tag{A9}$$

i.e.,

$$\begin{aligned}&\left(\mathbf{T}_{12}^{L}\mathbf{T}_{1}^{\theta}\right)\left(\mathbf{T}_{23}^{L}\mathbf{T}_{2}^{\theta}\right)\left(\mathbf{T}_{34}^{L}\mathbf{T}_{3}^{\theta}\right)\left(\mathbf{T}_{45}^{L}\mathbf{T}_{4}^{\theta}\right)\left(\mathbf{T}_{56}^{L}\mathbf{T}_{5}^{\theta}\right)\left(\mathbf{T}_{61}^{L}\mathbf{T}_{6}^{\theta}\right)\\ &+\left(\mathbf{T}_{12}^{L}\mathbf{T}_{1}'^{\theta}\right)\left(\mathbf{T}_{23}^{L}\mathbf{T}_{2}^{\theta}\right)\left(\mathbf{T}_{34}^{L}\mathbf{T}_{3}^{\theta}\right)\left(\mathbf{T}_{45}^{L}\mathbf{T}_{4}^{\theta}\right)\left(\mathbf{T}_{56}^{L}\mathbf{T}_{5}^{\theta}\right)\left(\mathbf{T}_{61}^{L}\mathbf{T}_{6}^{\theta}\right)\Delta\theta_1\\ &+\left(\mathbf{T}_{12}^{L}\mathbf{T}_{1}^{\theta}\right)\left(\mathbf{T}_{23}^{L}\mathbf{T}_{2}'^{\theta}\right)\left(\mathbf{T}_{34}^{L}\mathbf{T}_{3}^{\theta}\right)\left(\mathbf{T}_{45}^{L}\mathbf{T}_{4}^{\theta}\right)\left(\mathbf{T}_{56}^{L}\mathbf{T}_{5}^{\theta}\right)\left(\mathbf{T}_{61}^{L}\mathbf{T}_{6}^{\theta}\right)\Delta\theta_2\\ &\qquad\qquad...\\ &+\left(\mathbf{T}_{12}^{L}\mathbf{T}_{1}^{\theta}\right)\left(\mathbf{T}_{23}^{L}\mathbf{T}_{2}^{\theta}\right)\left(\mathbf{T}_{34}^{L}\mathbf{T}_{3}^{\theta}\right)\left(\mathbf{T}_{45}^{L}\mathbf{T}_{4}^{\theta}\right)\left(\mathbf{T}_{56}^{L}\mathbf{T}_{5}^{\theta}\right)\left(\mathbf{T}_{61}^{L}\mathbf{T}_{6}'^{\theta}\right)\Delta\theta_6=\mathbf{I}.\end{aligned} \tag{A10}$$

Because of (A6), it can be derived that

$$\mathbf{T}_1\Delta\theta_1 + \mathbf{T}_2\Delta\theta_2 + \mathbf{T}_3\Delta\theta_3 + \mathbf{T}_4\Delta\theta_4 + \mathbf{T}_5\Delta\theta_5 + \mathbf{T}_6\Delta\theta_6 = [\mathbf{0}], \tag{A11}$$

where $\mathbf{T}_1 = \left(\mathbf{T}_{12}^L\mathbf{T}_1'^{\theta}\right)\left(\mathbf{T}_{23}^L\mathbf{T}_2^{\theta}\right)\left(\mathbf{T}_{34}^L\mathbf{T}_3^{\theta}\right)\left(\mathbf{T}_{45}^L\mathbf{T}_4^{\theta}\right)\left(\mathbf{T}_{56}^L\mathbf{T}_5^{\theta}\right)\left(\mathbf{T}_{61}^L\mathbf{T}_6^{\theta}\right)$, etc., whose forms are similar as

$$\mathbf{T}_i = \begin{bmatrix} 0 & t_{i_{1,2}} & t_{i_{1,3}} & t_{i_{1,4}} \\ -t_{i_{1,2}} & 0 & t_{i_{2,3}} & t_{i_{2,4}} \\ -t_{i_{1,3}} & -t_{i_{2,3}} & 0 & t_{i_{3,4}} \\ 0 & 0 & 0 & 0 \end{bmatrix}. \tag{A12}$$

Due to the skew-symmetry property, each $\mathbf{T}_i$ has only 6 independent parameters, which will form the Plücker coordinates of each joint axis. This yields a 6×6 system of equations, whose coefficient matrix is known as the Jacobian of the system.

$$\begin{bmatrix} \mathbf{T}_{1_{1,2}} & \mathbf{T}_{2_{1,2}} & \mathbf{T}_{3_{1,2}} & \mathbf{T}_{4_{1,2}} & \mathbf{T}_{5_{1,2}} & \mathbf{T}_{6_{1,2}} \\ \mathbf{T}_{1_{1,3}} & \mathbf{T}_{2_{1,3}} & \mathbf{T}_{3_{1,3}} & \mathbf{T}_{4_{1,3}} & \mathbf{T}_{5_{1,3}} & \mathbf{T}_{6_{1,3}} \\ \mathbf{T}_{1_{2,3}} & \mathbf{T}_{2_{2,3}} & \mathbf{T}_{3_{2,3}} & \mathbf{T}_{4_{2,3}} & \mathbf{T}_{5_{2,3}} & \mathbf{T}_{6_{2,3}} \\ \mathbf{T}_{1_{1,4}} & \mathbf{T}_{2_{1,4}} & \mathbf{T}_{3_{1,4}} & \mathbf{T}_{4_{1,4}} & \mathbf{T}_{5_{1,4}} & \mathbf{T}_{6_{1,4}} \\ \mathbf{T}_{1_{2,4}} & \mathbf{T}_{2_{2,4}} & \mathbf{T}_{3_{2,4}} & \mathbf{T}_{4_{2,4}} & \mathbf{T}_{5_{2,4}} & \mathbf{T}_{6_{2,4}} \\ \mathbf{T}_{1_{3,4}} & \mathbf{T}_{2_{3,4}} & \mathbf{T}_{3_{3,4}} & \mathbf{T}_{4_{3,4}} & \mathbf{T}_{5_{3,4}} & \mathbf{T}_{6_{3,4}} \end{bmatrix} \begin{bmatrix} \Delta\theta_1 \\ \Delta\theta_2 \\ \Delta\theta_3 \\ \Delta\theta_4 \\ \Delta\theta_5 \\ \Delta\theta_6 \end{bmatrix} = \begin{bmatrix} 0 \\ 0 \\ 0 \\ 0 \\ 0 \\ 0 \end{bmatrix}. \tag{A13}$$

When the system has mobility one, the matrix in (A13) will be with rank of 5 rather than full rank 6. This implies that there is a single set of infinity solutions to the matrix in (A13) and the six Plücker coordinates of the linkage are linearly dependent, which leads to the conclusion that the linkage has an internal degree of mobility. The solution to (A13) is the infinitesimal displacement of the linkage at current configuration, which can be found by computing the singular value decomposition (SVD) of the Jacobian matrix.

In the numerical simulation, a small finite displacement, $\Delta\theta_i^p$ (i = 1, 2, …, 6), which is called predictor and is proportional to the infinitesimal solution of (A13), is added to θ_i to update the linkage in the predicted configuration, $\theta_i^p = \theta_i + \Delta\theta_i^p$. However, this linear

relationship is very likely to induce errors to the kinematic paths, which is mostly non-linear. Therefore, under the predicted configuration, (A6) becomes

$$\left(\mathbf{T}_{12}^{L}\mathbf{T}_{1}^{\theta p}\right)\left(\mathbf{T}_{23}^{L}\mathbf{T}_{2}^{\theta p}\right)\left(\mathbf{T}_{34}^{L}\mathbf{T}_{3}^{\theta p}\right)\left(\mathbf{T}_{45}^{L}\mathbf{T}_{4}^{\theta p}\right)\left(\mathbf{T}_{56}^{L}\mathbf{T}_{5}^{\theta p}\right)\left(\mathbf{T}_{61}^{L}\mathbf{T}_{6}^{\theta p}\right)=\mathbf{I}+\mathbf{E}, \tag{A14}$$

where $\mathbf{E}$ is the error matrix.

A corrector, $\Delta\theta_i^c$, is added to the predictor displacement so that the linkage moves towards to the corrected configuration on the kinematic paths, i.e.

$$\theta_i^n=\theta_i^p+\Delta\theta_i^c=\theta_i+\Delta\theta_i^p+\Delta\theta_i^c, \tag{A15}$$

under which (A6) is satisfied as

$$\left(\mathbf{T}_{12}^{L}\mathbf{T}_{1}^{\theta n}\right)\left(\mathbf{T}_{23}^{L}\mathbf{T}_{2}^{\theta n}\right)\left(\mathbf{T}_{34}^{L}\mathbf{T}_{3}^{\theta n}\right)\left(\mathbf{T}_{45}^{L}\mathbf{T}_{4}^{\theta n}\right)\left(\mathbf{T}_{56}^{L}\mathbf{T}_{5}^{\theta n}\right)\left(\mathbf{T}_{61}^{L}\mathbf{T}_{6}^{\theta n}\right)=\mathbf{I}. \tag{A16}$$

From (A16)-A(14), it can be obtained that

$$\mathbf{T}_1^p\Delta\theta_1^c+\mathbf{T}_2^p\Delta\theta_2^c+\mathbf{T}_3^p\Delta\theta_3^c+\mathbf{T}_4^p\Delta\theta_4^c+\mathbf{T}_5^p\Delta\theta_5^c+\mathbf{T}_6^p\Delta\theta_6^c=\mathbf{E}. \tag{A17}$$

where $\mathbf{T}_1^p=\left(\mathbf{T}_{12}^{L}\mathbf{T}_{1}^{\theta p}\right)\left(\mathbf{T}_{23}^{L}\mathbf{T}_{2}^{\theta p}\right)\left(\mathbf{T}_{34}^{L}\mathbf{T}_{3}^{\theta p}\right)\left(\mathbf{T}_{45}^{L}\mathbf{T}_{4}^{\theta p}\right)\left(\mathbf{T}_{56}^{L}\mathbf{T}_{5}^{\theta p}\right)\left(\mathbf{T}_{61}^{L}\mathbf{T}_{6}^{\theta p}\right)$, etc. The solution to (A17) can be obtained from the same SVD method as (A13). The new configuration will be used as the configuration for the next iteration in simulation. After a number of iterations, the full kinematic paths of the linkage could be found.

Appendix B:

Proof to the Relationship in Eq. (5.2.35)

After introducing the special geometry condition to the closure equations of double-subtractive-Goldberg linkage, we can simplify P_{DSG} in Eqs. (5.2.4) and (5.2.5) by $m_1 = -m_4$ and $m_6 = -m_3$ as follows.

$$P_{\mathrm{DSG}} = \frac{1}{2}\left[-\left(m_6 - m_1\right)\cdot \frac{m_6 + m_1 \tan^2\frac{\theta_1}{2}}{\left(m_6 - m_1\right)\tan\frac{\theta_1}{2}} \pm \sqrt{\left(m_6 - m_1\right)^2 \frac{\left(m_6 + m_1 \tan^2\frac{\theta_1}{2}\right)^2}{\left(m_6 - m_1\right)^2 \tan^2\frac{\theta_1}{2}} - 4m_1 m_6} \right] \tag{B1}$$

$$= \frac{1}{2}\left(-\frac{m_6 + m_1 \tan^2\frac{\theta_1}{2}}{\tan\frac{\theta_1}{2}} \pm \left| \frac{m_6 - m_1 \tan^2\frac{\theta_1}{2}}{\tan\frac{\theta_1}{2}} \right| \right).$$

For Form I linkage, we have

$$P_{\mathrm{DSG}} = \begin{cases} \dfrac{1}{2}\left(-\dfrac{m_6 + m_1 \tan^2\frac{\theta_1}{2}}{\tan\frac{\theta_1}{2}} + \left| \dfrac{m_6 - m_1 \tan^2\frac{\theta_1}{2}}{\tan\frac{\theta_1}{2}} \right| \right) & \left(-\pi \le \theta_1 < 0\right), \\ \dfrac{1}{2}\left(-\dfrac{m_6 + m_1 \tan^2\frac{\theta_1}{2}}{\tan\frac{\theta_1}{2}} - \left| \dfrac{m_6 - m_1 \tan^2\frac{\theta_1}{2}}{\tan\frac{\theta_1}{2}} \right| \right) & \left(0 \le \theta_1 < \pi\right). \end{cases} \tag{B2}$$

The sign of $\left| \dfrac{m_2 - m_1 \tan^2\frac{\theta_1}{2}}{\tan\frac{\theta_1}{2}} \right|$ determines the result, which is related to $m_{1,2}$ and $\tan\dfrac{\theta_1}{2}$.

- **Case 1**: $m_6 - m_1 \tan^2\dfrac{\theta_1}{2} > 0$ always hold

When $-\pi \le \theta_1 < 0$, $\tan\frac{\theta_1}{2} < 0$, therefore $\left|\frac{m_6 - m_1 \tan^2\frac{\theta_1}{2}}{\tan\frac{\theta_1}{2}}\right| < 0$. For Form I linkage,

$$P_{\text{DSG}} = \frac{1}{2}\left[-\frac{m_6 + m_1 \tan^2\frac{\theta_1}{2}}{\tan\frac{\theta_1}{2}} + \left(-\frac{m_6 - m_1 \tan^2\frac{\theta_1}{2}}{\tan\frac{\theta_1}{2}}\right)\right] = -\frac{m_6}{\tan\frac{\theta_1}{2}}, \tag{B3}$$

When $0 \le \theta_1 < \pi$, $\tan\frac{\theta_1}{2} > 0$, therefore $\left|\frac{m_6 - m_1 \tan^2\frac{\theta_1}{2}}{\tan\frac{\theta_1}{2}}\right| > 0$. For Form I linkage,

$$P_{\text{DSG}} = \frac{1}{2}\left[-\frac{m_6 + m_1 \tan^2\frac{\theta_1}{2}}{\tan\frac{\theta_1}{2}} - \left(+\frac{m_6 - m_1 \tan^2\frac{\theta_1}{2}}{\tan\frac{\theta_1}{2}}\right)\right] = -\frac{m_6}{\tan\frac{\theta_1}{2}}, \tag{B4}$$

For $\theta_1 \in [-\pi, 0)$ or $[0, \pi)$ in the Form I linkage, we will always have

$$\tan\frac{\theta_1}{2}\cdot\tan\frac{\theta_5}{2} = \tan\frac{\theta_1}{2}\cdot\frac{\left(-\frac{m_6}{\tan\frac{\theta_1}{2}}\right)}{-m_6} = 1 \text{ or } \theta_1 + \theta_5 = \pm\pi\,. \tag{B5}$$

which make the curve of θ_5 vs. θ_1 is a straight line. To be specific, for $\theta_1 \in [-\pi, 0)$, $\theta_1 + \theta_5 = -\pi$ and for $\theta_1 \in [0, \pi)$, $\theta_1 + \theta_5 = \pi$.

- **Case 2**: $m_6 - m_1 \tan^2\frac{\theta_1}{2} < 0$ always hold

When $-\pi \le \theta_1 < 0$, $\tan\frac{\theta_1}{2} < 0$, therefore $\left|\frac{m_6 - m_1 \tan^2\frac{\theta_1}{2}}{\tan\frac{\theta_1}{2}}\right| > 0$. For Form I linkage,

$$P_{\text{DSG}} = \frac{1}{2}\left[-\frac{m_6 + m_1 \tan^2\frac{\theta_1}{2}}{\tan\frac{\theta_1}{2}} + \left(+\frac{m_6 - m_1 \tan^2\frac{\theta_1}{2}}{\tan\frac{\theta_1}{2}}\right)\right] = -m_1 \tan\frac{\theta_1}{2}, \tag{B6}$$

When $0 \le \theta_1 < \pi$, $\tan\frac{\theta_1}{2} > 0$, therefore $\left|\frac{m_6 - m_1 \tan^2\frac{\theta_1}{2}}{\tan\frac{\theta_1}{2}}\right| < 0$. For Form I linkage,

$$P_{\text{DSG}} = \frac{1}{2}\left[-\frac{m_6 + m_1 \tan^2\frac{\theta_1}{2}}{\tan\frac{\theta_1}{2}} - \left(-\frac{m_6 - m_1 \tan^2\frac{\theta_1}{2}}{\tan\frac{\theta_1}{2}}\right)\right] = -m_1 \tan\frac{\theta_1}{2} \tag{B7}$$

For $\theta_1 \in [-\pi, 0)$ or $[0, \pi)$ in the Form I linkage, we will always have

$$\tan\frac{\theta_1}{2} \cdot \tan\frac{\theta_5}{2} = \tan\frac{\theta_1}{2} \cdot \frac{\left(-m_1 \tan\frac{\theta_1}{2}\right)}{-m_6} = \frac{m_1}{m_6}\tan^2\frac{\theta_1}{2} \text{ or } \theta_1 + \theta_5 \neq \pm\pi. \tag{B8}$$

Instead, for $\theta_1 \in [-\pi, 0)$ or $[0, \pi)$ in the Form II linkage, we will always have

$$\tan\frac{\theta_1}{2} \cdot \tan\frac{\theta_4}{2} = \tan\frac{\theta_1}{2} \cdot \frac{-m_1}{\left(-m_1 \tan\frac{\theta_1}{2}\right)} = 1 \text{ or } \theta_1 + \theta_4 = \pm\pi. \tag{B9}$$

In this case, the curve of θ_4 will become a straight line. To be specific, for the domain of $\theta_1 \in [-\pi, 0)$, $\theta_1 + \theta_4 = -\pi$ and for the domain of $\theta_1 \in [0, \pi)$, $\theta_1 + \theta_4 = \pi$.

- **Case 3**: the sign of $m_6 - m_1 \tan^2\frac{\theta_1}{2}$ changes with θ_1

By solving for the critical value, we have $\theta_1 = \pm 2\tan^{-1}\sqrt{\frac{m_2}{m_1}}$ when $m_2 - m_1 \tan^2\frac{\theta_1}{2} = 0$.

  - When $-\pi \le \theta_1 < -\tan^{-1}\sqrt{\frac{m_2}{m_1}}$, we have $\tan\frac{\theta_1}{2} < 0$ and $m_2 - m_1 \tan^2\frac{\theta_1}{2} < 0$. For Form I linkage, the same solution is the same as in Eq. (B6).
  - When $-\tan^{-1}\sqrt{\frac{m_2}{m_1}} \le \theta_1 < 0$, we have $\tan\frac{\theta_1}{2} < 0$ and $m_2 - m_1 \tan^2\frac{\theta_1}{2} > 0$. For Form I linkage, the same solution is the same as in Eq. (B3).

- When $0 < \theta_1 < \tan^{-1}\sqrt{\frac{m_2}{m_1}}$, we have $\tan\frac{\theta_1}{2} > 0$ and $m_2 - m_1\tan^2\frac{\theta_1}{2} > 0$. For Form I linkage, the same solution is the same as in Eq. (B4).

- When $\tan^{-1}\sqrt{\frac{m_2}{m_1}} \le \theta_1 < \pi$, we have $\tan\frac{\theta_1}{2} > 0$ and $m_2 - m_1\tan^2\frac{\theta_1}{2} < 0$. For Form I linkage, the same solution is the same as in Eq. (B7).

From the results in Case 1 and Case 2, it is obvious that in Case 3, only part of the curve of the Form I linkage will have $\theta_1 + \theta_5 = \pm\pi$. To be specific:

- for $\theta_1 \in \left[-\pi, -\tan^{-1}\sqrt{\frac{m_2}{m_1}}\right)$, $\theta_1 + \theta_5 = -\pi$;

- for of $\theta_1 \in \left[-\tan^{-1}\sqrt{\frac{m_2}{m_1}}, \tan^{-1}\sqrt{\frac{m_2}{m_1}}\right)$, $\theta_1 + \theta_5 \neq \pm\pi$; and

- for $\theta_1 \in \left[\tan^{-1}\sqrt{\frac{m_2}{m_1}}, \pi\right)$, $\theta_1 + \theta_5 = \pi$.

Therefore, on the kinematic paths, when θ_1 takes different values, part of the curves of Form I will present as a straight line, which also applies for the Form II linkage. Similar conclusions can be drawn between θ_1 and θ_4 when following exactly the same process as above.

The derivation and results for the Wohlhart's double-Goldberg linkage could be carried out in the same manner as the double-subtractive-Goldberg linkage shown above, where we will derive $\theta_1 + \theta_5 = 0$ for different cases of parameters and it is unavoidable to have part of the kinematic paths to present as a straight line.

Appendix C:

Solutions to Eqs. (5.3.16) and (5.3.17)

The solutions to Eqs. (5.3.16) and (5.3.17) could be generalized into the set of equations:

$$\tan\theta_2' = -\frac{\sin\delta\sin\theta_3'}{\sin\beta\cos\delta+\cos\beta\sin\delta\cos\theta_3'}, \tag{C1}$$

$$\tan\frac{\theta_2}{2} = \frac{-Bterm_2 \pm \sqrt{Bterm_2^2 - 4Aterm_2\cdot Cterm_2}}{2Aterm_2}, \tag{C2}$$

$$\tan\theta_2' = \tan\frac{\theta_2}{2}. \tag{C3}$$

By substituting Eqs. (C3) and (C1) into Eq. (C2) to eliminate θ_2, we will get

$$Aterm_2\cdot\tan^2\theta_2' + Bterm_2\cdot\tan\theta_2' + Cterm_2 = 0, \tag{C4}$$

where $Aterm_2$, $Bterm_2$ and $Cterm_2$ are functions of θ_1 as follows.

$$\begin{cases} Aterm_2 = \left(A_2\sin\theta_1 + B_2\cos\theta_1 + L_2\right) - \left(D_2 + F_2\sin\theta_1 + H_2\cos\theta_1\right) \\ Bterm_2 = 2\left(C_2 + E_2\sin\theta_1 + G_2\cos\theta_1\right) \\ Cterm_2 = \left(A_2\sin\theta_1 + B_2\cos\theta_1 + L_2\right) + \left(D_2 + F_2\sin\theta_1 + H_2\cos\theta_1\right). \end{cases} \tag{C5}$$

$$\begin{cases} A_2 = +\left(a_{34}\sin\alpha_{12}\cos\alpha_{23} + a_{12}\sin\alpha_{34}\right) \\ B_2 = -\left(R_3\sin\alpha_{12}\cos\alpha_{23}\sin\alpha_{34} + R_2\sin\alpha_{12}\sin\alpha_{34}\right) \\ C_2 = +\left(a_{23}\sin\alpha_{12}\cos\alpha_{34} + a_{12}\sin\alpha_{23}\right) \\ D_2 = -\left(R_3\sin\alpha_{12}\sin\alpha_{23}\cos\alpha_{34} + R_1\sin\alpha_{12}\sin\alpha_{23}\right) \\ E_2 = +R_3\sin\alpha_{23}\sin\alpha_{34} \\ F_2 = +\left(a_{34}\cos\alpha_{12}\sin\alpha_{23} + a_{23}\sin\alpha_{34}\right) \\ G_2 = +\left(a_{23}\cos\alpha_{12}\sin\alpha_{34} + a_{34}\sin\alpha_{23}\right) \\ H_2 = -R_3\cos\alpha_{12}\sin\alpha_{23}\sin\alpha_{34} \\ L_2 = +R_1\left(\cos\alpha_{12}\cos\alpha_{23} + \cos\alpha_{34}\right) + R_2\left(\cos\alpha_{23} + \cos\alpha_{12}\cos\alpha_{34}\right) \\ \qquad + R_3\left(1 + \cos\alpha_{12}\cos\alpha_{23}\cos\alpha_{34}\right). \end{cases} \tag{C6}$$

By substituting Eqs. (C5) and (C6) into Eq. (C4), we will get an equation about θ_1 as follows,

$$A\cdot\sin\theta_1+B\cdot\cos\theta_1+C=0\,, \tag{C7}$$

where

$$\begin{cases} A=\left(A_2-F_2\right)\tan^2\theta_2'+2E_2\tan\theta_2'+\left(A_2-F_2\right) \\ B=\left(B_2-H_2\right)\tan^2\theta_2'+2G_2\tan\theta_2'+\left(B_2-H_2\right) \\ C=\left(L_2-D_2\right)\tan^2\theta_2'+2C_2\tan\theta_2'+\left(L_2-D_2\right). \end{cases} \tag{C8}$$

After half-tangent transformation of the $\sin\theta_1$ and $\cos\theta_1$ in Eq. (C7), we can derive that

$$\left(C-B\right)\cdot\tan^2\frac{\theta_1}{2}+2A\cdot\tan\frac{\theta_1}{2}+\left(C+B\right)=0\,. \tag{C9}$$

By solving Eq. (C9), we can derive that

$$\tan\frac{\theta_1}{2}=\frac{-A\pm\sqrt{A^2+B^2-C^2}}{C-B}\,. \tag{C10}$$

Therefore, the positive result of Eq. (C10) is the solution to Eq. (5.3.16), while the negative result of Eq. (C10) is the solution to Eq. (5.3.17). The symbols are determined in Eqs. (C1), (C6) and (C8).

References

Altmann, P. G. (1954) Communications to Grodzinski, P. and M'Ewen, E.: Link mechanisms in modern kinematics. *Proceedings of the Institution of Mechanical Engineers* 168: 877-896, doi: 10.1243/PIME_PROC_1954_168_079_02.

Baker, J. E. (1978) On the investigation of extreme in linkage analysis, using screw system algebra. *Mechanism and Machine Theory* 13: 333-343, doi: 10.1016/0094-114X(78)90057-5.

Baker, J. E. (1979) The Bennett, Goldberg and Myard linkages - in perspective. *Mechanism and Machine Theory* 14: 239-253, doi: 10.1016/0094-114X(79)90011-9.

Baker, J. E. (1980) An analysis of the Bricard linkages. *Mechanism and Machine Theory* 15: 267-286, doi: 10.1016/0094-114X(80)90021-X.

Baker, J. E. (1983) An analysis of Goldberg's anconoidal linkage. *Mechanism and Machine Theory* 18: 371-376, doi: 10.1016/0094-114X(83)90133-7.

Baker, J. E. (1986) Limiting Positions of a Bricard Linkage and Their Possible Relevance to the Cyclohexane Molecule. *Mechanism and Machine Theory* 21: 253-260, doi: 10.1016/0094-114X(86)90101-1.

Baker, J. E. (1993a) A comparative survey of the Bennett-based, 6-revolute kinematic loops. *Mechanism and Machine Theory* 28: 83-96, doi: 10.1016/0094-114X(93)90049-2.

Baker, J. E. (1993b) A geometrico-algebraic exploration of Altmann's linkage. *Mechanism and Machine Theory* 28: 249-260, doi: 10.1016/0094-114X(93)90091-9.

Baker, J. E. (1997) The Single Screw Reciprocal to the General Plane-Symmetric Six-Screw Linkage. *Journal for Geometry and Graphics* 1: 5-12.

Baker, J. E. (2001) The axodes of the Bennett linkage. *Mechanism and Machine Theory* 36: 105-116, doi: 10.1016/S0094-114X(00)00026-4.

Baker, J. E. (2002) Displacement-closure equations of the unspecialised double-Hooke's-joint linkage. *Mechanism and Machine Theory* 37: 1127-1144, doi: 10.1016/S0094-114X(02)00042-3.

Baker, J. E. (2010) Using the Single Reciprocal Screw to Confirm Mobility of a Six-Revolute Linkage. *Proceedings of the Institution of Mechanical Engineers, Part C: Journal of Mechanical Engineering Science* 224: 2247-2255, doi: 10.1243/09544062JMES2062.

Baker, J. E., Duclong, T. and Khoo, P. S. H. (1982) On Attempting to Reduce Undesirable Inertial Characteristics of the Schatz Mechanism. *Transactions of the ASME: Journal of Mechanical Design* 104: 192-205, doi: 10.1115/1.3256310.

Baker, J. E. and Min, H. (1986) On spatial networks of overconstrained linkages. *Mechanism and Machine Theory* 21: 427-437, doi: 10.1016/0094-114X(86)90091-1.

Baker, J. E. and Wohlhart, K. (1994) On the Single Screw Reciprocal to the General Line-symmetric Six-screw Linkage. *Mechanism and Machine Theory* 29: 169-175, doi: 10.1016/0094-114X(94)90028-0.

Ball, R. S. (1876) *The theory of screws: a study in the dynamics of a rigid body*: Dublin: Hodges, Foster.

Barbarino, S., Bilgen, O., Ajaj, R. M., et al. (2011) A Review of Morphing Aircraft. *Journal of Intelligent Material Systems and Structures* 22: 823-877, doi: 10.1177/1045389X11414084.

Beggs, J. S. (1983) *Kinematics*: Hemisphere Publishing Corporation.

Bennett, G. T. (1903) A new mechanism. *Engineering* 76: 777–778.

Bennett, G. T. (1912) Deformable Octahedra. *Proceedings of the London Mathematical Society* s2-10: 309-343, doi: 10.1112/plms/s2-10.1.309.

Bennett, G. T. (1914) The skew isogram mechanism. *Proceedings London Mathematical Society* s2-13: 151–173, doi: 10.1112/plms/s2-13.1.151.

Bricard, R. (1897) Mémoire sur la théorie de l'octaèdre articulé. *Journal of Pure and Applied Mathematics* 3: 113-150.

Bricard, R. (1927) *Leçons de cinématique*, Paris: Gauthier-Villars.

Chai, W. H. and Chen, Y. (2010) The line-symmetric octahedral Bricard linkage and its structural closure. *Mechanism and Machine Theory* 45: 772-779, doi: 10.1016/j.mechmachtheory.2009.12.007.

Chen, I. M. (1994) Theory and applications of modular reconfigurable robotic systems. *Mechanical Engineering.* Pasadena, CA.: California Institute of Technology.

Chen, I. M. and Burdick, J. W. (1995) Determining Task Optimal Modular Robot Assembly Configurations. *Proceedings of the 1995 IEEE International Conference on Robotics and Automation.* Nagoya, Japan, 132-137.

Chen, I. M. and Yang, G. L. (1996) Configuration Independent Kinematics for Modular Robots. *IEEE International Conference on Robotics and Automation.* Minneapolis, MN, 1440-1445.

Chen, Y. and Baker, J. E. (2005) Using a Bennett linkage as a connector between other Bennett loops. *Proceedings of the Institution of Mechanical Engineers, Part K: Journal of Multi-body Dynamics* 219: 177-185, doi: 10.1243/146441905X9935.

Chen, Y. and Chai, W. H. (2011) Bifurcation of a special line and plane symmetric Bricard linkage. *Mechanism and Machine Theory* 46: 515-533, doi: 10.1016/j.mechmachtheory.2010.11.015.

Chen, Y. and You, Z. (2005) Mobile assemblies based on the Bennett linkage. *Proceedings of the Royal Society A: Mathematical, Physical and Engineering Science* 461: 1229-1245, doi: 10.1098/rspa.2004.1383.

Chen, Y. and You, Z. (2007) Spatial 6*R* linkages based on the combination of two Goldberg 5*R* linkages. *Mechanism and Machine Theory* 42: 1484-1498, doi: 10.1016/j.mechmachtheory.2006.12.008.

Chen, Y. and You, Z. (2008a) An Extended Myard Linkage and its Derived 6*R* Linkage. *Transactions of the ASME: Journal of Mechanical Design* 130: 8, doi: 10.1115/1.2885506.

Chen, Y. and You, Z. (2008b) On mobile assemblies of Bennett linkages. *Proceedings of the Royal Society A: Mathematical, Physical and Engineering Science* 464: 1275-1293, doi: 10.1098/rspa.2007.0188.

Chen, Y., You, Z. and Tarnai, T. (2005) Threefold-symmetric Bricard linkages for deployable structures. *International Journal of Solids and Structures* 42: 2287-2301, doi: 10.1016/j.ijsolstr.2004.09.014.

Dai, J. S. and Rees Jones, J. (1999) Mobility in Metamorphic Mechanisms of Foldable/Erectable Kinds. *Transactions of the ASME: Journal of Mechanical Design* 121: 375-382, doi: 10.1115/1.2829470.

Dai, J. S. and Rees Jones, J. (2005) Matrix Representation of Topological Changes in Metamorphic Mechanisms. *Transactions of the ASME: Journal of Mechanical Design* 127: 837-840, doi: 10.1115/1.1866159.

Dai, J. S. and Wang, D. (2007) Geometric Analysis and Synthesis of the Metamorphic Robotic Hand. *Transactions of the ASME: Journal of Mechanical Design* 129: 1191-1197, doi: 10.1115/1.2771576.

Dai, J. S. and Zhang, L. P. (2009) An Overview of the Development on Reconfiguration of Metamorphic Mechanisms. *2009 ASME/IFToMM International Conference on Reconfigurable Mechanisms and Robots.* King's College London, London, UK.

Dalha, C. (1982) Le Mécanisme de Bennett: propriétés et applications. Besançon, France: Laboratoire de Mécanique appliquée, 151.

Delassus, E. (1922) Les chaînes articulées fermées et déformables à quatre membres. *Bulletin des Sciences Mathématiques* 2nd Series: 283–304, doi: 10.1.1.41.7324.

Denavit, J. and Hartenberg, R. S. (1955) A kinematic notation for lower-pair mechanisms based on matrices. *Transactions of the ASME: Journal of Applied Mechanics* 23: 215-221.

Dietmaier, P. (1995a) Einfach übergeschlossene mechanismen mit drehgelenken. Graz, Austria: Technische Universität Graz.

Dietmaier, P. (1995b) A new 6R space mechanism. *Proceeding 9th World Congress IFToMM.* Milano, Italy, 52–56.

Fowler, P. W. and Guest, S. D. (2005) A symmetry analysis of mechanisms in rotating rings of tetrahedra. *Proceedings of the Royal Society A: Mathematical, Physical and Engineering Science* 461: 1829-1846, doi: 10.1098/rspa.2004.1439.

Fukuda, T. and Ueyama, T. (1994) *Cellular Robotics and Micro Robotic Systems*: World Scientific.

Galletti, C. and Fanghella, P. (1999) Kinematotropic Properties and Pair Connectivities in Single-Loop Spatial Mechanisms. *Proc. 10th World Congress on the Theory of Machines and Mechanisms.* Oulu, Finland, 560-565.

Galletti, C. and Fanghella, P. (2001) Single-loop kinematotropic mechanisms. *Mechanism and Machine Theory* 36: 743-761, doi: 10.1016/S0094-114X(01)00002-7.

Galletti, C. and Giannotti, E. (2002) Multiloop Kinematotropic Mechanisms. *ASME 2002 International Design Engineering Technical Conferences and Computers and Information in Engineering Conference (IDETC/CIE2002)* Montreal, Canada, 455-460.

Gan, W. W. and Pellegrino, S. (2006) A numerical approach to the kinematic analysis of deployable structures forming a closed loop. *Proceedings of the Institution of Mechanical Engineers, Part C: Journal of Mechanical Engineering Science* 220: 1045-1056, doi: 10.1243/09544062JMES245.

Gantes, C. J. (1989) *Deployable structures: analysis and design*: WIT Press.

Gogu, G. (2005a) Chebychev–Grübler–Kutzbach's criterion for mobility calculation of multi-loop mechanisms revisited via theory of linear transformations. *European Journal of Mechanics - A/Solids* 24: 427-441, doi: 10.1016/j.euromechsol.2004.12.003.

Gogu, G. (2005b) Mobility and spatiality of parallel robots revisited via theory of linear transformations. *European Journal of Mechanics - A/Solids* 24: 690-711, doi: 10.1016/j.euromechsol.2005.02.004.

Gogu, G. (2005c) Mobility of mechanisms: a critical review. *Mechanism and Machine Theory* 40: 1068-1097.

Gogu, G. (2008) *Structural synthesis of parallel robots: Methodology. Part 1*: Springer.

Goldberg, M. (1943) New five-bar and six-bar linkages in three dimensions. *Transactions of the ASME* 65: 649–663.

Goldberg, M. (1946) A three-dimensional analog of a plane kempe linkage. *Journal of Mathematics and Physics* 25: 96-110.

Goldberg, M. (1974) A 6-plate Linkage in Three Dimensions. *The Mathematical Gazette* 58: 287-289.

Guest, S. D. and Fowler, P. W. (2005) A symmetry-extended mobility rule. *Mechanism and Machine Theory* 40: 1002-1014, doi: 10.1016/j.mechmachtheory.2004.12.017.

Hervé, J. M. and Dahan, M. (1983) The two kinds of Bennett's mechanisms. *Proceedings of the Sixth World Congress on Theory of Machines and Mechanisms.* New Delhi, India, 116-119.

Ho, C. Y. (1978) A note on the existence of Bennett mechanism. *Mechanism and Machine Theory* 13: 269-271, doi: 10.1016/0094-114X(78)90050-2.

Huang, C. T. (1992) Application of Linear Algebra to Screw Systems and Position-force Synthesis of Closed-loop Linkages. *Department of Mechanical Engineering.* Stanford University, 298.

Huang, C. T. (2003) The Screw Triangle: Now and Then. In: McCarthy, M. (ed) *Bernard Roth Symposium.* Stanford.

Huang, C. T. and Chen, C. M. (1995) The Linear Representation of the Screw Triangle—A Unification of Finite and Infinitesimal Kinematics. *Transactions of the ASME: Journal of Mechanical Design* 117: 554-560, doi: 10.1115/1.2826718.

Hunt, K. H. (1990) *Kinematic geometry of mechanisms,* Oxford: Oxford University Press.

Husty, M. L. (2000) E. Borel's and R. Bricard's papers on displacements with spherical paths and their relevance to self-motions of parallel manipulators. In: Ceccarelli, M. (ed) *International Symposium on History of Machines and Mechanisms.* Cassino, Italy: Kluwer Acad. Pub., 163-172.

Husty, M. L. and Karger, A. (1996) On Self-Motions of a Class of Parallel Manipulators. In: Lenarcic, J. and Parenti-Castelli, V. (eds) *Advances in Robot Kinematics.* Kluwer Acad. Pub., 339-348.

Husty, M. L. and Zsombor-Murray, J. (1994) A Special Type of Singular Stewart Gough Platform. In: Lenarcic, J. and Ravani, B. (eds) *Advances in Robot Kinematics.* 439-449.

Kamimura, A., Kurokawa, H., Yoshida, E., et al. (2005) Automatic Locomotion Design and Experiments for a Modular Robotic System. *IEEE/ASME Transactions on Mechatronics* 10: 314-325, doi: 10.1109/TMECH.2005.848299.

Kong, X. and Huang, C. (2009) Type synthesis of single-DOF single-loop mechanisms with two operation modes. *Proceedings of the 2009 ASME/IFToMM International Conference on Reconfigurable Mechanisms and Robots.* London, UK, 136-141.

Kuo, C. H., Dai, J. S. and Yan, H. S. (2009) Reconfiguration Principles and Strategies for Reconfigurable Mechanisms. *Proceedings of the 2009 ASME/IFToMM International Conference on Reconfigurable Mechanisms and Robots.* London, UK, 1-7.

Lan, Z. H. and Du, R. (2008) Representation of Topological Changes in Metamorphic Mechanisms With Matrices of the Same Dimension. *Transactions of the ASME: Journal of Mechanical Design* 130: 074501, doi: 10.1115/1.2918917.

Lee, C. C. (1996) On the generation synthesis of movable octahedral 6*R* mechanisms. *ASME Design Engineering Technical Conferences and Computers in Engineering Conference.* Irvine, California, 1-8.

Lee, C. C. (2000) Computational and geometric investigation on the reciprocal screw axis of Bricard six-revolute mechanisms. *ASME Design Engineering Technical Conference and Computers and Informatin in Engineering Conference.* Baltimore, Maryland, 93-101.

Lee, C. C. (2002) Analysis and Synthesis of General-Type Goldberg Five-Revolute Mechanism. *JSME Int J., Ser. C* 45: 614-627.

Lee, C. C. and Hervé, J. M. (2005) Discontinuously Movable Seven-Link Mechanisms Via Group-Algebraic Approach. *Proceedings of the Institution of Mechanical Engineers, Part C: Journal of Mechanical Engineering Science* 219: 577-587, doi: 10.1243/095440605X31436.

Lee, H. Y. and Liang, C. G. (1988) A new vector theory for the analysis of spatial mechanisms. *Mechanism and Machine Theory* 23: 209-217, doi: 10.1016/0094-114X(88)90106-1.

Mavroidis, C. (1993) Inverse Kinematics of General and Special Serial Link Manipulators. Paris, France: University Paris VI.

Mavroidis, C. and Roth, B. (1995) New and Revised Overconstrained Mechanisms. *Transactions of the ASME: Journal of Mechanical Design* 117: 75, doi: 10.1115/1.2826120.

Mavroidis, C. and Roth, B. (1997) On the Geometry of Spatial Polygons and Screw Polygons. *Transactions of the ASME: Journal of Mechanical Design* 119: 246-252, doi: 10.1115/1.2826243.

Myard, F. E. (1931) Contribution à la géométrie des systèmes articulés. *Bulletin de la Société Mathématique de France* 59: 183-210.

Nawratil, G. (2010) Flexible octahedra in the projective extension of the Euclidean 3-space. *Journal for Geometry and Graphics* 14: 147-169.

Nawratil, G. (2011) Self-motions of TSSM manipulators with two parallel rotary axes. *Transactions of the ASME: Journal of Mechanisms and Robotics* 3: 031007, doi: 10.1115/1.4004030.

Nelson, G. D. (2010) Extending Bricard Octahedra. *arXiv.org*, arXiv:1011.5193 [math.MG].

Nelson, G. D. (2012) Generalizations of Bricard octahedra. *arXiv.org*, arXiv:1206.2588 [math.MG].

Pamidi, P. R., Soni, A. H. and Dukkipati, R. V. (1973) Necessary and sufficient existence criteria of overconstrained five-link spatial mechanisms with helical, cylinder, revolute and prism pairs. *Transactions of the ASME: Journal of Engineering for Industry* 95: 737-743, doi: 10.1115/1.3438218.

Pellegrino, S. (1993) Structural computations with the singular value decomposition of the equilibrium matrix. *International Journal of Solids and Structures* 30: 3025-3035, doi: 10.1016/0020-7683(93)90210-X.

Perez, A. and McCarthy, J. M. (2002) Bennett's linkage and the cylindroid. *Mechanism and Machine Theory* 37: 1245-1260, doi: 10.1016/S0094-114X(02)00055-1.

Phillips, J. (1984) *Freedom in Machinery I: Introducing screw theory*, Cambridge: Cambridge University Press.

Phillips, J. (1990) *Freedom in Machinery II: Screw theory exemplified*, Cambridge: Cambridge University Press.

Raghavan, M. and Roth, B. (1990) A general solution for the inverse kinematics of all series chains. *Proceedings of the 8th CISM-IFToMM Symposium on Robots and Manipulators.* Cracow, Poland, 24-31.

Sarrus, P. T. (1853) Note sur la transformation des mouvements rectilignes alternatifs, en mouvements circulaires, et reciproquement. *Academie des Sciences Comtes Rendus Hebdomataires Des séances* 36: 1036-1038.

Savage, M. (1972) Four-link mechanisms with cylindric, revolute and prismatic pairs. *Mechanism and Machine Theory* 7: 191-208, doi: 10.1016/0094-114X(72)90004-3.

Schatz, P. (1975) *Rhythmusf orschung and Technik*, Stuttgart: Freies Geisteslehen.

Seffen, K. A., You, Z. and Pellegrino, S. (2000) Folding and deployment of curved tape springs. *International Journal of Mechanical Sciences* 42: 2055-2073, doi: 10.1016/S0020-7403(99)00056-9.

Song, C. Y. and Chen, Y. (2011) The original double-Goldberg 6*R* linkage and its bifurcation analysis. *International Symposium on Multibody Systems and Mechatronics.* Valencia, Spain.

Stephanos, C. (1894) Problem 376: "*Do there exist polyhedra with invariant facets susceptible to continuous deformations that solely alter solid angles and dihedral angles?"*. *L'Intermédiaire des mathématiciens* 1: 228.

Stubbs, M. D., Whittier, W. B. and Reinholtz, C. F. (2004) Single Degree-of-Freedom Morphing Wing (Design and Synthesis). *ASME 2004 International Design Engineering Technical Conferences and Computers and Information in Engineering Conference.* Salt Lake City, USA: ASME, 33-41.

Waldron, K. J. (1968) Hybrid overconstrained linkages. *Journal of Mechanisms* 3: 73-78, doi: 10.1016/0022-2569(68)90016-5.

Waldron, K. J. (1979) Overconstrained linkages. *Environment and planning B* 6: 393-402, doi: 10.1068/b060393.

Wohlhart, K. (1987) A new 6R space mechanism. *Proceedings of the 7th World.Congress on the Theory of Machines and Mechanisms.* Sevilla, Spain, 193-198.

Wohlhart, K. (1991a) Merging two general goldberg 5*R* linkages to obtain a new 6*R* space mechanism. *Mechanism and Machine Theory* 26: 659-668, doi: 10.1016/0094-114X(91)90028-3.

Wohlhart, K. (1991b) On isomeric overconstrained space mechanisms. *Proeeedings of the Eights World Congress on the Theory of Machines and Mechanisms.* Prague, Czechoslovakia, 153-158.

Wohlhart, K. (1993) The Two Types of the Orthogonal Bricard Linkage. *Mechanism and Machine Theory* 28: 809-817, doi: 10.1016/0094-114X(93)90023-O.

Wohlhart, K. (1996) Kinematotropic linkages. In: Parenti-Castelli, J. L. a. V. (ed) *The fifth international symposium on Advances in Robots Kinematics.* Portoroz, Slovenia: Kulwer Academic Publishers, 359-368.

Wohlhart, K. (2010) Multifunctional 7R Linkages. *Proceedings of the International Symposium on Mechanisms and Machine Theory.* Izmir, Turkey: AzCIFToMM, 85-91.

Yan, H. S. and Kang, C. H. (2009) Configuration Synthesis of Mechanisms with Variable Topologies. *Mechanism and Machine Theory* 44: 896-911, doi: 10.1016/j.mechmachtheory.2008.06.006.

Yan, H. S. and Kuo, C. H. (2006a) Representations and Identifications of Structural and Motion State Characteristics of Mechanisms with Variable Topologies. *Transactions of the Canadian Society for Mechanical Engineering* 30: 19-40.

Yan, H. S. and Kuo, C. H. (2006b) Topological Representations and Characteristics of Variable Kinematic Joints. *Transactions of the ASME: Journal of Mechanical Design* 128: 384-391, doi: 10.1115/1.2166854.

Yang, A. T. (1963) Application of quaternion algebra and dual numbers to the analysis of spatial mechanisms. Columbia University.

Yim, M. (1994) Locomotion with a unit-modular reconfigurable robot. *Department of Mechanical Engineering.* Stanford University, 157.

Yu, H. C. (1981a) The Bennett linkage, its associated tetrahedron and the hyperboloid of its axes. *Mechanism and Machine Theory* 16: 105-114, doi: 10.1016/0094-114X(81)90056-2.

Yu, H. C. (1981b) The Deformable Hexahedron of Bricard. *Mechanism and Machine Theory* 16: 621-629, doi: 10.1016/0094-114X(81)90068-9.

Yu, H. C. and Baker, J. E. (1981) On the generation of new linkages from Bennett loops. *Mechanism and Machine Theory* 16: 473-485, doi: 10.1016/0094-114X(81)90019-7.

Zarrouk, D. and Shoham, M. (2011) A Note on the Screw Triangle. *Transactions of the ASME: Journal of Mechanisms and Robotics* 3: 4, doi: 10.1115/1.4002943.

Zhang, L. and Dai, J. S. (2008) Genome Reconfiguration of Metamorphic Manipulators Based on Lie Group Theory. *ASME 2008 International Design Engineering Technical*

Conferences and Computers and Information in Engineering Conference (IDETC/CIE2008). Brooklyn, New York, USA.

Zhang, L. P. and Dai, J. S. (2009a) An Overview of the Development on Reconfiguration of Metamorphic Mechanisms. In: J.S. Dai, M. Z. a. X. K. (ed) *Proceedings of the 2009 ASME/IFToMM International Conference on Reconfigurable Mechanisms and Robots.* London, UK, 8-12.

Zhang, L. P. and Dai, J. S. (2009b) Reconfiguration of Spatial Metamorphic Mechanisms. *Transactions of the ASME: Journal of Mechanisms and Robotics* 1: 8, doi: 10.1115/1.2963025.

Zhang, L. P., Wang, D. L. and Dai, J. S. (2008) Biological Modeling and Evolution Based Synthesis of Metamorphic Mechanisms. *Transactions of the ASME: Journal of Mechanical Design* 130: 072303, doi: 10.1115/1.2900719.